



**DEFINING THE PATHOPHYSIOLOGICAL  
IMPACT OF CIGARETTE SMOKE  
EXTRACT IN MICE AS A MODEL FOR  
CHRONIC OBSTRUCTIVE PULMONARY  
DISEASE (COPD)**

**Laura Grace Bartlett, MSc, BSc (Hons)**

Thesis submitted to the University of Nottingham for the  
degree of Doctor of Philosophy

**March 2024**

---

## CONTENTS

DECLARATION .....	I
ACKNOWLEDGEMENTS .....	II
PUBLICATIONS .....	IV
COMMUNICATIONS IN CONGRESS .....	VI
COVID-19 IMPACT STATEMENT .....	VIII
ABSTRACT .....	IX
INTRODUCTION: .....	IX
METHODS: .....	IX
RESULTS: .....	X
CONCLUSIONS: .....	X
LIST OF FIGURES .....	XI
LIST OF TABLES .....	XVII
ABBREVIATIONS .....	XVIII
CHAPTER 1 – GENERAL INTRODUCTION .....	1
1.1. CHRONIC OBSTRUCTIVE PULMONARY DISEASE .....	1
1.1.1. EPIDEMIOLOGY AND GLOBAL BURDEN .....	3
1.1.2. CAUSATIVE FACTORS .....	13
1.1.3. MECHANISMS AND PATHOGENESIS .....	20
1.1.4. IMMUNOPATHOLOGICAL MECHANISMS .....	24
1.2. ANIMAL MODELS OF COPD .....	38
1.2.1. MODELS OF COPD .....	39
1.2.2. CS EXPOSURE MURINE MODELS OF COPD .....	43
1.3. ANIMAL ETHICS AND WELFARE IN SCIENTIFIC PROCEDURES .....	49
1.3.1. UK LEGISLATION AND HISTORY .....	50
1.3.2. THE THREE RS AND THE CULTURE OF CARE .....	52
1.4. AIMS OF THIS PHD THESIS .....	57
CHAPTER 2 – MATERIALS AND METHODS .....	58
2.1. MATERIALS .....	58
2.1.1. MURINE MODEL .....	58
2.1.2. SPECTRAL FLOW CYTOMETRY .....	61
2.1.3. REVERSE PHASE PROTEIN MICROARRAY .....	65
2.1.4. RT-qPCR .....	72

---

2.1.5. HISTOLOGY .....	74
2.2. METHODS .....	75
2.2.1. MURINE COPD MODEL .....	75
2.2.2. SPECTRAL FLOW CYTOMETRY.....	84
2.2.3. REVERSE PHASE PROTEIN MICROARRAY .....	91
2.2.4. RT-QPCR.....	98
2.2.5. HISTOLOGY .....	105
2.2.6. DATA AND STATISTICAL ANALYSIS .....	106
CHAPTER 3 – VALIDATION OF ANALYTICAL TECHNIQUES .....	112
3.1. INTRODUCTION .....	112
3.2. METHODS .....	115
3.2.1. SPECTRAL FLOW CYTOMETRY.....	115
3.2.2. REVERSE PHASE PROTEIN MICROARRAY.....	119
3.2.3. RT-QPCR.....	121
3.3. RESULTS .....	124
3.3.1. SPECTRAL FLOW CYTOMETRY.....	124
3.3.2. REVERSE PHASE PROTEIN MICROARRAY.....	137
3.3.3. RT-QPCR.....	143
3.4. DISCUSSION.....	152
CHAPTER 4 – SYSTEMIC EFFECTS OF CSE EXPOSURE .....	157
4.1. INTRODUCTION .....	157
4.2. METHODS .....	159
4.2.1. MURINE MODEL.....	159
4.2.2. SPECTRAL FLOW CYTOMETRY.....	162
4.3. RESULTS .....	163
4.3.1. ANIMAL WELFARE .....	163
4.3.2. TOTAL PERIPHERAL IMMUNE CELLS .....	165
4.3.3. T CELLS.....	166
4.3.4. NK CELLS.....	180
4.3.5. MACROPHAGES.....	183
4.3.6. NEUTROPHILS.....	186
4.3.7. MONOCYTES.....	189
4.3.8. DENDRITIC CELLS.....	192
4.3.9. B CELLS .....	195

---

4.3.10. CLUSTERING ANALYSIS .....	198
4.4. DISCUSSION .....	211
CHAPTER 5 – PULMONARY EFFECTS OF CSE EXPOSURE .....	215
5.1. INTRODUCTION .....	215
5.2. METHODS .....	217
5.2.1. MURINE MODEL .....	217
5.2.2. RT-QPCR .....	217
5.2.3. HISTOLOGY .....	219
5.3. RESULTS .....	220
5.3.1. RNA PURITY FROM MURINE LUNG .....	220
5.3.2. RELATIVE GENE EXPRESSION .....	222
5.3.3. MAST CELL IDENTIFICATION .....	226
5.3.4. MAST CELL NUMBERS AND ACTIVITY .....	227
5.3.5. AIRWAY STRUCTURE, COLLAGEN DEPOSITION AND NEUTROPHIL IDENTIFICATION .....	230
5.3.6. PULMONARY NEUTROPHILIA .....	233
5.3.7. COLLAGEN DEPOSITION .....	239
5.3.8. SMALL AIRWAY AND ALVEOLAR REMODELLING .....	243
5.4. DISCUSSION .....	244
CHAPTER 6 – GENERAL DISCUSSION .....	249
6.1. OVERVIEW .....	249
6.2. EFFECTS OF CSE EXPOSURE ON SYSTEMIC IMMUNE CELL PROFILES .....	252
6.3. ALTERATIONS TO GENE EXPRESSION FOLLOWING CSE EXPOSURE .....	253
6.4. INCREASED ACTIVITY OF MAST CELLS IN THE TRACHEA .....	254
6.5. DOSE-DEPENDENT INCREASE IN PULMONARY NEUTROPHILIA AND AIRWAY REMODELLING .....	255
6.6. IMPACT OF SEX ON COPD PATHOPHYSIOLOGY .....	256
6.7. MOUSE MODEL DESIGN .....	257
6.8. GENERAL LIMITATIONS .....	258
6.9. APPLICATIONS AND FUTURE DIRECTIONS .....	262
6.10. CONCLUDING REMARKS .....	265
REFERENCES .....	267
APPENDIX A: BSU STUDY PROTOCOL .....	307

---

APPENDIX B: ANIMAL WELFARE MONITORING SHEET .....	316
APPENDIX C: STAIN INDEXES .....	317
APPENDIX D: PIPS REFLECTIVE STATEMENT .....	346
NOTE TO EXAMINERS:.....	346
PLACEMENT OUTLINE.....	346
PLACEMENT AIMS .....	347
PERSONAL AND PROFESSIONAL DEVELOPMENT.....	347

## DECLARATION

This work was funded through the University of Nottingham BBSRC DTP.

I declare that this thesis is the result of my own work, unless otherwise stated. It has not been presented as part of any other degree.

All animal work was conducted under Home Office Establishment Licence X653228F4 (Registered to the University of Nottingham and held by Paul Greatorix), Project Licence PP5215372 (Held by Adam Watkins) and Personal Licence I27390381 (Held by Laura Grace Bartlett) and in accordance with the regulations specified by the updated Animals (Scientific Procedures) Act 2012 under European Directive 2010/63/EU. Licences were obtained under guidance of the University of Nottingham Animal Welfare and Ethical Review Body (AWERB) and training and guidance for investigators were provided by the establishment's designated trainers including the Named Veterinary Surgeon (NVS) and Named Animal Care and Welfare Officers (NACWOs). Competency in all regulated procedures used in this study was assessed and authorised by the Named Training and Competency Officer (NTCO).

I accept responsibility as the primary investigator under PP5215372 from February 2023 to November 2023 for any perceived breach of the Animals (Scientific Procedures) Act 2012, or for any welfare concerns raised as a result of this study following the submission of this thesis.

## ACKNOWLEDGEMENTS

First and foremost, the greatest thanks go to my supervisors Professor Lucy Fairclough, Dr Adam Watkins and Professor Paddy Tighe, who over the last four and a half years have given me the most brilliant guidance and insight, as well as allowing me to have the freedom to really take charge and steer this project in the direction I best saw fit. I particularly want to thank Lucy for constantly pushing me forwards and giving me so many amazing opportunities to build on my skills both professionally and personally, whether it be funded work to assist in groundbreaking COVID research or giving lectures and presentations to share my work or knowledge of my PhD subject. Thank you for being my “Nottingham Mum”. Adam also deserves special thanks for all his patience and hard work as we fought to get the ethical approval necessary for our mouse model, I’m not quite sure how much he realises how appreciative we are of his efforts, knowledge and down-to-earth approach to all the hurdles we faced. Last but certainly not least, a big thank you to Paddy. It’s a shame that the RPPA didn’t work but we gave it our best shot, and your laissez-faire approach to science and life in general has at times been frustrating for someone who struggles with anxiety, but ultimately had a huge impact on me and I’ve become far more comfortable and confident with unexpected challenges and failure. Lucy, Adam and Paddy have gone above and beyond to make sure that I made it through to the very end, always putting my welfare at the forefront of everything, for which I’m incredibly grateful. I have always struggled with my confidence and sense of self-worth, and at every moment where I doubted myself and my capabilities, each of my supervisors has taken the time to listen to me and encouraged me with the most amazing amount of kindness and compassion. It’s safe to say that at the end of this journey, thanks to them, I’ve developed a newfound confidence in myself and achieved far more than I ever thought I could.

It goes without saying that this project wouldn’t have been possible without the help of a number of people across the University and beyond. Thank you to the BBSRC DTP team for all their help and support over the years, especially to Sara, Alice and Sandra for easing a lot of stress by helping sort out my much-needed voluntary interruption to study and helping me adjust to coming back. A big thank you to Vendula, Paola, Huw and Bev at Sony Biotechnology for all

their help and support in developing our flow cytometry panel, and of course to David and Nicki at the University of Nottingham Flow Cytometry Facility who helped save me from many migraines trying to optimise the panel. Thanks also to Alison (Imperial College London) and Amanda (University of Nottingham) for all their advice and guidance in the creation of our Project Licence, we wouldn't have been able to answer many of the technical questions the AWERB and Home Office threw at us without your insight. A massive thanks to Ian at the School of Life Sciences Imaging (SLIM) Facility and to Jeni for helping me navigate the weird and wonderful world of histology with nothing but excitement and a wicked sense of humour, this project wouldn't be as complete as it is without all your help! The biggest thanks goes to the tireless work and support of everyone at the University of Nottingham BioSupport Unit who provided the space and equipment necessary for our animal work. I particularly want to thank Ian, Debbie, Mark, Lauren and Callum for all their hands-on support over the thirteen incredibly tiring weeks that our model was running, and for being just as excited about seeing the results of the study as my supervisors and I were. You all helped reignite my passion for research more than you can imagine.

I can't express how grateful or thankful I am for the love and support shown to me over the years by my friends and family, which includes all the members of the Fairclough, Watkins and Tighe labs, and also the University of Nottingham Artistic Swimming Club. Big thanks to Georgie, Davis, Will and Tyler for bearing with my many emotional outbursts, and for somehow always being able to make me smile and laugh during some truly challenging times. Thank you to Yasmin, who has taken over this project with a sense of enthusiasm that I didn't even know was possible, I know that this project is in the best hands with you. Super special thanks also to Hannah M and Hannah J for always lending an ear when I needed it or just simply providing encouragement or a distraction when the stress was getting to me. The same can be said for my two best friends, Katie and Brittany, who no matter the distance or how long we went between talking always showed me the greatest love and support, I still maintain that you're more like sisters than friends to me. My family has and always will be one of the most important things to me, and I couldn't have made it without all their help and support over the years. Mum (Mumsie Beans), Dad (Doom), Sandra (Sangie Da), Matt (Gloom) and Jamie (Jimby Wimby), thank you for always being there for me and supporting me through all my (often



questionable) choices and adventures in life. And a big thanks to the Douglis too, for being the honorary (and somehow even madder) extended family I never knew I needed. I especially want to thank my Mum and Dad for being not only my parents, but also my best friends, and helping me get back up on my feet every time something knocked me down.

Last but not least, an honourable mention needs to be made for my cat, Zoe (AKA ZoBo, bubba, bubs, bubsies, bubba dubba, mizzog, rumbles, stinky baby, big stink, grampus, ratbag... and a whole heap of other names I definitely can't include in my thesis). As my unofficial therapy animal, I greatly appreciate all the cuddles, purrs, headbutts and slow blinks you've given me as I've been writing. Thanks to your ridiculousness often providing me with a good laugh, and your relentlessness for a cuddle forcing me to take a break every now and then, I've made it to the end and finished my PhD. Also, have you been smoking without us knowing? Because you meow, wheeze and snore like you've been smoking for 50+ years, and I can safely say at this point I happen to know a thing or two about COPD and the negative effects of smoking.



## PUBLICATIONS

Gumber L, Gomez N, Hopkins G, Tucis D, **Bartlett L**, Ayling K, Vedhara K, Steers G, Chakravorty M, Rutter M, Jackson H, Tighe P, Ferraro A, Power S, Pradère MJ, Onion D, Lanyon PC, Pearce FA, Fairclough L (2022). Humoral and cellular immunity in patients with rare autoimmune rheumatic diseases following SARS-CoV-2 vaccination. *Rheumatology (Oxford)*. (<https://doi.org/10.1093/rheumatology/keac574>)

**Bartlett LG**, Watkins AJ, Fairclough LC (2024). Immunopathological mechanisms of chronic obstructive pulmonary disease (COPD): A systematic review of lessons learned from murine models. *Thorax*. (In Preparation)

Hopkins GV, Gomez N, Tucis D, **Bartlett L**, Steers G, Jackson H, Tighe P, Onion D, Wills M, Godkin A, Fairclough L (2024). Decreased Humoral and T Cell Responses to Asymptomatic SARS-CoV-2 Infection in Education (The ACE Cohort). *Journal of Clinical Immunology*. (Under Review)

Jackson H, Hopkins GV, Gomez N, Tucis D, **Bartlett L**, Steers G, Tighe P, Onion D, Wills M, Godkin A, Fairclough L. Cross-reactive antibody responses in young adults following asymptomatic and symptomatic SARS-CoV-2 infection and vaccination. (In Preparation).

## COMMUNICATIONS IN CONGRESS

**Bartlett LG**, Tighe PJ, Watkins AJ, Fairclough LC. Development of a novel refined cigarette smoke exposure mouse model to define the immunopathophysiological mechanisms of chronic obstructive pulmonary disease (COPD). *Midlands National Centre for the 3Rs Symposium, Birmingham, UK, 2023*. Poster Presentation and Flash Talk

**Bartlett LG**, Tighe PJ, Watkins AJ, Fairclough LC. Fancy a cigarette? Addressing the need of an ethically sound mouse model to define the immunopathophysiological mechanisms of cigarette smoke-induced chronic obstructive pulmonary disease (COPD). *School of Life Sciences PGR Conference, Nottingham, UK, 2023*. Oral Presentation

**Bartlett LG**, Tighe PJ, Watkins AJ, Fairclough LC. Fancy a cigarette? Addressing the need of an ethically sound mouse model to define the immunopathophysiological mechanisms of cigarette smoke-induced chronic obstructive pulmonary disease (COPD). *British Society for Immunology Midlands Immunology Group Symposium 2023, Leicester, UK*. Poster Presentation

**Bartlett LG**, Tighe PJ, Watkins AJ, Fairclough LC. Development and validation of a novel murine spectral flow cytometry panel to investigate the immunopathogenic mechanisms of chronic obstructive pulmonary disease (COPD). *Midlands Innovation Flow Cytometry Group Meeting, Nottingham, UK, 2023*. Oral Presentation

**Bartlett LG**, Tighe PJ, Watkins AJ, Fairclough LC. Defining the pathophysiological impact of cigarette smoke extract in mice as a model of Chronic Obstructive Pulmonary Disease (COPD). *BBSRC Spring Conference, Nottingham, UK, 2023*. Oral Presentation (3-Minute Thesis)

**Bartlett LG**, Tighe PJ, Watkins AJ, Fairclough LC. Development of a novel murine model to investigate the immunopathogenic mechanisms of chronic obstructive pulmonary disease (COPD). *British Society for Immunology Congress 2022, Liverpool, UK*. Poster Presentation

**Bartlett LG**, Tighe PJ, Watkins AJ, Fairclough LC. Development of a novel murine spectral flow cytometry panel to investigate the immunopathogenic mechanisms of chronic obstructive pulmonary disease (COPD). *BBSRC Spring Conference, Nottingham, UK, 2022*. Oral Presentation

Hopkins G, Gomez N, Tucis D, **Bartlett L**, Browne W, Granata S, Jackson H, Steers G, James V, Watkins A, Onion D, Wills M, Godkin A, Tighe P, Fairclough L. The Fairclough Lab Research. *Midlands Health and Life Science Symposium, Birmingham, UK, 2021*. Poster Presentation

## COVID-19 IMPACT STATEMENT

As a result of the lockdowns imposed by the COVID-19 pandemic, our lab was closed for 6 months which resulted in the temporary shutdown of all wet lab work. Upon reopening of the lab, further difficulties were faced as a result of equipment and reagent shortages and delivery delays due to the pandemic and Brexit. These issues in addition to social distancing restrictions meant that limited wet lab work could take place for several months after labs being reopened. These restrictions also applied to the BSU and the impact of the pandemic further delayed the acquisition of our Home Office Licences, severely delaying the possibility of commencing animal studies. In addition, our lab group was heavily involved in a National Core Studies funded COVID-19 study, for which I was employed between February 2021 to May 2022. This involved the recruitment of participants to the study, phlebotomy training, blood collection and processing and conducting cellular based assays. These activities were performed alongside the PhD, and resulted in our team being awarded a Vice-Chancellor's medal for these efforts. As a result of the pandemic's impact on my mental health, I took a 3-month voluntary leave of study in June 2022, returning to my studies on 1<sup>st</sup> September 2022. Due to these significant impacts, in addition to issues faced with the BSU and Home Office, the BBSRC DTP team at the University of Nottingham allowed me to reduce the length of my PIP from 3 months to 1 month to allow me as much time as possible to complete wet lab work.

## ABSTRACT

### INTRODUCTION:

Chronic obstructive pulmonary disease (COPD) is a progressive, long-term group of respiratory diseases that encompasses chronic bronchitis and emphysema, and is typically caused by chronic cigarette smoke (CS) exposure. Although it is currently listed as the third leading cause of mortality worldwide by the WHO, current understanding of COPD pathophysiology is limited and as such the disease is frequently underdiagnosed or misdiagnosed. One of the hallmark characteristics of COPD is chronic and persistent inflammation, and much of our current understanding of the immunopathogenic mechanisms of COPD comes from the use of whole-body or nose-or-head only CS-exposure mouse models. Despite the existence of such models, these are not permitted for use under UK laws protecting the use of animals in science, as the model systems are considered to place mice under significant unnecessary stress and harm, and phenotypic outcomes do not accurately mimic human disease. Therefore, this project aims to develop a novel CS-exposure murine model of COPD that encompasses the three Rs of animal research (replacement, refinement and reduction) to improve model design in regards to both animal welfare and applicability to human disease.

### METHODS:

Prior to model development, a 24-colour spectral flow cytometry was developed and optimised for the characterisation of major innate and adaptive immune cells. In addition to this, a reverse phase protein microarray (RPPA) panel to assess proteomics of the lungs was tested for cross-reactivity to mouse samples, though after no cross-reactivity was detected an RT-qPCR panel was developed to assess changes in gene expression in tissues. Mice were exposed intranasally to an aqueous cigarette smoke extract (CSE) to minimise stress of restraint and handling, and provide an exposure methodology more reflective of human exposure methods. Once per week, microsampling of tail vein blood was obtained to assess impact of CSE exposure on peripheral immune cells via flow cytometry. Following 12 weeks of CSE exposure, mice were culled and tissues were isolated for RT-qPCR and histological analysis.

## RESULTS:

Due to low cell numbers in peripheral blood as a result of microsampling restrictions, no differences were detected in peripheral immune cell profiles between control groups and two disease groups (light-smoker and heavy-smoker). Despite this, both conventional gating strategies and unbiased clustering analysis displayed comparable cell profiles, demonstrating the effectiveness of the comprehensive flow panel. Although no differences in systemic immunopathophysiology were observed, significant differences in gene expression, neutrophilia and airway remodelling were observed in the lungs, dependent on either CSE dose or sex. In particular, whilst most inflammatory and immune signalling pathway genes were upregulated in males, these were downregulated in females. Additionally, pulmonary neutrophilia and alveolar diameter were significantly increased in both male and female heavy-smoker mice in comparison to control groups, and these findings were more pronounced in females in comparison to males.

## CONCLUSIONS:

Overall, we have developed the foundations of a novel murine model of COPD that better encompasses the 3Rs and mimics the pulmonary manifestations of COPD. Whilst no differences in systemic immune cell profiles were observed, marked alterations to lung structure were observed akin to results reported in both humans and mice with COPD, and these appeared to be exacerbated in females. In order to fully assess systemic inflammation, blood samples could be taken less frequently in order to increase blood volume permitted to be withdrawn, thus increasing the number of cells available for analysis and allowing differences to be better visualised. This model system provides a toolkit for researchers in the UK to further our current understanding of COPD immunopathophysiology, and may potentially be used in the future to assess pathophysiological differences dependent on other causative factors, such as environmental and household air pollutants and e-cigarette smoke.

## LIST OF FIGURES

Figure 1.1.1:- Common phenotypic presentations and symptoms of chronic obstructive pulmonary disease (COPD).	2
Figure 1.1.2:- Inverse distance weighted (IDW) interpolation map of global prevalence of COPD.	6
Figure 1.1.3:- Global risk factors of COPD according to sociodemographic index (SDI) (as highlighted for each country) and approximate prevalence of COPD by continent (as identified by percentage).	17
Figure 1.2.1:- Comparison between murine lung anatomy (left) and human lung anatomy (right).	40
Figure 1.2.2:- Diagrammatic demonstration of the two most commonly used CS-induced COPD models using mice.	47
Figure 2.2.1:- Murine COPD study design protocol.	76
Figure 2.2.2:- Diagrammatic overview of the restraint acclimatisation procedure.	77
Figure 2.2.3:- Diagrammatic overview of CSE generation apparatus.	80
Figure 2.2.4:- Intranasal dosing of CSE in mice.	82
Figure 2.2.5:- Tail vein blood sampling of mice.	83
Figure 2.2.6:- Diagrammatic protocol for splenocyte isolation and antibody titrations.	88
Figure 2.2.7:- Diagrammatic protocol for whole blood staining for peripheral immune cell phenotyping.	91
Figure 2.2.8:- Transfer stack assembly using XCell II Blot Module.	97
Figure 2.2.9:- Diagrammatic example of how to calculate stain index.	108
Figure 2.2.10:- Comprehensive gene stability of housekeeping genes using RefFinder.	110
Figure 3.2.1:- Gating strategy to obtain stain indexes using FlowJo.	118
Figure 3.3.1:- 24-Colour flow panel design.	127
Figure 3.3.2:- Gating strategy to determine adequate separation of positive and negative populations.	129
Figure 3.3.3:- Gating strategy for activation markers of T lymphocytes.	130
Figure 3.3.4:- Gating strategy for cytokines produced by T lymphocytes.	131
Figure 3.3.5:- Gating strategy for NK cells.	132



Figure 3.3.6:- Gating strategy for neutrophils and monocytes.....	133
Figure 3.3.7:- Gating strategy for macrophages.....	134
Figure 3.3.8:- Gating strategy for dendritic cells.....	135
Figure 3.3.9:- Gating strategy for B cells. ....	136
Figure 3.3.10:- Optimisation of wash steps for protein microarray.....	140
Figure 3.3.11:- Optimisation of amplification techniques and signal detection. .....	141
Figure 3.3.12:- Coomassie blue staining SDS-PAGEs to determine protein content of tissue types and cell lines following protein extraction.....	142
Figure 3.3.13:- Western blotting and chemiluminescent test scans to determine antibody cross-reactivity with mouse samples.....	143
Figure 3.3.14:- Melt curves for inflammasome genes for RT-qPCR panel.....	146
Figure 3.3.15:- Melt curves for TLR signalling genes for RT-qPCR panel. ....	147
Figure 3.3.16:- Melt curves for matrix metalloproteinase genes for RT-qPCR panel. .....	148
Figure 3.3.17:- Melt curves for IL6R signalling genes for RT-qPCR panel. ....	149
Figure 3.3.18:- Melt curves for other key inflammatory genes for RT-qPCR panel. .....	150
Figure 3.3.19:- Agarose gels to determine size of resulting products following RT- qPCR to determine primer specificity.....	151
Figure 4.3.1:- Average weight of male (A) and female (B) C57BL/6J mice per week during a 12-week exposure to CSE.....	163
Figure 4.3.2:- Relative weight gain in male and female C57BL/6J mice over a 12- week exposure to CSE. ....	165
Figure 4.3.3:- Total peripheral immune cells in whole blood of male and female C57BL/6J mice during 12-week exposure to CSE. ....	166
Figure 4.3.4:- Percentage of CD3+ and proportions of CD4+ and CD8+ T cells in peripheral blood of male C57BL/6J mice during 12 weeks of CSE exposure. ...	168
Figure 4.3.5:- Percentage of CD3+ and proportions of CD4+ and CD8+ T cells in peripheral blood of female C57BL/6J mice during 12 weeks of CSE exposure.169	
Figure 4.3.6:- Ratios of CD4+ and CD8+ T cells in male and female C57BL/6J mice over a 12-week exposure period to CSE. ....	170

Figure 4.3.7:- Percentage of activation marker-positive CD4+ T cells in peripheral blood of male C57BL/6J mice during 12 weeks of CSE exposure.....	172
Figure 4.3.8:- Percentage of activation marker-positive CD4+ T cells in peripheral blood of female C57BL/6J mice during 12 weeks of CSE exposure. ....	173
Figure 4.3.9:- Percentages of cytokine positive CD4+ T cells in peripheral blood of male C57BL/6J mice during 12 weeks of CSE exposure. ....	174
Figure 4.3.10:- Percentages of cytokine positive CD4+ T cells in peripheral blood of female C57BL/6J mice during 12 weeks of CSE exposure. ....	175
Figure 4.3.11:- Ratios of Th17 and Tregs in male and female C57BL/6J mice over a 12-week exposure period to CSE.....	176
Figure 4.3.12:- Percentage of activation marker-positive CD8+ T cells in peripheral blood of male C57BL/6J mice during 12 weeks of CSE exposure.....	177
Figure 4.3.13:- Percentage of activation marker-positive CD8+ T cells in peripheral blood of female C57BL/6J mice during 12 weeks of CSE exposure. ....	178
Figure 4.3.14:- Percentage of cytokine positive CD8+ T cells in peripheral blood of male C57BL/6J mice during 12 weeks of CSE exposure. ....	179
Figure 4.3.15:- Percentage of cytokine positive CD8+ T cells in peripheral blood of female C57BL/6J mice during 12 weeks of CSE exposure. ....	180
Figure 4.3.16:- Percentage of NK cells and cytokine positive NK cells in peripheral blood of male C57BL/6J mice during 12 weeks of CSE exposure.....	182
Figure 4.3.17:- Percentage of NK cells and cytokine positive NK cells in peripheral blood of female C57BL/6J mice during 12 weeks of CSE exposure. ....	183
Figure 4.3.18:- Percentage of macrophages and cytokine positive macrophages in peripheral blood of male C57BL/6J mice during 12 weeks of CSE exposure. ....	185
Figure 4.3.19:- Percentage of macrophages and cytokine positive macrophages in peripheral blood of female C57BL/6J mice during 12 weeks of CSE exposure. ....	186
Figure 4.3.20:- Percentage of neutrophils and cytokine positive neutrophils in peripheral blood of male C57BL/6J mice during 12 weeks of CSE exposure. ..	188
Figure 4.3.21:- Percentage of neutrophils and cytokine positive neutrophils in peripheral blood of female C57BL/6J mice during 12 weeks of CSE exposure.	189
Figure 4.3.22:- Percentage of monocytes and cytokine positive monocytes in peripheral blood of male C57BL/6J mice during 12 weeks of CSE exposure. ..	191

Figure 4.3.23:- Percentage of monocytes and cytokine positive monocytes in peripheral blood of female C57BL/6J mice during 12 weeks of CSE exposure.	192
Figure 4.3.24:- Percentage of dendritic cells and cytokine positive dendritic cells in peripheral blood of male C57BL/6J mice during 12 weeks of CSE exposure. ....	194
Figure 4.3.25:- Percentage of dendritic cells and cytokine positive dendritic cells in peripheral blood of female C57BL/6J mice during 12 weeks of CSE exposure. ....	195
Figure 4.3.26:- Percentage of B cells and cytokine positive B cells in peripheral blood of male C57BL/6J mice during 12 weeks of CSE exposure.....	197
Figure 4.3.27:- Percentage of B cells and cytokine positive B cells in peripheral blood of female C57BL/6J mice during 12 weeks of CSE exposure. ....	198
Figure 4.3.28:- Cluster location and marker expression by Cluster 3.....	199
Figure 4.3.29:- Cluster location and marker expression by Cluster 6.....	200
Figure 4.3.30:- Cluster location and marker expression by Cluster 7.....	201
Figure 4.3.31:- Cluster location and marker expression by Cluster 8.....	202
Figure 4.3.32:- Cluster location and marker expression by Cluster 4.....	203
Figure 4.3.33:- Cluster location and marker expression by Cluster 1.....	204
Figure 4.3.34:- Cluster location and marker expression by Cluster 5.....	205
Figure 4.3.35:- Total Immune Cell Clustering Analysis by sex. ....	206
Figure 4.3.36:- Total Immune Cell Clustering Analysis by smoking status.....	207
Figure 4.3.37:- Total Immune Cell Clustering Analysis by week. ....	209
Figure 4.3.38:- Total Immune Cell Clustering Analysis by disease group.....	211
Figure 5.3.1:- Relative gene expression and individual gene expressions in the right inferior lung lobe of male C57BL/6J mice following 12 weeks of CSE exposure.....	224
Figure 5.3.2:- Relative gene expression and individual gene expressions in the right inferior lung lobe of female C57BL/6J mice following 12 weeks of CSE exposure.....	225
Figure 5.3.3:- Mast cell identification using toluidine blue staining.....	226
Figure 5.3.4:- Toluidine blue staining of left middle lung, thymus and trachea of male C57BL/6J mice following 12 weeks of CSE exposure. ....	228

Figure 5.3.5:- Toluidine blue staining of left middle lung, thymus and trachea of female C57BL/6J mice following 12 weeks of CSE exposure. ....	230
Figure 5.3.6:- Airway structure and identification in mouse lung. ....	231
Figure 5.3.8:- Identification of neutrophils in mouse lung. ....	232
Figure 5.3.7:- Picosirius red staining identification of collagen deposition in the lung. ....	233
Figure 5.3.9:- H&E staining of left middle lung sections containing alveoli, major airways and major or minor blood vessels of male C57BL/6J mice following 12 weeks of CSE exposure. ....	235
Figure 5.3.10:- H&E staining of left middle lung sections containing alveoli, major airways and major or minor blood vessels of female C57BL/6J mice following 12 weeks of CSE exposure. ....	237
Figure 5.3.11:- Total neutrophil counts in left middle lung sections of C57BL/6J mice following 12 weeks of CSE exposure. ....	239
Figure 5.3.12:- Picosirius staining of left middle lung sections of male C57BL/6J mice following 12 weeks of CSE exposure. ....	240
Figure 5.3.13:- Picosirius red staining of left middle lung sections of female C57BL/6J mice following 12 weeks of CSE exposure. ....	242
Figure 5.3.14:- Mean linear intercept (MLI) analysis of C57BL/6J mice following 12 weeks of CSE exposure. ....	244
Figure C.1:- Stain index histograms and curve for CD45 (APC Fire810). ....	317
Figure C.2:- Stain index histograms and curve for CD3 (BUV496). ....	318
Figure C.3:- Dot plots and stain index curve for CD3 (BUV496). ....	319
Figure C.4:- Stain index histograms and curve for CD4 (FITC). ....	320
Figure C.5:- Stain index histograms and curve for CD8 (APC-Cy5.5). ....	321
Figure C.6:- Stain index histograms and curve for RORyt (PE-Cy5.5). ....	322
Figure C.7:- Stain index histograms and curve for FOXP3 (NovaFluorBlue610). ....	323
Figure C.8:- Stain index histograms and curve for CD25 (BV510). ....	324
Figure C.9:- Stain index histograms and curve for CD49b (PerCP-Cy5.5). ....	325
Figure C.10:- Dot plots and stain index curve for CD49b (PerCP-Cy5.5). ....	326
Figure C.11:- Stain index histograms and curve for CD11b (Pacific Blue). ....	327
Figure C.12:- Stain index histograms and curve for Ly6G/Ly6C (PE-Cy5). ....	328

---

Figure C.13:- Stain index histograms and curve for I-A/I-E (PE-Cy7).....	329
Figure C.14:- Stain index histograms and curve for F4/80 (CF568).....	330
Figure C.15:- Stain index histograms and curve for CD163 (PE).....	331
Figure C.16:- Stain index histograms and curve for CD169 (BV605). ....	332
Figure C.17:- Dot plots and stain index curve for CD163 (PE). ....	333
Figure C.18:- Dot plots and stain index curve for CD169 (BV605).....	334
Figure C.19:- Stain index histograms and curve for CD80 (BUV661).....	335
Figure C.20:- Stain index histograms and curve for CD86 (BV650). ....	336
Figure C.21:- Stain index histograms and curve for CD38 (PE-Dazzle594). ....	337
Figure C.22:- Stain index histograms and curve for CD69 (BV785). ....	338
Figure C.23:- Stain index histograms and curve for CCR7 (AF647). ....	339
Figure C.24:- Stain index histograms and curve for IFN- $\gamma$ (BV421).....	341
Figure C.25:- Stain index histograms and curve for IL-6 (PerCP-eFluor710). ...	342
Figure C.26:- Stain index histograms and curve for IL-17A (BV711).....	343
Figure C.27:- Stain index histograms and curve for TNF- $\alpha$ (BV750). ....	345

---

## LIST OF TABLES

Table 2.1.1:- 24-Colour Flow Cytometry panel.....	63
Table 2.1.2:- Conjugation kit details for in-house labelled antibodies.....	64
Table 2.1.3:- Antibody targets used in optimised anti-human RPPA panel.....	68
Table 2.1.4:- List of reagents used to prepare gels for SDS-PAGE.....	71
Table 2.1.5:- Primer sequences and details for housekeeping genes. ....	72
Table 2.2.1:- Extracellular and intracellular antibody panels for whole blood staining. ....	90
Table 2.2.2:- Standard curve dilutions using a Pierce BCA Protein Assay kit. ....	93
Table 2.2.3:- Reverse transcription reagent master mix dilutions.....	102
Table 2.2.4:- Cycle steps and conditions for reverse transcription generation of cDNA. ....	102
Table 2.2.5:- Polymerase chain reaction reagent master mix dilutions. ....	103
Table 2.2.6:- Cycle steps and conditions for polymerase chain reaction.....	104
Table 3.2.1:- Reagents selected for flow cytometry panel with details based on OMIP guidelines. ....	116
Table 3.2.2:- Target genes of interest for RT-qPCR panel.....	122
Table 3.3.1:- BCA results and yield for murine tissue samples.....	138
Table 3.3.2:- Dilutions required to obtain optimal staining concentration of 2 mg/mL. ....	139
Table 3.3.3:- Primers designed as a substitute for the RPPA panel.....	144
Table 5.3.1:- RNA concentrations (ng/ $\mu$ L), 260/280 and 260/230 values from murine lungs following 12 weeks of CSE exposure.....	221
Table 6.9.1:- Results of power calculation to determine effect size and required sample size per group for future experiments .....	264

---

## ABBREVIATIONS

3Rs	Three Rs
$\Delta\Delta Ct$	Double delta Ct
A1AT	$\alpha$ -1 Anti-Trypsin
AECOPD	Acute exacerbations of COPD
Akt1	RAC(Rho family)-alpha seroma/threonine-protein kinase
APC	Antigen presenting cell
ASPA	Animals (Scientific Procedures) Act
AWERB	Animal welfare and ethical review body
BALF	Bronchoalveolar lavage fluid
BCA	Bicinchoninic acid
BSA	Bovine serum albumin
BSU	BioSupport unit
CD	Cluster of differentiation
cDNA	Complementary DNA
COPD	Chronic obstructive pulmonary disease
CRP	C-reactive protein
CS	Cigarette smoke
CSE	Cigarette smoke extract
CYLD	CYLD lysine 63 deubiquitinase
DALY	Disability-adjusted life year
DAMP	Damage-associated molecular pattern
DC	Dendritic cell
dH <sub>2</sub> O	Deionised water
DMSO	Dimethyl sulfoxide
EtOH	Ethanol
EVALI	E-cigarette or vaping associated lung injury
FBS	Foetal bovine serum
FEV <sub>1</sub>	Forced expiratory volume in the first second

---

FSC	Forward scatter
FVC	Forced vital capacity
FWD	Forward primer
GOLD	Global Initiative for Chronic Obstructive Lung Disease
GWAS	Genome-wide Association Study
H&E	Haematoxylin and Eosin
Hprt1	Hypoxanthine-guanine phosphoribosyltransferase 1
HSF	Heavy-smoker Female
HSM	Heavy-smoker Male
I-A/I-E	Major histocompatibility complex class II I-A and I-E subregions
IFN- $\gamma$	Interferon gamma
IL	Interleukin
IL6R $\alpha$	Interleukin-6 receptor alpha
ILC	Innate lymphoid cell
IN	Intranasal
IP	Intraperitoneal
IRF3	Interferon regulatory factor 3
LASA	Laboratory Animals in Science Association
LLN	Lower limit of normal
LMIC	Low- and middle-income country
LPS	Lipopolysaccharide
LSF	Light-smoker Female
LSM	Light-smoker Male
Ly6C	Lymphocyte antigen 6 family member C
Ly6G	Lymphocyte antigen 6 family member G
MLI	Mean linear intercept
MMP	Matrix metalloproteinase
mTOR	Mammalian target of rapamycin
MyD88	Myeloid differentiation primary response 88
NACWO	Named Animal Care and Welfare Officer



---

NC3Rs	National Centre for the 3 Rs
NCBI	National Centre for Biotechnology Information
NFKBIA	NF-kappa-B inhibitor alpha
NHO	Nose-or-head only
NK	Natural killer cell
NKT	Natural killer T cell
NLRP3	NLR family pyrin domain containing 3
NOX2	NADPH oxidase 2
NRF2	Nuclear factor erythroid 2-related factor 2
NRT	No reverse transcriptase control
NSF	Never-smoker Female
NSM	Never-smoker Male
NTC	No template control
NTCO	Named Training and Competency Officer
NVS	Named Veterinary Surgeon
OMP	Optimised Multicolour Immunofluorescence Panel
PAMP	Pathogen-associated molecular pattern
PBA	Phosphate buffer albumin
PBS	Phosphate buffer saline
PMA	Phorbol 12-myristate 13-acetate
PEL	Establishment licence
PIL	Personal licence
PPL	Project licence
PRR	Patter recognition receptor
REV	Reverse primer
RPMI	Roswell Park Memorial Institute
RPPA	Reverse phase protein microarray
RT-qPCR	Reverse transcription-quantitative polymerase chain reaction
SDHA	Succinate dehydrogenase complex flavoprotein subunit A
SERPINA1a	Serpin family A member 1a

---

SDI	Sociodemographic index
SLIM	School of Life Sciences Imaging Facility
SSC	Side scatter
TBP	TATA-binding protein
Th17	T helper subset 17
TIRAP	TIR domain containing adaptor protein
TLR2	Toll-like receptor 2
TLR4	Toll-like receptor 4
TNF- $\alpha$	Tumour necrosis factor alpha
Treg	T regulatory subset
Tuba1	Tubulin alpha-1A
WB	Whole-body
WHO	World Health Organisation
YLD	Years of life lost due to disability
YLL	Years of life lost due to premature mortality

## CHAPTER 1 – GENERAL INTRODUCTION

### 1.1. CHRONIC OBSTRUCTIVE PULMONARY DISEASE

Throughout the course of our lifetime, we are exposed to and inhale a number of potentially harmful materials that can elicit an immune response and cause inflammation within the lungs and pulmonary spaces. Pulmonary inflammation is often caused either by infection with pathogens, such as bacteria, viruses and fungi, or by lung diseases such as asthma and lung cancer. Noxious particulate matter in the form of air pollutants and tobacco smoke may also cause immune responses, particularly if inhaled on a regular basis either passively (second-hand) or actively (first-hand). Over time, chronic exposure of such hazardous materials can cause persistent inflammation and lead to the development of a number of pulmonary diseases.

Chronic obstructive pulmonary disease (COPD) is an umbrella term to describe persistent and progressive respiratory disease with a multitude of causative factors and phenotypic characteristics, and is most often associated with chronic cigarette smoke (CS) exposure. Phenotypic presentations of COPD manifest in the form of airflow limitation and inflammation in conjunction with chronic cough (chronic bronchitis), or as significant airway remodelling and enlargement resulting in poor gaseous exchange mechanisms (emphysema) [1]. COPD also has a multitude of extra-pulmonary effects, including fatigue and weight loss, and is associated with abnormal inflammatory responses both within the lungs and systemically in response to noxious particulate matter (figure 1.1.1). These systemic effects are often accompanied by comorbidities which may either arise as a result of COPD or exacerbate pre-existing symptoms or underlying conditions. As of 2019, COPD is listed as the third leading cause of mortality worldwide by the World Health Organisation (WHO), though frequent underdiagnosis may infer that the global impact of COPD is considerably higher than estimated or reported in current literature [2, 3].

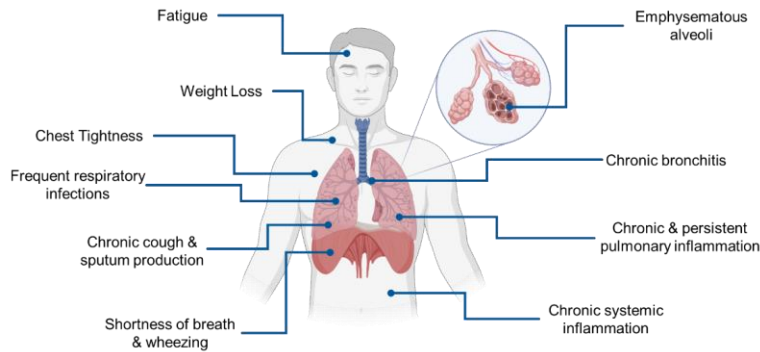


**Figure 1.1.1:- Common phenotypic presentations and symptoms of chronic obstructive pulmonary disease (COPD).** (Created with BioRender)

Despite being a disease of high morbidity worldwide, current understanding of COPD pathophysiology is limited. The lack of knowledge on the mechanisms that drive COPD pathology and persistence has meant that current therapies and treatment plans for COPD patients revolve largely around symptom management and intervention during exacerbations. Overall, this leads to a significant medical and economic burden, with patients frequently hospitalised as a result of exacerbations. Although a disease of significant burden, COPD is studied to a lesser extent than other respiratory diseases, and is there much less public awareness of the disease. Other conditions such as tuberculosis, HIV/AIDS, malaria and cancers are often given more of a focus, and research focus is often shifted heavily during outbreaks of infectious diseases of significant potential global burden [3]. Nonetheless, estimates of the epidemiology and global burden of COPD highlight the necessity of gaining better understanding of its pathophysiology so as to identify therapeutic targets or strategies and reduce strain on global resources.

1.1.1. EPIDEMIOLOGY AND GLOBAL BURDEN

1.1.1.1. Prevalence

It is estimated that approximately 300 – 400 million people are diagnosed with COPD worldwide [4]. Despite this, the prevalence of COPD was not widely studied until the 1980s, and even still estimates of global incidences vary significantly between publications [5]. This is often attributed to the lack of a well-established case definition across studies due to the use of different lung function tests for COPD diagnosis [6]. Quantitative analysis of airflow obstruction used to diagnose COPD is typically performed via spirometry. Spirometric analysis uses the ratio of the forced expiratory volume in the first second ( $FEV_1$ ) to the forced vital capacity (FVC) of the lungs to determine the degree of airway obstruction. The resulting ratio can then be defined as being less than the lower limit of normal (LLN) based on the lower fifth percentile of the individual's age, sex, height and race/ethnicity, or as less than 70%, both of which are indicative of obstructive airway disease. Spirometric measurements may also be taken either prior to or after the use of a bronchodilator, which may have an effect on diagnostic outcomes. According to GOLD standards, the preferred method for diagnosis is post-bronchodilator spirometry using the fixed ratio  $FEV_1/FVC$  of less than 70% (0.7) due to its simplicity and wider usage in comparison to the LLN method [7]. A National Health and Nutrition Examination Survey (NHANES) study conducted between 2007 - 2010 demonstrated that the prevalence of COPD in the United States changes significantly depending on the diagnostic criteria used to define a case. In this study, COPD prevalence increased from 10.2% when using post-bronchodilator spirometry with  $FEV_1/FVC < 0.7$  fixed ratio criterion to 20.9% when using pre-bronchodilator spirometry with  $FEV_1/FVC < LLN$  [8]. The argument of when bronchodilators are to be used for spirometric analysis is influenced by evidence that pre-bronchodilator spirometry can overestimate COPD diagnosis by up to 30%, and therefore post-bronchodilator spirometry should be the preferred option [9]. Further compounding the ability to accurately estimate the prevalence of COPD, many cases are often

diagnosed based on airway obstruction or reported symptoms alone in the absence of spirometry [10]. Diagnosis in this manner is credited as a result of lack of standardised spirometry testing methods as well as a poor definition of what constitutes COPD. This lack of diagnostic standards and criteria in turn results in the potential risk of either misdiagnosis of COPD or failure to diagnose patients with active COPD. In addition to the requirement of a post-bronchodilator  $FEV_1/FVC < 0.7$ , GOLD definitions also state that COPD diagnosis requires the presentation of persistent respiratory symptoms (e.g., dyspnoea, chronic cough or sputum production), in addition to a history of exposure to known risk factors (e.g., tobacco smoke, household air pollution, occupational dust and fumes etc.) [11]. As demonstrated by epidemiological studies however, these guidelines are not often followed for accurate COPD diagnosis, suggesting a lack of awareness of diagnostic methods for obstructive respiratory diseases [10, 12-14].

A large majority of COPD cases are found in low- and middle-income countries (LMICs), though COPD in high income countries is also frequently reported. This case incidence could be attributed to the fact that approximately 84% of the global smoking population reside in developing and transitional economy countries [15]. Although cigarette smoking is considered to be the primary aetiological factor of COPD, approximately 30% of all COPD patients are never-smokers [16]. COPD can also be the result of occupational, environmental and household air pollution exposure. One third of the world's population relies on the burning of biomass fuels to power and heat homes, which are often subject to poor ventilation [3]. Incomplete combustion of fuels and poor ventilation results in the inhalation of noxious particles which may lead to the development of COPD. It is potentially this factor which results in COPD being more prevalent in younger age groups in LMICs, as exposure to environmental or household air pollution during childhood has been demonstrated to prevent lungs from developing to their full potential, and may predispose individuals to developing COPD earlier in life in comparison to individuals who live in countries that do not rely on

biomass fuels for household heating [3, 17, 18]. Biomass-associated COPD also has a slightly different phenotype in comparison to tobacco smoke-induced COPD and has been implicated in asthma-COPD overlap syndrome, and may therefore go undiagnosed or misdiagnosed particularly in younger generations given that COPD is considered a "disease of old age" [19, 20]. Additionally, COPD as a result of occupational dust and fumes (often from industrial or agricultural workplaces) is frequently underreported and may comprise a large number of cases that would contribute to the overall global burden of COPD [21]. Despite the large number of epidemiological studies that have been conducted since the 1980s, most studies are conducted in Western countries (particularly the United States and European countries) [22-25]. Data is particularly lacking from South-east Asian and African countries, which is typically attributed to a lack of spirometers in general practice meaning that cases cannot be diagnosed [26]. Additionally, data from Africa is only partial and often primarily concerns pockets of populations exposed to occupational air pollution hazards or hospital environments [27]. Therefore, much of the data available on global prevalence of COPD is based on predictive statistical methods using data from available epidemiological studies from these countries or neighbouring countries (figure 1.1.2) [28, 29]. The lack of epidemiological data from Eastern and African countries, as well as LMICs, means that estimates into the overall prevalence and health and economic burdens of COPD may not reflect the true overall impact of COPD on a global scale, and may only be indicative of the situation in higher income and Western countries.

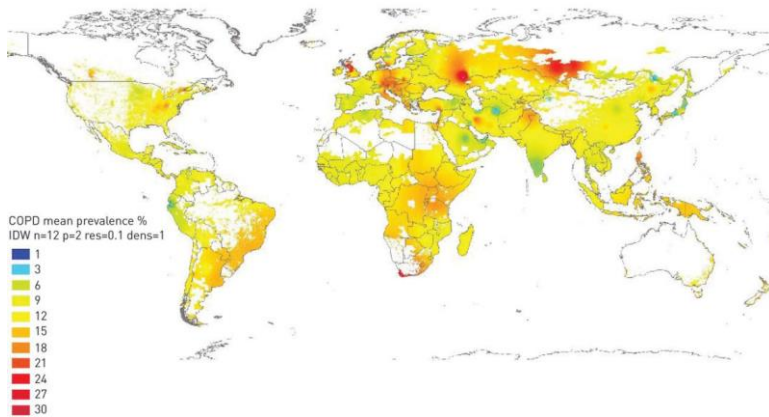


**Figure 1.1.2:- Inverse distance weighted (IDW) interpolation map of global prevalence of COPD.** Red and orange shadows indicate areas of high prevalence, with lighter shades of yellow and green indicating intermediate or low prevalence. Pockets of high prevalence of COPD can be observed in Northern England and Scotland, across the majority of Europe, Northern USA/Southern Canada within the area of the Great Lakes, Eastern and Southern Africa, Northern and Southern Asia and the Eastern coast of Southern America. Areas shaded in white represent areas where prevalence cannot be estimated due to sparse populations or lack of data (figure taken from Blanco et al. (2019)) [24]

#### 1.1.1.2. Morbidity and Mortality

Morbidity is typically defined as the condition of suffering from a medical disease or the rate of disease within a population, whereas mortality describes the number of deaths as a result of a specific condition. COPD is currently listed as the third leading cause of mortality worldwide, resulting in approximately 3.5 to 4 million deaths per year as a result of household air pollution and approximately 6 million deaths per year as a result of smoking [2, 30, 31]. Mortality within COPD is typically associated with low FVC, which is also closely related to poverty [32]. This could provide an explanation behind the higher probability of death from COPD in African countries and India, despite such countries typically having a lower prevalence of COPD overall [33]. Respiratory failure is attributed as the most common cause of death amongst COPD patients, though cardiovascular diseases and lung cancer are typically more common causes of death in early COPD [34-37]. However,



determining the burden of COPD through mortality rates alone fails to reflect the true total burden, as many cases are often not included due to misattribution of cause of death and also do not account for the impact of a disease throughout an individual's lifetime. Instead, COPD burden may be more accurately estimated through the measure of disability-adjusted life years (DALYs). A DALY is a time-based measurement of overall disease burden, which combines years of life lost as a result of premature death and poor health, or years of life lost as a result of disability. A single DALY therefore equates to the loss of a single year of full health [6]. As such, not only do DALYs take death as a result of COPD into consideration, but also include data from other factors that contribute to a disease's overall burden, such as inability to work and hospitalisations as a result of ill health. This provides a better estimation of a disease's burden by allowing it to be compared to other diseases that cause death but not disability, in order to ascertain the overall impact of the disease's disability burden in conjunction with its mortality burden. DALYs can further be separated into more specific statistical analyses, including years of life lost due to premature mortality (YLL) and years of life lost due to disability (YLD). Using these statistics, it was estimated that COPD accounted for 4.7% of all global DALYs between 1990 - 2010, with chronic respiratory diseases accounting for 6.3% of global YLDs, of which COPD was the largest contributor [38, 39]. Currently, the WHO lists COPD as the 7th largest cause of DALYs in 2019, though DALYs for many diseases including COPD have been dropping for a number of years due to advancements in medical treatments and disease knowledge [2].

Even with the use of DALYs, estimating the morbidity and mortality of COPD still poses significant challenges, and it is thought that global COPD morbidity and mortality may be considerably higher than currently estimated. This is due to the prevalence of comorbidities alongside COPD. Attribution of death is not universal, and therefore differences in diagnosis and cause of death between countries has a compounding effect on estimated global mortality rate of COPD [14, 40]. Often the

cause of death in COPD patients is attributed to one or more comorbidities, with COPD typically only being listed as an underlying compounding factor and not as a contributing or direct cause of death [41]. Previous studies have found that approximately only 40% of deaths amongst COPD patients were judged to be related to COPD, meaning the remaining 60% were attributed to comorbidities associated with COPD or to factors unrelated to health or disease [42]. Although comorbidities are widely reported, determining the prevalence of COPD alongside comorbid conditions is confounded by shared risk factors, underdiagnosis of COPD and related comorbidities, as well as overlapping phenotypic characteristics of COPD and common comorbidities [11, 43-46]. This can often make it difficult to ascertain the true morbidity of COPD, as a reduction in the quality of life of an individual may be due to an undiagnosed comorbid condition or misattributed to a comorbid condition in an individual with undiagnosed COPD. Nonetheless it is generally considered that 97% of all COPD patients possess one or more comorbidities, with approximately 53% of patients having four or more comorbidities [47]. For each diagnosed comorbidity, the incidence of self-rated poor health status by COPD patients is increased by 43%, with common comorbidities such as heart failure, diabetes and arthritis resulting in significant decreases in quality of life scores when compared to other comorbidities [48]. An increased number of diagnosed comorbidities is also often associated with exacerbations of COPD or diagnosed conditions, which can overall lead to a decrease in quality of life [49, 50]. Comorbidities common amongst COPD patients are not limited to physical conditions, anxiety disorders and clinical depression are widely reported diagnoses, with depression being far more prevalent concurrently with COPD in comparison to any other chronic disease [51-54]. The presence of anxiety and/or depression amongst COPD patients has a long-lasting impact on reported quality of life, which is made all the more difficult due to effectiveness of treatment and therapy programs for mental health conditions varying depending on an individual's needs and presentations of the condition. In particular, COPD patients with an anxiety and/or depression diagnosis are at an

elevated risk of exacerbations, hospitalisation, and increased mortality in comparison to COPD patients without anxiety or depression [55, 56]. For patients with spouses the presence of anxiety and/or depression is shown to lead to a significant decrease in the reported quality of life in both the COPD patient and spouse, and overall prevalence of anxiety and depression is greater amongst both COPD patients and their spouses [53]. This demonstrates that COPD and its comorbidities may not only have an impact on the quality of life of the patient themselves, but their immediate family as well. Although global morbidity and mortality of COPD has widely been studied, it is evident that the amount of duress placed upon the patient as a result of the disease itself and its comorbidities has indirect consequences on the quality of life of those around the patient, and should also be cause for consideration when investigating COPD burden.

#### 1.1.1.3. Economic and Healthcare Burden

Perhaps the greatest burden of COPD is its impact on global healthcare resources, which result in significant healthcare costs and have a negative effect on global economic resources. The healthcare burden of COPD is best highlighted by its impact during the recent pandemic caused by severe acute respiratory distress syndrome coronavirus 2 (SARS-CoV-2), during which strains on global healthcare resources were widely reported as a result of the virus itself. As a respiratory disease, COPD patients were classified as “high-risk” of severe infection and likely to require intensive care and hospitalisation in the event of infection [57, 58]. While data is limited due to research priorities at the time of the pandemic, generally the impact of COPD and outcomes as a result of coronavirus disease 2019 (COVID-19) are disputed and the topic is somewhat controversial in the field of respiratory medicine [59]. Nonetheless, evidence suggests that while patients with COPD are not at increased mortality as a result of COVID-19, admissions to intensive care units (ICU), advanced respiratory support and mechanical ventilation interventions were significantly higher in

comparison to those without COPD [60, 61]. COPD diagnosis was typically associated with severe outcomes as a result of infection, likely due to higher expression of the angiotensin-converting enzyme 2 (ACE2) receptor by which the virus enters cells typically seen in smokers and those with COPD, though increased susceptibility to disease through this mechanism alone remains an ongoing debate [62, 63]. Still, the greatest impact on healthcare resources as a result of COPD comes in the form of hospitalisation due to acute exacerbations, typically as a result of respiratory infections from bacteria, viruses and fungi [64]. It is therefore no surprise that COPD was typically associated with hospitalisation and admission to ICU throughout the course of the COVID-19 pandemic.

The economic impact of COPD primarily affects low- and middle-income countries (LMICs), particularly due to the scarcity of healthcare resources, and those that are available are ill equipped to treat chronic conditions [3, 65]. Even in high-income countries, the cost of COPD is still significantly high. It is estimated that COPD has an approximate global cost of US\$2.1 trillion, with at least half of the burden carried by LMICs [66]. Of this value, the vast majority is attributed to direct costs such as medication and hospitalisation, whilst US\$0.2 trillion can be attributed to indirect costs such as missed work and early retirement [67]. Some studies have found that medication is the largest contributor to a country's economic burden as a result of COPD, though hospitalisation and exacerbations pose the most significant challenge and greatest impact as they greatly affect both economic and healthcare resources [68]. In the US alone, hospitalisations as a result of COPD exacerbations can cost as much as US\$18 billion per year [69]. There is both a significant lack of understanding of COPD pathogenesis and awareness of COPD as a disease by both healthcare professionals and the general public, all of which contribute towards ineffective treatment interventions, underdiagnosis and failure to seek medical advice particularly for those exposed to risk factors [70-74]. While the current total global economic impact of COPD currently stands at US\$2.1 trillion, it is estimated that by 2030 the economic impact of COPD in LMICs alone will rise to US\$1.7

trillion as a result of an increasingly aged population and inadequate treatment interventions [75]. Though the prevalence of COPD itself is falling, its continuing impact on morbidity, mortality, healthcare and economic resources remains heavy due to lack of disease understanding, and therefore further research needs to be conducted in order to decrease global burden.

#### 1.1.1.4. Projections and Research Priorities

Currently COPD is listed as the third leading cause of mortality worldwide, however the WHO had not anticipated that this would occur until 2030 [76]. This sudden increase in COPD mortality and prevalence despite the effectiveness of smoking awareness and cessation programs is likely linked to an increasing aged population [6]. Advances in medical care and disease knowledge means that on average expected lifespan is increased, resulting in a larger demographic of elderly individuals and thus increasing burden of diseases typically considered those of old age (typically 60 + years) [33]. Whilst the prevalence of COPD in high-income countries has plateaued, it is expected that the number of COPD patients will double in low- and middle-income countries (LMICs) within the next decade [77]. However, given the increasing prevalence of COPD amongst younger individuals (> 60 years), it is no longer justifiable to classify COPD as only a disease of old age [20]. As previously described, many individuals in LMICs rely on the use of biofuels for heating and powering their homes, and chronic exposure to incompletely combusted particulate matter from a young age has detrimental effects on lung function and development [3]. It is estimated that the average amount of household air pollution generated as a result of burning biofuels individuals in these conditions are exposed to is equivalent to smoking two packs of cigarettes per day, and women and children are of particular risk of developing COPD as well as a multitude of other chronic respiratory conditions [78]. This often results in a growing demographic of younger individuals diagnosed with COPD in LMICs, whilst the reverse is observed in high-income countries where older individuals are more

likely to suffer from COPD [17, 18]. By considering COPD only a disease of old age or only a result of chronic cigarette smoking, little is done to manage and prevent COPD in younger individuals or in individuals with COPD as a consequence of chronic exposure to household air pollution or occupational hazards. Current strategies to minimise the global burden of COPD rely largely around these elderly patients with a history of smoking, and prevention methods are typically related to smoking awareness and cessation whilst interventions for those with COPD involve minimising exacerbations and the management or prevention of comorbid conditions [6]. Failure to develop strategies to deal with the growing incidence of COPD amongst those to which the above criteria does not apply means that only a fraction of the global burden is addressed, and further must be done to correct this.

Determining the research priorities of diseases with significant global burden is often an arduous task, as there are a number of questions that must be answered. It is difficult to ascertain where priorities should lie, and whether developing prevention or treatment strategies is more important than understanding a disease's pathogenesis is the subject of much debate. A study conducted by Adeloje et al. (2021) [79] aimed to investigate the opinions of 62 researchers in the field of COPD research to determine where researchers felt priorities should lie for future studies. Of 230 research ideas proposed, the top ranked priorities included strategies for improving access and effectiveness of treatment and prevention methods for COPD, as well as better defining diagnostic methodologies for accurate COPD diagnosis. Interestingly, the lowest ranked priorities included further research to understand the biological pathways involved in COPD pathophysiology and whether disease classification should be altered depending on phenotype. However, without sound understanding of a disease's mechanisms, finding more effective treatment strategies and improving diagnostics could prove challenging. Overall, the findings from this study highlight that while COPD research is often focused on

treatment and diagnostic strategies, investigations on pathogenic mechanisms and risk factors are often overlooked.

### 1.1.2. CAUSATIVE FACTORS

#### 1.1.2.1. Air Pollutants

Air pollutants account for 55% of all global COPD-associated DALYs, though these risk factors are far more common in countries with a lower SDI in comparison to high or high-middle SDI countries (figure 1.1.3) [80]. Air pollutants in regard to COPD can be distinguished into three separate categories: ambient particulate matter (including ambient ozone), occupational exposures and household air pollution. In lower SDI countries, household air pollution comprises the largest risk factor for COPD, and is particularly problematic for younger individuals and women [3, 81]. Given that as much as one third of the world's population relies on the burning of biomass or solid fuel (such as coal, wood and charcoal) to heat their homes and cook, standards have been set to ensure exposure to the products of incomplete combustion, including carbon monoxide, and particulate matter do not exceed a recommended level in order to minimise risk of damage to respiratory health. PM<sub>10</sub> is used as the standard indicator of health hazard of air pollutants within a given space, and the mean annual value for PM<sub>10</sub> in outdoor air is set at between 40 to 50 µg/m<sup>3</sup> depending on the country and regulating Environmental Protection Agency (EPA) [78]. It is estimated that in homes relying on biomass and solid fuels, PM<sub>10</sub> levels can reach up to 10,000 µg/m<sup>3</sup>, approximately 200 times higher than the standards set by the EU and US EPA [3]. These levels of particulate matter present a significant risk factor to children especially, as chronic exposure to household air pollutants during critical stages of lung development, including in utero and in early childhood, have been shown to prevent the lungs from developing to their full potential [82-84].

Occupational hazards resulting in compounded respiratory health have been reported as early as the 19<sup>th</sup> century, though it was only as

recently as the 1970s and 80s where the link between COPD and occupational exposures was established [85-87]. Unlike other risk factors of COPD, occupational exposures carry relatively the same risk between countries regardless of their SDI, and contribute towards 15% of all COPD-associated DALYs globally (figure 1.1.3) [80]. Global incidence of occupational COPD may be underestimated, especially for workers who smoke and present COPD-like disease, as this may frequently be diagnosed as smoking-induced COPD to avoid companies having to pay worker's compensation [88, 89]. Regardless, the association between occupational hazards including inorganic dust such as coal dust, asbestos and cement is well established and reported in a number of cohort studies, and there is increasing evidence of COPD amongst healthcare workers as a result of exposure to irritant gases and cleaning agents [90-93].

Unlike household air pollutants and occupational air hazards, the link between ambient air pollutants and COPD is poorly established. Nonetheless it is estimated that this accounts for 20% of all global COPD-associated DALYs. Most research associated with ambient particulate matter on respiratory health largely focuses on short-term effects, with long-term research and research investigating the role of air pollutants on COPD pathogenesis severely lacking [16, 94]. Regardless, evidence suggests that ambient air pollutants including nitrogen dioxide, ozone and byproducts of traffic may contribute towards COPD pathogenesis, and chronic exposure to such matter can cause hallmark pathophysiological characteristics reminiscent of COPD [95, 96]. Although the link between ambient air pollution and COPD remains up for debate, many researchers argue that it is a plausible risk factor in the development of COPD given the effects exposure to such particulate matter can generate even after short-term exposure.



#### 1.1.2.2. Tobacco and Cigarette Smoke

COPD is often considered a disease caused by chronic cigarette smoking, however only 45% of all COPD DALYs are a direct result of tobacco smoking (figure 1.1.3) [80]. This preconceived notion is likely a result of the fact that chronic cigarette smoking is most commonly associated with COPD onset in countries with a higher sociodemographic index (SDI) and typically in countries where the most amount of research into COPD and other respiratory diseases is conducted [22-25, 97]. Nonetheless, it has been reported that in high-income countries approximately 73% of COPD mortality is directly related to chronic smoking, and that of those who smoke regularly approximately 50% will develop COPD later in life [98-101]. Additionally, smoking during pregnancy has been shown to result in foetal lung injury and childhood lung injury, which may predispose children to the development of asthma and COPD-like disease [102]. Studies such as these and long-held opinions regarding COPD have meant that approaches to reducing disease burden comprise of a triad of strategies: smoking cessation and control of tobacco products or smoke exposure, protective measures to reduce acute exacerbations and effective management and prevention of the development of comorbidities [6]. Recent efforts to minimise or prevent the use of tobacco products, particularly cigarettes, have led to a decrease in overall global smoking populations, however the burden of COPD is still significantly present. Historically there is far more research providing evidence for the direct causal link between tobacco smoke and COPD, and it has only been in more recent years that research has focused on COPD as a result of other factors outside of tobacco smoke exposure that contribute towards this global burden.

#### 1.1.2.3. Electronic Cigarette and Vape Smoke

Electronic cigarettes (e-cigarettes) have been introduced in the last two decades as a safer alternative to cigarette smoking, intended for those aiming to quit or reduce their tobacco consumption [103]. Due to

their recent introduction and use, the link between COPD and e-cigarette smoking or vaping has yet to be fully established. Despite this, there is increasing evidence to support a direct causal link between chronic vaping and lung injury, particularly amongst adolescents within the last ten years [103-105]. The majority of research investigating the influence of e-cigarettes and vaping on lung function in humans has largely been conducted using data and case studies within adolescent populations, likely due to the severity and frequency of e-cigarette or vaping associated lung injury (EVALI) amongst this demographic, to the point where the use of e-cigarettes amongst adolescents and young adults has previously been described as an “epidemic” [104]. As a result of this focus, research relating to the influence between e-cigarettes and COPD or e-cigarette use amongst older adults is severely lacking, as is research on the long-term effects of e-cigarette use due to their novelty. Despite this, it has been demonstrated that the incidence of self-reported COPD is considerably higher amongst individuals who both smoke conventional cigarettes and e-cigarettes, individuals who smoke e-cigarettes and previously smoked conventional cigarettes and individuals who smoke e-cigarettes but have never smoked conventional cigarettes in comparison to individuals who had never smoked nor vaped. Incidentally however, individuals who used e-cigarettes reported self-diagnosis of COPD compared to individuals who currently smoked conventional cigarettes regardless of whether they had previously smoked cigarettes prior to their vaping status [106]. This suggests that although there are negative effects associated with the use of e-cigarettes, these effects are less severe than those associated with conventional cigarettes, though as demonstrated through research and case studies are still capable of causing significant lung damage [105]. E-cigarettes were purposely designed as a means to assist smokers in quitting from conventional cigarettes and improve their pulmonary health, but emerging evidence over the last decade has proven that not only do e-cigarettes possess the capability to cause lung injury akin to tobacco products, but an increasing number of individuals, particularly those of a young age, are using e-cigarettes in lieu of conventional cigarettes altogether. Whilst there is

some evidence to suggest the use of e-cigarettes may lessen the degree of exacerbations in COPD patients in comparison to those using conventional cigarettes, the long-term effects of e-cigarettes and their potential role in the onset of COPD itself is currently unknown [107]. Given the number of case studies related to EVALI reported over the last decade, it would be safe to assume that chronic use of e-cigarettes may lead to the development of COPD-like disease, though these devices have not existed for long enough for this association to be definitively proven or observed.

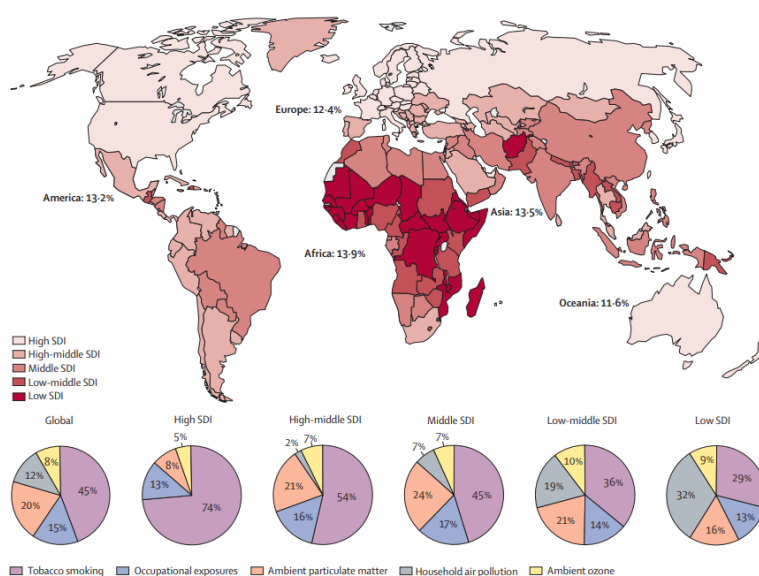


**Figure 1.1.3:- Global risk factors of COPD according to sociodemographic index (SDI) (as highlighted for each country) and approximate prevalence of COPD by continent (as identified by percentage).** Risk factors of COPD are demonstrated as a percentage of COPD-associated DALYs per 100,000 individuals globally and according to SDI. While tobacco smoking is considered the primary aetiological factor of COPD and is shown to be such in countries with a high or high-middle SDI, other risk factors such as occupational exposures, ambient particulate matter and household air pollution all contribute to a higher percentage of risk factors globally. This highlights that although attitudes towards COPD and treatment plans for COPD patients are largely focused on tobacco smoking, the global burden of COPD as a result of non-tobacco related risk factors is far greater particularly in countries with lower SDI (figure taken from Yang et al. (2022)) [80]

#### 1.1.2.4. Genetic association with COPD

Determining the genetic component of COPD has proven difficult throughout research history, much like many other complex chronic diseases. Nonetheless, studies have identified a number of genes which are both accepted and suggested to have influence over risk of COPD development [108]. Of these genes, a deficiency in the enzyme alpha-1-antitrypsin (A1AT) encoded by the SERPINA1 gene is the only widely accepted genetic predisposition towards COPD pathogenesis [109]. A1AT deficiency is believed to not be sufficient enough by itself to cause the development of COPD, and merely predisposes individuals to developing COPD earlier and to a much more severe degree than those without A1AT deficiency [110-112]. Whilst differences in gene expression can prove difficult to link to COPD pathogenesis, the link between genetic polymorphisms and relative risk of COPD is one that can be established somewhat more definitively. Generally, genetic polymorphisms are inherited, and while spontaneous mutations can occur most are silent and do not affect the resulting encoded protein structure. Genome wide association studies (GWAS) are useful in identifying both loci and variants of genes associated with a particular disease, and have previously been conducted on COPD [113]. As a result of GWAS studies, a number of genes and variants have been identified as risk factors of COPD, many of which are either linked to lung function or overlap as risk factors for asthma and pulmonary fibrosis [114]. Certain polymorphisms in the gene encoding for a disintegrin and metalloproteinase 33 (ADAM33) have been associated as risk factors for COPD amongst East Asian populations, and the resulting proteins may impact COPD pathogenesis [115]. ADAM33 is typically involved in tissue remodelling and proteolytic activity, including cleaving cytokines and receptors off of the surface of cells, and some polymorphisms have been associated with a dysregulation of ADAM33 activity [116, 117]. Additionally, certain variants of the genes encoding for proinflammatory cytokines including TNF- $\alpha$ , TGF- $\beta$ 1, IL1B and IL6, as well as variants of the TNFRSF1A and TNFRSF1B genes have been strongly associated with the development

of COPD [118, 119]. Although these associations have been made, the exact mechanistic effects of many genetic polymorphisms on COPD pathophysiology remain unclear.

#### 1.1.2.5. Sex as a risk factor

The influence of sex as a risk factor for COPD development and pathophysiology remains a topic of much debate [120]. While some argue that men and women are affected by COPD differently, the evidence to support this notion is significantly lacking in both quantity and robustness. Despite this, men and women have a number of sex-specific differences ranging from biological mechanisms including genetics, hormones and drug metabolism to behavioural and environmental differences, such as tobacco usage, work environments and willingness to seek and comply with medical advice and treatment plans. The consumption of tobacco products by women has steadily increased over the last few decades, though evidence to suggest increased susceptibility to the negative effects of tobacco products in women is disputed. Recent evidence however has suggested that women are more likely to develop COPD earlier and after having smoked fewer tobacco products than men, and display a greater annual decline in FEV<sub>1</sub> values compared to men [121, 122]. The exact mechanisms behind these observed differences are poorly understood, though it is believed that a number of biological and phenotypic difference contribute towards these findings. Oestrogen and progesterone have been demonstrated to have an influence on airway function particularly in asthmatic patients, though similar influence has yet to be observed for COPD, and bronchial hyperresponsiveness is reported more frequently in women than in men [123, 124]. A potential increased susceptibility to CS in females is often considered to be the result of women having smaller lungs than men, which results in a higher dose per cigarette in comparison, though it has also been suggested that differences in susceptibility may simply be the result of brand choice [125]. While these differences may possibly be dismissed by the fact that women appear to be more frequently diagnosed with COPD than men,

trends to suggest a susceptibility to COPD onset in women are frequently reported in the literature [126]. Of note, disparity between immune function and inflammatory responses between men and women have been previously observed, with women typically displaying a heightened immune response as a result of chronic smoking and COPD [127, 128]. Although such trends have been observed, the mechanisms behind COPD pathogenesis still remain poorly understood, which thus contributes towards a lack of understanding of the specific sex differences in COPD onset and pathophysiology. By fully characterising specific mechanisms of COPD pathogenesis, researchers can better understand the unique differences in disease phenotype that may be observed as a result of biological sex, race or background, and allow for better and more targeted treatment plans for the individual. Failure to account for potential sex differences in a given study may therefore result in potential mechanisms that may affect one sex greater than the other being overlooked or missed.

### 1.1.3. MECHANISMS AND PATHOGENESIS

#### 1.1.3.1. Extracellular matrix and airway remodelling

The pulmonary extracellular matrix (ECM) comprises a complex network of macromolecules that provides support to surrounding cells, and its dysregulation has been linked to airway remodelling. The majority of the components of the ECM are produced by fibroblasts, smooth muscle cells and epithelial cells, of which the main components are proteins and glycoproteins such as collagen, elastin and fibronectin [129, 130]. Collagens are the most abundant ECM components in the lungs and have a number of subtypes, the presence and ratios of which determine the mechanical properties of the lungs [131]. In the lung parenchyma, fibrillar collagen such as types I, III and V which possess high tensile strength and low elasticity are the most abundant, though type IV involved in cell migration and differentiation is also common [132]. Elastin, a protein responsible for the elasticity of tissues, allowing them to retain their shape following stretching or contracting, is also highly

abundant and typically associates with type I and III collagens in the alveoli [133]. Disproportionate ratios of ECM components and degradation of collagens and elastin are known to lead to alterations in lung rigidity and elasticity, resulting in lung injury due to poor resistance to mechanical tension and stretching [134]. The components of the ECM are controlled by proteases and antiproteases which may prevent or promote degradation of ECM components, and thus balance of these enzymes is pivotal for maintaining peak tissue function.

#### 1.1.3.2. Protease-antiprotease imbalance

Homeostasis of the ECM is dependent on careful balance of proteases and antiproteases, which are involved in regulating proteolysis and remodelling of the ECM and overarching tissue systems. Imbalance of proteases and antiproteases therefore results in alterations to the ECM which ultimately contributes to major tissue remodelling and reduction or loss of normal tissue function. In the context of COPD, an imbalance of elastase and its inhibitor,  $\alpha$ 1-antitrypsin, typically as a result of A1AT deficiency, is the most widely characterised and understood example of this [135]. However, other protease-antiproteases may contribute towards airway remodelling and additionally play a pivotal role in the hallmark persistent inflammation observed in COPD phenotypes. Matrix metalloproteinases (MMPs) and tissue inhibitors of metalloproteinases (TIMPs) are types of proteases and antiproteases involved in the breakdown of collagen and elastin, and an inflammation-driven imbalance of MMPs and TIMPs is known to contribute towards ECM degradation [136, 137]. In particular, certain MMPs such as MMP-9 and MMP-12 are shown to be increased in the bronchoalveolar lavage fluid (BALF) of COPD patients [138, 139]. MMP-9, also known as 92 kDa type IV collagenase, is involved in the degradation of type IV and V collagens. Conversely, MMP-12, or macrophage metalloelastase, degrades both soluble and insoluble elastin. An increase of these MMPs therefore results in increased degradation of collagens and elastin, reducing the elasticity of the lungs and leading to significant changes to airway

structure and dynamics [140]. These changes often result in lung injury and enlargement of airway spaces due to low tolerance to stretching and contracting mechanisms, which in turn elicit inflammatory responses through the release of damage associated molecular patterns (DAMPs) and thus result in the production of further MMPs [141, 142]. While many MMPs are involved in maintaining the structure and dynamics of the ECM, others are involved in cell-based mechanisms such as recruitment and activation. MMP-28 or epilysin is an MMP associated with inflammatory modulation, more specifically in the recruitment and activation of macrophages during inflammation. Typically lowly expressed in the pulmonary environment, MMP-28 has been demonstrated to contribute towards COPD pathophysiology by recruiting macrophages and a number of other key immune cells into the pulmonary spaces and therefore contributing to the persistent inflammatory microenvironment typically observed in COPD patients [143]. Therefore, although proteases, antiproteases and the ECM are not considered components of the immune system, homeostasis of the ECM is paramount in the maintenance of a stable tissue environment and preventing unnecessary inflammation.

#### 1.1.3.3. Structural changes to airway and vascular compartments

Alterations to the ECM and protease-antiprotease imbalance ultimately leads to remodelling of many key structures in the lungs. The lungs are made up of vascular compartments, including veins, arteries and capillaries, and airway compartments including the bronchi, bronchioles and the lung parenchyma. The lung parenchyma itself is comprised of a large number of alveoli, which are surrounded by a dense capillary network in order to facilitate gas exchange. In order to ensure efficient gas exchange, the surface area of the lung parenchyma must be as large as possible, whilst the distance between air contained within the alveoli and circulating deoxygenated blood must be as small as possible [144].



Pulmonary hypertension is a common comorbidity associated with COPD, as defined by increased blood pressure within the lungs which impairs blood flow, and thus reduces the efficiency of gaseous exchange mechanisms [145]. Exposure to CS has been demonstrated to result in significant vascular remodelling, causing decreased lumen size and increased thickness of the vascular smooth muscle wall [146]. These alterations are considered to be a result of collagen deposition as a result of ECM remodelling, as abundance of collagen is associated with increased thickening of blood vessel walls and narrowing of the lumen [129, 147]. Furthermore, vascular remodelling may also be characterised by the appearance of smooth muscle marker expressing cells within pre-capillary vessels, resulting in significant vasoconstriction [148, 149]. Vascular remodelling as a result of CS exposure is thought to be a result of chronic hypoxia, which triggers the expression of transcription factors such as hypoxia-inducible transcription factor 1 (HIF-1 $\alpha$ ), which promotes the innate immune response and arteriole inflammation [150]. Production of IL-6 by inflammatory cells has also been strongly associated with the development of COPD-associated pulmonary hypertension, and is shown to result in pulmonary arterial cell migration which contributes towards vasoconstriction and vascular remodelling [151]. Increased thickening of vascular walls and constriction of the lumen therefore results in impaired blood flow within the lungs, in addition to increased distance between circulating deoxygenated blood and alveolar air, which results in inefficient gas exchange and increased hypoxia which may drive inflammation.

Remodelling of the lung parenchyma has been shown to affect structure and integrity of the small airways, as loss of alveolar attachments is strongly associated with airflow limitation and neutrophilic inflammation in the small airways [152]. The emphysematous phenotype of COPD is characterised by alveolar destruction, which not only reduces the surface area of the lungs but also contributes towards loss of elastic recoil, causing a significant reduction in efficient gas exchange [153, 154]. As previously discussed, increased collagen deposition

surrounding the alveoli in combination with loss of elastin reduces the integrity and elasticity of the lungs, which causes elastolytic injury and alveolar destruction [155]. Overall, these alterations contribute towards a hypoxic environment, which in combination with remodelling of vascular compartments within the lungs may drive further remodelling of both airway and vascular compartments and increased inflammation which may damage the endothelial layers of vascular and airway compartments [156]. Understanding how inflammation may contribute towards ECM remodelling, which in turn results in vascular, airway and lung parenchyma remodelling, is therefore paramount to understanding the pathogenesis of COPD.

#### 1.1.4. IMMUNOPATHOLOGICAL MECHANISMS

Chronic and persistent inflammation is considered one of the hallmark pathophysiological characteristics of COPD, so much so that investigating the role of immunopathological mechanisms in disease pathogenesis is a common topic in COPD research. The immune system is composed of the innate immune system and the adaptive immune system. Innate immunity is considered the first line of defence in response to infection or tissue damage, and is largely nonspecific in its targets which may on occasion result in autoimmune damage [157, 158]. Conversely, the adaptive immune response is induced by antigen presenting cells (APCs) of the innate immune system and is more specific, often resulting in the generation of memory cells which circulate the body to swiftly detect and destroy the same pathogen in the event of reinfection [158, 159]. Regulation of the immune system, including both induction and resolution of inflammation, is highly influenced by small proteins produced by immune cells known as cytokines and chemokines. Cytokines and chemokines may be specific in that they only affect one cell type or have a broad range of activity, though cytokines are largely involved in the amplification of cell effector functions whilst chemokines are typically involved in cell migration to areas of inflammation, a process known as chemotaxis [158].

Whilst the main role of the immune system is to prevent tissue damage by clearing pathogens or materials considered foreign, it can in some cases be detrimental to human health. Cigarette smoke is considered a foreign body by the immune system, and thus elicits an immune response which can in turn result in impaired clearance of pathogens and autoimmune-like chronic inflammation [160]. These characteristics are considered hallmarks of COPD, yet despite this the immunopathogenic mechanisms involved in COPD pathogenesis are poorly characterised and understood. This is likely due to the fact that research into COPD is largely focused on treatment and diagnosis strategies, with research focused on understanding pathophysiological mechanisms considered low priority [79]. Given that COPD is often defined by its inflammatory nature, gaining a better understanding of its immunopathological mechanisms could be paramount to identifying effective treatment.

#### 1.1.4.1. Pulmonary epithelium

The epithelial layer of all tissue systems acts as a physical barrier to prevent infection and tissue damage. In the lungs, where constant gas exchange means a consistent exposure and turnover of potentially harmful materials, maintaining the integrity of the epithelial layer is paramount to preventing disease pathogenesis [161]. Naturally, because of this frequent exposure to harmful materials, the pulmonary epithelium is responsible for the induction of innate immunity when infection or tissue damage occurs [162]. Exposure to noxious particulate matter results in airway remodelling, which alters the composition of the pulmonary epithelium. The epithelial layer of the lungs is comprised of a number of cells, including basal cells, ciliated cells, goblet cells, club cells and alveolar epithelial cells type 1 and type 2 (AEC I and AEC II) [163]. In the small airways, goblet cells are often found in low numbers in healthy individuals, however these numbers are shown to be significantly increased in COPD patients [164, 165]. Increased numbers of goblet cells leads to mucus hypersecretion, and this in combination with increased

number of basal cells and poor mucociliary clearance results in thickening of the epithelial layer and airway obstruction [166, 167]. These phenotypic characteristics are associated with immune cell accumulation, which contributes towards a persistent inflammatory microenvironment [167]. Additionally, whilst apoptosis is part of the natural cell cycle and induces minimal inflammation, cell necroptosis leads to the production of DAMPs and elicits a strong inflammatory response. Chronic CS exposure leads to the necrosis of bronchial epithelial cells which release DAMPs, resulting in recruitment of immune cells into the pulmonary spaces and in turn induces further immune-driven cell death [168]. While not typically considered a component of the immune system, these findings demonstrate that the pulmonary epithelium plays a pivotal role in the induction of the immune response and its persistence in COPD pathogenesis.

#### 1.1.4.2. Macrophages

Macrophages are a type of innate immune cell known for their phagocytic activity, whereby foreign substances are engulfed and digested by the cell. Macrophages may also assist in immune cell recruitment and differentiation through antigen presentation, and as such is classified as a type of APC. As one of the first cells to respond to infection or tissue damage, macrophages are typically found in tissues rather than peripheral blood, but may be recruited to areas of inflammation by other cells. Accumulation of specialised alveolar macrophages within the lungs is a widely reported mechanism of COPD and are known to have a reduced efficiency in performing their effector functions [169, 170]. Classic macrophage dichotomy divides macrophages into M1 and M2 phenotypes *in vitro* depending on the type of stimulation, surface molecules, secreted cytokine patterns, and functional characteristics. However, *in vivo* systems possess more complicated environments and therefore macrophage stimulation results in significant macrophage heterogeneity. Using the simple dichotomy, M1 or classically activated macrophages possess proinflammatory effector

functions, whilst M2 or alternatively activated macrophages are anti-inflammatory in nature [171]. M2 macrophages are known to be involved in the processes of tissue repair and remodelling, and it is demonstrated that in COPD macrophages are polarised towards an M2 phenotype and are the most abundant phenotype identified in BALF [172, 173]. Cytokines produced by this subtype are known to contribute towards mucus hypersecretion and airway obstruction, overall leading to significant airway remodelling [174]. M1 macrophages are widely reported to be significant contributors to elevated levels of proinflammatory cytokines such as IL-6 and TNF- $\alpha$  within the lungs, which are known to be elevated in COPD pathophysiology [175, 176]. Macrophages are also major sources of MMPs, which as previously discussed may cause the degradation of ECM components and lead to loss of integrity and elasticity of the lungs and chest cavity [177]. While migration and influence of macrophages in the periphery or other tissue systems is not widely researched, an association has previously been made regarding elevated macrophages in BALF and loss of integrity of the blood brain barrier and elevated microglia activation, leading to altered behavioural affects [178]. Given their abundance and accumulation in COPD pathophysiology, macrophage biology and effector functions following CS exposure is a topic of much research in the field of respiratory immunology, though their presence and effects in the periphery and other tissues are often overlooked as a result.

#### 1.1.4.3. Neutrophils

Typically found in the bloodstream, neutrophils are a type of granulocyte of the innate immune system with phagocytic activity, and are considered one of the first responders in the event of inflammation [179]. Increased presence and migration of neutrophils into the lungs, termed pulmonary neutrophilia, is widely recognised as a hallmark characteristic of COPD so much so that it is often used as a diagnostic marker of COPD progression [180]. Neutrophils possess a large number of receptors on their cell surface known as pattern recognition receptors

(PRRs), which recognise specific markers on the surface of pathogens or molecular markers of tissue injury such as DAMPs. Activation of these receptor signalling pathways therefore elicits neutrophil-driven inflammation. In patients with COPD, both peripheral and pulmonary neutrophils display an overexpression of PRRs such as toll-like receptors (TLRs) on their surface, amplifying neutrophil recruitment and activation and promoting persistent inflammation [180, 181]. Much like macrophages, neutrophils are a contributing source of MMPs such as MMP-8 (neutrophil collagenase) and MMP-9, as well as neutrophil elastase. Accumulation and hyperactivation of neutrophils in the lungs is shown to result in a protease-antiprotease imbalance through an increased production of MMPs and neutrophil elastase, which result in the degradation of the ECM [182]. In a similar manner to macrophages, neutrophils are a topic of much focus in COPD research and are possibly amongst the most well characterised immune cell type in the pathogenesis of COPD.

#### 1.1.4.4. Dendritic cells

Dendritic cells (DCs) are professional APCs of the innate immune system, their primary role being the activation of naïve T cells in the draining lymph nodes [183]. Despite being a critical link between the innate and adaptive immune responses, the role of DCs in COPD has not been investigated as widely as other cells of the immune system. Nonetheless, DC recruitment into the lungs is associated with COPD pathophysiology, though exposure to noxious particulate matter is known to impair DC maturation thereby limiting their antigen-presenting capabilities [184, 185]. Immature DCs produce chemotactic proteins which drive neutrophil recruitment and induce T cell differentiation into proinflammatory phenotypes [186, 187]. While there is some evidence to suggest DCs may play a role in elastin degradation, their role beyond antigen presentation and cell recruitment and differentiation has not been extensively studied in COPD research [187].

#### 1.1.4.5. Natural killer and natural killer T cells

Natural killer (NK) cells belong to the innate lymphoid cell (ILC) family and possess cytotoxic activity. Unlike similar cytotoxic cells of the adaptive immune system, NK cells do not require antigen presentation for their activation, and are hence classified as cells of the innate immune system despite being of lymphoid origin. As such, they are highly specialised in providing a rapid response to virus-infected cells and tumour cells, which typically prevent the presentation of antigens on their cell surface to allow for rapid replication without eliciting an immune response [158]. By contrast, natural killer T (NKT) cells possess qualities of both NK and T cells and lie between innate and adaptive immunity. They have similar cytotoxic activity to NK cells, but possess a distinct T cell receptor and require antigen presentation for activation, and are therefore not classified as ILCs. In order to perform their cytotoxic activity, both NK and NKT cells produce and secrete perforin and granzyme B, which create pores in cell surface membranes and induce apoptosis respectively [188]. Although critical in preventing the replication of potentially harmful or cancerous cells, current research investigating the role of NK and NKT cells in COPD pathogenesis is somewhat lacking [189]. However, data from COPD patients has demonstrated that the numbers of peripheral NK and NKT cells are reduced in comparison to healthy smoker and non-smoking healthy participants, and that these cells possess blunted cytotoxic capabilities. Blunted cytotoxic activity is attributed to lower expression of perforin and granzyme B, as the same effect was observed in NK and NKT cells exposed to perforin and granzyme B inhibitors from smokers and healthy participants [190]. While proportions and effector functions of NK and NKT cells are reduced in the periphery, their numbers are significantly increased in the sputum of COPD patients. These cells both expressed perforin and granzyme B in significantly higher amounts in comparison to healthy smoking and healthy non-smoking participants [191, 192]. These results provide evidence that NK and NKT cells are trafficked out of the periphery and

into the pulmonary spaces, where their cytotoxic activity is overexpressed and result in nonspecific damage to the epithelial layer [192]. NK and NKT cells are both the largest contributing sources of IFN- $\gamma$  and TNF- $\alpha$ , two major proinflammatory cytokines involved in macrophage and endothelial cell activation in addition to immune regulation [193]. Despite these findings, investigations into the role of NK and NKT cells in COPD pathogenesis are often overlooked, and most research is focused on peripheral NK and NKT cells as opposed to those found in the lungs [194].

#### 1.1.4.6. T cells

T cells are lymphocytes of the adaptive immune system, often classified into two main subtypes based on the expression and presence of their surface cluster of differentiation (CD) marker. Similar to NK and NKT cells, CD8<sup>+</sup> or killer T cells possess cytotoxic activity to kill potentially harmful cells such as cancerous cells or virus-infected cells. An increased presence of CD8<sup>+</sup> T cells in the airways and BALF of COPD patients is widely reported in the literature, whilst peripheral numbers are shown to be reduced [195-197]. Cytotoxic activity of CD8<sup>+</sup> T cells is shown to be increased in the pulmonary spaces, as evidenced by increased expression of perforin and granzyme B, though peripheral CD8<sup>+</sup> T cells are identified as being less cytotoxic by comparison [191, 198-200]. These characteristics follow the same trend observed in NK and NKT cells, and suggest that highly cytotoxic cells migrate into the pulmonary spaces from the periphery where their cytotoxic activity leads to ECM degradation and airway remodelling [140]. Cytokine production by CD8<sup>+</sup> T cells is also widely reported. CS exposure has been associated with the production of IFN- $\gamma$  and TNF- $\alpha$  in both the lungs and the periphery [201, 202]. CD8<sup>+</sup> T cells are also significant contributors to IL-17A levels in the lungs, a cytokine which is important in the induction of another proinflammatory T cell subtype [203]. Despite this evidence to support the key role of CD8<sup>+</sup> T cells in COPD pathogenesis, the phenotypic characteristics and CD8<sup>+</sup> T cell-driven mechanisms of COPD



pathophysiology remain poorly characterised, particularly in the periphery [204].

CD4<sup>+</sup> or helper T cells are the other major subtype of T cell, characterised by their expression of the CD4 marker on their surface. The role of CD4<sup>+</sup> T cells in the immune system lies in the production and secretion of cytokines which may either promote or resolve inflammation. As such, there are a wide variety of further subsets within the CD4<sup>+</sup> subtype defined by the cytokines they produce and their overall role in the inflammatory process. Like many other cells, influx of CD4<sup>+</sup> T cells into the lungs is widely reported, though it is the disproportion of CD4<sup>+</sup> T cell subsets that is considered their primary contribution towards COPD pathophysiology [205, 206]. T helper 1 (Th1) and T helper 2 (Th2) subtypes induce different types of immune response, with Th1 inducing cell-mediated responses whilst Th2 induces a humoral response. These differing types of immune responses lead to the activation and proliferation of different types of immune cells and production of different types of cytokines and chemokines. Of note, Th1 responses are often associated with neutrophilic inflammation and tissue destruction, whilst Th2 responses may result in allergic-type responses particularly in allergic inflammatory diseases [205]. It has been demonstrated that an imbalance of Th1/Th2 subsets leads to dysregulation of cell-mediated and humoral immune responses in COPD, resulting in persistent inflammation and airway remodelling [207]. In acute exacerbations of COPD (AECOPD) particularly, the CD4<sup>+</sup> T cell response shifts towards a Th2 phenotype, resulting in allergic inflammation [208, 209]. While Th1 and Th2 responses induce different immune responses to combat different pathogens respectively, Th17 and T regulatory cells (Tregs) induce and resolve inflammation. Th17 cells produce the proinflammatory cytokine IL-17A and induce the production of antimicrobial peptides and chemokines by epithelial cells in addition to recruiting neutrophils to inflammation sites [210]. By comparison, Tregs are a primary source of IL-10, an anti-inflammatory cytokine, and are pivotal in preventing overactivation of innate and adaptive immune cells

to minimise severe inflammation and tissue damage [211]. An increase in Th17 cells in both the BALF and periphery of COPD patients has been reported in the literature, with their presence associated with the production of a number of proinflammatory cytokines driving the recruitment of neutrophils and macrophages [212-214]. The proportions of Th17 cells to Tregs are significantly altered in COPD, with Th17 populations typically being negatively correlated to Treg populations [215]. This imbalance is observed in both the periphery and in the lungs [216, 217]. Ultimately, this imbalance leads to a persistent inflammatory environment, inducing cellular recruitment and production of proinflammatory mediators, whilst anti-inflammatory and immune resolution mechanisms are typically suppressed [205].

#### 1.1.4.7. B cells

B cells are antibody producing cells of the adaptive immune system, critical in the humoral immune response and development of long-term immunity [218]. They may also present antigens to T cells, resulting in their differentiation and activation. In the lungs, B cells are largely found in tertiary lymphoid aggregates named inducible bronchus-associated lymphoid tissues (iBALTs), the presence of which is positively correlated with COPD severity [219, 220]. iBALTs are formed by activated mesenchymal cells such as endothelial cells, podoplanin-expressing fibroblasts and follicular dendritic cells, which in turn results in ILC-driven recruitment of T and B cells [206, 221]. The presence of iBALTs allows for localised antigen presentation and swift lymphocyte differentiation in order to combat and remove perceived threats, such as pathogens. However, in COPD B cells both within and outside of iBALTs are demonstrated to possess autoreactive characteristics and generate autoantibodies which target host cells and molecules. These include antibodies which recognise host cells and molecules critical for lung health and homeostasis, such as epithelial cells and elastin fragments [222-225]. The presence of autoantibodies has been correlated particularly to the development of emphysematous phenotypes, and

smoking-induced emphysema has demonstrated a similar phenotype to that of autoimmune diseases such as systemic lupus erythematosus (SLE) [226]. Increased presence of autoantibodies in the sputum of COPD patients is associated with an increased risk of AECOPD and decreased lung function compared to that of systemic autoantibodies [227]. Whilst these studies demonstrate a critical role for B cell prevalence and the production of autoantibodies in the generation of an autoimmune-like environment within the lungs as a driving factor for COPD pathology, their exact contribution towards health decline is unclear [206].

#### 1.1.4.8. Cytokines and chemokines

Cytokines and chemokines are produced and secreted by a number of immune cells during the inflammatory process and may contribute towards either the progression or resolution of inflammation. Whilst a number of cytokines and chemokines have been implicated in COPD pathogenesis, the role of cytokines is more widely researched and understood than that of chemokines. Major proinflammatory cytokines associated with COPD pathophysiology include IL-1 $\beta$ , IL-6, IL-17A, IFN- $\gamma$  and TNF- $\alpha$  [228]. Each of these cytokines has distinct effects on different cell types, though are all involved in inflammatory cell activation or cellular recruitment. Macrophages are a major source of cytokines in inflammation, in particular TNF- $\alpha$  which induces the expression of adhesion molecules resulting in cell migration into the pulmonary spaces [229]. TNF- $\alpha$  is also secreted by NK, NKT, Th1 and CD8<sup>+</sup> T cells, and elevated levels in both serum and BALF has been associated with COPD pathogenesis [189, 202, 230]. IL-1 $\beta$  is a proinflammatory cytokine of the interleukin family critical in protection against noxious particulate matter including CS, and are one of the first cytokines to be secreted by epithelial cells following exposure to particulate matter or pathogens [231, 232]. Much like TNF- $\alpha$ , increase of IL-1 $\beta$  in the periphery, lungs and BALF is associated with COPD pathophysiology, with higher levels being indicative of more severe disease phenotype [233]. IL-1 $\beta$  is also

associated with the development of lung cancer, as indicated by a reduction in cancer incidence and mortality in patients treated with canakinumab, an anti-IL-1 $\beta$  antibody [234]. Given the overlap in pathological symptoms between COPD and lung cancer and that the two diseases are often comorbid, such data suggests that the IL-1 $\beta$  pathway may be a suitable target for future therapeutic options. Similarly, IL-6 has been implicated in the pathogenesis of a number of pulmonary diseases including asthma, lung fibrosis, lung cancer and COPD [235]. Increased upregulation of IL-6 in serum and BALF can be observed in COPD patients, though no association between IL-6 levels and degree of disease severity has been established [236, 237]. As previously mentioned, IL-17A is a major proinflammatory cytokine produced largely by Th17 cells and is involved in the production of antimicrobial peptides and neutrophil recruitment [210]. Elevated IL-17A levels in serum and sputum of COPD patients are associated with increased disease progression, and also with imbalanced Th17/Treg ratios [238, 239]. IFN- $\gamma$  is largely produced by adaptive immune cells and ILCs, with the main contributors in COPD pathogenesis being NK/NKT cells and CD8<sup>+</sup> T cells [193, 201]. Inflammation is driven by IFN- $\gamma$  through macrophage activation and the proliferation and differentiation of immune cells into proinflammatory phenotypes, and increased levels of CD8<sup>+</sup> T cell-derived IFN- $\gamma$  is associated with disease severity [212]. Studies such as these demonstrate that no one cytokine is responsible for COPD pathogenesis, and that disease progression and persistence is driven by a multitude of contributing proinflammatory cytokines which decrease the expression and secretion of anti-inflammatory mediators [228, 240].

Chemokines are a distinct subdivision of cytokines with chemotactic effects, and are thus pivotal in the trafficking and migration of immune cells during inflammation [241]. Chemokines are subclassified into distinct families depending on their amino acid sequence, the two main groups being CC, with two adjacent conserved cysteines next to each other, and CXC, which possess a single variable amino acid between two conserved cysteines [242]. In the context of COPD, the chemokine

CXCL8 (also known as IL-8) is the most widely associated with pathogenesis and pathophysiology, and is implicated as a driving factor in AECOPD and neutrophil-driven inflammation [243]. Alveolar macrophages and epithelial cells are thought to be the most significant contributors to CXCL8 levels, and its association with CXC-chemokine receptor (CXCR) 2 is known to trigger neutrophil and monocyte recruitment [244]. An elevation of CXCL8 in serum and sputum is associated with severe AECOPD, as indicated by an increased number of neutrophils, increased airway bacterial load and increased blood myeloperoxidase (a proinflammatory enzyme secreted by neutrophils) [245, 246]. Higher levels of CXCL8 are also associated with an increased risk of consistent AECOPD in comparison to COPD patients with lower CXCL8 [247]. Other chemokines implicated in COPD pathogenesis are CXCL9, CXCL10, CXCL11 and CCL2, all of which are mainly produced by alveolar macrophages and drive either T cell or monocyte recruitment [243, 248]. In particular, CXCL10 is associated as a biomarker of viral AECOPD, as elevated serum levels have been detected in COPD patients suffering from rhinovirus-associated exacerbations [249, 250]. Although associations have been made for these chemokines in COPD, particularly in the context of AECOPD, their exact impact on COPD pathophysiology is not well characterised unlike that of cytokine-driven mechanisms.

#### 1.1.4.9. Interplay between immune cell types

Inflammation in COPD is driven by complex interactions among various immune cell types. These interactions create a self-perpetuating cycle of immune activation, tissue damage, and impaired repair mechanisms, which contribute to the progression of COPD. Recent studies have provided deeper insights into the synergistic relationships among these immune cells, highlighting the intricate network that underlies COPD pathogenesis.

Neutrophils and macrophages are central players in the chronic inflammation observed in COPD. Neutrophils release proteases such as neutrophil elastase and MMPs which contribute to the breakdown of extracellular matrix components, leading to emphysema and airway remodelling. Macrophages, on the other hand, secrete chemokines such as CCL2 that further recruit neutrophils to the site of inflammation, creating a positive feedback loop [167]. Macrophages activated in the COPD lung also exhibit a pro-inflammatory M1 phenotype, characterized by the production of cytokines such as TNF- $\alpha$  and IL-1 $\beta$  [171]. These cytokines not only sustain neutrophil recruitment but also promote the survival and activation of these cells, exacerbating tissue damage. Recent evidence suggests that neutrophils can also influence macrophage function by releasing ROS and proteases that alter macrophage polarisation, thus enhancing their pro-inflammatory capacity [251, 252]. This bidirectional interaction between neutrophils and macrophages underscores their synergistic role in maintaining chronic inflammation in COPD.

The interplay between T cells and macrophages is another crucial aspect of COPD pathogenesis. CD8<sup>+</sup> T cells are significantly elevated in the lungs of COPD patients and are involved in the direct killing of epithelial cells, contributing to tissue destruction [253]. These T cells are activated in part by macrophages, which present antigens and secrete cytokines that promote T cell differentiation and activation. In turn, hyperactivated CD8<sup>+</sup> T cells have increased secretion of IFN- $\gamma$ , which enhances the pro-inflammatory activity of macrophages [189].

CD4<sup>+</sup> T helper cells, particularly the Th1 and Th17 subsets, further amplify this crosstalk. IFN- $\gamma$  producing Th1 subsets drive M1 macrophage polarisation and increase the secretion of inflammatory mediators [229]. Th17 cells produce IL-17, which is crucial for neutrophil recruitment and activation, linking the adaptive immune response to innate immune mechanisms [206]. The synergy between these T cell subsets, macrophages and neutrophils not only sustains chronic inflammation but also facilitates the transition from acute to chronic

immune responses, which results in persistent inflammation typically observed in COPD [254].

DCs act as key regulators of immune responses in COPD by bridging innate and adaptive immunity. DCs capture and process antigens from inhaled irritants and apoptotic cells, subsequently presenting these antigens to T cells. In COPD, DCs exhibit a heightened capacity to activate T cells, particularly CD8+ T cells, through increased expression of co-stimulatory molecules and secretion of cytokines such as IL-12 [255]. This enhanced antigen presentation by DCs drives the chronic activation of T cells, thereby reinforcing the inflammatory cascade. Additionally, DCs influence the activity of other immune cells by releasing chemokines such as CCL20, which attracts Th17 cells, further linking the activation of innate and adaptive immune cells [187]. The interplay between DCs, macrophages, and T cells creates a network of synergistic interactions that sustain and amplify the inflammatory response in COPD.

The interplay and synergy among immune cells in COPD pathophysiology represent a complex network of interactions that drive chronic inflammation, tissue damage, and disease progression. Neutrophils, macrophages, T cells, and DCs interact in a manner that amplifies the inflammatory response, leading to a self-perpetuating cycle of immune activation and tissue destruction. Understanding these interactions is crucial for developing targeted therapies that can disrupt these pathogenic feedback loops, potentially altering the course of COPD.

#### 1.1.4.9-1.1.4.10. Other immunopathogenic mechanisms

Due to the overlap between asthma and COPD pathophysiology, it is suggested that a number of mechanisms known to drive asthma pathology may contribute to COPD pathogenesis and persistence. Despite this overlap in symptoms and many pathophysiological characteristics, many of the mechanisms of asthma believed to

contribute towards COPD have not been widely studied and their association is merely suggestive [256]. Eosinophilic inflammation is a hallmark characteristic of asthma, though it is typically only observed in severe COPD or during AECOPD [257]. Eosinophils are highly specialised granulocytic cells of the innate immune system that combat infection by helminths or multicellular parasites, and are known to contribute towards and drive allergy. Unlike many other immunopathological mechanisms, eosinophilic inflammation is phenotypically indicative of chronic bronchitis phenotypes as opposed to emphysematous phenotypes and is associated with only very mild alveolar damage [258]. Mast cells are another type of granulocytic cell of the innate immune system thought to have a role in COPD pathophysiology, given their role in asthma and allergy. Despite this, mast cells are perhaps the most overlooked immune cell in COPD research, and their role in COPD pathophysiology is purely speculative [259]. It is suggested that mast cells may contribute towards COPD pathophysiology through the production and secretion of TNF- $\alpha$  and CXCL8 and interactions with various other immune cells to drive inflammation and airway remodelling, though evidence to suggest this is limited [259, 260]. Overall, studies investigating the immunopathogenic mechanisms of COPD demonstrate the critical role each cell type plays in both disease progression, persistence and severity. Nonetheless, these studies also highlight the lack of definitive understanding in how each mechanism is induced and drives COPD, as well as how each mechanism is in turn influenced by other mechanisms.

## 1.2. ANIMAL MODELS OF COPD

Due to the difficulties and ethical regulations surrounding access to COPD patient samples, much of our current understanding of COPD pathogenesis and pathophysiology has come from studies making use of animal models of disease. Model systems are simplified systems that aim to mimic or reflect human disease, and by definition must be easily accessible and manipulated. There are a multitude of factors that must



be considered when using an animal model to investigate COPD, including sex and age of the animals, as well as the method and irritant used to induce COPD [261]. Given that COPD takes a number of years to develop in humans, animals with a shorter lifespan and developmental process, such as mice and rats, are favoured as they are able to mimic the phenotypic characteristics of COPD within a shorter timeframe. Although frequently used in COPD research, there is no set standard for model design, and as such there is high variability in species used, exposure methods and methods to confirm the presence of COPD [262].

### 1.2.1. MODELS OF COPD

#### 1.2.1.1. Elastase models

Elastases are a class of serine proteases that break down elastin, thereby causing alterations to connective tissue and the ECM. As previously discussed, elastin degradation results in impaired airway dynamics, in particular reduced tolerance to stretching and contracting mechanisms. Because of this, exposure to elastases (particularly porcine pancreatic elastase (PPE) or human neutrophil elastase (HNE)) is a frequently used methodology in inducing COPD in animals. The role of elastases in COPD pathogenesis has been well documented since the 1960s, and the first protease-induced animal model of COPD was developed as early as 1965 [263, 264]. Elastase instillation is typically given intratracheally (directly into the trachea) or endotracheally (via the mouth or nose cavity into the trachea), though other routes particularly in larger animals may be used [261]. Some of the main benefits of using elastases to induce COPD in animals are that they are relatively inexpensive and lung injury can be observed after singular or minimal doses. However, whilst the dose of elastases such as PPE or HNE can be tightly controlled, it has a very narrow dose window. Doses below the threshold are insufficient in inducing lung injury or tissue remodelling, whilst doses above the threshold result in haemorrhage and mortality [265, 266]. As a result, the use of elastase to induce COPD may result in unnecessary harm or suffering to animals if given incorrect doses.

Furthermore, it is known that direct elastase instillation does not provide insight into disease pathogenesis and bypasses immune cell involvement, resulting in a more “artificial” emphysematous phenotype and is insufficient in the study of chronic bronchitis phenotypes [267-269]. Although small rodents such as rats and mice are preferred species for animal studies, some argue that, in respiratory disease research, such species are not suitable for a model system. This is due to differences in lung structure between humans and rodents, particularly in the context of total lung capacity, lobe structure (figure 1.2.1), parenchyma percentage and alveoli size [270, 271]. Larger animals such as pigs, dogs and sheep provide model systems more reflective of human disease and physiology, however such species possess their own challenges in scientific research. In particular, larger animals induce higher costs for housing and husbandry, in addition to a lack of reagents specific for such species being commercially available [261]. As a result of this, the majority of research using large animals to study COPD was conducted some 40 or more years ago prior to advancements in both investigative techniques and equipment available to study lung function [272-274].

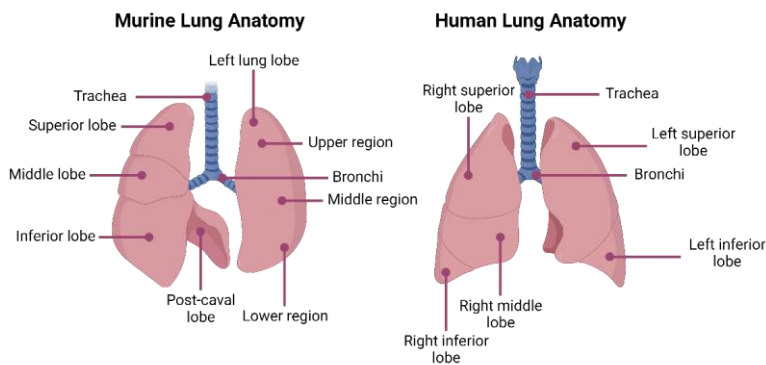


**Figure 1.2.1:- Comparison between murine lung anatomy (left) and human lung anatomy (right).** Whilst the human right lobe is comprised of three lobes whilst the left is comprised of two, mouse lungs have a significantly different anatomy. In mice, the right lung is comprised of four lobes: the superior lobe, middle lobe, inferior lobe and the post-caval lobe. The left is a singular large lobe split into the upper, middle and lower regions [271]. (Created with BioRender)

#### 1.2.1.2. Cigarette smoke models

As one of the primary aetiological factors in COPD pathogenesis, CS is frequently used to induce COPD in animals. Due to the types of equipment required for CS exposure, small animals including mice, rats, hamsters and guinea pigs are favoured species [261]. Although such models are well established, there is a high degree of variation in reported findings, likely as a result of model design. While mice are the preferred species for COPD research, it has been demonstrated that different strains possess unique susceptibilities and resistances to COPD development [275]. Additionally, exposure is typically performed either via a whole-body (WB) or nose-or-head only (NHO) system which may influence the phenotypic presentation of resulting COPD [276] (as described below in section 1.2.2). There are no standardised techniques or model systems for COPD research, even when it comes to the types of cigarettes animals are exposed to. Many research groups choose to utilise Kentucky reference cigarettes (Center for Tobacco Reference Products) in order to standardise findings, though this is not mandatory in model design [268]. Despite this, CS exposure is considered to result in the most clinically relevant model of COPD due to it being a proven direct cause of COPD [277]. Exposure to CS is shown to induce an emphysematous COPD phenotype with hallmark inflammatory characteristics in a number of species, and is thus the most widely used and reported exposure type in respiratory research [278].

#### 1.2.1.3. Genetic models

In the majority of genetic models of COPD, disease is induced in transgenic or knockout animals through PPE or CS exposure, and are thus used to identify relative risks of COPD development [261]. Given that their genome is more widely studied and understood, mice are the species of choice in transgenic and knockout studies. Additionally, rapid development, large litter sizes and fast reproductive cycle mean that mice

are favoured due to their ease of selecting genetic traits as well as housing and husbandry conditions [279]. Translational ability of genetically-altered murine models to human disease is a topic of much debate. As such it is paramount that research groups ensure that target genes for COPD research are either expressed in humans or orthologues of human genes [280]. Studies typically focus on overexpression or knockout of genes involved in major signalling or inflammatory mechanisms, including genes encoding receptors, enzymes and cytokines. These models have provided significant insight into the degree of which certain mechanisms may protect against or induce COPD phenotypes. For example, an MMP-12 knockout model demonstrated that mice were largely resistant to macrophage accumulation in the lungs and to development of emphysema [281]. Furthermore, knockout of other inflammatory mechanisms has been shown to partially protect mice from some hallmark inflammatory mechanisms of COPD. Knockout of IL-17A is demonstrated to protect against COPD as a result of limited migration of macrophages into the lungs and reduced production of MMPs [282], and specific knockout of IL-17A in CD4<sup>+</sup> and CD8<sup>+</sup> T cells exemplified the critical role of innate lymphoid cells as major sources of IL-17A [283]. As such, although these models are not typically used to identify specific genes leading to COPD development, they are critical in providing evidence for the role of particular genes and mechanisms in COPD pathogenesis and persistence.

#### 1.2.1.4. Exacerbation models

AECOPD is a common symptom of COPD that places significant burden on both patient health and medical resources. It is widely reported that the pulmonary environment and immune system of COPD patients may respond differently to infection in comparison to healthy individuals [189, 204], as such exacerbation models to mimic human AECOPD are used to study these responses. Much like genetic models, exacerbation models of COPD typically use mice and are induced through elastase or CS exposure. After COPD has been established, animals are exposed to

either pathogens or pathogen associated molecular patterns (PAMPs) which trigger the immune response. As COPD is a respiratory disease and in order to maintain relevance to human disease, most models expose animals to respiratory pathogens such as influenza [284], rhinovirus [285], RSV [286] and *Streptococcus pneumoniae* [287]. PAMPs such as lipopolysaccharide (LPS) or polyinosinic:polycytidylic acid (poly I:C) may also be used to simulate either bacterial or viral infection respectively. As a component of gram-negative bacterial cell walls, LPS is a well characterised PAMP known to elicit immune responses and is more accessible and affordable than whole pathogens, as specialist facilities are required for particularly hazardous pathogens [261]. Additionally, evidence has demonstrated that LPS is present in CS, air pollution and organic dusts, and may therefore contribute towards COPD pathogenesis [288, 289]. Although mouse models are favoured, larger rodent models such as rats and guinea pigs have been used previously to investigate responses to infection within the COPD lung [290, 291]. Exacerbation models may not investigate COPD pathogenesis, with the exception of LPS exposure models, but they are critical in understanding the responses to infection and resulting tissue injury and repair processes following pathogen clearance. This is particularly relevant in recurrent infections in current-smoker COPD patients, as models mimicking these characteristics can provide significant insight as to why these reinfections occur and how this contributes towards further exacerbations and worsening severity of COPD [286].

#### 1.2.2. CS EXPOSURE MURINE MODELS OF COPD

Mice are the most frequently used species in scientific research involving animal studies due to their rapid development, strain choices, low cost of housing and husbandry and availability of target reagents [292]. As previously mentioned, CS exposure is the most frequently used methodology to induce COPD in mice due to its clinical relevance to human disease and ability to elicit an inflammatory emphysematous

phenotype [277, 278]. Although frequently used, model design varies significantly between research groups and countries. This can lead to discrepancies between study findings, particularly in cases where different sexes, strains and ages of mice are used. The most frequently used strain is C57BL/6J, which is demonstrated to have mild susceptibility to the development of emphysema but is more resistant to acute lung injury and complications than other common strains such as BALB/cJ and A/J [275, 292, 293]. The age of mice used may also be a compounding factor in a study's findings. Typically most studies utilise mice between 6 – 10 weeks of age, which is considered juvenile and is the equivalent of a human below the age of 20 [294]. COPD is often considered a disease of old age, and ageing influences a number of biological functions and processes within the body and thus increases risk of developing COPD. The same influence of age on COPD pathogenesis has been observed in mice, where 12-month-old mice display marked inflammation and airway remodelling following 3 months of CS exposure in comparison to 8-week-old mice [295]. The length of exposure to CS is also a critical consideration, as naturally the longer mice are exposed to CS the more severe the resulting pathophysiology is [296]. The types of cigarettes used to generate CS for exposure are also critical impacting factors. A wide variety of cigarette brands are available commercially, and thus contain different components which may affect both smoking habits and the composition of CS [297]. Composition of CS, as well as exposure to mainstream (first-hand) or sidestream (second-hand) CS, can result in different phenotypic presentations of COPD in mice. Mainstream smoke exposure, particularly with greater masses of total particulate matter (TPM), is shown to elicit a stronger acute inflammatory response in comparison to sidestream exposure and lower TPM, which generates a solely macrophage response [298]. Despite each of these variables, the most compounding factor in determining the outcome of COPD generation in mice lies in the methodology used to administer CS. Currently, most models follow one of two designs: whole-body (WB) exposure or nose-or-head only (NHO) exposure (figure 1.2.2). While both models are

effective in generating COPD in mice, each presents its own limitations which must be considered when designing studies.

#### 1.2.2.1. Whole-body models

Whole-body (WB) exposure to CS is the most frequently utilised model design for murine COPD models, likely due to their ease of use and ability to expose large numbers of animals at once [299]. Smoke burned directly from a cigarette is pumped into chambers housing mice, which are unrestrained and have free access to necessities such as food and water (figure 1.2.2). As a result of this, mice can be exposed to CS for long durations throughout a 24-hour period, for as many times per week as specified by their study protocols and design. Many systems are available commercially, allowing researchers to automate the exposure process [261]. Most studies utilising this design typically expose mice to CS for a longer duration in comparison to other methods, with exposure periods lasting approximately 24 weeks (6 months), this is considered chronic exposure [275, 300-305]. While the WB system is beneficial in its ease of use, there are significant limitations of the model design relating to the exposure method. In particular, in a comparison between a WB and NHO model, Serré et al. (2021) [276] demonstrated that WB models elicit a stronger inflammatory response. This is attributed to the ingestion of particulate matter generated from CS via grooming, as a result of particulate matter clinging to fur [306]. Additionally, particulate matter was suggested to have been absorbed via the skin, which contributed to higher serum cotinine (a metabolite of nicotine) levels in comparison to controls and an NHO model [276]. Although humans may naturally be exposed to CS through this manner, the degree to which mice are exposed to CS via the skin or digestive tract using the WB method is not reflective of true human CS exposure.

#### 1.2.2.2. Nose-or-head only models

The nose-or-head only (NHO) model is a more targeted method of CS exposure, and is also more specified than WB methods in that it allows the concentration of CS delivered to each animal to be tightly regulated [306, 307]. Unlike the WB system, mice are placed into restraints in the NHO system where a cone is inserted into their nose to allow direct inhalation of CS (figure 1.2.2). Although mice are typically exposed for shorter durations in comparison to WB methods, the process of restraint and being unable to access water and food places animals under a significant amount of stress which may impact study data [308, 309]. Additionally, because of the system setup, NHO models limit the number of animals that can be used at any one time. These limitations may explain why NHO systems are typically used less frequently than WB systems. Nonetheless, due to targeted delivery and control of CS concentrations, NHO model exposure periods are typically 24 weeks (6 months) or less in length, which may reduce the costs of housing and husbandry [276, 296, 310-312]. Furthermore, as CS is delivered directly into the lungs the NHO system removes the risk of particulate matter being ingested or absorbed, and therefore the resulting COPD phenotype is generated via inhalation only. NHO models display a marked increase in airway remodelling in comparison to WB methods, whilst still retaining the hallmark inflammatory characteristics of COPD [276]. Because of this, the NHO system is considered to be more clinically representative of human COPD [313]. Although reflective of human disease, the degree of stress and potential suffering animals may endure as a result of



prolonged periods of restraint is a serious ethical welfare concern in many countries in the EU and the UK.

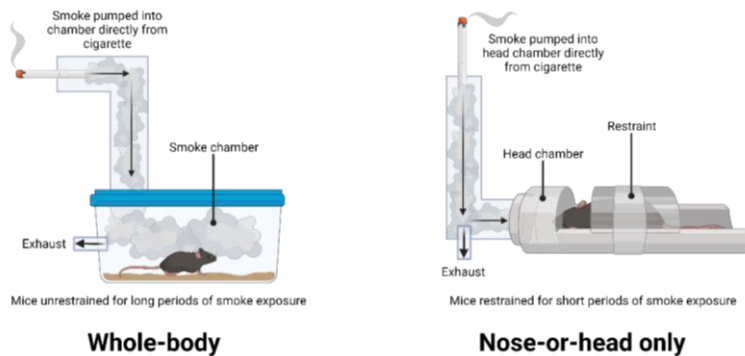


**Figure 1.2.2:- Diagrammatic demonstration of the two most commonly used CS- induced COPD models using mice.** Both models utilise direct exposure of mice to unfiltered CS either via a whole-body (WB) or nose-or-head only (NHO) route and require specialist equipment for exposure. While both models are effective in inducing a COPD phenotype in mice, both possess their own limitations, in particular unnecessary stress and/or suffering of animals in addition to failure to reflect human exposure methods that induce COPD. It is widely reported that the majority of noxious particulate matter generated by CS in these exposure methods elicits immune responses and induction of COPD phenotypes through ingestion via grooming or absorption via the skin rather than inhalation [276, 307]. (Created with BioRender)

### 1.2.2.3. Other exposure method models

Although the WB and NHO methods are widely used, these model systems are typically only used in North America and Asia where ethical and welfare considerations for animals in research are less tightly governed than in Europe [314]. Alternative model designs have been utilised in the past, though these are not as widespread as current model systems. These model systems typically expose mice to cigarette smoke extract (CSE) in lieu of direct cigarette smoke. In order to generate CSE, unfiltered cigarettes are typically pumped through a liquid culture medium, and typically one cigarette per 1 mL of media is classified as 100% CSE [315]. The resulting CSE is then diluted down to clinically relevant concentrations and determined by the researchers. Lee et al.

(2017) [316] utilised a model of COPD generated through intratracheal CSE exposure, which eliminated many of the limitations of WB and NHO systems. In particular, mice were prevented from being exposed to CS by the skin or digestive system due to direct tracheal exposure and were only restrained for a brief period in order to receive doses. However, intratracheal exposure is typically a complex and difficult dosing strategy, with incorrect administration resulting in either accidental overspill into the oesophagus or injury to the animal [317]. Due to the small size of mice, the risk of incorrect placement of an intubation tube or needle into the trachea is somewhat high. An alternative methodology demonstrated by Miller et al. (2002) [318] is intranasal CSE exposure. For this, mice are given doses of CSE into the nasal cavity to be inhaled naturally. While this is technically easier than intratracheal administration, the risk of overspill into the oesophagus may still be present.

#### 1.2.2.4. Limitations with current model systems

It is evident that each model design possesses its own strengths and limitations, though there are additional considerations that often fail to be addressed in COPD research using mouse models. Although sex differences in COPD are disputed, the majority of murine COPD studies are subject to a degree of sex bias in that often mice of only one sex (typically female) are used during investigation [178, 303, 319, 320]. Furthermore, many studies often fail to report or disclose the sex of mice used [283, 321-323]. Inability to report or include both sexes, particularly in the study of diseases where sex differences are either reported or suspected, fails to solidify the robustness of the reported outcomes of a study. Additionally, many murine model studies display an element of investigator bias, as typically only mechanisms in the lungs are investigated and defined in COPD [302, 322, 324]. COPD is known to be a whole-body disease, with inflammatory mechanisms reported in the peripheral blood of human patients [190, 212]. A model utilising both sexes and used to study both pulmonary and systemic mechanisms is therefore paramount to maintain robustness of generated data. These

factors in combination with the limitations of the WB and NHO systems compound the efforts of research groups, particularly in countries where animal welfare laws and rights are strictly governed. As a result of these same laws, developing novel model designs is often an arduous task, as researchers must be able to definitively justify the necessity for both a novel system and the harm and suffering animals may endure throughout a given study.

### 1.3. ANIMAL ETHICS AND WELFARE IN SCIENTIFIC PROCEDURES

Animals have been used to study anatomy and physiology in lieu of human dissections, which in many ancient cultures was considered taboo, for centuries [325]. Many of these studies were performed as “vivisections”, and made use of live animals [326]. Up until the eighteenth century, ethical and welfare concerns were overshadowed by the perceived view of animals being less sentient than humans and as tools to aid in medical research [327]. At the turn of the eighteenth century and into the nineteenth century, attitudes towards the use of animals in scientific procedures, particularly vivisections, began to change. Amongst the most influential of those opposing inhumane experimentation on or using animals was Jeremy Bentham. As a philosopher, Bentham advocated for the idea of granting animals moral standing as a result of their sentience. His founding philosophical ideas of utilitarianism helped shape the future of animals in scientific research, promoting the idea that animal research is acceptable on the condition that the benefit to human knowledge and medical advancement outweighed the cost of suffering on animals [328]. Bentham’s most famous statement; “The question is not, can they reason? Nor, can they talk? But, can they suffer?”, is one that continues to influence the perceptions and legal legislations of animal ethics and welfare in science to this date [329].

### 1.3.1. UK LEGISLATION AND HISTORY

#### 1.3.1.1. History of animal welfare laws in the UK

The introduction of laws and legislations regarding animal welfare in the UK did not commence until the late 1870s following rising opposition towards vivisections. The National Anti-Vivisection Society, spearheaded by Irish feminist Frances Power Cobbe, opposed the use of animals in scientific procedures so strongly that a Royal Commission was led in 1875 [330]. This led to the introduction of the first legislation regarding animals in science: The Cruelty to Animals Act of 1876. Under this legislation, researchers were now required to justify their experiments on all vertebrate species and demonstrate that the benefit of their research outweighed the cost of harm or suffering caused to any animals used. This legislation remained in effect and unchanged for over 100 years until the introduction of the Animals (Scientific Procedures) Act in 1986, which further required researchers to find suitable alternatives or methodologies in order to minimise harm and suffering caused to animals [331].

#### 1.3.1.2. Animals (Scientific Procedures) Act

The Animals (Scientific Procedures) Act (ASPA) is a UK legislation introduced under the 1986 European Directive 86/609/EEC which permits the use of animals in scientific procedures provided certain criteria are met [332]. In order to comply with the European Directive 2010/63/EU, ASPA was amended in 2012. ASPA is founded on the principles of the three Rs (3Rs) framework of animal research, an idea first proposed by British scientists of the Universities Federation for Animal Welfare (UFAW) William Russell and Rex Burch in 1959 [333]. Although first introduced in the late 1950s, the 3Rs framework of replacement, refinement and reduction did not garner much attention until the 1980s which led to the implementation of European Directive 86/609/EEC in 1986 [331]. While the 3Rs are not explicitly mentioned in the original directive, much of the framework ideology is reflected by the

directive's requirements. This includes avoidance of distress and unnecessary pain or suffering (refinement) and encouragement of use of alternative model systems for all or part of a study (reduction/replacement). The updated directive further expands on the 3Rs principals with improved measures, such as ensuring housing and husbandry needs are met, performing harm-benefit analysis prior to study applications and ensuring ethical reviews are performed when study applications are received. The conditions under which ASPA applies are highly specific, and when ASPA applies researchers cannot perform procedures without acquisition of a number of licences from the UK Home Office.

#### 1.3.1.3. Authorisation of animal studies

Obtaining authorisation to perform scientific studies involving animals in the UK is done so through the UK Home Office. Before applications are to be submitted, researchers must first determine whether ASPA applies and therefore whether or not licences are required to carry out the desired study. ASPA applies if two criteria are met: 1 – the study involves the use of a protected species, and 2 – protected species may undergo regulated procedures. Protected species are defined as any living vertebrate or cephalopod other than man, though the point at which protection begins to apply depends on the lifecycle of the animal in question [334]. As such, commonly used research animals, such as mice, rats, hamsters, guinea pigs, zebrafish and axolotls, are protected under ASPA, usually after two thirds of their gestational period or when able to independently feed. Regulated procedures are defined as any procedure which may cause lasting harm, distress or suffering to a protected species [334]. The threshold of what constitutes a regulated procedure is typically measured as anything equivalent to or exceeding the harm, stress or suffering caused as a result of the insertion of a hypodermic needle according to good veterinary practice. If ASPA applies to a given study, three licences are required from the Home Office to authorise the study to take place, which are applied to person, project

and place. First and foremost, the institution (typically a University or commercial research institute) where the intended study is expected to take place must hold an establishment licence (PEL), which is typically held by an executive individual at the institution such as a Vice-Chancellor or Chief Executive Officer [335]. Secondly, a project licence (PPL) is required to authorise the procedures expected to be carried out on animals placed on a given study [336]. PPLs must also specify the species used in the study and where the study must take place, as well as justify why the study and procedures are being carried out in accordance with the 3Rs. A PPL is typically held by the researcher leading the study, and is typically someone with a strong background in prior research using animal models. Finally, the personal licence (PIL) authorises an individual to carry out regulated procedures on animals as specified in the PPL [337]. All PIL holders are required by law to ensure that they seek and receive the appropriate training and competency checks to ensure that regulated procedures are carried out in a manner consistent with the 3Rs. PPL and PIL licences are subject to review every 5 years by the Home Office in order to regulate and evaluate all research involving animals so as to maintain adherence to the 3Rs and promote a culture of care [338].

### 1.3.2. THE THREE RS AND THE CULTURE OF CARE

The UK is considered one of the leading countries in the world for animal welfare in research, but is also reported to be the largest contributor for procedures carried out on animals by EU member states [338]. The concern over lack of animal welfare particularly in scientific research is one that has only grown over the last few centuries. While there is no one right answer to ensure that all needs or opinions are met, it is paramount that all individuals at each stage of an animal study remain mindful of both the ethical and welfare obligations placed upon them when conducting their research. Attitudes regarding policies, ethics and animal welfare are often impacted by an individual's experience or knowledge of the field. For example, one study found that confidence in

the translational ability of animal models was highest amongst researchers in biological sciences at the University of Wisconsin-Madison, with those in the arts and humanities departments having the least confidence [319]. Even amongst those involved in animal research, there is often a lack of sound understanding or appreciation for the necessities of animal welfare in scientific research. Researchers are often reported to view animals as “tools” to distance themselves from the harm and suffering they may cause to animals, and as a result render themselves desensitised to the basic welfare needs of animals [320]. Some studies have reported that researchers would consider emigrating to other countries if legislations and policies in their own country became too restrictive on the use of animals in research [321].

Current murine COPD models are not authorised to take place in the UK as the harm and suffering caused to mice during WB and NHO CS exposure is deemed too severe and unnecessary. As such, COPD research in the UK is conducted only on *in vitro* systems or using patient samples, which in itself poses its own ethical concerns and does not allow the ability to fully investigate disease pathogenesis. For the sake of producing robust, reliable and reproducible data when using animal studies, it is important that researchers ensure that the model system used can be effectively used by other research groups and reflect human disease. To ensure this, the 3Rs underpins all animal studies in the UK in order to promote what is known as a culture of care. While the definition of the culture of care is conveyed in different ways, the overall aims of the culture of care are to provide an environment where societal expectations of respect and humane attitudes towards animals in research are met [339]. The National Centre for the Replacement, Refinement and Reduction of Animals in Research (NC3Rs) is a UK-based organisation that provides guidance, funding and support both nationally and internationally to researchers using animal models, and is critical in triggering changes in policy, regulations and practice. As part of this, the NC3Rs has led to the development of the Animal Research: Reporting of In Vivo Experiments (ARRIVE) guidelines. These guidelines

are designed to ensure that *in vivo* studies are reported with full transparency to ensure reproducibility and scrutinise methods that may not be in accordance with the 3Rs [340]. Despite these guidelines however, transparent reporting of animal studies has been largely inconsistent, and as such there is still much left to be done when it comes to implementing the 3Rs in research.

#### 1.3.2.1. Replacement

The NC3Rs provide both basic definitions of the 3Rs, as specified by Russell and Burch, and updated definitions based on the context of the 3Rs in modern research practices. Replacement is defined as avoiding or replacing the use of animals in a given study. In the context of scientific practice, this is further elaborated as “accelerating the development and use of predictive and robust models and tools, based on the latest science and technologies, to address important scientific questions without the use of animals” [341]. In other words, if a suitable replacement is available such as a cell line, organ-on-a-chip, or patient material that can effectively address and answer a research hypothesis, then animals should not be used. Replacement is typically considered the main priority of the 3Rs, as partial or total replacement of animals in a given study overall eliminates the potential harm or suffering animals are exposed to. Advances in organ-on-a-chip technology have meant that efforts to replace animals in research are now becoming a reality, whether it be as part of a study or in full [342]. Nonetheless, at current these replacements cannot encapsulate or simulate a whole-body system and are ineffective in the study of complex or whole-body diseases such as COPD [343].

In the context of COPD research, replacement of animal model systems is largely reliant on the use of human participants and samples from COPD patients. However, with growing advancements in *in vitro* and *in silico* technologies, it may be possible in future to conduct pulmonary and COPD research without the use of animals. Total replacement of



animal models for COPD research would eliminate the risks of findings from a given model system not being truly reflective of human disease, as an *in vitro* or *in silico* model could be manipulated and engineered in order to perfectly replicate human disease manifestations [344]. One such example of this is the use of human air-liquid-interface organotypic airway tissue models, which simulate an *in vivo*-like airway system without requiring the use of animals [345].

#### 1.3.2.2. Refinement

Refinement refers to the minimisation of the pain, suffering, distress or lasting harm that animals may experience throughout the duration of a research study. In the context of modern research, refinement may be used to define advancements in animal welfare methodology and technology to minimise the impact of poor welfare conditions on scientific outcomes [341]. This can apply to both techniques related to handling, dosing and sampling of animals, as well as housing and husbandry conditions. An example of refinement relates to the handling practices of mice. Previously, mice were handled by the tail, but recent studies demonstrated the stressful impact this had on mice which ultimately influences study outcomes [346]. As a result, new handling methodologies were developed for mice to minimise stress and improve the quality of both animal welfare and study outcomes [347].

For CS-induced COPD in mice, refinement largely focuses on aspects of CS inhalation and dosing schedules in order to induce COPD. As previously discussed, there are no standardised methodologies to generate COPD in mice, and different research groups typically display slight nuances in their methodologies with regards to exposure method and frequency. The aim of refinement in COPD research seeks to ensure that disease simulation is as reflective of human disease as possible, whilst also ensuring minimal impact to stress and welfare of the animal in question. Comparative studies investigating different CS exposure techniques in murine COPD models highlight the necessity of refining

such model systems, as the resulting COPD phenotype may be the result of exposure to particulate matter via a non-inhalational route [276]. Despite reported concerns regarding these model systems, refinement of CS exposure methodologies and frequencies is often overlooked in favour of using models which have already been widely accepted for use in COPD research [268]. Therefore, there is a significant need to conduct further research to refine current model systems to both improve study animal welfare and applicability to human disease, until such a time that *in vivo* model systems can be fully replaced by nonanimal systems.

### 1.3.2.3. Reduction

Reduction refers to the minimisation of the number of animals used in scientific research, which in the context of modern research refers to ensuring that animal experiments are designed and analysed appropriately for robustness and reproducibility [341]. While reduction may seem like an arduous task, and the use of animals in many studies is often necessary to achieve set aims, there are a variety of methodologies researchers can employ to reduce animal numbers. This includes the use of online or virtual tools for PIL training in techniques to prevent the unnecessary use of animals for training purposes [348, 349]. Additionally, researchers are encouraged to employ multiplexed and highly comprehensive analysis of samples obtained from animals in order to maximise information output without the need for additional animals. Data and sample sharing between research groups is also widely suggested. Despite these efforts however, animals continue to be used widely in research, and there are a number of issues in regards to the 3Rs with most current models of COPD as described above in section 1.2.2.4.

Efforts to reduce the numbers of animals used in COPD research are often as a result of replacement and refinement methods. For example, use of *in vitro* and *in silico* models where an animal model may have been used would naturally result in fewer animals being used as

consequence. Perhaps the greatest example of the need to reduce the numbers of animals used in COPD research comes from the use of preclinical animal models. It is estimated that approximately 7 out of 10 orally inhaled drugs fail to reach the clinic, likely attributed to poor predictive and translational ability of current animal models of COPD [350]. As such, the animals used to both develop and investigate a drug's efficacy have failed to contribute towards the robustness and reproducibility of the given aims of the research, and thus compound the efforts of reducing the numbers of animals used in scientific research. Opting to use *in vitro* or patient samples for COPD research in lieu of animal models, particularly for research on disease pathogenesis, is perhaps the most effective way to reduce the numbers of animals used in COPD research.

#### 1.4. AIMS OF THIS PHD THESIS

COPD presents a significant global burden on health and economic resources and is a leading cause of mortality as specified by the WHO. There is still much left to discover and understand in regards to COPD pathogenesis and persistence, though it is known that the immune system plays a critical role in disease severity. Much of our current understanding of COPD pathophysiology has come from the use of CS exposure murine models, though under current UK legislations these models are considered too inhumane for use. As a result, we aim to develop a novel murine model of CS-exposure COPD that focuses on the 3Rs principle of refinement, to build on and improve current model systems to characterise and identify the immunopathogenic mechanisms of COPD. We anticipate that this new model system will better encapsulate the phenotypic presentations of human COPD without compounding the welfare of animals involved or the quality of science generated, and allow British researchers access to an animal model to study new targets for therapeutic intervention.

## CHAPTER 2 – MATERIALS AND METHODS

### 2.1. MATERIALS

#### 2.1.1. MURINE MODEL

##### 2.1.1.1. Home Office Licences and welfare checks

All procedures were performed under PEL X653228F4 registered to the University of Nottingham, PPL PP5215372 registered to Dr Adam Watkins, and PIL I27390381 registered to Laura Bartlett. All PIL holders were licenced to perform regulated procedures on mice and rats in PIL categories A (minor invasive procedures without anaesthesia), B (minor invasive procedures with anaesthesia (< 15 minutes)) and C (surgical procedures with anaesthesia ( $\geq$  15 minutes)). A study protocol summarising the contents and restrictions of these licences was submitted to the University of Nottingham BioSupport Unit (BSU) in accordance with the standard protocols of the unit (see Appendix A: BSU Study Protocol for a copy of the submitted documentation). Welfare checks were performed using a set of scales to determine weight and observational checks were performed by the primary investigator to determine body condition score according to the guidelines set by the NC3Rs. Weight, body condition scores and other reported details of aberrant health or behaviour were recorded on health monitoring record sheets (1 sheet per animal; see Appendix B: Health Monitoring Record Sheet for an example copy of the monitoring sheet used) which were stored within a ring binder in the mouse holding room alongside the study protocol for ease of access by all investigators and BSU staff.

##### 2.1.1.2. Animals and housing conditions

Twelve 8-week-old male and twelve 8-week-old female (24 total) C57BL/6J mice were obtained from Charles River Laboratories (Strain code 632, Batch Number 25042023-7869, UK) and housed in sex-specific cages (3 males per cage (4 cages) and 4 females per cage (3 cages)) within the University of Nottingham BioSupport Unit (BSU).

Animals were housed under specific pathogen-free conditions and regulated temperature and air control conditions, with a light-dark cycle of 12 hour. Designated procedure rooms separate to housing rooms were used to perform regulated procedures. Due to delays to the study start as a result of staff and space issues, mice did not undergo any regulated procedures until 11-weeks of age.

### 2.1.1.3. Cigarette smoke extract

Phenol-Red Free Roswell Park Memorial Institute (RPMI)-1640 Culture Medium containing 2mM L-glutamine (Cat no. R8755, Merck, UK) was used as the media to generate cigarette smoke extract (CSE). A smoke collection apparatus was used to generate and collect CS. This consisted of plastic piping leading to a three-way stopcock, which was then connected to tubing leading to a 50mL BD Plastipak Polypropylene Disposable Luer-Lok Concentric Tip Syringe (Cat no. SYR6168, Scientific Laboratory Supplies, UK) on one side and tubing leading to a modified 25 mL sterlin tube lid with the tubing attached to allow for easy attachment of the CSE media tube. 1 mL pipette tips with the conical end cut off were used to attach Marlboro Red brand cigarettes (purchased locally from general stores). Generated CSE was sterile filtered to remove large particulate matter using a Sartorius Minisart 0.45 µm Luer Lock Syringe Filter (Cat no. FIL6588, Scientific Laboratory Supplies, UK) and a BD Emerald 10 mL Luer Slip Concentric Tip Syringe (Cat no. SYR1040, Scientific Laboratory Supplies, UK).

### 2.1.1.4. Materials for regulated procedures

Isoflurane (99% Purity) (Cat no. PC2045, Apollo Scientific, UK) was used as the anaesthetic agent during intranasal dosing, mixed with medical grade oxygen (O<sub>2</sub>) supplied by BOC, UK. Anaesthesia procedures were performed using a standard anaesthesia Boyle's trolley with an anaesthesia induction chamber for mice and appropriate scavenger system with fluosorber active charcoal scavenger attached,

these were kindly supplied by the BSU. CSE was administered using a P200 pipette and sterile P200 tips.

Restraint procedures were performed using standard 50 mL Falcon tubes with 1/3 of the conical end cut off using a sterile box cutter or surgical scalpel blade. Sunflower hearts were purchased from Amazon (Garden Ting brand suitable for wild birds and animals). Hibiscrub containing 40 mg/mL chlorhexidine glutamate and sterile gauze pads were supplied by the BSU. Puncture of the lateral caudal vein was performed using either BD Microlance Stainless Steel 25G Hypodermic needles (Cat no. SYR6116, Scientific Laboratory Supplies, UK) or Terumo Agani 25G Disposable needles (Cat no. SYR6247, Scientific Laboratory Supplies, UK) depending on product availability. Vitrex 50 mL End-To-End Capillary Tubes containing sodium heparin (Cat no. 177513, IMS Euro, UK) were used to collect blood, and blood was expelled into 1.5 mL Eppendorf tubes using an in-house modified BD Emerald Disposable Luer Slip Concentric Tip 5 mL syringe (Cat no. SYR1038, Scientific Laboratory Supplies, UK).

For instances where veterinary treatment was necessary as a result of overgrooming, subcutaneous Metacam (0.5 mg/mL oral suspension for cats and guinea pigs) and topical EMLA cream were administered by a Senior Animal Technician under guidance of the Named Veterinary Surgeon (NVS) and Named Animal Care and Welfare Officer (NACWO).

Dolethal 200 mg/mL solution for injection containing pentobarbital sodium as the active ingredient (Vetoquinol, UK) was supplied by the BSU for Schedule 1 cull (intraperitoneal overdose). BD Microlance Stainless Steel 27G Hypodermic needles (Cat no. BD300635, Scientific Laboratory Supplies, UK) and BD Plastipak Disposable Concentric Tip Sterile 1 mL syringes (Cat no. SYR6000, Scientific Laboratory Supplies, UK) were used to perform IP injections.

### 2.1.2. SPECTRAL FLOW CYTOMETRY

#### 2.1.2.1. Cell culture media

RPMI-1640 Culture Medium containing 2mM L-glutamine (Cat no. R6504, Merck, UK) supplemented with Penicillin (100 IU)-Streptomycin (100µg/mL) (Cat no. P0781, Merck, UK), 10 mM HEPES (Cat no. H0887, Merck, UK), and 5% foetal bovine serum (FBS) (Cat no. F7524, Sigma, UK) was used for splenocyte cultures unless otherwise specified.

#### 2.1.2.2. Murine splenocytes and whole blood

Murine spleens and whole blood from cardiac puncture for the validation of analytical methods were kindly provided fresh from mice set for S1 cull by the Watkins lab. Whole blood for examination of systemic effects of CSE was obtained from the lateral caudal veins of mice on PPL PP521573 using the materials specified in section 2.1.1.4.

Splenocytes were isolated from murine spleens using mechanical disruption in a petri dish containing cell culture medium using sterile surgical scissors and the based of a BD Emerald Luer Slip Concentric Tip 5 mL syringe. Cells were isolated from tissue debris using a Falcon 100µm Yellow Cell Strainer for 50mL tube (Cat no. 352360, Scientific Laboratory Supplies, UK). A Countess 3 Automated Cell Counter (Thermofisher, UK) was used to determine cell count. For this, trypan blue and countess disposable slides were used.

Isolated splenocytes were frozen down at  $1 \times 10^7$  cells per mL using FBS and 10% DMSO. Defrosting media comprised of the reagents listed in section 2.1.2.1 plus 10% FBS (as opposed to 5%) and 0.01 U/µL of  $\geq 250$  U/µL benzonase (Cat no. 1016540001, Merck, UK). PMA 5 mg/mL in DMSO (Cat no. P1585, Sigma-Aldrich, UK) and ionomycin 10 mg/mL in DMSO (Cat no. I0634, Sigma-Aldrich, UK) were used for T cell stimulation assays. Lipopolysaccharides (LPS) from *Escherichia coli* O111:B4 1 mg/mL (Cat no. L5293, Sigma-Aldrich, UK) was used for myeloid and granulocyte activation assays.

Splenocytes and whole blood both required the use of a red blood cell (RBC) lysis buffer. For splenocytes a dual RBC Lysis/Fixation buffer was used (Cat no. 422401, Biolegend, UK) and for whole blood a RBC Lysis buffer without fixation was used (Cat no. 420302, Biolegend, UK). A protein transport inhibitor cocktail 500x (Cat No. 00-4980-93, Thermo Fisher, UK) was used to prevent secretion of intracellular markers for intracellular staining. Fc receptors were blocked to prevent non-specific binding of antibodies using a 0.5 mg/mL TruStain FcX (anti-mouse CD16/32) antibody (Cat no. 101320, Biolegend, UK).

#### 2.1.2.3. Flow cytometry antibodies and equipment

Due to the size and high-throughput nature of the 24-colour panel generated for flow cytometry, all flow cytometry was performed using the ID7000 (Sony, UK) available at the University of Nottingham Flow Cytometry Facility. Antibodies were selected and sourced from a number of companies and allowed for the detection of T cells and T cell subsets, NK cells, macrophages, monocytes, neutrophils, DCs and B cells, as shown in table 2.1.1. Where pre-conjugated antibodies were not commercially available, purified antibodies were purchased (table 2.1.1) and appropriate conjugation kits for desired fluorophores were sourced from the providers listed in table 2.1.2.



## CHAPTER 2 – MATERIALS AND METHODS

**Table 2.1.1:- 24-Colour Flow Cytometry panel.** Details of all antibodies including conjugate, brightness (according to supplier's specifications), company purchased from, catalogue number and concentration used during analysis. FOXP3 was dropped from the panel due to staining issues and replaced with CD25 to isolate Treg populations. Purified antibodies were conjugated in-house using fluorophore conjugation kits as detailed in table 2.1.2 below.

<u>Antibody</u>	<u>Fluorophore</u>	<u>Brightness</u>	<u>Clone</u>	<u>Company</u>	<u>Cat No.</u>	<u>Cell Type</u>
<u>CD45</u>	<u>APC-Fire810</u>	1	<u>30-F11</u>	<u>Sony Biotechnology</u>	<u>1115865</u>	<u>Pan-immune cells</u>
<u>CD3</u>	<u>BUV496</u>	2	<u>17A2</u>	<u>BD Biosciences</u>	<u>741117</u>	<u>Pan-T cells</u>
<u>CD4</u>	<u>FITC</u>	3	<u>RM4-5</u>	<u>Sony Biotechnology</u>	<u>1102550</u>	<u>CD4* Helper T cells</u>
<u>CD8a</u>	<u>APC/Cy5.5</u>	3	<u>53-6.7</u>	<u>Abcam</u>	<u>ab82005</u>	<u>CD8* Cytotoxic T cells</u>
<u>RORyt</u>	<u>Purified</u>	-	<u>W19344C</u>	<u>Biologend</u>	<u>603151</u>	<u>Th17 cells</u>
<u>FOXP3</u>	<u>Purified</u>	-	<u>MF-14</u>	<u>Biologend</u>	<u>126401</u>	<u>Tregs</u>
<u>CD25</u>	<u>BV510</u>	3	<u>PC61</u>	<u>Biologend</u>	<u>102042</u>	<u>Tregs/Activated T cells</u>
<u>CD49b</u>	<u>PerCP/Cy5.5</u>	3	<u>DX5</u>	<u>Biologend</u>	<u>108915</u>	<u>NK cells</u>
<u>CD11b</u>	<u>Pacific Blue</u>	1	<u>M1/70</u>	<u>Sony Biotechnology</u>	<u>1106120</u>	<u>Myeloid and NK cells</u>
<u>Lv6G/Lv6C</u>	<u>PE/Cy5</u>	5	<u>RB6-8C5</u>	<u>Sony Biotechnology</u>	<u>1142050</u>	<u>Monocytes, granulocytes and neutrophils</u>
<u>I-A/I-E</u>	<u>PE/Cy7</u>	4	<u>M5/114.14.2</u>	<u>Sony Biotechnology</u>	<u>1138150</u>	<u>MHCII – Antigen presenting cells</u>
<u>F4/80</u>	<u>Purified</u>	-	<u>T45-2342</u>	<u>BD Biosciences</u>	<u>565409</u>	<u>Macrophages</u>
<u>CD163</u>	<u>PE</u>	5	<u>S15049F</u>	<u>Sony Biotechnology</u>	<u>1383515</u>	<u>Monocytes and macrophages</u>
<u>CD169</u>	<u>BV605</u>	4	<u>3D6.112</u>	<u>Biologend</u>	<u>142413</u>	<u>Alveolar macrophages</u>
<u>CD80</u>	<u>BUV661</u>	3	<u>16-10A1</u>	<u>BD Biosciences</u>	<u>741515</u>	<u>DCs, B cells, Monocytes and Macrophages</u>

## CHAPTER 2 – MATERIALS AND METHODS

<b>CD86</b>	<a href="#">BV650</a>	3	<a href="#">GL-1</a>	<a href="#">Sony Biotechnology</a>	<a href="#">1125175</a>	<a href="#">DCs, B cells, Monocytes and Macrophages</a>
<b>CD38</b>	<a href="#">PE/Dazzle 594</a>	5	90	<a href="#">Sony Biotechnology</a>	<a href="#">1113650</a>	<a href="#">B and T cells</a>
<b>CD69</b>	<a href="#">BV785</a>	3	<a href="#">H1.2F3</a>	<a href="#">Sony Biotechnology</a>	<a href="#">1122715</a>	<a href="#">Activated T cells</a>
<b>CCR7</b>	<a href="#">AF647</a>	4	<a href="#">4B12</a>	<a href="#">Sony Biotechnology</a>	<a href="#">1200545</a>	<a href="#">B cells</a>
<b>IFN-<math>\gamma</math></b>	<a href="#">BV421</a>	5	<a href="#">XMG1.2</a>	<a href="#">Sony Biotechnology</a>	<a href="#">3129150</a>	<a href="#">T cells, NK cells and neutrophils</a>
<b>IL-6</b>	<a href="#">PerCP-eFluor 710</a>	4	<a href="#">MP5-20F3</a>	<a href="#">Thermo Fisher</a>	<a href="#">46-7061-82</a>	<a href="#">T cells, B cells and macrophages</a>
<b>IL-17A</b>	<a href="#">BV711</a>	3	<a href="#">TC11-18H10.1</a>	<a href="#">Sony Biotechnology</a>	<a href="#">3134705</a>	<a href="#">Th17 cells, CD8<sup>+</sup> T cells and NK cells</a>
<b>TNF-<math>\alpha</math></b>	<a href="#">BV750</a>	3	<a href="#">MP6-XT22</a>	<a href="#">Biolegend</a>	<a href="#">506358</a>	<a href="#">Macrophages, NK cells and T cells</a>
<b>Zombie</b>	<a href="#">NIR</a>	4	-	<a href="#">Biolegend</a>	<a href="#">423106</a>	<a href="#">Dead cells</a>

**Table 2.1.2:- Conjugation kit details for in-house labelled antibodies.**

Dye:antibody ratio was confirmed via NanoDrop spectrophotometry unless extinction coefficients could not be obtained due to restrictions as a result of proprietary information.

Marker	Fluorophore	Brightness	Company	Cat No.	Dye:Antibody Ratio
<b>ROR<math>\gamma</math>t</b>	<a href="#">PE/Cy5.5</a>	3	<a href="#">Novus Biologicals</a>	<a href="#">761-0005</a>	1:1
<b>FOXP3</b>	<a href="#">NovaFluorBlue 610 70S</a>	3	<a href="#">Thermo Fisher</a>	<a href="#">K06T04 L011</a>	1:1
<b>F4/80</b>	<a href="#">CF568</a>	4	<a href="#">Sigma-Aldrich</a>	<a href="#">MX568S 100-1KT</a>	3:1

#### 2.1.2.4. Intracellular and extracellular staining reagents

Phosphate buffer albumin (PBA) wash buffer was made in-house, consisting of PBS with 30% bovine serum albumin (BSA) (Cat no. A7284, Merck, UK) and 20% Sodium Azide (Cat no. S2002, Merck, UK). Standard PBS was made using deionised water (dH<sub>2</sub>O) and PBS tablets (Cat no. BR0014G, Thermo Fisher, UK,). The solution was sterile-filtered and stored at 4°C. Sterile cell culture-grade pH 7.2 PBS was obtained from Merck (Cat no. P2272, UK) and used to make all solutions that required sterile PBS asides from PBA.

Intracellular staining was performed using an eBioscience FOXP3/Transcription factor fixation/permeabilisation kit (Cat no. 00-5521-00, Thermo Fisher, UK) and fixation buffer for the final fix step was purchased from Biolegend (Cat no. 420801, UK).

Splenocyte assays were performed in Corning Costar Ultra-Low Attachment 96-well plates (Cat no. 7007, Scientific Laboratory Supplies, UK) whilst whole blood assays were performed in 1.5 mL Eppendorf tubes.

#### 2.1.3. REVERSE PHASE PROTEIN MICROARRAY

##### 2.1.3.1. Slides and printing equipment

Nitrocellulose coated slides for array printing were produced in-house using SLS Select Economy 76 x 26 x 1 mm Microscope Slides (Cat no. MIC2000, Scientific Laboratory Supplies, UK) and Amersham Protran Western Blotting nitrocellulose membrane (Cat no. GE10600002, Merck, UK). Nitrocellulose membrane was fixed to slides using adhesive clear polyurethane glue (Gorilla brand purchased locally from general stores) and vacuum sealed during the drying process using a BioRad Model 583 Gel Dryer.

Samples for printing were prepared in Corning 384 well plates (Cat no. CLS3680, Merck, UK) in 4 x 4 arrangements according to grid layout

programs set by a MicroGrid II Microarrayer (BioRobotics). A 4 x 4 pinhead designed for mechanical microspotting was used for printing.

#### 2.1.3.2. Murine tissues

Tissue samples from the heart, liver, kidney, muscle and gonad fat of 5 male mice and spleen samples from a female mouse were kindly provided by the Watkins lab. RAW 264.7 murine macrophages were kindly prepared and provided by Prof Paddy Tighe.

#### 2.1.3.3. Tissue lysis reagents

Lysis buffer was prepared using 10 mL radioimmunoprecipitation assay (RIPA) buffer (Cat no. R0278, Sigma-Aldrich, UK) and contained 2 mM sodium orthovanadate and 2 mM sodium fluoride. Sodium vanadate ( $\text{NaVO}_3$ ) was prepared using 300 – 400 mM sodium orthovanadate ( $\text{Na}_3\text{VO}_4$ )  $\geq$  90% (Cat no. S6508, Sigma-Aldrich, UK) in  $\text{dH}_2\text{O}$ , which was heated until colourless and adjusted to pH 10 using NaOH or HCl. Volume was adjusted for a final concentration of 200 mM (100 x stock solution). Sodium fluoride (NaF) 500 mM was purchased from Sigma-Aldrich (Cat no. 67414, UK).

Round bottom 2 mL Eppendorf tubes (Cat no. E0030120094, Scientific Laboratory Supplies, UK) containing 5 mm stainless steel beads (Cat no. 69989, Qiagen, UK) were used to lyse tissues in a Qiagen TissueLyser II.

#### 2.1.3.4. BCA assay

A Pierce BCA Protein assay kit was purchased from Thermo Fisher (Cat no. 23225, UK) for quantification of proteins following tissue lysis. Plates were read using a Promega GloMax Discover Microplate Reader.

#### 2.1.3.5. Print buffers and staining reagents

2 x concentrated print buffer was prepared in dH<sub>2</sub>O used 4 M betaine monohydrate (Cat no. B2754, Sigma-Aldrich, UK) and 50% 2,3-butanediol (Cat no. B84904, Sigma-Aldrich, UK). Isolated proteins were diluted with dH<sub>2</sub>O and 4x SDS sample buffer (Cat no. 70607, Merck Millipore, UK) in a 96-well half-skirted PCR microplate (Cat no. AXYPECR96M2HSC, Merck, UK) to denature proteins required for printing and validation methodologies using a PCR thermocycler.

Streptavidin-Cy5 1 mg/mL (Cat no. SA-1500-1, Vector Laboratories, UK) and goat anti-human IgG IRDye 680 RD 1 mg/mL (Cat no. 926-68078, Li-Cor, UK) were used as “landing lights” to determine slide orientation during scanning and as an indicator of print quality.

An AF647 conjugated rabbit anti-mouse alpha tubulin 1 mg/mL (Cat no. 5046, Cell Signaling Technology, USA) was used as a primary antibody to test printing and staining efficiency. Biotinylated goat polyclonal anti-rabbit IgG 2 mg/mL (Cat no. B8895, Sigma-Aldrich, UK) was used as a secondary antibody. Streptavidin-Cy5 1 mg/mL and biotinylated goat anti-streptavidin (Cat no. BA-0500-5, Vector Laboratories, UK) were used to test optimal signal amplification. All antibodies were diluted in PBS for staining.

PBS made using the materials listed in section 2.1.2.4 was used to make PBST wash buffer (PBS + 0.05% Tween 20 (Cat no. P1379, Sigma-Aldrich, UK)) and blocking buffer (PBST 0.01% Tween 20 + 3% Skim Milk Powder (Cat no. 70166, Merck Millipore, UK)). Liquid Plate Sealer (Cat no. #160, Candor Biosciences, UK) was used to test efficiency of probe binding. Slide scans were taken using a GenePix 4000b Microarray System.

A full panel of primary rabbit anti-human antibodies against immune signalling pathways involved in COPD pathogenesis were kindly supplied by a previous PhD student. These antibodies were sourced from Cell Signaling Technology (USA) and reported to be cross-reactive with mouse. The targets and details of each antibody are listed in table 2.1.3.

## CHAPTER 2 – MATERIALS AND METHODS

**Table 2.1.3:- Antibody targets used in optimised anti-human RPPA panel.**

All antibodies were obtained from Cell Signaling at 1 mg/mL concentration and tested for cross-reactivity against murine samples. Details of pathways and justifications for inclusion are shown below. (Abbreviations: p – phosphorylated)

Target	Pathway	Justification
<b>Zap-70</b> <b>pZap-70</b>	T cell receptor signalling (via CD3)	Stimulation via $\alpha$ -CD3 and $\alpha$ -CD28 so T cells and NK cells will be activated via this pathway, so does CSE suppress signalling or enhance it?
<b>Erk1/2</b>	T cell receptor signalling (via CD3) MAPK/Erk signalling	As above Signalling to lead to activation and production of perforin
<b>p38 MAPK</b>	T cell receptor signalling (via CD3) MAPK signalling p38 MAP Kinase signalling	As above Signalling to lead to activation and production of perforin
<b>MKK4/7</b> <b>pMKK4/7</b>	T cell receptor signalling (via CD3) JNK Signalling	As above Signalling to lead to activation and production of perforin
<b>JNK</b> <b>pJNK</b>	T cell receptor signalling (via CD3) NKG2D signalling SAPK/JNK signalling	As above Signalling to lead to activation and production of perforin
<b>PDK1</b>	T cell receptor signalling (via CD28)	As above
<b>PI3K</b> <b>pPI3K</b>	T cell receptor signalling (via CD28) Oxidative stress	As above Oxidative stress seen in exposure to CSE will switch on PI3K to lead to accelerated lung aging and inflammation
<b>p65/RelA</b> <b>NFkB</b>	Inflammasome signalling TLR4	Signal 1 Inflammasome signalling (via particulates from CSE) LPS in cigarette smoke activates TLR4 signalling

		- ultimately activates p65 for nuclear shuttle in and out of nucleus
<b>IKK<math>\alpha</math>/IKK<math>\beta</math></b>	Inflammasome signalling (via particulates from CSE)	Signal 1 Inflammasome signalling – LPS in cigarette smoke
<b>Caspase-1 (total and cleaved)</b>	Inflammasome signalling (via particulates from CSE)	Signal 2 Inflammasome signalling – stimulated by particulates in Cigarette smoke
<b>p50 NF<math>\kappa</math>B</b>	Cell activation	All routes lead to NF- $\kappa$ B i.e. Oxidative stress seen in exposure to CSE will switch on PI3K to lead to accelerated lung aging and inflammation
<b>Cathepsins</b>	Inflammasome signalling (via particulates from CSE)	Signal 2 Inflammasome signalling – stimulated by particulates in Cigarette smoke
<b>MKK4/7</b> <b>pMKK4/7</b>	SAPK/JNK signalling cascade	Signalling to lead to activation and production of perforin
<b>Stat1</b> <b>pSTAT1</b>	Key role in many gene expressions that cause survival of the cell, viability or pathogen response	Cell survival as well as response to pathogen
<b>Stat3</b> <b>pStat3</b>	Key role in many cellular processes (such as cell growth and apoptosis)	Increased activity of STAT3 in cancer cells
<b>Perforin</b>	Killing/damage mechanism	Mediator to “punch holes” in target cells/cause tissue damage
<b>Granzyme</b>	Killing/damage mechanism	Mediator to activate Caspase 8 in target cells/cause tissue damage
<b>Caspase 8</b>	Leads to apoptosis	Mechanism to lead to tissue damage
<b>TRAIL</b>	Regulation of apoptosis	Can assist in regulating apoptosis
<b>HSP27</b> <b>HSP70</b> <b>HSP90</b>	Heat shock proteins	Stress related proteins that one might expect to be up-regulated on exposure to CSE

<b>PIP3</b>	NKG2D/DAP10 signalling	Activation pathway for NK cells
<b>Cdc42 or Rac or Rho</b>	NKG2D/DAP10 signalling	Activation pathway for NK cells
<b>SHP-1 or Src</b>	KIR signalling	Inhibition pathway for NK cells
<b>Crk or Abl</b>	KIR signalling	Inhibition pathway for NK cells
<b>p53</b>	Tumour suppressor protein	Protein that regulates cell cycle so does CSE affect its' expression?
<b>Caspase 3</b>	Induces Apoptosis	Cell survival – does CSE increase expression?
<b>SYK</b>	Spleen tyrosine kinase (SYK) has a role in adaptive immune receptor signalling	SYK also mediates other, unexpectedly diverse biological functions, including cellular adhesion and innate immune recognition. SYK is activated by C-type lectins and integrins

#### 2.1.3.6. SDS-PAGE reagents

SDS-PAGE was performed using an XCell Surelock Mini-Cell electrophoresis system. Gels for SDS-PAGE were made in-house using Bolt Mini Gel Cassettes (Cat no. NW2010, Thermo Fisher, UK). Reagents used to prepare gels are listed in table 2.1.4 below. 1.5 M Tris-HCl pH 8.8 and 1 M Tris-HCl pH 6.8 were prepared using Trizma base in dH<sub>2</sub>O and pH adjusted using 6N HCl. 10% Ammonium persulfate (APS) was prepared by adding 1 g of APS to 10 mL of dH<sub>2</sub>O, 20% SDS was kindly prepared and supplied by Tyler Harvey-Cowlishaw. Samples were diluted with dH<sub>2</sub>O and 4 x SDS sample buffer and heated in a thermocycler for denaturation. A 0.3% Bromophenol Blue solution (Cat no. B8026, Sigma-Aldrich, UK) was prepared to improve visibility of wells in stacking gel. 10 x Running buffer was prepared using 25 mM Tris HCl, 200 mM glycine and 0.1% SDS in dH<sub>2</sub>O and diluted to 1x running buffer as necessary. A Broad Range (10 – 250 kDa) Color Prestained Protein



Standard (Cat no. P7719L, New England Biolabs, UK) was used as an estimate of protein size and a Biotinylated Protein Ladder (9 – 200 kDa) (Cat no. 81851, Cell Signaling, USA) was used as a positive control for Western Blot transfer. SimplyBlue SafeStain (Cat no. LC6060, Thermo Fisher, UK) was used to stain gels for viewing. Gel images were taken using a NuGenius Gel Doc Scanner under standard light.

*Table 2.1.4:- List of reagents used to prepare gels for SDS-PAGE.*

Reagent	Cat No.	Supplier	Country
Acrylamide/Bis-acrylamide solution (30%)	A3574	Sigma-Aldrich	UK
Trizma Base	93362	Sigma-Aldrich	UK
Glycine	G8898	Sigma-Aldrich	UK
Ammonium Persulfate	A3678	Sigma-Aldrich	UK
Sodium Dodecyl Sulphate	L3771	Sigma-Aldrich	UK
TEMED	1610800	Bio-Rad	UK

#### 2.1.3.7. Western Blot reagents

Amersham Protran Western Blotting nitrocellulose membrane (Cat no. GE10600002, Merck, UK) was used as a protein transfer membrane. Blot transfer was performed using an XCell Surelock Mini-Cell electrophoresis system containing an XCell II Blot Module. Filter paper and foam pads were kindly provided by Prof Paddy Tighe. Transfer buffer was prepared using Novex 25 x Tris-Glycine Transfer Buffer (Cat no. LC3675, Thermo Fisher, UK) diluted to 1 x using dH<sub>2</sub>O and methanol to obtain a final concentration of 20% methanol. Probing was performed using an Immunetics Miniblotter 16 system (Cat no. S31580, Interchim Biotech, France). Probe antibodies consisted of a selection of

constitutively expressed markers in all tissue types from table 2.1.3 (p50 NFkB, p53, STAT3, SAP/JNK and mTOR). Streptavidin-HRP 1 mg/mL (Cat no. 4800-30-06, RnD Systems, UK) was used for chemiluminescent assays. Chemiluminescent assays were performed using a Novex ECL Chemiluminescent Substrate Reagent Kit (Cat no. WP20005, Thermo Fisher, UK). Chemiluminescent blots were scanned using a SynGene G:Box.

#### 2.1.4. RT-qPCR

##### 2.1.4.1. Primers

Genes were identified in literature and the National Centre for Biotechnology Information (NCBI) website (USA) was used to identify mRNA sequences to be used for primer design. The NCBI Primer Blast tool was used to identify possible primer sequences and the Human BLAT Search website was used to identify exon-exon boundaries and to check primer binding locations. NCBI Standard Nucleotide BLAST suite was used to check for nonspecific binding of primers to ensure amplification of desired target gene. Primer sequences were sent to Eurofins Genomics (Germany) for Oligonucleotide Salt-Free Primer synthesis. Housekeeping gene primers were already available in-house and are detailed in table 2.1.5 below.

**Table 2.1.5:- Primer sequences and details for housekeeping genes. These genes were used to normalise target genes to calculate relative gene expression.**

Gene Name	Primer	Primer Sequence	Tm	GC%	Product Length	Accession Number
SDHA	FWD	TGTTCAAGTCCACCCACA	60	53	66	NM_023281
	REV	TCTCCACGACACCCTTCTGT	60	55		
Tuba1	FWD	CTGGAACCCACGGTCATC	59	61	114	NM_011653
	REV	GTGGCCACGAGCATAGTTATT	59	48		

#### 2.1.4.2. RNA purification kit and equipment

Round bottom 2 mL Eppendorf tubes (Cat no. E0030120094, Scientific Laboratory Supplies, UK) containing 5 mm stainless steel beads (Cat no. 69989, Qiagen, UK) were used to lyse tissues in a Qiagen TissueLyser II. An RNeasy Mini Kit was purchased to isolate RNA from tissues (Cat no. 74104, Qiagen, UK). On-column DNase digestion was performed using an RNase-free DNase Set (Cat no. 79254, Qiagen, UK).

#### 2.1.4.3. Reverse transcription reagents

A TaqMan Reverse Transcription kit (Cat no. N8080234, Thermo Fisher, UK) was used to generate cDNA from isolated RNA. Reverse transcription reactions took place in a PCR thermocycler.

#### 2.1.4.4. Polymerase chain reaction reagents

Precision FAST qPCR Master Mix with ROX at a reduced level, premixed with SYBRgreen (Cat no. PFAST-ABI7500, PrimerDesign, UK) was used as qPCR master mix and RNase-free H<sub>2</sub>O from the Qiagen RNeasy Mini Kit was used as the H<sub>2</sub>O negative control. Samples were loaded into Bright White real-time PCR 96-well plates for ABI FAST and StepOnePlus machines (Cat no. BW-FAST, PrimerDesign, UK) and sealed using Optical adhesive seals (Cat no. BW-ADVSEAL, PrimerDesign, UK). PCRs were run using an ABI Fast 7500 qPCR machine and the resulting data was analysed using a relative gene expression formula template on Microsoft Excel (kindly provided by Dr Adam Watkins) and plotted using GraphPad Prism.

#### 2.1.4.5. Agarose gel electrophoresis reagents

Agarose gel electrophoresis was performed using a ReadyAgarose Precast Gel System (Bio-Rad, UK) and gels were cast in-house using combs appropriate for gel size. Gels were prepared using 1% Agarose (Cat no. 05066, Sigma-Aldrich, UK) and tris-borate-EDTA (TBE) buffer

using a 10 x TBE buffer stock solution (Cat no. 574795, Sigma-Aldrich, UK). GelRed Nucleic Acid stain (Cat no. SCT123, Merck Millipore, UK) was used as a fluorescent nucleic acid stain and a GeneRuler 50 bp DNA Ladder (Cat no. 11813973, Fisher Scientific, UK) was used as an indicator of product size. Gel images were taken using a NuGenius Gel Doc Scanner under UV light.

### 2.1.5. HISTOLOGY

#### 2.1.5.1. Tissue processing

After dissection, tissues for histology were placed into 5 mL bijoux containing 10% formalin (Cat no. HT5012-1CS, Scientific Laboratory Supplies, UK) which were then transferred into 70% ethanol (EtOH). A Leica TP1020 Tissue Processor (Leica Biosystems, UK) was used for tissue processing, and a Leica EG1150 Embedding Station (Leica Biosystems, UK) was used to embed tissues into paraffin wax blocks using Simport embedding cassettes kindly supplied by Dr Jeni Luckett.

#### 2.1.5.2. Microtomy

A Leica 2245 microtome (Leica Biosystems, UK) was used to prepare wax cuttings, which were embedded onto Corning 75 mm x 25 mm microscope slides (Cat no. CLS294875X25, Merck, UK) using a mounting bath.

#### 2.1.5.3. Staining reagents

The following reagents for hydration and dehydration of slides were kindly supplied by the University of Nottingham School of Life Sciences Imaging Facility (SLIM): xylene, EtOH (70%, 80%, 95% and 100%), 1% acid alcohol and Scott's tap water. Harris Haematoxylin Solution (Cat no. HHS128, Sigma-Aldrich, UK) and Eosin Y Solution (Cat no. HT1102128, Sigma-Aldrich, UK) were used for H&E staining. Toluidine blue 1% stain solution (Cat no. 89640, Sigma-Aldrich, UK) was kindly supplied by Dr

Jeni Lockett (University of Nottingham). [Weigert's haematoxylin, Picrosirius red and acidified water were kindly supplied by Dr Amanda Tatler \(University of Nottingham\).](#) Slides were mounted using Hydromount histology mounting media (Cat no. NAT1324, Scientific Laboratory Supplies, UK) and Corning 22 mm x 50 mm cover slips (Cat no. CLS2975225, Merck, UK).

Stained slides were processed using a Zeiss Axioscan 7 Slide Scanner (Zeiss, UK) and corresponding Zeiss Zen Blue software. Image analysis was performed in ImageJ.

## 2.2. METHODS

### 2.2.1. MURINE COPD MODEL

#### 2.2.1.1. Welfare checks and study design

The murine COPD study was designed to ascertain the optimal dosing regimen to elicit a moderate COPD phenotype in mice. For this, mice were exposed to CSE three times per week (Mondays, Wednesdays and Fridays) for 12 weeks. To minimise workload on investigators, mice were split into two groups: Group 1 and Group 2, containing two mice from each dose group and each sex. Group 1 commenced CSE exposure on the first week of the study and had tail vein bleeds performed on Tuesdays, whereas Group 2 did not commence CSE exposure until the second week of the study and had tail vein bleeds performed on Thursdays (figure 2.2.1). As such, each group was culled a week apart to streamline dissection protocols. Weekly tail vein bleeds were performed to examine peripheral immune cell changes in response to CSE exposure, the results of which were also used as a welfare indicator.

Full welfare checks were performed three times per week prior to administration of anaesthesia. This consisted of behavioural examinations (activity levels and interactions with cage-mates) and physical examinations (coat condition, evidence of injury, weight loss, respiratory changes). In particular, mice had their weight recorded three

times per week and respiratory rate closely monitored for signs of increased respiration rate or laboured breathing. In the event of signs of adverse effects, concerns were reported to the designated NACWOs and

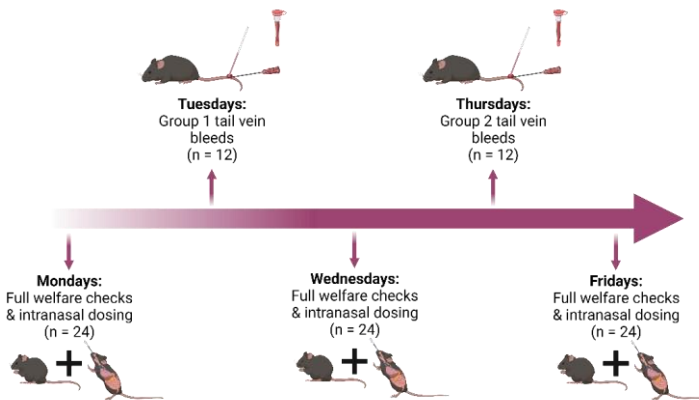


**Figure 2.2.1:- Murine COPD study design protocol.** Full welfare checks and intranasal dosing was performed on all mice three times per week on Mondays, Wednesdays and Fridays. To minimise workload, mice were split into Group 1 and Group 2 and had tail vein bleeds performed on either Tuesdays or Thursdays respectively. (Created with Biorender.com)

veterinary intervention or close monitoring were performed as directed and necessary.

#### 2.2.1.2. Acclimatisation to restraint procedures

In order to minimise the impact of stress on study outcomes, mice were acclimatised to handling and restraint procedures through positive reinforcement (figure 2.2.2). For this, sunflower hearts were used as a reward following handling and restraint. The week before the murine COPD study was due to begin, mice were first introduced to the reward by placing sunflower hearts into home cages. The next day, mice were handled and shown restraint tubes briefly before being returned to their home cages and provided with a reward. On day three, mice were handled and allowed to freely enter restraint tubes before being returned to home cages with a reward, and on day four the same procedure was

repeated but mice were placed into restraint tubes and immediately withdrawn prior to returning to the home cage. On the final day of acclimatisation, mice were placed into restraint tubes and their leg or tail was restrained at the base for up to 30 seconds, after which mice were returned to their home cages with a reward. Positive reinforcement was

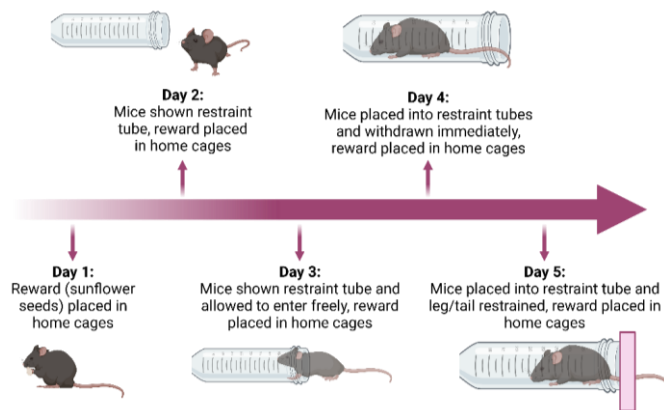


**Figure 2.2.2:- Diagrammatic overview of the restraint acclimatisation procedure.** Mice were acclimatised to handling and restraint procedures during a week-long process, and were rewarded with sunflower hearts following each period of handling or restraint. Following the acclimatisation period, positive reinforcement was maintained through provision of sunflower hearts following regulated procedures. (Created with Biorender.com)

maintained throughout the murine COPD study by providing sunflower hearts following all regulated procedures, thus minimising stress of handling and also encouraging more docile behaviour.

### 2.2.1.3. Calculation of cigarette smoke extract concentration

Due to the novelty of our model system, an optimal dose concentration for cigarette smoke extract (CSE) was not available in the literature. Therefore, to ascertain the appropriate dose concentration to elicit a moderate COPD phenotype, calculations were made to determine the percentage of CSE to be used. This was performed by calculating the number of cigarettes smoked per day per gram of average human weight,

and calculating how many cigarettes smoked per week per average weight of an 8-week-old mouse in percentage form. While this method does not account for factors such as metabolic and lung structure differences, this method provides a crude and justifiable reasoning behind the concentrations mice would be exposed to. As such, the following calculations were performed to determine CSE doses:

$$\begin{aligned}
 & \text{no. cigarettes per day} \div \text{average human weight (kg)} \\
 & \quad = \text{cigarettes per kg} \\
 & \text{cigarettes per kg} \div 1000 = \text{cigarettes per gram (g)} \\
 & \text{cigarettes per g} \times \text{average weight of 8 week old mouse (g)} \\
 & \quad = \text{no. cigarettes per mouse} \\
 & (\text{no. cigarettes per mouse} \times 7) \times 100 \\
 & \quad = \% \text{ of cigarette smoke extract required}
 \end{aligned}$$

According to health statistics from 2019, the average smoker in the UK smoked 10 cigarettes per day [351]. To determine optimal dose concentration, we opted to use two different CSE concentrations based on the median number of cigarettes smoked per day by the average UK smoker  $\pm$  5. As such, 5 cigarettes per day (35 per week) was classified as “Light-smoker” (LS) and 15 cigarettes per day (105 cigarettes per week) was classified as “Heavy-smoker” (HS). Average weights of UK men and women were obtained from the Health Survey for England 2021 [352] and average weights for 8-week-old male and female C57BL/6J mice were obtained from the Jackson Laboratories [353]. Using this information, the following calculations were made:

$$\begin{aligned}
 & \text{Light Smoker Males:} \\
 & 5 \div 84.5 = 0.05855 \text{ cigarettes per kg} \\
 & 0.05855 \div 1000 = 0.00005855 \text{ cigarettes per g} \\
 & 0.00005855 \times 25 = 0.001464 \\
 & (0.001464 \times 7) \times 100 = 1.02 \%
 \end{aligned}$$



*Light Smoker Females:*

$$\begin{aligned}5 \div 72.1 &= 0.06935 \text{ cigarettes per kg} \\0.06935 \div 1000 &= 0.00006935 \text{ cigarettes per g} \\0.00006935 \times 20 &= 0.001387 \\(0.001387 \times 7) \times 100 &= 0.97 \%\end{aligned}$$

*Heavy Smoker Males:*

$$\begin{aligned}15 \div 84.5 &= 0.17564 \text{ cigarettes per kg} \\0.17564 \div 1000 &= 0.00017564 \text{ cigarettes per g} \\0.00017564 \times 25 &= 0.004391 \\(0.004391 \times 7) \times 100 &= 3.07 \%\end{aligned}$$

*Heavy Smoker Females:*

$$\begin{aligned}15 \div 72.1 &= 0.20804 \text{ cigarettes per kg} \\0.20804 \div 1000 &= 0.00020804 \text{ cigarettes per g} \\0.00020804 \times 20 &= 0.0041608 \\(0.0041608 \times 7) \times 100 &= 2.91 \%\end{aligned}$$

Using these values, it was determined that 1% CSE would be appropriate for the LS groups and 3% CSE would be appropriate for the HS groups.

#### 2.2.1.4. Generation of cigarette smoke extract

CSE was generated in-house fresh on assigned dosing days (3 x per week). For this, 10 mL of phenol red-free RPMI was added to a 25 mL sterilin tube and attached to the CSE apparatus as shown in figure 2.2.3. The end of a 1 mL pipette tip was cut off to improve airflow and attached to tubing at the top of the apparatus, to which a single Marlboro

Red cigarette with the filter broken off was attached. The cigarette was lit and a 50 mL syringe was used to draw in cigarette smoke, which was then used to expel the smoke into the sterilin tube. A three-way stopcock was used to control the direction of airflow, and the apparatus was designed to simulate human respiration and inhalation/exhalation of cigarette smoke. This process was repeated until the full cigarette had been smoked, and the resulting medium was classified as 10% CSE (1 cigarette per 1 mL of media = 100% CSE). 10% CSE was sterile filtered into a clean 25 mL sterilin tube through a 0.45 µm filter to remove large debris, and the resulting filtrate was then used to create 1% and 3% CSE in a total volume of 1 mL using phenol red-free RPMI. A separate 1.5 mL

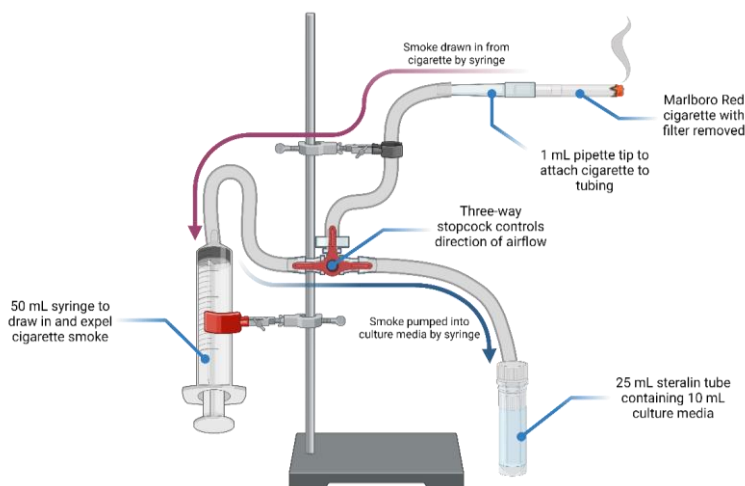


**Figure 2.2.3:- Diagrammatic overview of CSE generation apparatus.** Smoke is drawn in from a Marlboro Red cigarette with the filter removed using a 50 mL syringe (as demonstrated by the dark pink arrow), which is then used to slowly pump smoke into a 25 mL sterilin tube containing 10 mL of phenol red-free RPMI-1640 culture media (as demonstrated by the dark blue arrow). Airflow direction is controlled by use of a three-way stopcock. (Created with BioRender.com)

Eppendorf tube containing 1 mL of sterile phenol red-free RPMI was used as a control for the “Never Smoking” (NS) group. Tubes containing CSE were temperature and pH checked and maintained at room temperature and neutral pH in preparation for intranasal dosing.

#### 2.2.1.5. Intranasal dosing

Prior to intranasal (IN) dosing, a full welfare check was performed on mice to check for signs of ill health or welfare concerns (see section 2.2.1.6 for details). After conducting welfare checks, mice were placed into an anaesthesia chamber on a cage-by-cage basis. Mice were first exposed to 2.5% isoflurane mixed with O<sub>2</sub> until sedated and loss of righting reflex occurred. After this, mice were placed onto their sides to monitor respiration rate and isoflurane was increased to 3.5%. Respiration rate was monitored until deep respiration (gasping mechanism) was observed, after which mice were individually removed from the chamber and held in an upright position with the head tilted back to open airways. 25 µL of CSE or control media was carefully administered into the nasal cavity using a P200 pipette and the mouse was kept in an upright position until the dose had been inhaled and respiratory rate stabilised. Mice were then returned to their home cages for recover, after which the anaesthetic chamber was purged of isoflurane in preparation for the next cage. When all mice had regained consciousness, a brief welfare check was conducted to detect signs of ill health following anaesthesia and sunflower hearts were placed into the cage to reinforce acclimatisation to handling and restraint procedures. Mice were under anaesthesia for ≤ 15 minutes in accordance with Category B anaesthesia protocols, and recovery following brief anaesthesia was approximately ≤ 2 minutes. Figure 2.2.4 provides a graphical demonstration of the IN dosing protocol.

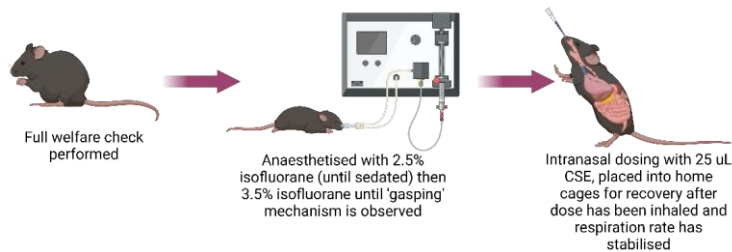


**Figure 2.2.4:- Intranasal dosing of CSE in mice.** Full welfare checks were performed prior to administration of anaesthesia, after which mice were placed into an anaesthetic chamber and exposed to 2.5% isoflurane until sedated. After sedation and lack of righting reflex, isoflurane was increased to 3.5% until deep respiration (gaspings mechanism) was observed. Mice were then individually removed from the chamber and 25  $\mu$ L CSE was carefully administered through the nasal cavity using a P200 whilst the mouse was held in an upright position to ensure delivery into the respiratory system. Once the full dose was inhaled and respiratory rate had stabilised, mice were returned to their home cages for recovery. (Created with Biorender.com)

#### 2.2.1.6. Tail vein blood sampling

Tail vein blood sampling was performed once per week, and in accordance with the Laboratory Animals in Science Association (LASA) and NC3Rs guidelines for microsampling [354, 355]. Body temperature water was mixed with hibiscrub in a small beaker to encourage vasodilation and sterilise the puncture area. Mice were placed into restraint tubes and restrained at the base of the tail, which was placed into the beaker for 30 seconds. After this, the tail was wiped dry with a sterile gauze pad and the lateral caudal vein was located. The lateral caudal vein was punctured using a 25G needle approximately 2/3 distance from the base of the tail. Blood was gently massaged out of the vein and 20  $\mu$ L was collected using a heparinised capillary tube, one mouse each week had 30  $\mu$ L collected so that an unstained control was available. In accordance with microsampling guidelines, mice that had 30  $\mu$ L collected only had 20  $\mu$ L collected within a given 4-week period. After blood was collected, it was expelled into 1.5 mL Eppendorf tubes using a modified syringe and pressure was applied to the puncture site on the

tail using sterile gauze pad. Once bleeding had stopped, mice were returned to their home cages and rewarded with sunflower hearts to reinforce acclimatisation to restraint and handling procedures. Figure 2.2.5 provides a graphical example of this protocol.

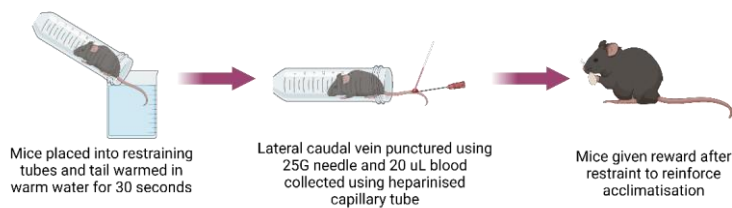


**Figure 2.2.5:- Tail vein blood sampling of mice.** Mice were placed into restraint tubes and the tail was warmed in body temperature water with hibiscrub for 30 seconds, after which the tail was wiped dry. The lateral caudal vein was punctured using a 25G needle and 20  $\mu$ L blood was collected using a heparinised capillary tube. After bleeding had stopped, mice were returned to their home cages and given sunflower hearts to reinforce acclimatisation. (Created with Biorender.com)

#### 2.2.1.7. S1 cull and dissection

Following 12 weeks of CSE exposure, mice were culled by intraperitoneal (IP) overdose of anaesthetic using dolethal. Mice were first weighed and 100  $\mu$ L dolethal per 10 g of weight was drawn into a 1 mL syringe using a sterile 27G needle, which was then disposed and replaced with a new sterile 27G needle. Mice were scruffed and injected intraperitoneally into the left side of the abdomen (as viewed ventrally) to avoid accidental injection into the caecum. Following administration of the full dose of dolethal, mice were placed into a spare cage and monitored to allow the IP overdose to take effect. Upon loss of the pedal withdrawal reflex and detectible heartbeat (checked via placing the index and middle fingers on either side of the chest) and visual signs of permanent cessation of respiration (defined as observation of Cheyne-Stokes respiration followed by permanent arrest of the respiratory system), mice were removed from the cage and death was confirmed via

laceration of the femoral artery (cessation of blood circulation). Once death was confirmed, the lungs and spleen were collected for histological, genetic and immunological analysis. The testes, epididymis, ovaries and uterus were collected for histological and genetic analysis by the Watkins lab, and the caecum was collected by request of Dr Jeni Lockett for microbiome analysis.

### 2.2.2. SPECTRAL FLOW CYTOMETRY

#### 2.2.2.1. Generation of panel and antibody selection

Markers for flow cytometry were identified through literature searches and resources available via the Biolegend website. To determine appropriate fluorophore designation, the Gene Expression Atlas was used to determine the expression levels of each marker in the periphery and the lungs [356]. Immune cell frequencies in mouse were obtained using a resource on the BioRad website [357]. A panel design tool was kindly provided by Sony Biotechnology that automatically calculated the R-squared values of fluorophores and spectral patterns within a given panel to determine the spillover matrix of each fluorophore. Markers that were lowly expressed in both the periphery and lungs were assigned to bright fluorophores whilst highly expressed markers were assigned to dim fluorophores. Markers with variable expression as a result of effector functions or tissue origin were assigned to moderate fluorophores. Where an R-squared value above 0.7 was detected between two fluorophores using the panel designer tool, alternative fluorophores were selected to ensure accurate unmixing during analysis.

Once markers and fluorophores had been assigned, antibodies were purchased from suppliers (see table 2.1.1). For antibodies with pre-conjugated fluorophores were not available, purified antibodies and conjugation kits were purchased for the necessary antibodies and fluorophores (see table 2.1.2). Antibodies were conjugated to fluorophores according to the protocols outlined by each conjugation kit

and dye to antibody ratio was determined using a NanoDrop Spectrophotometer [358-360].

Conjugation of ROR $\gamma$ t antibody was performed using a Lightning-Link PE-Cy5.5 labelling kit. Briefly, for every 10  $\mu$ L of antibody, 1  $\mu$ L of modifier reagent was added and mixed gently by pipetting. Modified antibody was then added to a PE-Cy5.5 conjugation mix and mixed by pipetting before being left to incubate in the dark for 3 hours. Following incubation, 1  $\mu$ L quencher per 10  $\mu$ L antibody was added and mixed gently. Dye to antibody ratio was determined to be 1:1 by NanoDrop Spectrophotometer.

Conjugation of F4/80 antibody was performed using a Mix-n-Stain CF568 labelling kit. Briefly, the 10 x mix-n-stain buffer was diluted to 1 x using purified F4/80 and mixed by pipetting. The mixed solution was then added to a vial containing dye solution and vortexed briefly before being incubated in the dark for 15 minutes. Following incubation, the conjugated antibody was diluted in storage buffer containing 2 mM sodium azide and dye to antibody ratio was determined to be 1:3 by NanoDrop Spectrophotometer.

Conjugation of FOXP3 antibody was performed using a NovaFluor Blue610 70S conjugation kit. Briefly, spin columns in 2 mL collection tubes from the kit were centrifuged for 1 minute at 1500 g and the eluent was discarded. 300  $\mu$ L reaction buffer was added to spin columns for buffer exchange and centrifuged for 1 minute at 1500 g. Buffer exchange was repeated three times for a total of four buffer exchanges. Following the fourth exchange, one spin column was set aside after discarding the eluent, whilst another was transferred to a 1.5 mL Eppendorf tube. 100  $\mu$ L of FOXP3 antibody was added to the spin column and centrifuged at 1,500 g for 2 minutes, after which the spin column was discarded. The buffer exchanged antibody was then added to a tube of activation reagent and mixed by pipetting. The tube was vortexed and mixed by inversion, which was repeated twice over the course of 1 minute, after which the tube was centrifuged at 1,500 g for 30 seconds. The antibody solution was then left to incubate for 1 hour at room temperature, after which the

spin column that was set aside was spun for 1 minute at 1,500 g and placed into a 1.5 mL Eppendorf tube after discarding the eluent. The antibody solution was then transferred to the spin column and centrifuged for 2 minutes at 1,500 g, after which the spin column was disposed of. The activated antibody solution was transferred to a tube of NovaFluor Linker, vortexed and mixed by inversion before being centrifuged briefly for 30 seconds at 1,500 g and left to incubate overnight at room temperature. After overnight incubation, 80  $\mu$ L PBS was added to the antibody solution and mixed by pipetting. 200  $\mu$ L ammonium sulphate was then added and mixed by pipetting up and down 10 times and left to incubate on ice for 10 minutes. After incubation, the tube was centrifuged for 5 minutes at 13,500 g, after which the supernatant was carefully removed using a pipette. The pellet was resuspended in 200  $\mu$ L PBS and ammonium sulphate washing was repeated. After the second wash with ammonium sulphate, the pellet was resuspended in 100  $\mu$ L PBS and 300  $\mu$ L NovaFluor conjugate was added to the antibody solution. The solution was vortexed and mixed by inversion before being centrifuged for 30 seconds at 1,500 g and left to incubate overnight at 4°C in the dark. Due to proprietary restrictions, dye:antibody ratio could not be determined via NanoDrop Spectrophotometry, but the manufacturer advised that conjugation would yield a 1:1 ratio.

#### 2.2.2.2. Isolation, activation and staining of murine splenocytes

Murine spleens were acquired from mice scheduled for cull at the BSU, where the spleens would have otherwise gone to waste. Splenocytes were isolated via mechanical disruption, this was performed by cutting spleens using sterile surgical scissors and grinding tissue in a petri dish containing 3 mL RPMI + 5% FBS using the plunger of a 5 mL syringe until only fibrous tissue remained. The media was then carefully poured into a 50 mL falcon tube through a 100  $\mu$ M mesh cell strainer. The petri dish was then washed twice with 4 mL RPMI + 5% FBS and added to the falcon tube through the cell strainer. The resulting media was then centrifuged for 10 minutes at 200 g (3↑ 3↓) and the supernatant



was discarded. The cell pellet was resuspended in 20 mL RPMI + 5% FBS and centrifuged again under the same settings before discarding the supernatant. The cell pellet was then resuspended in 10 mL RPMI + 5% RPMI and a cell count was performed to determine number of cells per mL. The resuspended cells were centrifuged for 10 minutes at 200 g (3↑ 3↓) before being resuspended in FBS + 10% DMSO at a concentration of  $1 \times 10^7$  cells per mL. Cells were then transferred to cryotubes in 1 mL aliquots and stored in liquid nitrogen until use.

Frozen splenocytes were defrosted by warming in a water bath set at 37°C until a small amount of ice remained. 2 vials of splenocytes from the same mouse were slowly diluted in 20 mL defrosting media using a Pasteur pipette and then centrifuged for 10 minutes at 500 g (3↑ 3↓). Cells were then resuspended in 20 mL fresh defrosting media and incubated for 1 hour at 37°C. After incubation, a cell count was performed to determine the number of cells per mL and the cells were centrifuged under the same settings as before. Cells were then resuspended in resuspension media at approximately  $8 - 10 \times 10^6$  cells per mL. For activation, splenocytes were either exposed to 100 ng/mL LPS (macrophage/granulocyte/DC activation) or 25 ng/mL PMA and 1 µg/mL ionomycin (T cell activation) for between 6 – 48 hours. For intracellular staining, a protein cocktail inhibitor was added during the last 4 hours of activation to prevent secretion of cytokines. 10 µg/mL Fc receptor block was added during the last 30 minutes of incubation to prevent nonspecific binding of antibodies. All incubation took place in a sterile incubator at 37°C. After incubation was finished, cells were topped up with 10 mL RPMI + 5% FBS and centrifuged for 10 minutes at 500g (3↑ 3↓), and were then resuspended in resuspension media at a concentration of  $8 - 10 \times 10^6$  cells per mL. For intracellular staining, splenocytes were washed twice with 2 mL perm wash buffer for 5 minutes at 350 g (3↑ 3↓) before being added to 96-well plates for staining.

Serial dilutions of antibodies ranging from 1:10 to 1:1280 in a 25  $\mu$ L volume were prepared in PBA in a 96-well low bind plate. Following incubation, 6  $\mu$ L splenocytes (approximately 48 – 50,000 cells) was added to each well and the plate was incubated at room temperature in the dark for 20 minutes. An unstained control containing 50  $\mu$ L PBA and 12  $\mu$ L splenocytes and single colour controls for unmixing were prepared in FACS tubes and incubated in the same manner as the plate. After incubation, 225  $\mu$ L RBC lysis/fixation buffer was added to each well of the plate and 350  $\mu$ L was added to the FACS tubes, which were then incubated for 15 minutes at room temperature in the dark before being analysed using the Sony ID7000. Figure 2.2.6 below provides a diagrammatic overview of the splenocyte isolation and staining protocol without activation or intracellular staining.

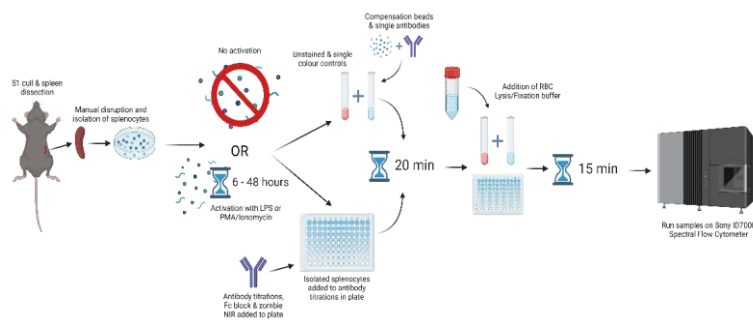


**Figure 2.2.6:- Diagrammatic protocol for splenocyte isolation and antibody titrations.** (Created with BioRender.com)

### 2.2.2.3. Gating strategies

Cell gating was performed in FlowJo, in all instances, cells were first gated according to their forward scatter area (FSC-A) and side scatter area (SSC-A) profiles. Following this, singlets were isolated using FSC-A against forward scatter height (FSC-H), after which live cells were gated according to cells stained negative for ZOMBIE-NIR. Specific gating strategies are presented in Chapters 3 and 4.

#### 2.2.2.4. Whole blood staining

Whole blood staining was performed immediately after tail vein bleeds were performed (see section 2.2.1.6). After transferring whole blood to 1.5 mL Eppendorf tubes, a protein transport inhibitor was added to each sample and incubated for 3.5 hours at 37°C, after which an Fc receptor block was added. After a further 30 minutes of incubation at 37°C, 1 mL of a RBC lysis buffer was added and samples were left to incubate at room temperature for 5 minutes. Following incubation, samples were centrifuged for 5 minutes at 350 g (3↑ 3↓) in a microcentrifuge, after which supernatants were discarded and cells were resuspended by gentle tapping. 1 mL of PBA was added to each tube and the samples were washed and the supernatant was discarded. Utilising the stain index data generated, the cells were resuspended in 50 µL of extracellular panel master mix using the concentrations shown in table 2.2.1. Samples were incubated at room temperature in the dark for 20 minutes, after which cells were washed with 1 mL PBA. Samples were then resuspended in 1 mL fix/perm working solution after supernatants were discarded, and left to incubate for 30 minutes at room temperature in the dark. Following incubation, cells were washed twice with 1 mL perm wash buffer and then resuspended in 50 µL of intracellular panel master mix (table 2.2.1). Samples were left to incubate for 20 minutes at room temperature in the dark, after which they were washed twice with 1 mL perm wash buffer. Cells were resuspended in 500 µL fixation buffer and transferred to FACS tubes and either analysed immediately using a Sony ID7000 or stored overnight at 4°C in the dark for analysis the following day. Figure 2.2.7 demonstrates this protocol in graphical format.

CHAPTER 2 – MATERIALS AND METHODS

Table 2.2.1:- Extracellular and intracellular antibody panels for whole blood staining.

Cell Marker	Fluorophore	Cell Type	Concentration (µg/mL)
<b>Extracellular Panel Master Mix</b>			
CD45	APC-Fire810	All haematopoietic cells	2
CD3	BUV496	T cells	2
CD4	FITC	CD4 <sup>+</sup> T cells	0.5
CD8a	APC/Cy5.5	CD8 <sup>+</sup> T cells	1
CD25	BV510	T cell activation/Tregs	5
CD49b	PerCP/Cy5.5	Pan NK cells	2
CD11b	Pacific Blue	Myeloid and NK cells	0.5
Ly6G/Ly6C	PE/Cy5	Monocytes/Granulocytes	2
I-A/I-E	PE/Cy7	MHC II, APCs	0.2
F4/80	CF568	Macrophages	5
CD163	PE	Macrophages/Monocytes	0.2
CD169	BV605	Alveolar/Splenic macrophages	0.2
CD80	BUV661	Monocytes/B cells/DCs	2
CD86	BV650	Monocytes/B cells/DCs	2
CD38	PE/Dazzle 594	B cells, activation	0.5
CD69	BV785	T cell activation	4
CCR7	AF647	B cells, activation	10
Zombie	NIR	Live/Dead stain	1
<b>Intracellular Panel Master Mix</b>			
RORγt	PE/Cy5.5	Th17 subset	5
IFN-γ	BV421	T cells/NK cells/Neutrophils	2
IL-6	PerCP-efluor 710	T cells/B cells/Macrophages	2

IL-17A	BV711	Th17/CD8 <sup>+</sup> T cells/NK cells	2
TNF- $\alpha$	BV750	Macrophages/NK cells/T cells	2

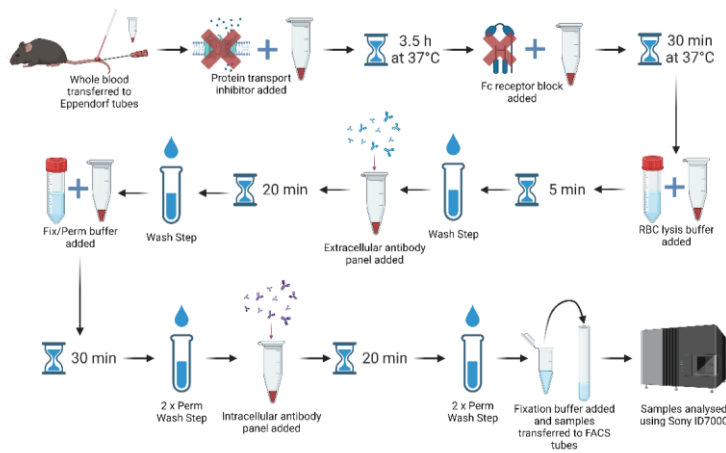


**Figure 2.2.7:- Diagrammatic protocol for whole blood staining for peripheral immune cell phenotyping. (Created with BioRender.com)**

### 2.2.3. REVERSE PHASE PROTEIN MICROARRAY

#### 2.2.3.1. Slide manufacture

24 glass slides were arranged into a BioRad Model 583 gel dryer and a sheet of nitrocellulose membrane was cut to size enough to cover three quarters of each slide. Painter’s tape was applied to the outer edges of the arrangement to hold the slides in place. The nitrocellulose membrane was adhered to the slide arrangement using polyurethane glue and was vacuum sealed overnight to allow adhesion to take place. Slides were then carefully removed from the arrangement and excess nitrocellulose was trimmed from the edges of the slide using a scalpel blade. Slides were then stored in a slide box within a vacuum sealed container until ready for use to preserve the nitrocellulose membrane.

#### 2.2.3.2. Tissue lysis

Frozen tissues collected from 5 male mice from a previous study by the Watkins lab were donated in addition to one female spleen from a mouse removed from a current study due to presence of a congenital birth defect. Approximately 30 mg (between 25 mg to 35 mg) of each tissue was excised and placed into a round bottom Eppendorf tube containing 300  $\mu$ L lysis buffer and a steel bead. Tubes were homogenised using a Qiagen TissueLyser II for 2 minutes at 23 Hz, after which the adapters were reversed and homogenisation was repeated to ensure uniform homogenisation across samples. This was repeated until tissue samples were fully homogenised. The steel beads were removed from the tubes and centrifuged at 14,000 g for 15 minutes at 4°C. Supernatants were then transferred into new 1.5 mL Eppendorf tubes and spun again under the same settings. This process was repeated until supernatants appeared clear and free of any large clumps or noticeable debris. The resulting samples were then stored at -80°C until use.

#### 2.2.3.3. BCA assay and protein concentration

BCA assays were performed using a Pierce BCA Protein Assay kit according to the manufacturer's directions [361]. Standards were prepared as specified by the kit using a BSA standard as shown in table 2.2.2. Working reagent was prepared using reagents A and B according to the manufacturer's directions. 25  $\mu$ L of each standard or sample and 200  $\mu$ L of working reagent was added to a 96 well plate, left to mix on a plate shaker for 30 seconds and then incubated at 37°C for 30 minutes. The plate was then left to briefly cool before being read on a Promega GloMax Discover Microplate Reader at 560 nm. The resulting readings were oversaturated with proteins and exceeded the limits of the standard curve, and the assay was therefore repeated using a dilution series of each sample in PBS ranging from 1:100 to 1:3200 to determine the optimal dilution factor to accurately calculate the protein concentrations in each sample. The assay was then repeated using an optimal dilution

factor of 1:50 for the tissue samples in a volume of 0.3 mL. Readings from the unknown samples were analysed against a standard curve from known standards using the standard curve interpolation function on Graphpad Prism (line, robust fit). The resulting data was then multiplied by 50 to account for the dilution factor to calculate the protein concentration in the undiluted stocks. Protein yield was calculated using the following equation:

$$\begin{aligned} & \text{Protein concentration} \times \text{volume of stock} \\ & = \text{total protein} \div \text{tissue weight} = \text{yield} \end{aligned}$$

The resulting protein concentrations were used to calculate the dilutions required for a minimum of 2 mg/mL required for optimal printing, the yield was used to indicate the minimum weight of sample required to achieve sufficient protein concentration for analysis. Samples were transferred into a 96 well PCR plate at 2 mg/mL by diluting with dH<sub>2</sub>O and 30 µL 4 x SDS to a total volume of 120 µL. The PCR plate was heated at 90°C for 2 minutes to denature proteins, and was then cooled, sealed with foil and placed into a -20°C freezer until ready for use.

*Table 2.2.2:- Standard curve dilutions using a Pierce BCA Protein Assay kit.*

Vial	PBS Vol (µL)	BSA Vol (µL)	BSA Conc (µL/mg)
A	0	300 stock	2000
B	125	375 stock	1500
C	325	325 stock	1000
D	175	175 vial B	750
E	325	325 vial C	500
F	325	325 vial E	250
G	325	325 vial F	125
H	400	100 vial G	25
I	400	0	0

#### 2.2.3.4. Printing and staining optimisation

Individual samples for printing were prepared on a 384-well plate with a 1:1 dilution of 2 x print buffer arranged in a 4 x 4 well grid to comply with printing pins. Landing lights consisting of streptavidin-Cy5 and goat anti-human IgG IRDye 680 RD were loaded into the twenty-third and twenty-fourth quadrants to be used as landing lights. Each array was printed with 8 replicates and landing lights were printed in each outer corner to define grids and slide orientation.

For wash optimisation, the printed slides were scanned at 635 nm using a GenePix 4000b Microarray System to determine print quality, before being washed in PBST to determine optimal wash time to remove autofluorescence and debris. Slides were washed for either 30 minutes or 1 hour, with PBST being changed approximately every 10 minutes and were scanned again to determine effect of washing.

To determine optimal staining and signal amplification protocols, six printed slides were placed vertically into slide cassettes and an in-house 3D printed cassette holder sufficient so that aqueous solutions ran slowly down the nitrocellulose membrane. The conditions tested consisted of no amplification, 1 x amplification and 2 x amplification, and each amplification level was either treated with or without liquid plate sealer. 480  $\mu$ L blocking buffer was first added and the slides were left to block for 1 hour, before being washed three times in PBST. Three slides were then dipped into liquid plate sealer and allowed to air dry before moving on to the next step. 240  $\mu$ L of rabbit anti-mouse  $\alpha$ -tubulin antibody was added at a concentration of 1.25  $\mu$ g/mL and left to incubate for 1 hour. The slides with no amplification were then washed once in PBS for 5 minutes before being rinsed briefly in dH<sub>2</sub>O and spun dry using a slide centrifuge at 1200 rpm for 3 minutes. The remaining four slides were washed three times with PBST. To perform signal amplification, 50  $\mu$ L streptavidin-Cy5 at a concentration of 0.5 ng/mL was added and left to incubate for 20 minutes in the dark. 1 x amplification slides were washed once in PBS for 5 minutes and spun dry after being rinsed briefly in dH<sub>2</sub>O as described above. The remaining plates were washed three times with



PBST, then 50  $\mu$ L of biotinylated anti-streptavidin antibody was added and left to incubate in the dark for 30 minutes. Slides were washed three times in PBST and a second round of 50  $\mu$ L streptavidin-Cy5 was added before incubating in the dark for 20 minutes. After incubation, slides were washed once in PBS for 5 minutes, rinsed with dH<sub>2</sub>O and spun dry before being scanned at 635 nm using a GenePix 4000b Microarray System.

#### 2.2.3.5. SDS-PAGE

Isolated proteins from murine heart, spleen and RAW 264.7 macrophages at a final concentration of 2 mg/mL each were used for SDS-PAGE. Gels were prepared in an empty Bolt cassette held upright using an in-house 3D printed cassette holder. 10 mL of 10% resolving gel was prepared in a 25 mL sterilin tube using 3.4 mL dH<sub>2</sub>O, 4 mL 30% acrylamide, 2.5 mL 1.5 M Tris-HCl pH 8.8 and 50  $\mu$ L 20% SDS. Immediately before pouring into the cassette, 100  $\mu$ L 10% APS and 10  $\mu$ L TEMED were added and the tube was gently mixed by inverting. The solution was poured into 3/4 of the cassette and a thin layer of 50% 2,3-butanediol was laid over the gel solution to maintain an even gel surface. The gel was left to set for approximately 30 minutes at room temperature. During this time, 4 mL of 6% stacking gel was prepared in a new 25 mL sterilin tube using 2.7 mL dH<sub>2</sub>O, 0.8 mL 30% acrylamide, 0.5 mL 1 M Tris-HCl pH 6.8, 20  $\mu$ L 20% SDS and 40  $\mu$ L 0.3% bromophenol blue. Once the resolving gel was set, the butanediol was poured off and the gel surface was washed briefly with dH<sub>2</sub>O and carefully blotted dry. Immediately before adding to the cassette, 40  $\mu$ L APS and 4  $\mu$ L TEMED were added to the solution, which was gently inverted to mix before being poured into the cassette. A 12-well comb was placed into the top of the cassette and the gel was left to set for 30 minutes at room temperature.

Samples were mixed with 4 x SDS sample buffer sufficient to obtain protein concentrations of 2 mg/mL in a volume of 20  $\mu$ L per sample using 0.5 mL PCR tubes. Samples, along with protein ladder standards, were

then heated in a thermocycler at 95°C for 5 minutes and briefly centrifuged to remove droplets from the lids.

After the stacking gel had dried and the protective strip was removed, the gel cassette was placed into an XCell Surelock Mini gel electrophoresis system with the wells facing the inner section of the tank. A plastic block was added on the opposite side in the event that only one gel cassette was used, and the cassettes were locked into place. Running buffer was added to the inner section of the gel tank sufficient to cover gel wells, and also added to the outer section up to the bottom of the wells. The comb was carefully removed from the gel cassette and the inner portion of the tank was topped up with running buffer to ensure wells were sufficiently covered if necessary. The full volume of prepared samples was added to each well, and 20 µL protein standard ladder was added to the wells at either end of the gel. The gel tank was then plugged in and set to run for 1 hour 45 minutes at 125 V constant. Expected current was 40 mA until samples were run through the stacking gel, after which current dropped to 10 mA.

Once complete, the gel was either used for staining to visualise protein bands (if using colour pre-stained protein ladder) or for Western Blot (if using biotinylated protein ladder) (see section 2.2.3.6). For staining, the cassette was carefully opened and the gel was removed from the cassette after trimming away the stacking gel and any excess resolving gel. Staining was performed using the SimplyBlue SafeStain microwave method. After transferring the gel to heatproof container with 100 mL dH<sub>2</sub>O, the container was heated in a 1000 W microwave for 1 minute or until the solution almost boiled. The gel was then agitated on an orbital plate shaker for 1 minute before the dH<sub>2</sub>O was discarded and replaced with a fresh 100 mL and heated again. This procedure was repeated once more, and after the final wash with dH<sub>2</sub>O, 20 mL of SimplyBlue was added to the container and it was heated until the solution almost boiled. The gel was then agitated for 10 minutes on an orbital plate shaker. After this, the gel was washed in 100 mL dH<sub>2</sub>O for 10 minutes on an orbital plate shaker, after which it was incubated in 20

mL 20% NaCl solution for 5 minutes. After the final incubation, the gel was imaged using standard light settings in a NuGenius Gel Doc Scanner.

#### 2.2.3.6. Western Blot

Following SDS-PAGE, gels using the biotinylated protein standard were carefully removed from cassettes after trimming away stacking gel and excess resolving gel. The gel was immersed in transfer buffer for 10 minutes for equilibration. Whilst the gel was equilibrating, nitrocellulose membrane was cut to size with the top right corner notched to indicate membrane orientation, and soaked in transfer buffer for 5 minutes. The transfer stack was assembled in an XCell II Blot Module from the cathode (-) side to the anode (+) side. For this, filter papers and foam pads were soaked in transfer buffer and stacked according to figure 2.2.8 below, ensuring bubbles between layers were removed using a blot roller:

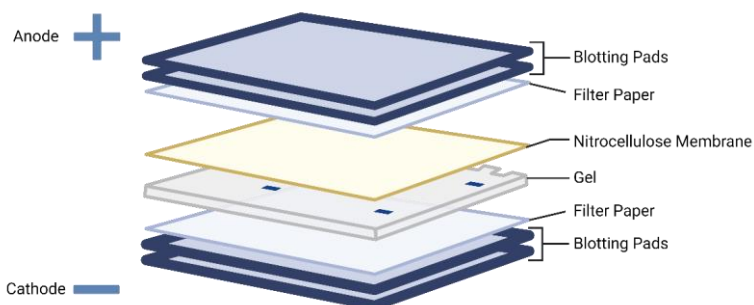


**Figure 2.2.8:- Transfer stack assembly using XCell II Blot Module.** (Created with BioRender.com)

Once the transfer stack was assembled, the blot module was closed and placed into an XCell Surelock Mini gel electrophoresis system in the correct orientation to ensure transfer from the cathode side to the anode side. Transfer buffer was added to the blot module sufficient to cover the transfer stack and dH<sub>2</sub>O was added to the outer tank up to 2 cm below

the top of the blot module to dissipate heat. The transfer was then run for 2 hours at 25 V constant with an expected current of 100 mA.

Once the transfer was complete, the nitrocellulose membrane was carefully removed from the transfer stack and placed into a container with blocking buffer and incubated with agitation for 1 hour. During this time, probing antibodies were diluted to 1 µg/mL in PBS and streptavidin-HRP was diluted to 25 µg/mL in PBS. After blocking, the blot membrane was washed in PBST and placed into a Miniblotter 16. 200 µL of probing antibodies were added to each chamber on the miniblotter and was left to incubate for 20 minutes with gentle agitation. After incubating, the membrane was washed for 5 minutes with PBST and removed from the miniblotter into a container with streptavidin-HRP solution for 20 minutes with agitation. Following incubation, the membrane was washed with PBST and placed onto a sheet of A4 projector film. Equal parts of reagent A and reagent B from the Novex Chemiluminescence kit were mixed and 2 mL was added to the surface of the blot membrane. The projector film was carefully folded over the top of the blot membrane to remove air bubbles and to ensure the chemiluminescent solution covered the entire surface of the membrane. The membrane was then exposed under blacklight in a SynGene G:Box for 5 – 15 minutes and images were taken accordingly.

#### 2.2.4. RT-qPCR

##### 2.2.4.1. Target gene identification

Target genes were identified from those encoding for markers from the RPPA panel or by using GWAS of COPD to select genes of interest suggested to have an association with COPD pathogenesis. Murine orthologues to human genes were identified from the NCBI website and used for primer design.

#### 2.2.4.2. Primer design

To design primers, mRNA sequences for genes of interest were identified using the NCBI website. Where multiple splice variants were reported, the most common or validated splice variants were used as a basis for primer generation. Mouse BLAT search was used to identify exon-exon boundaries within identified sequences, and this information was input into Microsoft Word. The NCBI Primer Blast tool (which functions using Primer3) was then used to generate suitable primer pairs for the target gene using its accession number from the NCBI database. Ideal primers were selected based on their melting temperatures ( $T_m$ ) being within the range of 59 – 61°C (optimum 60°C) and forward and reverse primer melting temperatures being within 1°C of each other. Ideal guanine-cytosine (GC) content range was between 50 – 55%, though for some primers this was not possible due to sequence nature. All primers were designed to span exon-exon junctions so that only mRNA encoding portions were amplified. After the primer pair was selected, the forward primer sequence was searched for in the mRNA sequence placed into word and highlighted to identify where in the sequence it would bind. For the reverse primer, reverse complement was performed on the sequence and the resulting sequence was identified in the mRNA sequence in the same way as the forward primer. The resulting sequence between the forward and reverse primers was checked to ensure that an exon-exon junction was either spanned or included in the product sequence. Finally, the sequences of the forward and reverse primers were searched for on the Nucleotide BLAST suite to check for any nonspecific binding of primers to other gene targets. Where potential amplification of nonspecific genes was likely, primers were redesigned using the same steps as above. Once primer sequences were obtained, their details were sent to Eurofins Genomics for primer manufacture. After primers were obtained, each primer was reconstituted in RNase-free H<sub>2</sub>O to the volumes specified on the datasheets provided by Eurofins in order to obtain concentrations of 100 pmol/μL per primer. Primers were then diluted 1:100 in a total volume of 200 μL with RNase-free H<sub>2</sub>O, then

forward and reverse 1:100 dilutions were added 1:1 in a total volume of 100  $\mu$ L ready for use in PCR reactions. These mixtures were stored at -20°C until use.

#### 2.2.4.3. RNA isolation and reverse transcription

Murine spleens for validation of primers were kindly provided by mice from the Watkins group, whereas the right inferior lobe of the lungs was excised from mice on the COPD study. To extract RNA for reverse transcription, a Qiagen RNeasy mini kit was used and all procedures were performed on ice unless specified. ~30 mg of tissue was placed in a round bottom 2 mL Eppendorf tube containing a 5 mm steel bead and 600  $\mu$ L of buffer RLT from the mini kit. Samples were lysed using a Qiagen TissueLyser II at 23 Hz for 2 minutes, after which the adaptors were reversed and lysis repeated to ensure uniform homogenisation. This was repeated until tissues were sufficiently homogenised, after which samples were centrifuged at max speed for 3 minutes. Supernatants were removed and placed into new 1.5 mL Eppendorf tubes, after which 600  $\mu$ L of 70% EtOH was added and the samples were mixed by gentle pipetting. 700  $\mu$ L of each sample was added to an RNeasy Mini spin column in a 2 mL collection tube and centrifuged for 15 seconds at 8000 g.

After discarding the flow-through, an on-column DNase digest was performed using a Qiagen RNase-free DNase Set. 350  $\mu$ L of buffer RW1 was added to the spin column and samples were spun for 15 seconds at 8000 g, after which the flow-through was discarded. 10  $\mu$ L DNase stock I solution per sample was added to 70  $\mu$ L buffer RDD per sample and mixed gently by inversion and briefly centrifuged to remove droplets from the lid. 80  $\mu$ L of the DNase I incubation mix was added directly onto the RNeasy column membrane and left to incubate for 15 minutes at room temperature (25°C). After incubation, 350  $\mu$ L buffer RW1 was added to each spin column and samples were centrifuged for 15 seconds at 8000 g. The flow-through was discarded and 500  $\mu$ L buffer RPE was added to

spin columns before centrifuging for 15 seconds at 8000 g and the flow-through was discarded. Another 500  $\mu$ L buffer RPE was added to each column and centrifuged for 2 minutes at 8000 g, after which the spin columns were placed into new collection tubes and centrifuged at max speed for 1 minute to dry the membranes. Spin columns were transferred to new 1.5 mL collection tubes and 30  $\mu$ L RNase-free H<sub>2</sub>O was added directly to the spin column membrane. Samples were centrifuged for 1 minute at 8000 g to elute RNA, after which the resulting flow-through was used on a NanoDrop spectrophotometer to determine RNA concentrations and 260/280 values.

For reverse transcription, 1  $\mu$ g of RNA was required for optimal synthesis of cDNA. Reverse transcription was performed using a TaqMan Reverse Transcription kit using a 40  $\mu$ L mixture per reaction. A master mix of reverse transcription reaction reagents was prepared sufficient for the number of samples + 10% using the volumes listed in table 2.2.3. Negative controls including a no reverse transcription control (NRT) and no template control (NTC) using the same reaction mixture as shown in table 2.2.3 were also prepared. The multiscribe enzyme was substituted for RNase-free H<sub>2</sub>O for the NRT and all RNA was substituted for RNase-free H<sub>2</sub>O for the NTC. RNA was diluted to 1  $\mu$ g in 0.5  $\mu$ L PCR tube a total volume of 15.4  $\mu$ L RNase-free H<sub>2</sub>O, to which 24.6  $\mu$ L of reverse transcription reaction master mix was added (table 2.2.3). Each tube was vortexed to mix the reaction and placed into a thermocycler using a cycle program as detailed in table 2.2.4. After reactions were complete, 160  $\mu$ L RNase-free H<sub>2</sub>O was added to each sample for a final concentration of 5 ng of cDNA per sample, and tubes were stored at -20°C until use.

## CHAPTER 2 – MATERIALS AND METHODS

**Table 2.2.3:- Reverse transcription reagent master mix dilutions.** For negative controls, multiscribe was substituted for RNase-free H<sub>2</sub>O (no reverse transcription (NRT)) and only RNase-free H<sub>2</sub>O was added instead of 1 µg RNA (no template control (NTC)).

Reagent	Concentration	Volume per Reaction (µL)
10 x Buffer	-	4
MgCl <sub>2</sub>	25 mM	8.8
dNTPs	2.5 mM each	8
Random Hexamers	50 µM	2
RNase Inhibitor	20 U/µL	0.8
Multiscribe	50 U/µL	1
Reaction Master mix	-	24.6
RNA + H <sub>2</sub> O	-	15.4
<b>Total</b>	1 µg RNA	40

**Table 2.2.4:- Cycle steps and conditions for reverse transcription generation of cDNA.**

Cycle Step	Temperature (°C)	Time (minutes)	Purpose
1	25	10	Primer annealing
2	48	30	DNA polymerisation
3	95	5	Deactivation of multiscribe enzyme
4	4	Indefinite	Prevents degradation of cDNA after reaction has stopped



## 2.2.4.4. Polymerase chain reaction

PCRs were performed in triplicate in 96-well PCR plates for ABI FAST machines. A master mix of reagents necessary for PCR reactions was calculated for the number of wells required (+ 10%) using the reagents and volumes listed below in table 2.2.5. 9  $\mu\text{L}$  of PCR master mix was added to each well using reverse pipetting, and 1  $\mu\text{L}$  of cDNA or control sample was added to the corresponding wells according to a predefined plate map. The plate was then sealed with an optical adhesive seal from PrimerDesign and briefly spun in a benchtop plate spinner to ensure all reagents were in the bottom of the wells. The plate was then run on an ABI Fast 7500 qPCR machine using a standard protocol to measure  $\Delta\Delta\text{Ct}$  output using SYBR green reagents in a 10  $\mu\text{L}$  volume reaction. The cycle steps and conditions used in this protocol are shown below in table 2.2.6.

*Table 2.2.5:- Polymerase chain reaction reagent master mix dilutions. All reagents minus cDNA were prepared in 1.5 mL Eppendorf tubes, and cDNA was added directly to PCR plates.*

Reagent	Volume per Reaction ( $\mu\text{L}$ )
<b>SYBR Master Mix (2 x)</b>	5
<b>1:1 FWD/REV Primer mix</b>	0.35
<b>RNase-free H<sub>2</sub>O</b>	3.65
<b>cDNA (added directly to plate)</b>	1
<b>Total</b>	10

*Table 2.2.6:- Cycle steps and conditions for polymerase chain reaction.*

Cycle Step	Time (seconds)	Temperature (°C)
Pre-cycle	20	95
Extension cycle (x 40)	3	95
	30	60
Melt Curve cycle	15	95
	60	60
	15	95
	15	60

#### 2.2.4.5. Agarose gel electrophoresis

For agarose gel electrophoresis, gel chambers were prepared in non-spill trays. 1 g of agarose per 100 mL of TBE was used to prepare 1% agarose gels, the volume of which was dependent on the size of the gel chamber used. The solution was prepared in a conical flask, which was microwaved at 400W for approximately 2 minutes until the agarose had dissolved. 5  $\mu$ L of Gel Red per 100 mL of gel was added to the solution and gently mixed before adding to the gel chamber with combs and dams in place and allowed to set (approximately 30 minutes at room temperature). During this time, samples were mixed 1:1 with 2 x loading dye. After the gel had set, dams were removed and the chamber was placed into a gel tank so that samples would run from the cathode (-) to the anode (+). 1 x TBE was poured over the gel to cover it and the combs were removed. 6  $\mu$ L of GeneRuler 50 bp DNA ladder was added to the first and last lanes of the gel, and 12  $\mu$ L of each sample was added to the remaining lanes. The gel was then run for 45 minutes at 100V and then visualised under UV light using a NuGenius Gel Doc Scanner for image capture.

### 2.2.5. HISTOLOGY

#### 2.2.5.1. Tissue processing and microtomy

Following dissection, tissues were placed in 5 mL 10% formalin solution overnight before being transferred to 70% EtOH. Tissues were then placed into cassettes and processed using a Leica TP1020 Tissue Processor overnight using a standard protocol for fixation, dehydration and processing in formalin, 70%, 80%, 95% and 100% EtOH, xylene and paraffin wax. Processed tissues were then embedded in paraffin wax blocks using an embedding station and left to solidify, after which sections were cut at 10 µm using a microtome. Three sections per slide were mounted and allowed to dry overnight, after which slides were placed into storage in a slide box until ready for staining.

#### 2.2.5.2. H&E staining

In order to perform staining, slides were deparaffinised and rehydrated by soaking in xylene for 15 minutes before being dipped consecutively in 100% EtOH, 95% EtOH, 80% EtOH and 70% EtOH. The slides were then washed in slow running water for approximately 2 minutes, after which they were submerged in Harris haematoxylin solution for 5 minutes. Following incubation, slides were washed under running water, differentiated by submerging in 1% acid alcohol for 5 seconds and then submerged in Scott's tap water for 2 minutes. After this, the slides were placed into an eosin solution for 2 minutes. Slides were then briefly rinsed in running water before being dehydrated by dipping consecutively into 70% EtOH, 80% EtOH, 95% EtOH and 100% EtOH and finally soaked in xylene for 5 minutes. Slides were then mounted using Hydromount and 22 x 50 mm cover slips and left to dry overnight in preparation for imaging.

#### 2.2.5.3. Toluidine blue staining

Consecutive sections following on from those used for H&E staining were used for toluidine blue staining to allow for comparison between

sections and staining types. Slides were first deparaffinised, as above. 1% toluidine blue solution was then added to each slide using a Pasteur pipette and left to stain for approximately 2 minutes, after which slides were washed three times gently with dH<sub>2</sub>O. Slides were then dehydrated and mounted as above, and left to dry overnight in preparation for imaging.

#### 2.2.5.4. Picrosirius red staining

Consecutive sections following on from those used for H&E and toluidine blue staining were used for picrosirius red staining to allow for comparison between sections and staining types. Slides were first deparaffinised as described in section 2.2.5.2. Slides were then submerged in Weigert's haematoxylin for 8 minutes before being rinsed in running tap water for 5 minutes. The slides were then stained in a solution of picrosirius red for 1 hour, followed by two washes with acidified water for 3 minutes per wash. Water was removed from each slide by vigorous shaking, and the slides were then dehydrated and mounted as described in section 2.2.5.2 and left to dry overnight in preparation for imaging.

#### 2.2.6. DATA AND STATISTICAL ANALYSIS

##### 2.2.6.1. Minimisation of bias according to ARRIVE guidelines

In order to minimise bias, random allocation of mice to treatment groups and blinding of samples was conducted according to the ARRIVE 2.0 guidelines where possible [340]. For group allocation and to ensure group sizes were consistent, block randomisation was used according to each cage of mice. Given that females were housed in groups of 4, each cage was randomly assigned to NS, LS or HS conditions based on a random number generator (1 – NS, 2 – LS, and 3 – HS). Males were housed in groups of 3, as such were assigned based on the random order in which they were removed for ear notching, with a maximum of 2 mice in the same cage assigned to one treatment group and the remaining third mouse assigned to a different random group based on a random

**Formatted:** Font: 10 pt

**Formatted:** Justified, Indent: First line: 1 cm, Space Before: 6 pt, After: 6 pt, Line spacing: 1.5 lines

number generator. Given the novelty of the study and to ensure adverse welfare effects could be detected easily, all investigators and BSU staff were aware of which treatment group individuals belonged to.

Flow cytometry analysis could not be blinded due to potential issues of samples being unable to be traced back to the original individual, and only one investigator was available to conduct the necessary techniques. For histological analysis, images were randomly named by Zeiss ZenBlue image capture software and identifying label was hidden during image analysis by the same software. Once regions of interest and histological analysis techniques had been performed, the identifying label of each sample was unhidden and data was assigned to the relevant individual.

#### 2.2.6.2. Stain index calculations

Histograms were generated for each antibody dilution to identify negative and positively stained cell populations. The positive and negative peaks were defined using the bisector tool in FlowJo and median and standard deviation statistics were applied to the negative peak. Median statistics were applied to the positive peak. Statistical data for each dilution factor was then exported to Microsoft Excel and stain indexes were calculated using the formula shown in figure 2.2.9. Stain index values were then plotted as a standard curve in GraphPad Prism to determine the optimal dilution factor for each antibody. This was defined as the point at which the standard curve plateaued or where positive and negative populations could be clearly distinguished according to SSC-A and FSC-A profiles.

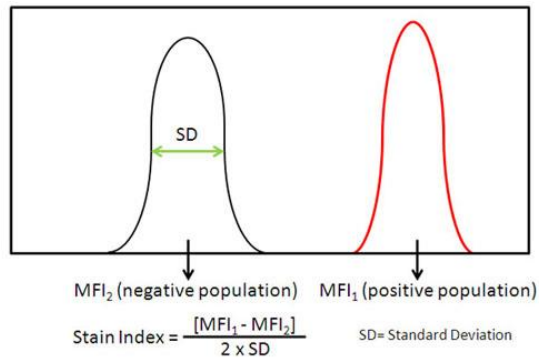


**Figure 2.2.9:- Diagrammatic example of how to calculate stain index.** Histograms created using FlowJo and were analysed using the bisector tool to discriminate positive and negative peaks similar to the example shown above. Median and standard deviation statistics were applied to the negative population whilst only the median was applied to the positive in order to generate the values required to calculate stain indexes according to the formula shown above. (Figure taken from Biolegend.com)

### 2.2.6.3. Interpretation of longitudinal data

Longitudinal data from weekly tail vein bleeds was plotted according to the percentage of cell type or marker expressed by cell type as a total percentage of all immune cells. Total peripheral immune cells were defined as live singlet CD45+ cells. Data was plotted as a linear XY graph in GraphPad Prism  $\pm$  standard error. As event counts were highly variable and, in some instances, low, statistical analysis was not performed and the data was instead presented in a manner designed to determine potential trends or areas for future investigation.

### 2.2.6.4. Clustering analysis

Multi-dimensional clustering analysis was performed on all cell populations isolated from whole blood (T cells, NK cells, macrophages, monocytes, neutrophils, DCs and B cells) using all markers included in the flow cytometry panel (see table 2.2.1). Single viable cells were first gated in FlowJo before equal sampling of events from males and females

Formatted: Normal, No bullets or numbering

from control, light-smoker and heavy-smoker groups. Due to analysis requiring equal numbers of subjects per group, and the male control group comprising only of three individuals instead of four, clustering analysis was performed using three subjects per group. Analysis was performed in FlowJo using FlowSOM clustering and presented using t-distributed stochastic neighbour embedding (tSNE) plots. Statistical analysis was performed by 2way ANOVA.

#### 2.2.6.5. Relative gene expression

Relative gene expression was calculated using the double delta Ct ( $\Delta\Delta Ct$ ) method [362]. This was performed using the following equation:

$$\text{Relative Quantification} = 2^{-\Delta\Delta Ct}$$

Where:  $\Delta\Delta Ct = \Delta Ct(\text{test samples}) - \Delta Ct(\text{calibrator samples})$

$\Delta Ct(\text{test samples}) = Ct(\text{target gene in test}) - \Delta Ct(\text{reference genes in test})$

$\Delta Ct(\text{calibrator samples})$

$= Ct(\text{target gene in calibrator})$

$- \Delta Ct(\text{reference genes in calibrator})$

Given that the input concentration of cDNA was the same for all samples, three random wells were selected to act as the calibrator in the above equation. Calibrator location assignment was uniform across all PCR plates and spanned two samples (A12, B1, B2). RefFinder was used to determine the stability of housekeeping genes, which were then used to normalise data and quantify relative gene expression (figure 2.2.10) [363]. According to RefFinder results, Tuba1 and SDHA were selected as housekeeping genes for normalisation factor (NF). Geomeans were calculated for housekeeping genes using the  $2^{-\Delta\Delta Ct}$  values of housekeeping genes for each sample, which were then divided by the total geomean of all  $2^{-\Delta\Delta Ct}$  values across both genes and all samples to provide the NF. Rescale means were then used to calculate rescaled individual values for each gene of interest (GOI). This was performed using the following equation:

Formatted: Normal, No bullets or numbering

$2^{-\Delta\Delta Ct(GOI)} \div NF = \text{normalised gene}(NG)$   
*average of NGs across dose groups*  
 $\div$  *average of NGs of control groups (male or female)*  
 $=$  *rescale mean (RM)*  
 $NG \div RM = \text{relative gene expression}$

Relative gene expressions were then plotted as a heat map in GraphPad Prism.

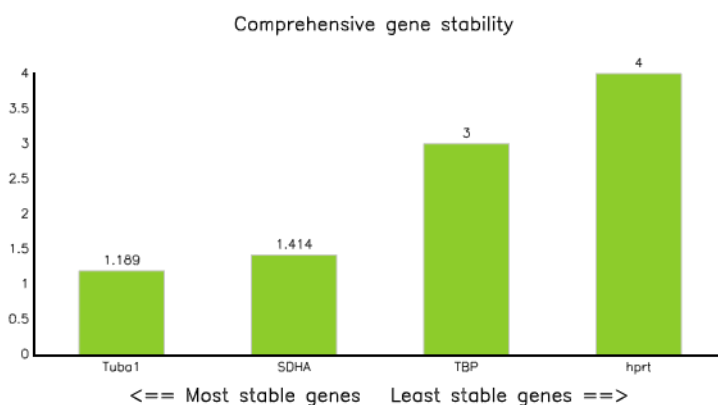


**Figure 2.2.10:- Comprehensive gene stability of housekeeping genes using RefFinder.** Based on the results, the most stable genes (*Tuba1* and *SDHA*) were used for normalisation and calculation of relative gene expression.

#### 2.2.6.6. Histology imaging and analysis

Following staining procedures, slide images were captured at 20x objective using a Zeiss AxioScan 7 Slide Scanner and 500 x 500  $\mu\text{m}$  regions of interest were exported from Zeiss ZenBlue software for analysis in ImageJ. Neutrophil cell counts and general analysis of cellular influx was performed using 500 x 500  $\mu\text{m}$  regions from the middle region of the left lung lobe containing alveoli and at least one major airway vessel (bronchus or bronchiole) in addition to one or more major or minor blood vessels. Neutrophil cell counts were performed manually. For mean linear intercept analysis, five random 500 x 500  $\mu\text{m}$  regions of

Formatted: Font: Cambria Math

Formatted: Font: Cambria Math

Formatted: Font: Cambria Math

Formatted: Font: Cambria Math

Formatted: Font: Cambria Math

Formatted: Normal, No bullets or numbering

Formatted: No bullets or numbering

Formatted: Heading 4



interest from the left lung lobe (2 from the inferior region, 2 from the middle region and 1 from the upper region) containing only alveoli were selected for each mouse and the degree of airway remodelling was measured using the mean linear intercept plugin for ImageJ [364]. The average alveolus diameter was then calculated from the resulting measurements and exported into Prism where data was analysed for statistical differences using a 2way ANOVA.

#### 2.2.6.7. Power calculation

A power analysis was performed using pilot study data to determine the required sample size to adequately detect expected differences between control and disease groups in future experiments. This was performed using mean linear intercept, lung neutrophil count and total peripheral immune cell count data from never-smoker mice and heavy-smoker mice. Male and female data was pooled together and mean difference and standard deviation for each of these parameters was calculated per group. Mean difference was calculated by subtracting the mean values of the never-smoker group per parameter from that of the heavy-smoker group for each respective parameter. Effect size was determined by standardising the mean difference by the pooled standard deviation of both groups to give a measure of the magnitude of effect (Cohen's d).

Power calculations were then conducted to determine the minimum sample size required to achieve a desired power level of 0.9 (90%) with a significance level  $\alpha = 0.05$ . This was performed using the SamplePower function in SPSS as a two-tailed test. Power calculations were not performed using longitudinal data due to the complexities of performing statistical analysis on repeated measures, and was also not performed using RT-qPCR data due to concerns regarding primer binding efficiency.

**Formatted:** Heading 4, Outline numbered + Level: 4 + Numbering Style: 1, 2, 3, ... + Start at: 1 + Alignment: Left + Aligned at: 1 cm + Indent at: 2 cm

**Formatted:** Indent: First line: 1 cm

## CHAPTER 3 – VALIDATION OF ANALYTICAL TECHNIQUES

### 3.1. INTRODUCTION

In the design of animal models, reduction is typically achieved through collaborative efforts to ensure animals or animal-derived samples do not go to waste, or through the use of high-throughput analytical techniques to maximise data output of available samples. Since COPD is known to have a number of pathological mechanisms ranging from immune cell mechanisms to genetic mechanisms, it is important to design panels and use appropriate analytical techniques to investigate pathological markers of choice without unnecessary use or waste of both whole animals or animal-derived samples.

Flow cytometry is an analytical technique commonly used in immunological studies to investigate both cell populations and effector functions, with its capabilities evolving significantly alongside technological advancements. Using flow cytometry, investigators are able to detect and gather data on multiple markers from a single sample, the limit of which is determined depending on the laser and detector capabilities of a given machine. Conventional flow cytometry employs a one laser – one detector principle, and uses dichroic mirrors and band pass filters in order to capture fluorescent wavelengths emitted by fluorophores using point detector photomultiplier tubes (PMTs) [365]. Because this method is only able to capture and analyse data based on the peak of emission of a fluorophore, conventional flow cytometry limits the number of markers in a given panel as fluorophores with similar or the same emission wavelengths cannot be used in tandem. Spectral flow cytometry is a higher-throughput methodology employing similar principles to conventional flow cytometry, but makes use of different detector techniques. Rather than using mirrors and point detectors, spectral flow cytometry functions by using prisms or gratings which disperse wavelengths and are captured using detector arrays, therefore allowing for the measurement of the entire emission spectra for a given

fluorophore across all laser lines. This allows the user to discern between fluorophores with overlapping emission wavelengths as markers are differentiated, or “unmixed”, based on their spectral pattern as opposed to their peak emission. Since fluorophores with similar emission wavelengths can be used in tandem (providing their spectral patterns are distinct enough from one another), spectral flow cytometry allows for the development of high-throughput multiparameter panels that would otherwise be limited under conventional flow cytometry conditions [366].

Given the high-throughput nature of spectral flow cytometry, it is important to ensure that panels are fully optimised so that researchers can be assured they are isolating the correct analytes [367]. Such optimised panels are published as Optimised Multicolour Immunofluorescence Panels (OMIPs) to provide researchers with the details of available panels for either use or as a basis to develop novel panels. Many spectral flow cytometry panels are typically designed with ten or more markers, with forty markers considered the limit [366]. Despite this, the large majority of published OMIPs are for human samples, and those designed for mouse samples are typically intended for specific tissue or cell types [368-370]. Even those that are considered more broad in their scope require the use of two separate panels to fully characterise desired cell populations [371]. It is unclear precisely why murine panels are less characterised or available than those of human panels, especially given that there is no shortage of available anti-mouse fluorescent antibodies designed specifically for flow cytometry. A possible explanation could be that there may be some difficulty in the translational ability of a mouse panel to that of human disease, as murine cells may express different cell markers or markers in different intensities under normal conditions in comparison to human cells [372]. Despite this, analysis by a broad flow cytometry panel allows for the identification of potential cell subsets or effector functions in a mouse model which may be of interest when using human samples, thus allowing highly in-depth panels to be used in humans to fully characterise an identified mechanism of disease pathology.

Whilst comprehensive flow cytometry panels for mice are somewhat lacking, techniques to characterise protein or gene expression are far more readily available and optimised in the literature. Enzyme-linked immunosorbent assays (ELISAs) have commonly been used to investigate changes in proteomics and for cytokine detection, though are limited in their multiplex capabilities. Reverse phase protein microarray (RPPA) is a type of protein microarray which functions by directly spotting the target antigen onto glass slides and probing with detector antibodies which may or may not be dye-labelled [373]. Protein microarrays are a technique built on DNA microarray technology which allow for the simultaneous analysis of multiple proteins whilst using a minimal amount of available sample [374]. These techniques have been pivotal in the identification and characterisation of protein-driven molecular interactions as well as novel biomarkers for autoinflammatory diseases [375]. In addition, techniques such as polymerase chain reaction (PCR) or more specifically reverse transcription-quantitative PCR (RT-qPCR) allow for the rapid and quantitative analysis of alterations in gene expressions within tissue samples. In RT-qPCR, RNA is used to generate single-stranded complementary DNA (cDNA) during the reverse transcription (RT) step, which is then measured during the quantitative PCR (qPCR) process when a fluorescent dye (such as SYBR green) intercalates with newly synthesised double-stranded DNA and emits signal [376]. The level of fluorescence detected during the qPCR process therefore provides a quantification of the degree of expression of the target gene. All forms of PCR have the benefit of requiring minimal quantities of DNA or RNA in order to function, as the number of genetic copies is amplified during the process to allow for detection.

As previously discussed, COPD pathophysiology is comprised of a complex interplay between cellular mechanisms, protein imbalances and alterations to gene expressions. Therefore, to fully characterise the immunopathogenic mechanisms of COPD, a multi-faceted approach is needed. In order to encompass and capture as many potential targets for further investigation as possible, we aimed to develop novel high-

throughput panels to allow us to identify suspected pathogenic mechanisms. For this, we developed a novel 24-colour spectral flow cytometry panel to allow us to examine peripheral immune cells in whole-blood, and aimed to validate a human RPPA panel for use on murine tissues. Unfortunately, cross-reactivity could not be detected on the RPPA panel, and this technique was dropped in favour of an 18-gene RT-qPCR panel to characterise key immune signalling pathways and genes known to play a role in COPD pathophysiology. This chapter details the validation and optimisation of the techniques used during our murine study in order to minimise and reduce the number of mice needed to achieve the project's aims and retain samples for future work.

## 3.2. METHODS

### 3.2.1. SPECTRAL FLOW CYTOMETRY

#### 3.2.1.1. Generation of panel and antibody selection

Full methods for spectral flow cytometry are found in section 2.2.2 Methods – Spectral Flow Cytometry. Briefly, markers for flow cytometry were identified and selected according to the literature. Markers were assigned to fluorophores appropriate for their expression levels in whole blood, spleen and lung tissues and the spillover matrix was determined using a panel builder tool provided by Sony Biotechnology. Conjugated antibodies were either purchased from suppliers or conjugated in-house using purified antibodies and conjugation kits for relevant fluorophores. Table 3.2.1 outlines the reagents and markers used for the panel according to OMIP guidelines.

*Table 3.2.1:- Reagents selected for flow cytometry panel with details based on OMIP guidelines.*

Specificity	Fluorophore	Clone	Purpose
<b>CD45</b>	APC-Fire810	30-F11	Pan haematopoietic cells
<b>CD3</b>	BUV496	17A2	Pan T cells
<b>CD4</b>	FITC	RM4-5	CD4 <sup>+</sup> T cells
<b>CD8a</b>	APC/Cy5.5	53-6.7	CD8 <sup>+</sup> T cells
<b>ROR<math>\gamma</math>t</b>	PE/Cy5.5	W19344C	Th17 cells
<b>FOXP3</b>	NovaFluorBlue 610 70S	MF-14	Tregs
<b>CD25</b>	BV510	PC61	Tregs/T cell activation
<b>CD49b</b>	PerCP/Cy5.5	DX5	Pan NK cells
<b>CD11b</b>	Pacific Blue	M1/70	Myeloid/NK/Granulocytes
<b>Ly6G/Ly6C</b>	PE/Cy5	RB6-8C5	Neutrophils/monocytes
<b>I-A/I-E</b>	PE/Cy7	M5/114.14.2	MHC II/APCs
<b>F4/80</b>	CF568	T45-2342	Macrophages
<b>CD163</b>	PE	S15049F	Macrophage subsets
<b>CD169</b>	BV605	3D6.112	Alveolar macrophages
<b>CD80</b>	BUV661	16-10A1	Co-stimulation of APCs
<b>CD86</b>	BV650	GL-1	Co-stimulation of APCs
<b>CD38</b>	PE/Dazzle 594	90	DC/B cell activation
<b>CD69</b>	BV785	H1.2F3	T cell activation
<b>CCR7</b>	AF647	4B12	DC/T/B cell activation/trafficking
<b>IFN-<math>\gamma</math></b>	BV421	XMG1.2	Inflammation/NK cells
<b>IL-6</b>	PerCP-eFluor 710	MP5-20F3	Inflammation/ CD4 <sup>+</sup> T cells
<b>IL-17A</b>	BV711	TC11-18H10.1	Inflammation/ Th17 cells
<b>TNF-<math>\alpha</math></b>	BV750	MP6-XT22	Inflammation/Macrophages
<b>Zombie</b>	NIR	-	Viability stain

#### 3.2.1.2. Isolation, activation and staining of murine splenocytes

Murine splenocytes were isolated via mechanical disruption and straining through a 100 µm cell strainer (see section 2.2.2.2 Isolation, activation and staining of murine splenocytes for more details). Isolated splenocytes were frozen down at  $1 \times 10^7$  cells per mL in FBS + 10% DMSO to preserve cells for future assays. Frozen splenocytes were defrosted and counted before being reconstituted at a concentration of between 8 – 10 million cells per mL. For activation assays, cells were either exposed to 100 ng/mL LPS or 25 ng/mL PMA and 1 µg/mL ionomycin for between 6 – 48 hours alongside an Fc block and protein transport inhibitor. Serial dilutions of antibodies from 1:10 to 1:1280 were prepared in a 96-well low bind plate, to which splenocytes were added. Samples along with unstained and single colour controls were incubated before a RBC lysis/fixation buffer was added. Experiments were analysed using a Sony ID7000 spectral flow cytometer and data was analysed using FlowJo.

#### 3.2.1.3. Gating strategies

For all gating, cells were first gated according to FSC-A and SSC-A profiles for either lymphocytes (figure 3.2.1 A.i) or large cells (figure 3.2.1 B.i) and then for single cells (figure 3.2.1 A.ii and B.ii). Viable live cells were then gated for according to negative staining for ZOMBIE-NIR (figure 3.2.1 A.iii and B.iii). For calculation of stain indexes, histograms were then generated for each fluorophore and dilution factor and the positive and negative population peaks were defined using the bisector tool in FlowJo.

#### 3.2.1.4. Stain index calculations

Stain indexes were calculated by applying median statistics to positive and negative histogram peaks, in addition to standard deviation statistics applied to the negative peak only. Stain indexes and stain index curves were then calculated and generated using Excel and GraphPad

Prism according to the methods specified in section 2.2.2.4 Stain index calculations.

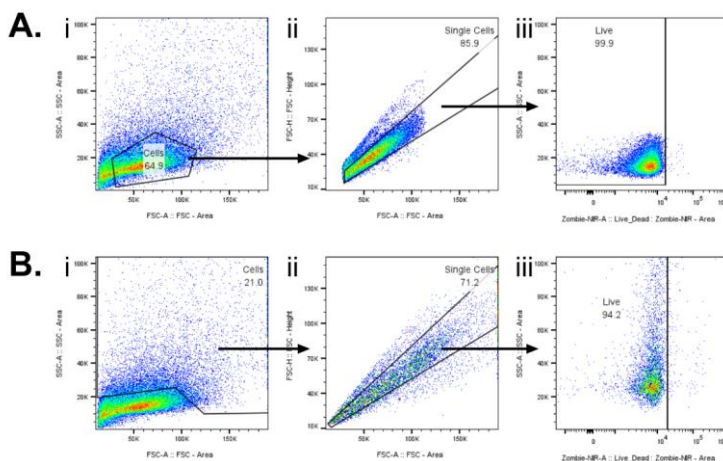


**Figure 3.2.1:- Gating strategy to obtain stain indexes using FlowJo.** Cells were gated according to size with two strategies to isolate lymphocytes (A) or larger cells such as granulocytes and macrophages (B). Cells were first gated according to side scatter area (SSC-A) against forward scatter area (FSC-A) to determine cell size and granularity (A.i and B.i). Gated cells were then gated forward scatter height (FSC-H) against FSC-A to isolate single cells and exclude doublets and debris (A.ii and B.ii). Single cells were then gated SSC-A against Zombie-NIR to exclude positively stained dead cells (A.iii and B.iii). Histograms were then prepared using the live cell populations and selected markers, and the negative and positive peaks were defined using the bisector tool (not shown).

#### 3.2.1.5. Whole blood staining

Whole blood staining was performed to determine panel efficiency and adjustments, full methods can be found in section 2.2.2.5. Whole blood staining. In brief, whole blood was provided from a mouse set for S1 cull. Protein transport inhibitor and Fc receptor block were added prior to the addition of a RBC lysis buffer. Samples were washed with PBA and an extracellular panel master mix was added (see table 2.2.1 for details). Following incubation, cells were washed and resuspended in a fix/perm working solution and incubated for 30 minutes. Cells were then washed twice with perm wash buffer before the addition of an intracellular



panel master mix (see table 2.2.1). After incubation, cells were washed twice with perm wash buffer and resuspended in fixation buffer in FACS tubes to be run on a spectral flow cytometer.

### 3.2.2. REVERSE PHASE PROTEIN MICROARRAY

#### 3.2.2.1. Slide development

Full methods for reverse phase protein microarray (RPPA) are found in section 2.2.3 Methods – Reverse Phase Protein Microarray. Briefly, nitrocellulose membrane was bound to two thirds of glass slides using polyurethane glue and a gel dryer. Slides were stored in a vacuum sealed container to preserve the membrane for printing (see section 2.2.3.1. Slide development).

#### 3.2.2.2. Tissue lysis

For tissue lysis and protein extraction, approximately 30 mg tissue was excised and placed into a round bottom Eppendorf tube with lysis buffer and a 5 mm steel bead. Tissues were lysed until complete and uniform homogenisation, after which the steel beads were removed and samples were centrifuged multiple times using the supernatant until clear and free of clumps. Samples were stored at -80°C until use (see section 2.2.3.2. Tissue lysis).

#### 3.2.2.3. BCA assay and protein concentration

A BCA assay was performed to determine protein concentrations from lysed tissues, this was performed according to the manufacturer's directions (see section 2.2.3.3. BCA assay and protein concentration). Protein concentrations were determined using GraphPad Prism's standard curve interpolation function (line, robust fit) and protein yield was also calculated to determine minimum tissue weight required to achieve optimal protein concentrations from lysis. Samples were then diluted to 2 mg/mL in a 96-well PCR plate using dH<sub>2</sub>O and 4 x SDS

sample buffer. The plate was heated to denature proteins and then stored at -20°C until ready for use.

#### 3.2.2.4. Printing and staining optimisation

Samples for printing were prepared in a 384-well plate with a 1:1 dilution of 2 x print buffer. Arrays were printed with 8 replicates and landing lights were printed in the outer corners to define grid and slide orientation (see section 2.2.3.4. Printing and staining optimisation). Optimal wash steps were determined by washing slides in PBST for up to 1 hour, changing PBST every 10 minutes. Optimal staining and amplification was determined through the addition or absence of liquid plate sealer in addition or absence of one or two rounds of amplification with streptavidin-Cy5 and biotinylated anti-streptavidin after incubation with an anti-mouse  $\alpha$ -tubulin antibody. Slides were scanned using a GenePix Microarray system at 635 nm to determine effects of wash steps and amplification on signal:noise ratio.

#### 3.2.2.5. SDS-PAGE

SDS-PAGE was performed using gels poured in-house according to the protocol specified in section 2.2.3.5. SDS-PAGE. Briefly, a 10% resolving gel was used to separate proteins whilst a 6% stacking gel was used to align samples for separation. Samples from murine heart, spleen and RAW 264.7 macrophages were used at a concentration of 2 mg/mL and run using an XCell Surelock Mini gel electrophoresis system for 1 hour 45 minutes at 125 V constant. Standards consisted of either colour prestained protein ladder or biotinylated protein ladder, the former of which was used for gels for visualisation whilst the latter was used for gels intended for Western Blot. Gels that were used for visualisation were stained with SimplyBlue SafeStain after trimming away stacking gel and excess resolving gel according to manufacturer's protocols for microwave staining. Gels were then imaged under standard light settings in a NuGenius Gel Doc Scanner.

#### 3.2.2.6. Western Blot

Gels using a biotinylated protein standard ladder were used for Western Blotting (see section 2.2.3.6. Western Blot). Gels and nitrocellulose membranes were equilibrated in transfer buffer and assembled in a transfer stack within an XCell II Blot Module and run for 2 hours at 25 V constant in an XCell Surelock Mini gel electrophoresis system. Following transfer, the nitrocellulose membrane was placed in blocking buffer for 1 hour with agitation. After washing with PBST, the membrane was placed into a Miniblotter 16 and probing antibodies were added to each chamber for 20 minutes with agitation. The membrane was washed and then placed into a solution containing streptavidin-HRP and incubated for 20 minutes with agitation. Following a wash step, the nitrocellulose membrane was placed onto a sheet of A4 projector film and a Novex Chemiluminescence kit was used for chemiluminescent detection of antibodies. Images were taken under blacklight in a SynGene G:Box under 5 – 15 minutes exposure.

#### 3.2.3. RT-qPCR

##### 3.2.3.1. Target gene identification

Full methods for RT-qPCR are found in section 2.2.4. Methods – RT-qPCR. In brief, target genes for primer design were identified using markers from the RPPA panel or using GWAS of COPD. Murine orthologues to human genes were identified from the NCBI website and accession numbers were recorded (table 3.2.2).

Table 3.2.2:- Target genes of interest for RT-qPCR panel.

Gene Name	Accession Number	Reason for Inclusion
<b>NLRP3</b>	NM_145827.4	Inflammasome signalling - production of proinflammatory cytokines, upregulated in COPD
<b>NOX2</b>	NM_007807.5	Inflammasome signalling - production of reactive oxygen species, modulates MMP9 pathway
<b>TLR2</b>	NM_011905.3	Pathogen recognition and regulation of innate immunity, balance of Th17/Tregs, excessive activation and expression in COPD
<b>TLR4</b>	NM_021297.3	Pathogen recognition and regulation of immunity, balance of Th1/Th2 responses, overexpressed in COPD but signalling disrupted
<b>MyD88</b>	NM_010851.3	TLR2/TLR4 signalling cascade (MyD88 dependent), activation of NFkB transcription factors and interferon regulatory factors
<b>TIRAP</b>	NM_001177845.1	TLR2/TLR4 signalling cascade (MyD88 dependent), activation of NFkB transcription factors and interferon regulatory factors
<b>IRF3</b>	NM_016849.4	Interferon regulatory factor 3, production of type I interferons
<b>MMP9</b>	NM_013599.5	Inflammation and lung remodelling in COPD
<b>MMP12</b>	NM_008605.3	Inflammation and recruitment of immune cells in COPD
<b>MMP28</b>	NM_080453.3	Reported driver of inflammation and persistence of emphysema in COPD, not often found in lungs but highly upregulated in COPD
<b>mTOR</b>	NM_020009.2	Downstream signalling of IL6R
<b>IL6Ra</b>	NM_010559.3	IL6 receptor alpha subunit
<b>Akt1</b>	NM_009652.4	Downstream signalling of IL6R
<b>Serpina1a</b>	NM_009243.4	Ortholog of human alpha 1 antitrypsin, deficiency reported to exacerbate COPD
<b>CYLD</b>	NM_001128170.2	Regulation of NFkB pathway, cell survival and proliferation
<b>NFKBIA (Ikbα)</b>	NM_010907.2	Inhibits NFkB and prevents transcription of DNA
<b>CRP</b>	NM_007768.4	Acute phase inflammation, upregulated in response to IL-6 secretion by macrophages and T cells
<b>NRF2</b>	NM_010902.5	Antioxidant marker of oxidative stress response, upregulated in COPD

#### 3.2.3.2. Primer design

mRNA sequences for genes of interest were identified using the NCBI website, and where multiple splice variants were reported the most common or validated variant was used as a basis for primer generation. Mouse BLAT was used to identify exon-exon boundaries, and the NCBI Primer Blast tool was used to generate suitable primer pairs using each gene's mRNA accession number. Ideal primers were selected based on T<sub>m</sub>, GC percentage, product size and exon-exon spanning. Forward and reverse primer sequences were checked on the Nucleotide BLAST suite to check for nonspecific binding, after which primer sequences were sent to Eurofins Genomics for synthesis. Primers were then reconstituted to 100 pmol/μL and 1:1 forward and reverse primer mixes were generated as specified in section 2.2.4.2 Primer design.

#### 3.2.3.3. RNA isolation and reverse transcription

For primer validation, RNA was extracted from murine spleens scheduled for cull. A Qiagen RNeasy mini kit was used to isolate RNA according to the manufacturer's protocols, in addition to an optional on-column DNase digest step using a Qiagen RNase-free DNase set (see section 2.2.4.3 RNA isolation and reverse transcription). After successful isolation of RNA, concentrations were determined by NanoDrop spectrophotometer.

For reverse transcription, 1 μg of RNA was used for optimal cDNA synthesis (see section 2.2.4.3 RNA isolation and reverse transcription). A TaqMan Reverse Transcription kit was used to generate cDNA for all samples in addition to no reverse transcriptase controls (NRT) and no template controls (NTC). Samples containing reaction mixture were placed into a thermocycler to allow reverse transcription to take place, after which resulting cDNA was diluted to 5 ng and stored at - 20°C until use.

#### 3.2.3.4. Polymerase chain reaction

PCRs were performed in triplicate in 96-well PCR plates using a master mix of SYBR green reagents and FWD/REV primer mixes (see section 2.2.4.4. Polymerase chain reaction). Plates were sealed with an optical adhesive seal after addition of cDNA and run on an ABI Fast 7500 qPCR machine using a standard protocol for SYBR green reagents in a 10  $\mu$ L volume reaction. Melt curves for each gene were exported to examine primer binding efficiency.

#### 3.2.3.5. Agarose gel electrophoresis

Agarose gel electrophoresis was performed using 1% agarose gel containing Gel Red prepared in-house (see section 2.2.4.5. Agarose gel electrophoresis). After gels were set, samples mixed with loading dye were added to wells alongside a GeneRuler 50 bp DNA ladder and the gel was run for 45 minutes at 100V. After separation of DNA products, the gel was visualised under UV light using a NuGenius Gel Doc scanner.

### 3.3. RESULTS

#### 3.3.1. SPECTRAL FLOW CYTOMETRY

##### 3.3.1.1. Panel generation

Originally, 23 markers were selected for inclusion in order to provide general phenotyping of major immune cells from both the innate and adaptive immune systems, but a 24<sup>th</sup> marker was added due to issues faced during validation of the panel. The panel design for these 24 targets is presented in figure 3.3.1. To ensure that only immune cells would be included in analysis, the first marker added was CD45 (approximately  $1 \times 10^8$  cells per spleen, 2,000 – 10,000 cells/ $\mu$ L in peripheral blood), which was assigned a dim fluorophore (APC-Fire810) due to being expressed by all haematopoietic cells and therefore found in high abundance. ZOMBIE-NIR was selected as a viability marker to isolate live cells from dead cells.

Common T cell markers CD3, CD4 and CD8a were selected to isolate and define lymphocyte populations and to differentiate T helper (13 – 20% of immune cells in spleen, 8 – 12% in peripheral blood) and cytotoxic T cell (7 – 15% of immune cells in spleen, 7 – 10% in peripheral blood) populations from one another. CD69 and CCR7 were also selected to characterise activation of T lymphocytes, and IFN- $\gamma$ , IL-6, IL-17A and TNF- $\alpha$  were selected as effector function markers based on existing literature regarding immunopathogenic mechanisms of COPD. FOXP3 and ROR $\gamma$ t were added to further define Treg and Th17 subsets of CD4<sup>+</sup> T cells respectively. During the course of validation, staining issues were observed with FOXP3, therefore CD25 was added as a substitute in order to isolate Treg populations and further characterise T cell activation. Fluorophores for extracellular markers (CD3, CD4 and CD8a) were selected with dim to moderate brightness (BUV496, FITC and APC/Cy5.5 respectively) based on higher expression levels and abundance in the periphery and lungs. Activation markers (CD69, CD25 and CCR7) and intracellular markers (FOXP3, ROR $\gamma$ t, IFN- $\gamma$ , IL-6, IL-17A and TNF- $\alpha$ ) were assigned moderate to very bright fluorophores (BV785, BV510, AF647, NovaFluorBlue610 70S, PE/Cy5.5, BV421, PerCP-eFluor 710, BV711 and BV750 respectively) due to variable expression (as a result of activation) or typically low abundance.

The addition of CD3 also used for the definitive isolation of CD3 negative populations, such as NK cells (1 – 5% of immune cells in spleen, 4 – 7% in peripheral blood), macrophages (3.5 – 5% of immune cells in spleen, 2 – 3% in peripheral blood), monocytes (3.5 – 5% of immune cells in spleen, 2 – 3% in peripheral blood), neutrophils (1 – 5% of immune cells in spleen, 4 – 6 % in peripheral blood), DCs (0.5 – 2% of immune cells in spleen, no data for peripheral blood) and B cells (44 – 58% of immune cells in spleen, 35 – 58% in peripheral blood). To further characterise these cell types, additional markers were selected to determine phenotype and effector functions. In mice, CD49b clone DX5 is used to isolate NK cells, and a moderate fluorophore (PerCP/Cy5.5) was selected due to variable abundance. CD11b (Pacific Blue) was also

selected as a marker due to being expressed by a high number of different cells, including NK cells, macrophages, monocytes and neutrophils. Since CD11b was expressed by a number of cells, I-A/I-E (the murine orthologue to HLA-DR) was added with a bright fluorophore (PE/Cy7) in order to isolate APCs. To conserve spectral options for additional markers, an antibody specific for both Ly6G and Ly6C (often referred to collectively as Gr-1) was selected. Specifically, clone RB6-8C5 was selected due to its capacity to bind with higher specificity to Ly6G and to a lesser extent to Ly6C. This allowed for the isolation of both neutrophils (Ly6G<sup>hi</sup>/Ly6C<sup>lo/neg</sup>) and monocytes (Ly6G<sup>lo/neg</sup>/Ly6C<sup>hi</sup>) using a single antibody (PE/Cy5). Several markers were selected for macrophage phenotyping, including F4/80, CD163 and CD169. These were assigned to moderate to very bright fluorophores (CF568, PE and BV605 respectively) due to low abundance in the periphery and variable abundance in tissues. CD163 allowed for the general identification of macrophages involved in the acute phase of inflammation, whilst CD169 would allow the identification of specific alveolar macrophage subsets. Activation markers for APCs included CD80 and CD86, which were assigned to moderate fluorophores (BUV661 and BV650 respectively) due to variable expression. CD38 was also selected as a specific marker for DC/B cell activation, and assigned a very bright fluorophore (PE/Dazzle 594) due to low cell populations for DCs. Specific percentages for immune cell populations in the lungs could not be found, and therefore fluorophore brightness was selected based on cell frequencies in spleen and peripheral blood as well as from reported results from previous COPD studies in mice. In all instances, spectral patterns were distinct enough that R-squared values did not exceed 0.7 for all markers.



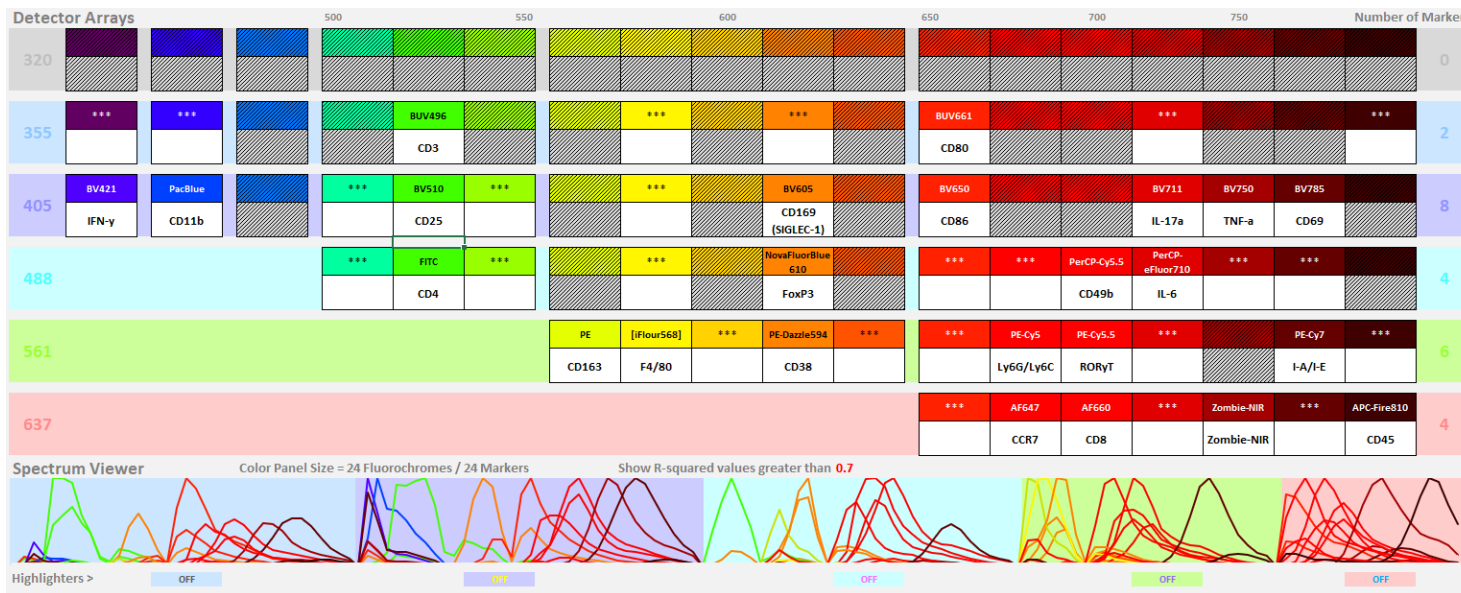


**Figure 3.3.1:- 24-Colour flow panel design.** Markers and fluorophores are outlined according to their emission wavelength (top) and which detector array they are detected by (left). Spectral patterns for each fluorophore are displayed on the Spectrum Viewer below to panel design table. Markers were assigned to appropriate fluorophores for relative brightness according to their expression levels in mouse periphery, spleen and lung and the panel designer automatically calculated the R-squared values to determine spillover matrix of selected fluorophores. Where R-squared values above 0.7 were detected for markers intended to be gated together, an alternative fluorophore was assigned to ensure accurate unmixing.

#### 3.3.1.2. Stain indexes

Due to the novelty of the panel and the lack of existing data regarding validated murine flow cytometry panels, optimal dilution and antibody concentrations were determined for each marker through the use of stain indexes. These were determined according to histograms generated from an 8-fold dilution series and resulting stain index curves. In some cases where low cell populations were reported (e.g. NK cells), stain index was determined according to SSC-A and FSC-A profiles and the difference between median values of the positive and negative populations. Cells were either gated according to the lymphocyte or macrophage/granulocyte strategy demonstrated in figure 3.2.1. Details of stain index calculations along with figures are found in Appendix C, the gating strategy used to calculate each stain index is specified in the figure legend for each marker.

#### 3.3.1.3. Multiplex panel capabilities

Once antibody concentrations for each target had been determined, the panel was tested in a multiplex format in whole blood. For this, antibodies were pooled together in extracellular and intracellular master mixes for staining. Once run on the Sony ID7000, ability to discern markers from one another was analysed by generating gating strategies to isolate specific cell types and markers of activation. As an example, ability to isolate CD4<sup>+</sup> and CD8<sup>+</sup> T cells was tested (figure 3.3.2). Initially, cells were gated to exclude debris (figure 3.3.2Ai), then single cells were selected (figure 3.3.2Aii), followed by selection of viable cells (figure 3.3.2Aiii) and finally CD45<sup>+</sup> cells were gated (figure 3.3.2Aiv). Clear separation between CD3<sup>+</sup> and CD3<sup>-</sup> populations were observed (figure 3.3.2B) which were then gated for both CD4 and CD8. As shown in figure 3.3.2C, the isolated CD3<sup>-</sup> population demonstrates minimal staining for CD4 and CD8 as would be expected. Using the same gating strategy applied to the CD3<sup>+</sup> population, the majority of cells are stained positive for either CD4 or CD8, with a small population of double positives and

double negatives (figure 3.3.2D). This demonstrates that CD4 and CD8 populations can not only be distinguished from negative populations, but also from each other, allowing for the identification of specific T cell subsets. This same strategy was applied for all other markers to ensure adequate separation of positive and negative populations. Given that all cells could be isolated based on whether or not they expressed CD3, the initial gating strategy to isolate populations for all cells using this panel followed the steps from figure 3.3.2A and B to define viable, singlets, that are positive for CD45 and either CD3+ or CD3- based on the desired population to be isolated.

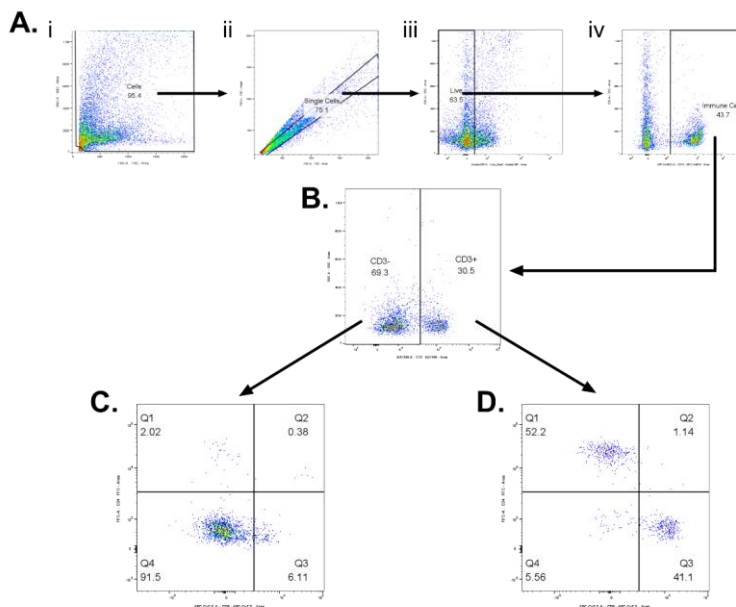


**Figure 3.3.2:- Gating strategy to determine adequate separation of positive and negative populations.** All cells were first gated (A.i) and then gated for singlets (A.ii) followed by live cells (A.iii). Live single cells were then gated for CD45 to isolate immune cells (A.iv). Immune cells were then gated for CD3 to determine positive and negative gate positions (B), with each population gated for CD4 and CD8 to determine correct positioning of CD3 gates (C and D).

After ensuring all markers could be isolated, gating strategies were then created to allow for the definition and characterisation of major immune cells. Gates were placed either where distinct separation was observed between positive and negative populations in a similar manner to calculating stain indexes, or where small cell populations caused difficulty defining positive and negative populations, where the positive population was expected to lie according to results from stain index histograms. Firstly, T cell subsets were defined as CD45+CD3+ and either CD4+ or CD8+ according to the same gating strategy defined in figure 3.3.2A, B and D. CD4+ and CD8+ were then gated for activation markers CCR7 (figure 3.3.3 B.i and C.i) and CD69 and CD25 (figure 3.3.3 B.ii and C.ii). Activated T cells were defined as either CCR7+, CD69+CD25- (early activation), CD69+CD25+ (mid activation) or CD69-CD25+ (late activation). In addition, for CD4+ cells, CD69-CD25+ cells were classified as containing Tregs in addition to conventionally activated CD4+ T cells (figure 3.3.3 B.ii Q3).

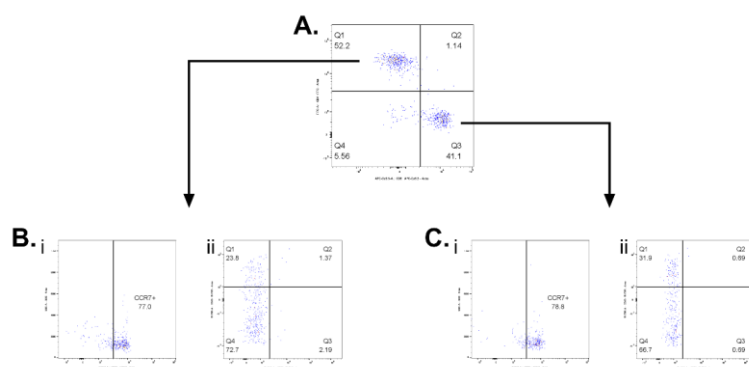


**Figure 3.3.3:- Gating strategy for activation markers of T lymphocytes.** Cells were first gated for viable singlets positive for CD45 and CD3 as shown in figure 3.3.2A and B. CD45+CD3+ cells were then gated for CD4 and CD8 (A). CD4+CD8- cells (A.Q1) were then gated for either CCR7 (B.i) or CD69 and CD25 (B.ii) to determine both activated (CCR7+ or CD69+CD25- or CD69+CD25+) and Treg populations (CD69-CD25+). The same gating strategy was applied to CD4-CD8+ cells (A.Q3) to determine number of CCR7+ cells (C.i) and CD69+CD25+ cells (C.ii).

A similar strategy was also used to gate for cytokine production by CD4<sup>+</sup> and CD8<sup>+</sup> T cells, with CD4+IL-17A<sup>+</sup> T cells defined as potentially containing Th17 subset populations (figure 3.3.4).

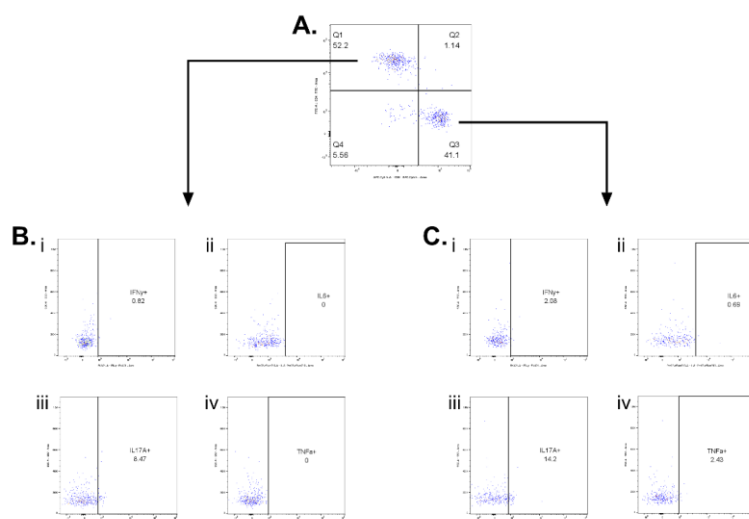


**Figure 3.3.4:- Gating strategy for cytokines produced by T lymphocytes.**

Cells were first gated for viable singlets positive for CD45 and CD3 as shown in figure 3.3.2A and B. CD45+CD3<sup>+</sup> cells were then gated for CD4 and CD8 (A). CD4+CD8<sup>-</sup> cells (A.Q1) were then gated for either IFN- $\gamma$  (B.i), IL-6 (B.ii), IL-17A (B.iii) or TNF- $\alpha$  (B.iv). The same gating strategy was applied to CD4-CD8<sup>+</sup> cells (A.Q3) to determine production of IFN- $\gamma$  (C.i), IL-6 (C.ii), IL-17A (C.iii) or TNF- $\alpha$  (C.iv).

All remaining cell types were then gated on the CD3<sup>-</sup> population according to the gating strategy defined in figure 3.3.2 A – C. NK cells were defined as CD45+CD3<sup>-</sup>CD49b<sup>+</sup> (figure 3.3.5A), and were then gated for cytokine production in the same manner as T cells (figure 3.3.5B).

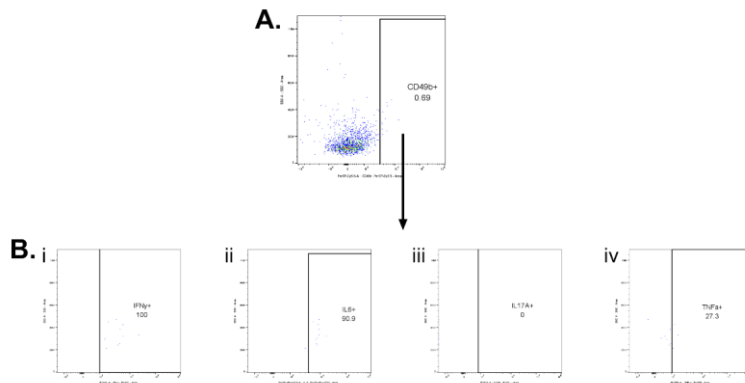


**Figure 3.3.5:- Gating strategy for NK cells.** Cells were first gated for viable singlets positive for CD45 and negative for CD3 as shown in figure 3.3.2A and B. CD45<sup>+</sup>CD3<sup>-</sup> cells were then gated for CD49b to isolate NK cells (A). NK cells were then gated to determine production of cytokines IFN- $\gamma$  (B.i), IL-6 (B.ii), IL-17A (B.iii) and TNF- $\alpha$  (B.iv).

Neutrophils and monocytes were gated on CD45<sup>+</sup>CD3<sup>-</sup> cells using both CD11b and Ly6G/Ly6C (Gr-1). As previously mentioned, the antibody used to select for Gr-1 binds with higher specificity to Ly6G than Ly6C, allowing neutrophils to be distinguished from monocytes. Neutrophils were therefore defined as CD11b<sup>+</sup>Gr-1<sup>hi</sup>, whilst monocytes were gated as CD11b<sup>+</sup>Gr-1<sup>med</sup> (figure 3.3.6A). Monocytes and neutrophils could then be gated for cytokines (figure 3.3.6B and C).

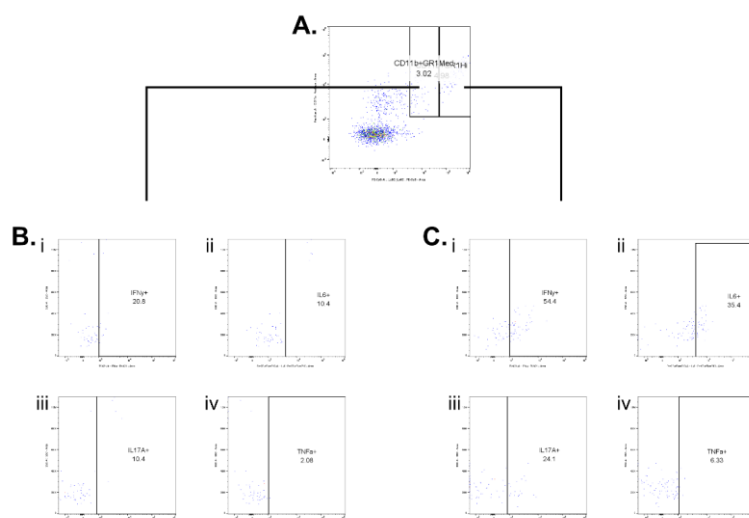


**Figure 3.3.6:- Gating strategy for neutrophils and monocytes.** Cells were first gated for viable singlets positive for CD45 and negative for CD3 as shown in figure 3.3.2A and B. CD45+CD3<sup>-</sup> cells were gated for CD11b and Ly6G/Ly6C (Gr-1) to isolate neutrophils and monocytes (A). Monocytes were defined as CD11b<sup>+</sup> and Gr-1 medium, and then gated for cytokines IFN- $\gamma$  (B.i), IL-6 (B.ii), IL-17A (B.iii) and TNF- $\alpha$  (B.iv). Neutrophils were defined as CD11b<sup>+</sup> and Gr-1 high, and then gated for cytokines IFN- $\gamma$  (C.i), IL-6 (C.ii), IL-17A (C.iii) and TNF- $\alpha$  (C.iv).

Since macrophages are known to express a wide variety of surface markers, CD45+CD3<sup>-</sup> cells were first gated for I-A/I-E (MHCII) and CD11b (figure 3.3.7A.i). Double positive MHCII and CD11b cells were then gated for CD80 and CD86 (figure 3.3.7A.ii), with CD80+CD86<sup>+</sup> cells then gated for CD163 (figure 3.3.7A.iii). These CD163<sup>+</sup> cells were then defined as macrophage populations. Given that macrophages are not typically found in peripheral blood, both F4/80 and CD169 could not be used to identify macrophages due to lack of staining, likely due to being specific markers of tissue resident macrophages. Identified macrophages were then gated for cytokines to determine activation status and production levels (figure 3.3.7B).

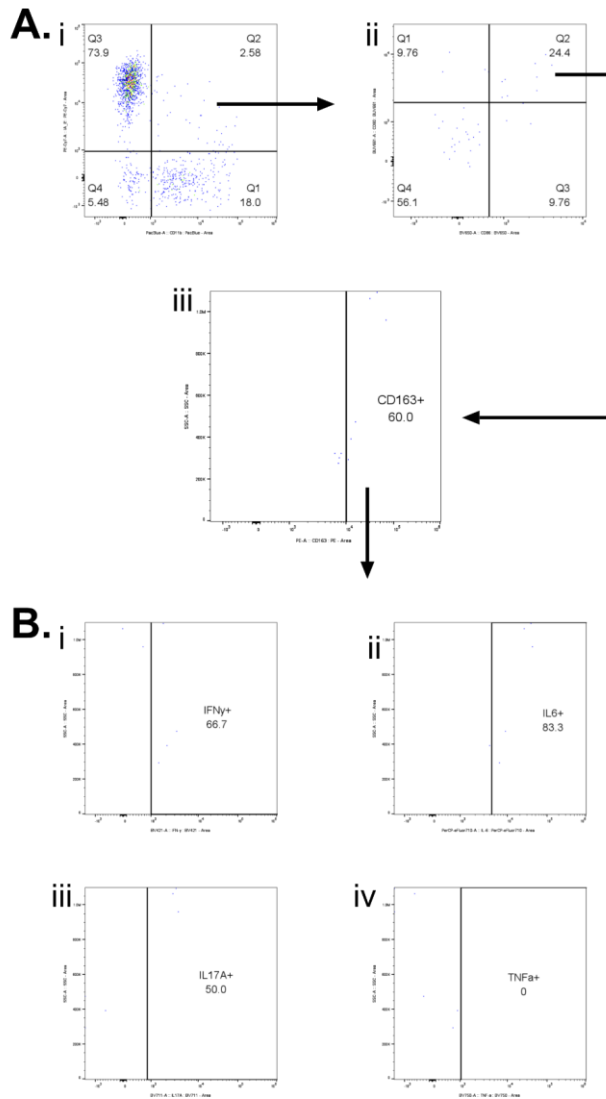


**Figure 3.3.7:- Gating strategy for macrophages.** Cells were first gated for viable singlets positive for CD45 and negative for CD3 as shown in figure 3.3.2A and B. CD45+CD3- cells were gated for I-A/I-E (MHCII) and CD11b to define populations of macrophages, dendritic cells and B cells (A.i). MHCII+CD11b+ cells (A.i Q2) were then gated for CD80 and CD86, with double positive cells (A.ii Q2) being further gated for CD163 to define macrophage populations (A.iii). Resulting macrophages were then gated for cytokines IFN- $\gamma$  (B.i), IL-6 (B.ii), IL-17A (B.iii) and TNF- $\alpha$  (B.iv).



DCs and B cells were gated for in a similar manner to macrophages, with CD45+CD3- cells being gated for CD11b and MHCII. DCs and B cells were defined as MHCII+CD11b- (figure 3.3.8A.i and figure 3.3.9A.i), which were then gated for CCR7 and CD38 (figure 3.3.8A.ii and 3.3.36A.ii). CCR7+CD38+ populations were identified as DCs, which were then gated for cytokines (figure 3.3.8B), whereas CCR7-CD38+ populations were identified as B cells and similarly gated for cytokines (figure 3.3.9B). Overall, these results and gating strategies demonstrate the high throughput efficiency of this panel and its ability to identify and characterise a multitude of cell types and their respective effector functions.

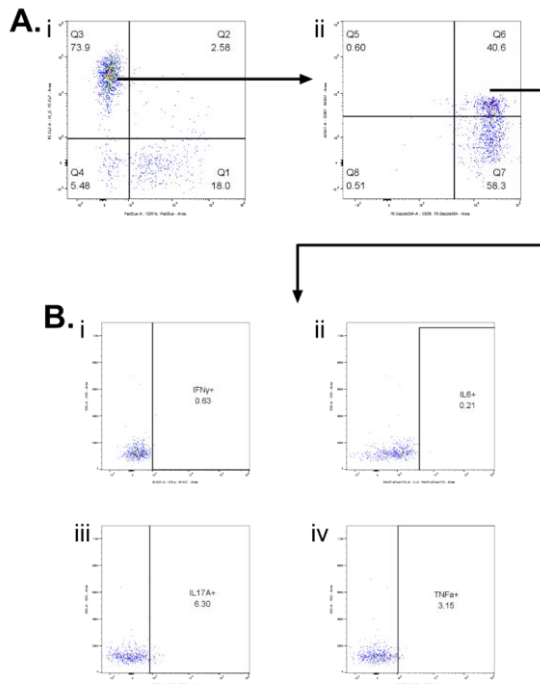


**Figure 3.3.8:- Gating strategy for dendritic cells.** Cells were first gated for viable singlets positive for CD45 and negative for CD3 as shown in figure 3.3.2A and B. CD45+CD3- cells were gated for I-A/I-E (MHCII) and CD11b to define populations of macrophages, dendritic cells and B cells (A.i). MHCII+ cells (A.i Q3) were then gated for CCR7 and CD38, with double positive cells (A.ii Q6) being defined as dendritic cells. Resulting dendritic cells were then gated for cytokines IFN- $\gamma$  (B.i), IL-6 (B.ii), IL-17A (B.iii) and TNF- $\alpha$  (B.iv).

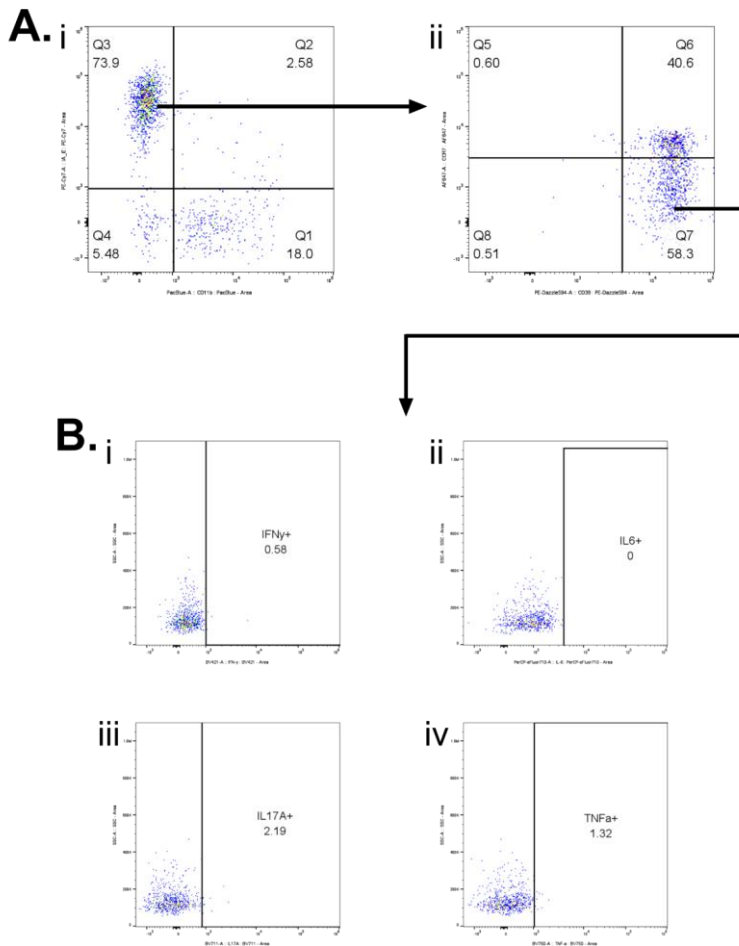


**Figure 3.3.9:- Gating strategy for B cells.** Cells were first gated for viable singlets positive for CD45 and negative for CD3 as shown in figure 3.3.2A and B. CD45+CD3- cells were gated for I-A/I-E (MHCII) and CD11b to define populations of macrophages, dendritic cells and B cells (A.i). MHCII+ cells (A.i Q3) were then gated for CCR7 and CD38, with CCR7-CD38+ cells (A.ii Q7) being defined as B cells. Resulting B cells were then gated for cytokines IFN- $\gamma$  (B.i), IL-6 (B.ii), IL-17A (B.iii) and TNF- $\alpha$  (B.iv).

### 3.3.2. REVERSE PHASE PROTEIN MICROARRAY

#### 3.3.2.1. Protein concentration calculations

In order to obtain optimal printing concentrations for RPPA, total protein concentrations were determined from lysed tissues. In addition, the yield ( $\mu\text{g}$  protein per mg tissue) was also calculated to determine the minimum weight of tissue required to obtain sufficient protein concentration for printing. This was performed using a BCA assay, and for validation purposes samples from murine heart (H), kidney (K), liver (L), gonad fat (GF) and muscle (M).

Based on BCA results, all tissue samples could be used for RPPA asides from gonad fat, which contained less than the required 2 mg/mL for printing (table 3.3.1). After calculating protein yield in  $\mu\text{g}$  per mg of tissue, it was determined that a minimum of 20 mg of tissue would be required to obtain the minimum 2 mg/mL concentration necessary for optimal printing. As a result, it was determined that future protein isolation would use initial tissue weights of between 25 – 30 mg in order to ensure sufficient protein extraction whilst preserving samples for potential future analysis. Due to low protein yield for gonad fat, it was concluded that this tissue type was not suitable for RPPA analysis. After determining protein concentrations, required dilutions for 2 mg/mL for printing were determined. As shown in table 3.3.2, minimal volumes were required to obtain the necessary concentrations and therefore there was enough stock left to perform repeated prints after diluted concentrations were used up, thereby reducing the amount of sample required for analysis.

**Table 3.3.1:- BCA results and yield for murine tissue samples.** Samples are identified according to the animal from which they came and the tissue of origin as follows: M9H1 = M (male) 9 (mouse 9) H (heart) 1 (sample 1).

Sample ID	Tissue Weight (mg)	Protein Concentration (mg/mL)	Total Protein (mg)	Yield ( $\mu\text{g}$ per mg tissue)
M9H1	35.1	23.64	7.08	202
M10H2	38.9	23.34	6.99	180
M11H3	27.2	13.26	3.99	147
M12H4	37.7	15.83	4.74	126
M15H5	25.8	12.83	3.84	149
M9K1	27.8	14.64	4.38	158
M10K2	25.1	13.42	4.02	160
M11K3	27.2	11.50	3.45	127
M12K4	25.4	15.02	4.50	177
M15K5	20.2	13.75	4.11	203
M9L1	20.9	8.27	2.49	119
M10L2	29.7	19.17	5.76	194
M11L3	25.2	15.08	4.53	180
M12L4	29.0	17.38	5.22	180
M15L5	25.5	16.05	4.83	189
M9GF1	31.5	1.67	0.51	16
M10GF2	35.8	1.65	0.51	14
M11GF3	23.8	0.95	0.27	11
M12GF4	29.1	0.97	0.30	10
M15GF5	26.2	0.83	0.24	9
M9M1	27.1	9.17	2.76	102
M10M2	26.6	6.21	1.86	70
M11M3	30.4	5.92	1.77	58
M12M4	28.9	6.76	2.04	71

*Table 3.3.2:- Dilutions required to obtain optimal staining concentration of 2 mg/mL. 30  $\mu$ L of 4x SDS was added to each sample. Gonad fat samples were not included as the protein concentration of each sample was below 2 mg/mL.*

Sample ID	Protein Concentration (mg/mL)	Sample Volume ( $\mu$ L)	Diluent Volume ( $\mu$ L)
M9H1	23.64	10.2	79.8
M10H2	23.34	10.3	79.7
M11H3	13.26	18.0	72.0
M12H4	15.83	15.2	74.8
M15H5	12.83	18.8	71.2
M9K1	14.64	16.4	73.6
M10K2	13.42	17.9	72.1
M11K3	11.50	20.9	69.1
M12K4	15.02	16.0	74.0
M15K5	13.75	17.5	72.5
M9L1	8.27	28.9	61.1
M10L2	19.17	12.5	77.5
M11L3	15.08	15.9	74.1
M12L4	17.38	13.8	76.2
M15L5	16.05	14.9	75.1
M9M1	9.17	26.1	63.9
M10M2	6.21	38.7	51.3
M11M3	5.92	40.7	49.3
M12M4	6.76	35.3	54.7

### 3.3.2.2. Slide staining optimisation

After printing in the appropriate format, the methodology for slide analysis was optimised. In order to reduce autofluorescence, wash steps were first optimised. As shown in figure 3.3.10A, immediately after printing arrays display a high degree of autofluorescence, particularly for the landing lights which minimises visualisation of the sample array. After washing for 30 minutes with PBST, much of this autofluorescence is reduced and the arrays can still be visualised (figure 3.3.10B). 1 hour of washing with PBST resulted in further reduction of autofluorescence, though background noise was increased and visualisation of arrays became more difficult (figure 3.3.10C). The optimal wash step was therefore determined to be 30 minutes.

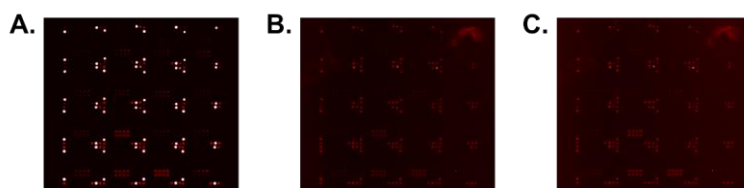


**Figure 3.3.10:- Optimisation of wash steps for protein microarray.** Slides were scanned at 635 nm wavelength before washing (A), after washing with PBST for 30 minutes (B) and after washing with PBST for 1 hour (C).

Optimal staining procedures were then tested, examining the effects of both a liquid plate sealer added prior to staining and signal amplification following staining to improve signal-to-noise ratio (SNR). Without amplification, slides demonstrated a low SNR, though this was marginally improved with the addition of liquid plate sealer (figure 3.3.11A). One round of amplification improved SNR and arrays were able to be visualised and detected more easily, particularly with liquid plate sealer (figure 3.3.11B). Although a second round of amplification improved SNR, this increase in signal was marginal in comparison to one round of amplification and results were highly varied without the addition of liquid plate sealer (figure 3.3.11C). As a result, optimal staining

procedures were amended to include the addition of liquid plate sealer and one round of signal amplification for optimal SNR.

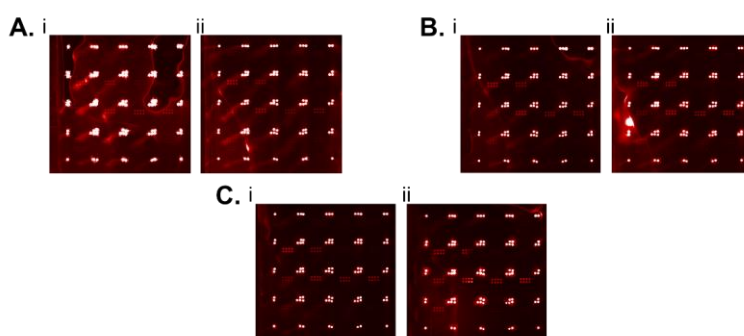


**Figure 3.3.11:- Optimisation of amplification techniques and signal detection.** Slides were either treated without (i) or with (ii) the addition of a plate sealer and underwent no amplification (A), one round of amplification (B) or two rounds of amplification (C) with biotinylated antibodies and streptavidin-cy5.

### 3.3.2.3. SDS-PAGE

To determine cross-reactivity of the RPPA panel to murine samples, proteins from murine heart, RAW 264.7 macrophages and murine spleen were separated via SDS-PAGE. As shown in figure 3.3.12, samples from both murine heart and spleen display high protein content across an 8-fold dilution series, however proteins from RAW 264.7 macrophages are poorly visualised. Due to both high protein content and likelihood of containing the majority of immune markers within the RPPA panel, murine spleen (figure 3.3.12C) was selected for Western Blot transfer to test for cross-reactivity.

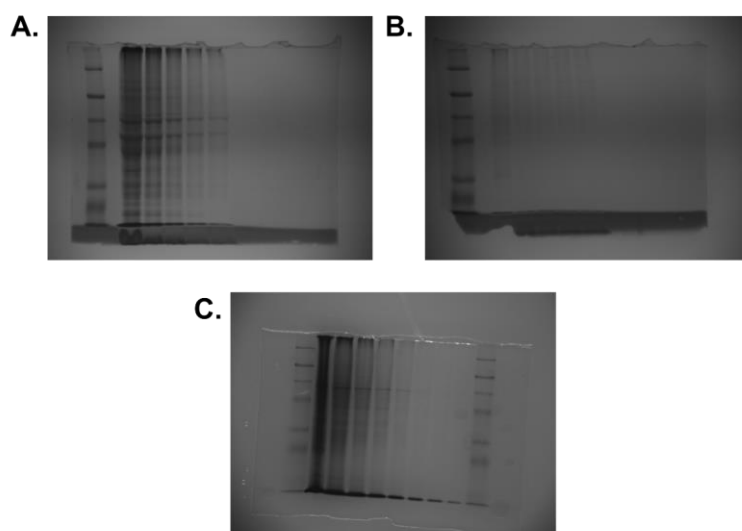


**Figure 3.3.12:-** *Coomassie blue staining SDS-PAGEs to determine protein content of tissue types and cell lines following protein extraction. Tissue types used were murine heart (A), RAW 264.7 murine macrophages (B) and murine spleen (C). A broad-range protein ladder (10 - 250 kDA) was used as a control and to determine presence of proteins.*

#### 3.3.2.4. Western Blots

Following Western Blot transfer of a dilution series of murine spleen samples, membranes were first probed with anti-mouse  $\alpha$ -tubulin to determine transfer efficiency. As shown in figure 3.3.13A, positive bands for  $\alpha$ -tubulin can be visualised across the entire dilution series. To then determine cross-reactivity of antibodies to mouse samples, a selection of markers from the RPPA panel which were constitutively expressed were chosen for probing. This included NF $\kappa$ B, STAT3, SAP/JNK and mTOR, with a biotinylated protein ladder standard as a positive control to ensure transfer had occurred. Following chemiluminescent staining however, detection of these markers could not be determined, though transfer was shown to have occurred (figure 3.3.13B and C). To determine whether there were issues with staining reagents, nitrocellulose slides were dotted with a dilution series of streptavidin-HRP and subject to



chemiluminescent staining, though no reported issues were detected with either staining reagents or the chemiluminescent kit (figure 3.3.13D). Western Blots were repeated though no signal was detected, and as a result it was concluded that the RPPA panel was not cross-reactive with mouse samples and was dropped from the project and an RT-qPCR panel was generated as a substitute.

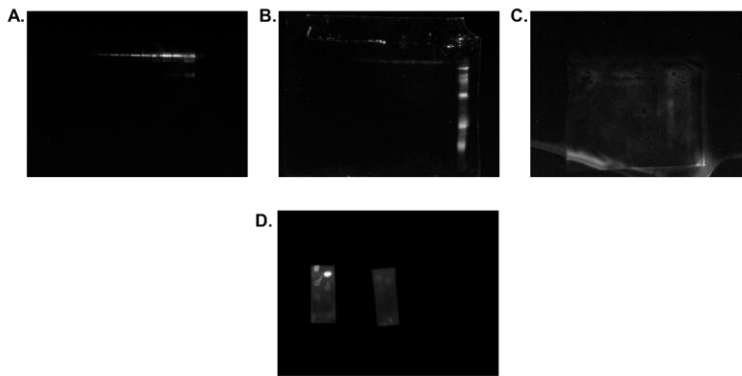


**Figure 3.3.13:- Western blotting and chemiluminescent test scans to determine antibody cross-reactivity with mouse samples.** Western Blot and chemiluminescent staining techniques were first tested using an anti-alpha tubulin antibody and spleen samples (A) before numerous antibodies from a validated RPPA panel were tested to determine cross-reactivity though no signal was detected except from standards (B and C). The chemiluminescent staining method was then tested using slides with dots of streptavidin-HRP at different concentrations to determine any issues in staining techniques (D). After troubleshooting, it was determined that the panel was not cross-reactive and RPPA was dropped from the project.

### 3.3.3. RT-qPCR

#### 3.3.3.1. Primer design

Primers were generated and selected according to their melting temperature ( $T_m$ ) and GC content. Where possible, primers with  $T_m$  within 1°C of the forward (FWD) and reverse (REV) primer were selected, and optimal GC percentage between 50 – 55%. Primers were able to be generated for 18 genes identified as contributing factors towards COPD pathogenesis, including those involved in inflammasome signalling

(NLRP3 and NOX2), toll-like receptor (TLR) signalling (TLR2, TLR4, MyD88, TIRAP and IRF3), matrix metalloproteinases (MMP9, MMP12 and MMP28), IL-6 receptor signalling (mTOR, IL6Ra and Akt1) in addition to genes involved in inflammation, oxidative stress or ECM alteration (Serpina1a, CYLD, NFKBIA, CRP and NRF2) (table 3.3.3). These primers were then generated by Eurofins and validated in-house.

**Table 3.3.3:- Primers designed as a substitute for the RPPA panel.** Genes were selected after being identified using GWAS studies or as orthologues from markers in the RPPA panel.

Gene Name	Primer	Primer Sequence	Tm (°C)	GC%	Product Length
NLRP3	FWD	CTCGCATTGGTTCTGAGCTC	58.99	55.00	153
	REV	AGTAAGGCCGGAATTCACCA	59.01	50.00	
NOX2	FWD	GATGATAGCACTGCACACCG	59.07	55.00	222
	REV	ATTCCTGTGATCCCAGCCAA	59.00	50.00	
TLR2	FWD	AAGGAGGTGCGGACTGTTTC	60.25	55.00	177
	REV	GAGCCAAAGAGCTCGTAGCA	60.11	55.00	
TLR4	FWD	CCTGACACCAGGAAGCTTGA	59.60	55.00	142
	REV	CTTCAAGGGTTGAAGCTCAGA	60.22	50.00	
MyD88	FWD	GAGGCATCACCACCCTTGAT	59.74	55.00	107
	REV	CCGGATCATCTCCTGCACAA	59.82	55.00	
TIRAP	FWD	AGTTTGGAGGCCTGCACTAT	59.00	50.00	233
	REV	CTCTCCGGTGAAGTGTGACT	59.04	55.00	
IRF3	FWD	TGGGTCAAGAGGCTTGTGAT	58.93	50.00	182
	REV	ATGTCCTCCACCAAGTCCTG	59.01	55.00	
MMP9	FWD	GAAAACCTCCAACCTCACGGA	60.20	52.38	224
	REV	TTTGGAATCGACCCACGTCT	59.32	50.00	
MMP12	FWD	GCTGCTCCCATGAATGACAG	58.98	55.00	186
	REV	TGCCAGAGTTGAGTTGTCCA	59.16	50.00	
MMP28	FWD	CAACTTGTTCTGTTGCTGG	59.97	55.00	354
	REV	CGAGGCTCTGAAACATTGCC	59.55	55.00	
mTOR	FWD	ATCCGCTACTGTGTTGGC	60.11	55.00	239
	REV	TTGATTCTCCAATGCCGCT	60.03	50.00	
IL6Ra	FWD	TCACTGTGCGTTGCAAACAG	59.90	50.00	102
	REV	TACCACAAGGTTGGCAGGTG	60.18	55.00	
Akt1	FWD	CTGCCCTTCTACAACCAGGA	59.02	55.00	214
	REV	CATACACATCCTGCCACACG	58.99	55.00	
Serpina1a	FWD	ACTGCTGTCTTCTTCTGCC	59.96	55.00	210
	REV	GAGGTCAGCCCCATTGTTGA	59.96	55.00	
CYLD	FWD	CCAGGTAGCAGGTTCCGGC	60.13	66.67	250
	REV	TCCGTTCTTCCCAGTAGGGT	59.88	55.00	
NFKBIA (IkBa)	FWD	AGGACGAGGAGTACGAGCAA	60.32	55.00	141
	REV	CGTGGATGATTGCCAAGTGC	60.18	55.00	

CRP	FWD	AGCTACTCTGGTGCCTTCTG	59.10	55.00	208
	REV	GAGAAGACTGAAGCTGCG	58.93	55.00	
NRF2	FWD	ACATGGAGCAAGTTGGCAG	59.04	50.00	234
	REV	TGGAGAGGATGCTGCTGAAA	59.01	50.00	

### 3.3.3.2. Melt curves

As part of the primer validation process, RT-qPCR was performed on spleen samples using the primers shown in table 3.3.3. Melt curves were used to determine primer binding specificity and amplification of target gene sequence. Housekeeping genes (Hprt1, TBP, Tuba1 and SDHA) had previously been validated in-house and routinely used in other projects and published data, and so validation for these primers was not deemed necessary. The peak of a melt curve is expected to lie between 85 – 90°C, where double stranded DNA (dsDNA) denatures into single stranded DNA (ssDNA) and thus fluorescent signal from amplification is lost as a result of dissociation of intercalating dye (SYBR green). This provides an indication of the specificity of primers, as dsDNA amplified from nonspecific sites will likely have different melting temperatures and thus produce peaks at lower temperatures. The same can be observed in the case of primer dimers, where FWD and REV primers bind to each other due to complimentary sequences and cause shorter amplification than the target DNA sequence.

Melt curves for generated primers largely showed a high degree of specificity. Although some primer dimers were observed for NLRP3, the majority of peaks fell in the expected position in comparison to negative controls (figure 3.3.14A). NOX2 primers displayed high specificity, with negative controls producing peaks indicative of nonspecific binding and primer dimers (figure 3.3.14B).

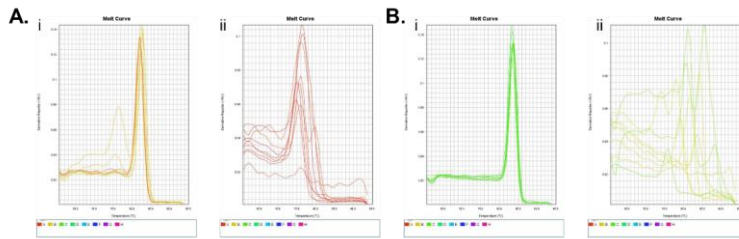


**Figure 3.3.14:- Melt curves for inflammasome genes for RT-qPCR panel.** Curves were generated for NLRP3 (A.i (positive sample) and A.ii (negative controls (dH<sub>2</sub>O, no template control (NTC) and no reverse transcriptase (NRT))) and NOX2 (B.i (positive sample) and B.ii (negative controls (dH<sub>2</sub>O, NTC and NRT))).

Some primer dimers for TLR2 and TLR4 were observed, likely due to these genes being variable in expression in an inflammation-dependent manner (figure 3.3.15A and B). MyD88, TIRAP and IRF3 displayed some evidence of primer dimers or nonspecific binding, but were shown to be highly specific in binding capacity in comparison to negative controls (figure 3.3.15C, D and E).

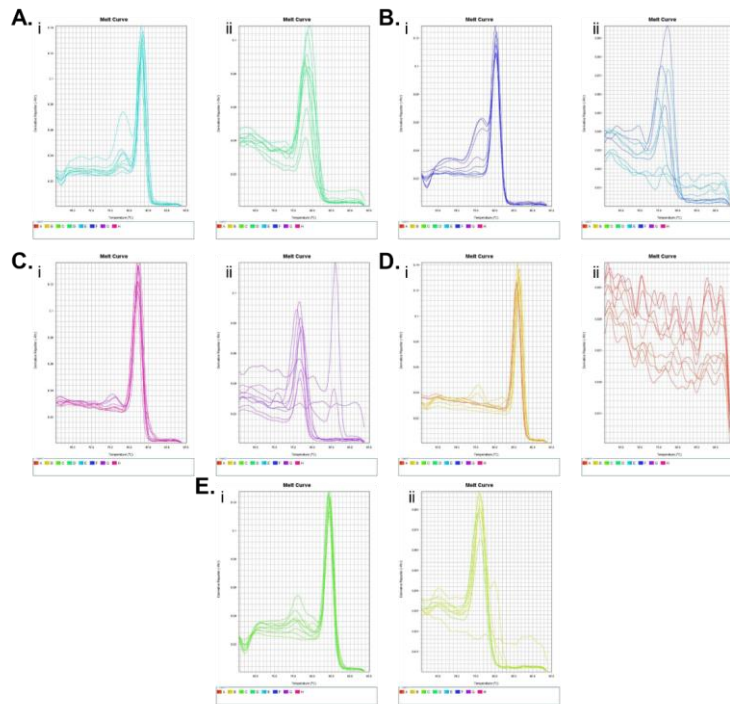


**Figure 3.3.15:- Melt curves for TLR signalling genes for RT-qPCR panel.**

Curves were generated for TLR2 (A.i (positivesample) and A.ii (negative controls dH<sub>2</sub>O, no template control (NTC) and no reverse transcriptase (NRT))), TLR4 (B.i (positivesample) and B.ii (negative controls dH<sub>2</sub>O, NTC and NRT)), MyD88 (C.i (positivesample) and C.ii (negative controls dH<sub>2</sub>O, NTC and NRT)), TIRAP (D.i (positivesample) and D.ii (negative controls dH<sub>2</sub>O, NTC and NRT)) and IRF3 (E.i (positivesample) and E.ii (negative controls dH<sub>2</sub>O, NTC and NRT)).

MMP primer specificity was difficult to ascertain from melt curve analysis alone, as potential primer dimers and nonspecific binding were observed for all three genes (figure 3.3.16). In a similar way to TLR2 and TLR4, this is likely the result of such genes typically only being expressed to a high degree in the event of inflammation or ECM changes, to which originating samples had not been subjected. In particular, specificity for MMP28 could not be determined (figure 3.3.16C).

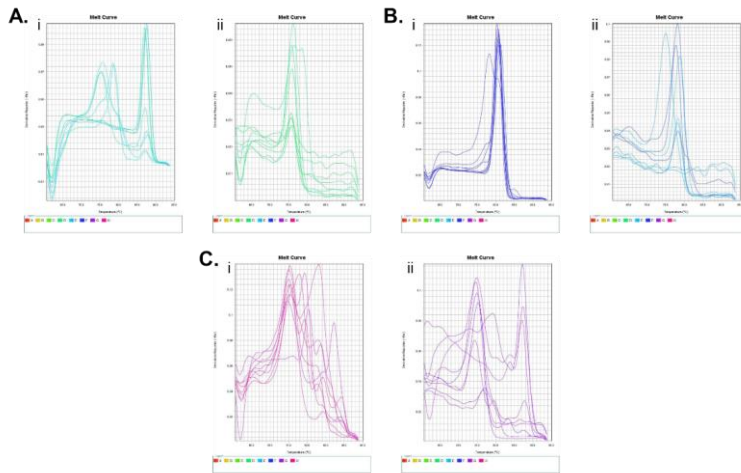


**Figure 3.3.16:- Melt curves for matrix metalloproteinase genes for RT-qPCR panel.** Curves were generated for MMP9 (A.i (*positivesample*) and A.ii (negative controls *(dH<sub>2</sub>O, no template control (NTC) and no reverse transcriptase (NRT))*)), MMP12 (B.i (*positivesample*) and B.ii (negative controls *(dH<sub>2</sub>O, NTC and NRT)*)) and MMP28 (C.i (*positivesample*) and C.ii (negative controls *(dH<sub>2</sub>O, NTC and NRT)*)).

Primers for IL6R signalling showed similar trends to TLR signalling primers, with some primer dimers or nonspecific binding present for all three genes (figure 3.3.17). Despite this, significant specificity was observed to conclude effective primer binding to the desired amplicon.

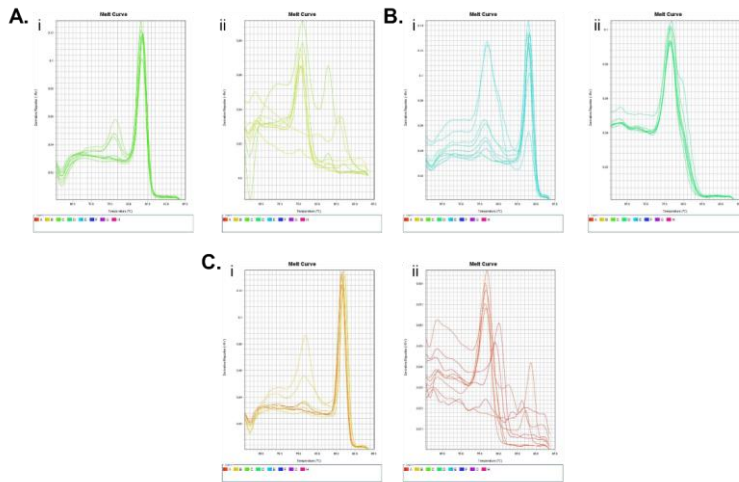


**Figure 3.3.17:- Melt curves for IL6R signalling genes for RT-qPCR panel.**

Curves were generated for IL6RA (A.i (*positivesample*) and A.ii (negative controls (*dH<sub>2</sub>O*, no template control (NTC) and no reverse transcriptase (NRT))), Akt1 (B.i (*positivesample*) and B.ii (negative controls (*dH<sub>2</sub>O*, NTC and NRT))) and mTOR (C.i (*positivesample*) and C.ii (negative controls (*dH<sub>2</sub>O*, NTC and NRT))).

Primer specificity for remaining genes displayed notable evidence of nonspecific binding in many cases. In particular, primers for Serpina1a showed significant amplification at a nonspecific site, though this was likely due to generally low expression of Serpina1a in spleen (figure 3.3.18A). Binding to CYLD displayed high specificity (figure 3.3.18B), though NFKBIA, CRP and **NOX2-NRF2** showed evidence of nonspecific binding (figure 3.3.18C, D and E). The degree of nonspecific binding in these cases is likely due to these genes typically being involved in induction or resolution of inflammation, which in tissues in homeostatic conditions would neither be upregulated nor downregulated. Whilst some primers displayed evidence of nonspecific binding or primer dimers, these findings could be explained by the fact that their target amplicons are typically influenced by inflammatory conditions which were not present in the sample material.

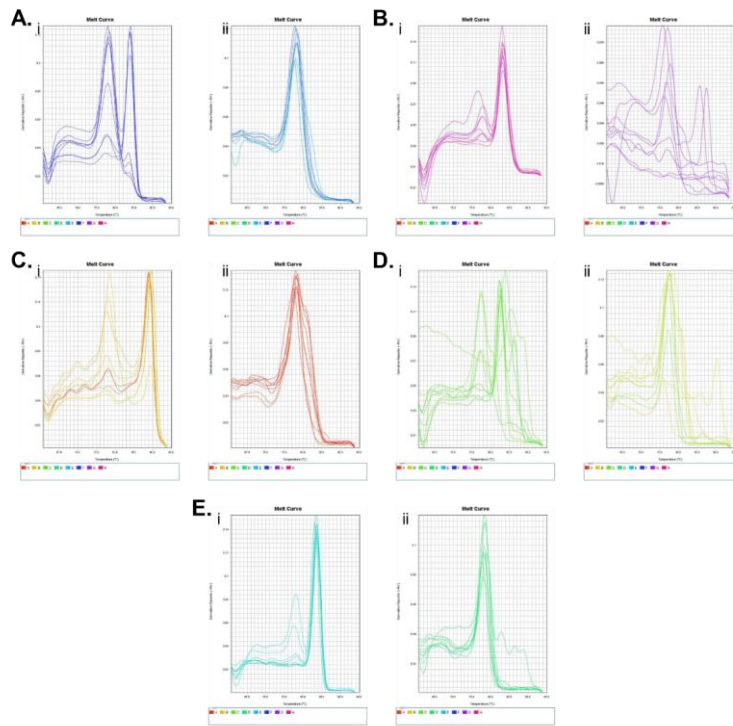


**Figure 3.3.18:- Melt curves for other key inflammatory genes for RT-qPCR panel.** Curves were generated for *Serpina1a* (A.i (positivesample) and A.ii (negative controls (dH<sub>2</sub>O, no template control (NTC) and no reverse transcriptase (NRT)))), *CYLD* (B.i (positivesample) and B.ii (negative controls (dH<sub>2</sub>O, NTC and NRT))), *NFKBIA* (C.i (positivesample) and C.ii (negative controls (dH<sub>2</sub>O, NTC and NRT))), *CRP* (D.i (positivesample) and D.ii (negative controls (dH<sub>2</sub>O, NTC and NRT))) and *NRF1X2* (E.i (positivesample) and E.ii (negative controls (dH<sub>2</sub>O, NTC and NRT))).



### 3.3.3.3. Agarose gel electrophoresis

To further validate the specificity of primers, a selection of amplified samples following RT-qPCR were subject to agarose gel electrophoresis to determine amplicon size. As most products fell into the range of between 150 – 250 bp, bands were anticipated within this region at the bottom of the gel once it had been run. As shown in figure 3.3.19, the majority of product bands can be observed within the 100 – 300 bp range of the DNA ladder, thus demonstrating amplification of the desired amplicon. Some primer dimers and nonspecific binding can be observed, particularly for MMP amplicons which was to be expected (figure 3.3.19A), however given that clear bands were observed at the expected size, it was concluded that all primers within the panel were specific for their targets.

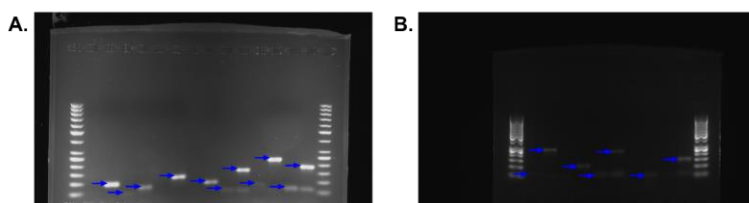


**Figure 3.3.19:- Agarose gels to determine size of resulting products following RT-qPCR to determine primer specificity.** Product bands are identified and marked with blue arrows, several gels were run and only a selection of amplicon targets were used due to the large number of genes. One gel tested the products of inflammasome, TLR signalling and MMP primers (A) and the second testing the other genes and housekeeper primers (B). A GeneRuler 50 bp DNA ladder was used as a control to estimate the size of products.

### 3.4. DISCUSSION

Reduction is one of the integral foundations of minimising the impact of animal use in science, typically achieved through collaborative efforts with other research groups or the use of high-throughput analytical techniques. Despite this, large-scale panels for mouse sample analysis are few and far between. Here, we have produced two panels that will allow the comprehensive identification and characterisation of peripheral immune cells in mice through spectral flow cytometry, and analysis of inflammatory gene alterations in mouse tissues.

While mouse flow cytometry panels do exist, these are often designed for deep phenotyping of one cell type or split across multiple panels [368, 371]. Deep phenotyping allows for the full characterisation of cells and their effector functions, but also means that cells and effector functions outside of those targeted are not detected. For complex diseases with multiple mechanisms, and where immunopathogenic mechanisms are not fully understood, this results in failure to report potential mechanisms or abnormal cell phenotypes and behaviour. Although this panel does not provide the deep phenotyping other current panels possess, it allows for the identification of all major immune cells known to influence COPD pathogenesis, in addition to broad activation markers and cytokines. This will allow for the identification of potential cell types or markers that can be further characterised in future research using purpose-built deep phenotyping panels. Despite the widespread availability of anti-mouse reagents for scientific research, panel design is often still limited by these reagents. During panel design, once common fluorophores had been assigned to markers the availability of appropriate commercial antibody-fluorophore conjugates was severely diminished. As a result, a selection of these antibodies had to be conjugated in-house using purified antibodies and appropriate conjugation kits. Furthermore, addition of future markers to this panel is limited.

The development of this flow cytometry panel has highlighted the challenges for the design of analytical techniques for mouse studies, and these are even more pronounced for less commonly used species, such

as rat, hamster and guinea pig. Additionally, the majority of high-throughput flow cytometry panels for mouse are designed for the analysis of tissue samples as opposed to whole blood. As discussed in section 3.3.1.1, immune cells vary in abundance dependent on the tissue type, and as such panels optimised and developed for specific tissue types may not have the same isolation efficiency if used in a different tissue type. For example, cells not typically found in high abundance in the peripheral blood, such as NK cells, are widely reported to be difficult to isolate and phenotype [377]. This was evident during the validation stages of our panel, as low populations of NK cells were reported even in murine spleen, such that we could not rely on standard methodology to calculate optimal dilutions for CD49b, our NK cell-specific marker (Appendix C figure C.9 and C.10). Although we were able to determine an optimal dilution factor for this marker's antibody using a different strategy, the challenges of NK cell isolation in whole blood were highlighted in our multiplex validation. NK cells comprised only 0.69% of all CD3- immune cells found in peripheral blood (figure 3.3.5A), and had an alternate fluorophore or different dilution factor been selected that would have been more appropriate for tissues where NK cells are found in higher abundance (for example, the bone marrow, lymph nodes and uterus), this population may not have been able to have been isolated. In addition, other high-throughput panels show similar limitations in reagent availability and demonstrate the necessity of using in-house conjugation kits to maximise panel output [378]. Despite these challenges however, we have successfully designed, optimised and validated a novel high-throughput flow cytometry panel for the identification and characterisation of murine peripheral immune cells in whole blood, making it the first of its kind, to the best of our knowledge.

Although RPPA allows for the generation of large-scale datasets with minimal samples, this technique comes with its own challenges. Cross-reactivity is often considered to be an unwanted and impeding problem with regards to antibody-based immunoassays, and is often widely reported in the literature [379]. Here, we had anticipated to see

cross-reactivity between the anti-human antibodies and our murine samples, as the manufacturer specifications reported mouse cross-reactivity. As this panel had previously been validated for human COPD patient samples, we had intended to translate this panel into mice to further bolster evidence of the translational ability of our mouse model design. However, as shown in figure 3.3.13, it was found that this panel did not bind to mouse samples, despite manufacturer specifications reporting mouse cross-reactivity. Although this panel could not be validated for murine samples, this nonetheless provides a prime example of the necessity of optimising and validating analytical techniques prior to a study's start so as not to waste samples in short supply [380]. This is critical, particularly if a study involves the use of animals, as it minimises the potential risk of unnecessary animals being used. To further highlight this, all murine-derived samples used for the validation and optimisation of our analytical techniques were sourced from studies that had already been conducted or from animals on other studies where the source material would have otherwise gone to waste.

Whilst the RPPA panel was dropped from the project and thus proteomic analysis of mouse samples would not be possible, we were able to design and validate an alternative RT-qPCR panel. This would allow us to examine the effects of cigarette smoke on the upregulation or downregulation of key inflammatory genes, in addition to genes identified as linked to COPD in GWAS studies. Although RT-qPCR is widely used in biomedical research, in addition for diagnostic purposes, there are concerns regarding the reproducibility of data obtained from this method. While the exact reasons for issues in reproducing published data are unknown, it is speculated that poor quality samples, inappropriate methodology or analysis techniques may contribute towards lack of reproducibility [381]. In recent years, one of the most prevalent uses of RT-qPCR has been for the diagnosis of SARS-CoV2 infection. Failure to validate the binding efficiency of primer-probe sets can lead to false positives or negatives, which in the case of diagnostics can lead to significant consequences. For example, in one study it was found that a

commercially available primer-probe set for diagnosis of SARS-CoV2 infection had a mismatched reverse primer for circulating virus RNA, thus leading to low sensitivity and an increased possibility of false negative results [382]. Additionally, with no specified universal methodology, RT-qPCR displays differing degrees of sensitivity and specificity, which proves to be a significant roadblock in the comparison of data both between and within research and diagnostic laboratories [383]. Lack of reproducibility has also been linked to the use of outdated methods to normalise gene expression [384] or use of unstable housekeeping genes for normalisation [385]. Genes are also heterogeneously expressed even in the same tissue type, as such samples taken from the same tissue, but different regions, may show differences in gene expression unrelated to tissue state (e.g. diseased vs control). This provides an explanation as to why for some genes melt curves displayed evidence of primer dimers or nonspecific amplification, as cDNA was generated from unspecified regions of the spleen. It also highlights why testing housekeeping genes for stability is pivotal to analysis, as different housekeeping genes may be more or less stable within different regions of the same tissue [386]. Whilst we did not conduct normalisation analysis on the genes and primers included in our panel, these are important factors to take note of for the analysis of RT-qPCR data. Common housekeeping genes were previously validated using the same methods to validate primers for the RT-qPCR panel, and therefore prior to any normalisation and expression analysis a selection of these housekeeping genes would be tested in lung tissues to identify the most stable housekeepers for normalisation. Additionally, cDNA would be generated from the same region of the lung in each sample and full details of RT-qPCR methodology including RNA quality for cDNA generation would be reported, thereby increasing reproducibility power of our analysis. Nonetheless, primers for TLR4, IRF3, MMP9, MMP28, Akt1, mTOR, Serpina1a, CYLD, NFKBIA, CRP and NRF2 were dropped, as data may not be reflective of actual gene expression due to the presence of consistent nonspecific binding during the validation process as shown by the presence of peaks outside of the expected melting temperature. Primers for NLRP3, NOX2, TLR2,

MyD88, TIRAP, MMP12 and IL6RA were used for analysis of samples as these displayed high specificity with minimal evidence of nonspecific binding which could be attributed to instances of human or experimental errors within repeats.

Overall, these results demonstrate the challenges faced during optimisation and validation of high-throughput techniques. These findings provide an example of the considerations and steps needed for target selection and panel design, and also demonstrate the quality and quantity of data that can be obtained following validation. In all, these techniques and the resulting outputs highlight the necessity of building multiplexed and high-throughput panels for analysis of mouse samples, as large datasets can be obtained without having to increase the numbers of animals used or rapidly depleting sample stocks.

## CHAPTER 4 – SYSTEMIC EFFECTS OF CSE EXPOSURE

### 4.1. INTRODUCTION

COPD is primarily a disease of the respiratory system, but it also displays a multitude of whole-body symptoms, including chronic fatigue and weight loss, as well as systemic inflammation. Given the prevalence of comorbidities in COPD patients, it is important to gain an understanding of whole-body mechanisms which may either contribute towards COPD itself or result in, or exacerbate, pre-existing comorbid conditions. Even within the lungs, while the presence of tissue-resident immune cells is generally considered to be a part of the normal pulmonary environment, an increased presence of both tissue-resident and circulatory immune cells within the airways is considered a hallmark of COPD. These cells are often trafficked into the lungs from other areas, such as the circulatory system, and thus alterations to immune cell profiles in systemic blood may provide insight into both pulmonary and whole-body aspects of COPD pathophysiology.

Immune homeostasis in the blood and tissues is pivotal for the maintenance of healthy function, and altered populations or effector functions of otherwise normal conditions can lead to inflammation, tissue injury or disease. Skewed distribution of inflammatory to anti-inflammatory cell types and effector functions in circulatory blood, for example, has been linked to poor outcomes in smokers and increased risk of cancer development due to reduced clearance of nascent tumour cells [387]. Th17/Treg imbalance is widely reported as a contributing factor to COPD pathophysiology, though this imbalance is typically reported within the pulmonary spaces. It has been shown that although peripheral Treg numbers and function do not appear to be affected by CS, impaired function is widely reported in the lungs [388]. In some instances, disproportion of CD4<sup>+</sup> to CD8<sup>+</sup> T cells in the periphery has been reported amongst COPD patients, though these findings are not universal [190, 389]. Despite this, altered effector functions of both CD4<sup>+</sup>

and CD8<sup>+</sup> T cells in COPD patients are widely reported, and these mechanisms are often considered abnormal and inflammatory in nature [389]. Understanding how cell function changes between the periphery and the pulmonary environment may provide insight as to how immunoregulatory function can be restored in COPD patients.

Neutrophils are granulocytes of the innate immune system, and are well characterised in COPD, with pulmonary neutrophilia often used as a diagnostic criterion for COPD. Despite their presence in the lungs being well documented in COPD, neutrophils by nature are generally found in peripheral blood, and are trafficked into tissue systems in response to infection or inflammation. In the periphery, neutrophils are shown to overexpress PRRs which amplify neutrophil recruitment and migration, and can thus result in increased production of proinflammatory effector functions [180].

-Whilst macrophages are not typically found in peripheral blood, it has been demonstrated that macrophages derived from peripheral monocytes of COPD patients display impaired phagocytic function, and contribute towards risk or frequency of AECOPD [390]. Furthermore, peripheral monocytes are shown to display altered gene transcript profiles in COPD patients which suggested enhanced inflammatory mechanisms, and cessation of smoking was not found to correlate to the reversal of these findings unless cessation began at an early age [391].

-Deep phenotyping of NK cell populations has also demonstrated that the identification of NK cell subtypes can be used as a predictor of AECOPD, as certain phenotypes display significant associations with individuals who had previously experienced exacerbations [392]. Thus, not only is it important to understand the contribution of inflammatory/anti-inflammatory cell type imbalances in COPD pathogenesis, but also their effector functions, as these are often indicative of disease severity and prognosis.

To determine the systemic effects of CSE on immune cell populations and distributions, we examined the whole blood of mice



exposed to CSE over a 12-week period. This would enable us to not only examine the effects of CSE on systemic immune cell phenotypes and effector functions, but also examine how CSE would affect immune cell populations over time. Once per week, tail vein bleeds were collected from each mouse and immune cell populations were examined via a comprehensive spectral flow cytometry panel. This panel enabled us to characterise populations of T cells (CD4<sup>+</sup> and CD8<sup>+</sup> subsets, including Tregs and Th17), NK cells, macrophages, neutrophils, monocytes, DCs and B cells. Effector functions including production of proinflammatory cytokines (IFN- $\gamma$ , IL-6, IL-17A and TNF- $\alpha$ ) were also examined. Clustering analysis was also performed as an unbiased analysis of specific cell types and distribution amongst groups according to sex, CSE dose, week or overall experimental group. Here, we present data gathered from analysis of whole-blood isolated from mice during our intranasal CSE model of COPD, to determine the potential peripheral immunopathogenic mechanisms of COPD.

## 4.2. METHODS

### 4.2.1. MURINE MODEL

#### 4.2.1.1. Home Office Licences

Full details and methods of Home Office Licences are found in Section 2.1.1.1. Materials – Home Office Licences and welfare checks. Briefly, all procedures were performed under PEL, PPL and PILs registered with the University of Nottingham in accordance with ASPA guidelines.

#### 4.2.1.2. Animals and housing conditions

Further details can be found in Section 2.1.1.2. Materials – Animals and housing conditions. Briefly, twenty-four 8-week-old male and female C57BL/6J mice (12 per sex) were supplied by Charles River Laboratories. Animals were housed in single-sex cages of 3 or 4

individuals under specific pathogen-free, temperature and air control conditions with a 12-hour light-dark cycle. Regulated procedures did not commence on animals until 11-weeks of age due to staff and spacing issues. Furthermore, a single male mouse was withdrawn prior to the study start as a result of injuries sustained from fighting with littermates making the total number of animals used on the study twenty-three.

### 4.2.1.3. Monitoring of animal welfare

In-depth methodology for all regulated procedures performed using animals can be found in Section 2.2.1. Methods – Murine COPD Model. Briefly, full welfare checks were performed three times per week prior to intranasal dosing to check for aberrations of normal health. This included recording of weight and scoring of behavioural and physical health indicators according to a predefined welfare score sheet (see Appendix B). In the event of signs of adverse effects, NACWOs were notified and veterinary intervention was sought as directed or necessary.

### 4.2.1.4. Acclimatisation to restraint procedures

Mice were acclimatised to restraint procedures over a week-long period, with positive reinforcement to handling and remaining in restraint tubes performed using sunflower hearts. This took place through repeated exposure to increasingly invasive handling and restraint methods to desensitise animals to stress of methods, commencing with basic handling at the beginning of the week and finishing acclimatisation by restraining mice in restraint tubes for up to 30 seconds.

### 4.2.1.5. Generation of cigarette smoke extract

Cigarette smoke extract was generated by expelling smoke from a single Marlboro Red cigarette with the filter broken off into 10 mL phenol red-free RPMI. The resulting media was sterile filtered through a 0.45 µm filter, and was used to generate 1% and 3% CSE in a total volume of 1

mL phenol red-free RPMI. 1 mL sterile phenol red-free RPMI containing no CSE was used as a control. All media was temperature and pH checked and maintained at room temperature and neutral pH in preparation for intranasal dosing.

#### 4.2.1.6. Intranasal dosing

Full welfare checks were performed prior to intranasal dosing to check for signs of ill health or adverse welfare effects. Following this, mice were placed into an anaesthesia chamber on a cage-by-cage basis and exposed to 2.5% isoflurane mixed with O<sub>2</sub>. After sedation and loss of righting reflex, mice were placed onto their sides and isoflurane was increased to 3.5%. After observation of gasping mechanism, mice were individually removed from the chamber and held in an upright position with the head tilted back to open airways. 25 µL CSE or control media was administered into the nasal cavity, and after the dose had been inhaled and respiratory rate had stabilised mice were returned to their home cages. After all mice had regained consciousness, a brief welfare check was performed to check for signs of adverse effects following anaesthesia.

#### 4.2.1.7. Tail vein blood sampling

Tail vein blood sampling was performed once per week. Mice were placed into restraint tubes and restrained at the base of the tail, the rest of the tail was then placed into a beaker of body temperature water containing hibiscrub to encourage vasodilation and sterilise the sampling area. After 30 seconds, the tail was wiped dry with a sterile gauze pad and the lateral caudal vein was located and punctured with a 25G needle. 20 µL blood was collected using a heparinised capillary tube and then expelled into an Eppendorf tube. Pressure was applied to the puncture site using a sterile gauze pad until bleeding had stopped, after which mice were returned to their home cages and rewarded with sunflower hearts to reinforce acclimatisation to restraint and handling procedures.

#### 4.2.2. SPECTRAL FLOW CYTOMETRY

##### 4.2.2.1. Whole blood staining

Full details of spectral flow cytometry methods can be found in section 2.2.2. Methods – Spectral Flow Cytometry. Briefly, for whole blood staining, a protein transport inhibitor was added to 20  $\mu$ L murine whole blood and incubated for 3.5 hours at 37°C. Fc block was then added and the blood was incubated for a further 30 minutes at 37°C. A RBC lysis buffer was added to each sample, and centrifuged following a 5 minute incubation at room temperature. Supernatants were discarded and cells were resuspended in PBA before being centrifuged. After discarding the supernatant, cells were resuspended in an extracellular panel master mix (see section 2.2.2.5. Whole blood staining; table 2.2.1) and incubated at room temperature for 20 minutes in the dark. Cells were then washed once with PBA and were then resuspended in fix/perm working solution after discarding the supernatant. Following a 30-minute incubation at room temperature in the dark, cells were washed twice with perm wash buffer and resuspended in an intracellular panel master mix and left to incubate for 20 minutes at room temperature in the dark. Afterwards, cells were washed twice with perm wash buffer and resuspended in 500  $\mu$ L fixation buffer, transferred to FACS tubes and analysed using a Sony ID7000.

##### 4.2.2.2. Conventional flow analysis

Conventional gating and flow cytometry was performed in FlowJo. Gating strategies are shown along with results from flow cytometric analysis in section 4.3. Results. Statistical analysis was not performed due to low cell numbers.

## 4.2.2.3. Clustering analysis

Multi-dimensional clustering analysis was performed on live, single immune cells isolated from whole blood using equal sampling. Analysis was performed in FlowJo using FlowSOM clustering and presented using t-distributed stochastic neighbour embedding (tSNE) plots. Statistical analysis was performed by 2way ANOVA.

## 4.3. RESULTS

## 4.3.1. ANIMAL WELFARE

No adverse effects as a result of CSE exposure were reported throughout the 12-week exposure period, and any welfare concerns reported were as a result of typical mouse behaviour (e.g. overgrooming in females and fighting to establish social hierarchy in males). Changes in weight are typically used as the best indicator of poor health in mouse studies, as such, given the novelty of our study, animals were weighed three times per week prior to intranasal dosing. As shown in figure 4.3.1, both male and female mice consistently gained weight as expected over the 12-week period. At week 8, heavy-smoker males (figure 4.3.1A), light-smoker females and heavy-smoker females (figure 4.3.1B) showed some weight loss, though this weight was regained in addition to an incremental amount reflective of weight gain from previous weeks. While it is uncertain whether this weight loss was a result of regulated procedures, this observation coincides with the period at which the mice were moved

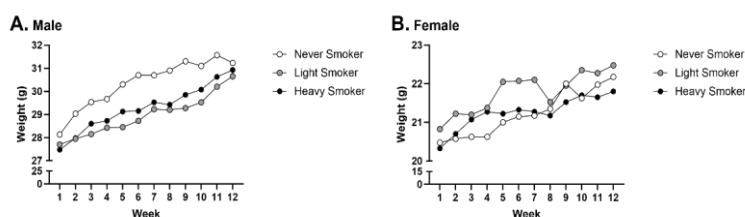


Figure 4.3.1:- Average weight of male (A) and female (B) C57BL/6J mice per week during a 12-week exposure to CSE. (n = 3 – 4)

to a new holding room. Therefore, these weight changes may be a result

of stress from a change in environment or brief transportation to the new room.

To determine if CSE dose impacted the rate of weight gain, the relative weight gain for each mouse was calculated. This was performed using the following calculation:

$$\begin{aligned} & \textit{relative weight gain} \\ &= ((\textit{end weight} - \textit{start weight}) \div \textit{number of weeks}) \\ &\times 100 \end{aligned}$$

Although no statistical differences were found by conducting a 2way ANOVA, small differences in relative weight gain were observed as a result of both dose group and sex. In particular, male mice displayed higher relative weight gain ( $\approx 24 - 29\%$ ) in comparison to female mice ( $\approx 12 - 14\%$ ), though this can be attributed to general mouse biology and characteristic sex differences based on predicted weight charts from suppliers (figure 4.3.2). Despite this, concentration of CSE appeared to have differing effects on relative weight gain dependent on sex. Male mice exposed to 3% CSE displayed higher relative weight gain ( $\approx 29\%$ ) in comparison to the never-smoker (0% CSE) control group ( $\approx 26\%$ ), whereas female mice exposed to 3% CSE showed lower relative weight gain ( $\approx 12\%$ ) by comparison to the control group ( $\approx 14\%$ ). Although not statistically significant, this data could suggest that females are more predisposed to reduction in relative weight gain than males, which may therefore contribute towards increased risk of weight loss amongst female COPD patients.

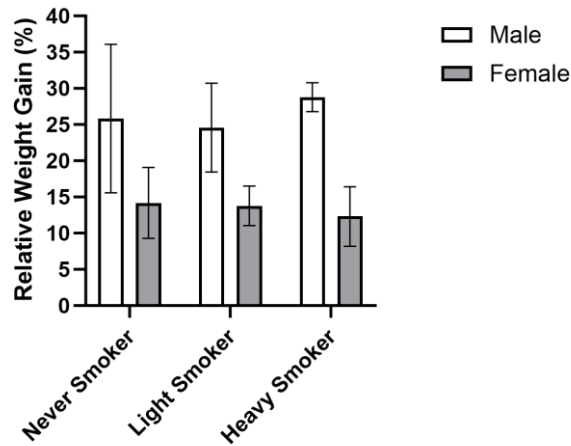
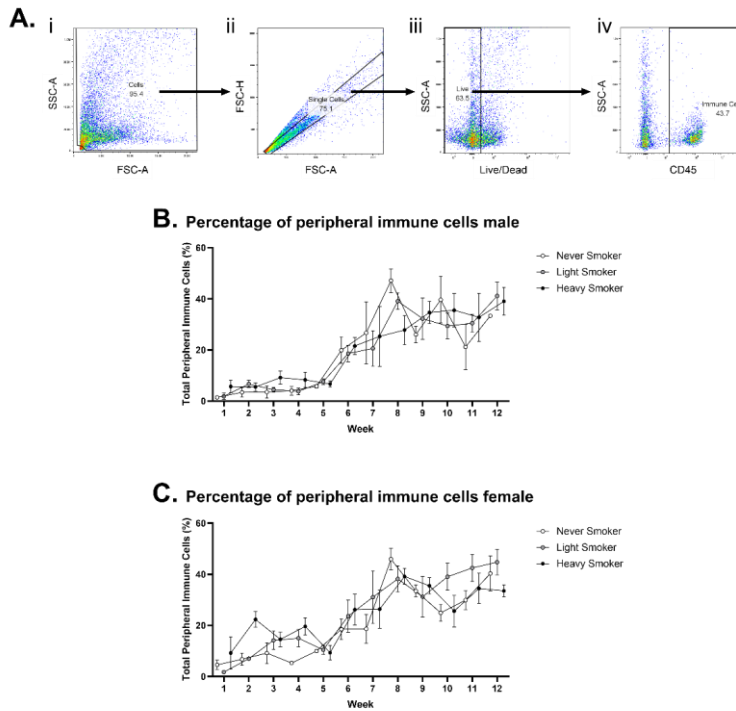


Figure 4.3.2:- Relative weight gain in male and female C57BL/6J mice over a 12-week exposure to CSE. Data plotted as mean  $\pm$  SEM, no statistical differences were identified via 2way ANOVA ( $n = 3 - 4$ )

#### 4.3.2. TOTAL PERIPHERAL IMMUNE CELLS

Total peripheral immune cells were defined according to the gating strategy shown in figure 4.3.3A. Although minimal differences in total peripheral immune cells were detected between dose groups, overall alterations to percentage were observed over the 12-week exposure period (figure 4.3.3B and C). This is demonstrated by an initial slight increase in total peripheral immune cells at week 2 for all groups, followed by a second increase at week 5, and a third increase at week 8 for male mice (figure 4.3.3B) and week 7 for female mice (figure 4.3.3C). These trends appear to demonstrate two separate increases in peripheral immune cells at week 2 and again at week 5, followed by sustained or regulated immune cell populations beyond week 7/8. What is important to note is that these changes to total immune cell numbers occur approximately one week earlier in females than in males, suggesting that female mice may be more susceptible to earlier exacerbations as a result of CSE exposure than males. Given that these trends are also demonstrated in both control groups however, it cannot be concluded that

these trends are a result of CSE concentration itself, but instead possibly a change in immune function as a result of ageing (figure 4.3.3B and C).



**Figure 4.3.3:- Total peripheral immune cells in whole blood of male and female C57BL/6J mice during 12-week exposure to CSE.** Gating strategy for single, live, and CD45+ immune cells shown in A. Peripheral immune cells are displayed as a percentage of total live single cells in male (B) and female (C) C57BL/6J mice. (n = 3 – 4; event count range = 22 – 9887 cells)

### 4.3.3. T CELLS

Total CD3+ T cells were gated according to the strategy defined in figure 4.3.4A. CSE exposure did not appear to have any noticeable effects on percentage of peripheral T cells, as all groups displayed similar trends and profiles for CD3+ T cells over time (figure 4.3.4B and figure 4.3.5A). However, data displayed a reduction in total peripheral T cells in all groups after week 2, with a gradual increase observed at week 5, followed by a second decrease in numbers after week 7. Whilst the exact



cause for these changes cannot be determined, it is possible that this trend further demonstrates two distinct increases in total T cell numbers, in a similar manner to that observed for total peripheral immune cells. Between weeks 1 and 2, total peripheral T cells increased, and in most groups (with the exception of never-smoker males) total peripheral T cells dropped below the baseline total recorded at week 1 (figure 4.3.4B and figure 4.3.5A). A second increase in total peripheral T cells at week 6/7 was observed, as percentage of T cells in peripheral blood return to a level just below the week 1 baseline (figure 4.3.4B and figure 4.3.5A). Following this increase, T cell numbers decreased to similar levels observed between weeks 3 – 5. Given that these observations were present for all dose groups, it cannot be concluded that CSE is the causative factor for the separate increases in T cell numbers, and therefore these trends may be a result of ageing or general immune homeostasis regulation.

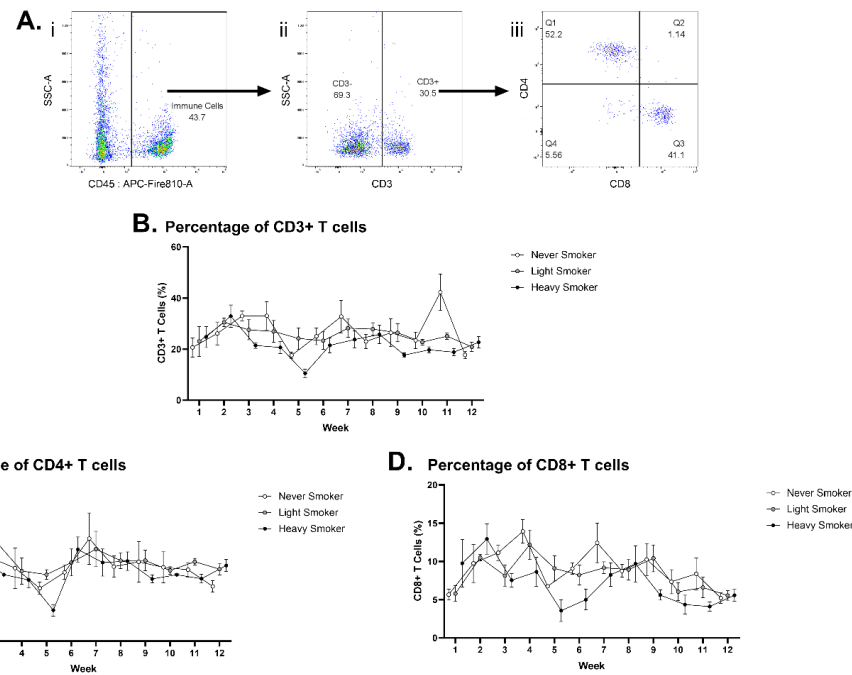


**Figure 4.3.4:- Percentage of CD3+ and proportions of CD4+ and CD8+ T cells in peripheral blood of male C57BL/6J mice during 12 weeks of CSE exposure.** Gating strategy is shown in A. Graphs show the total percentage of CD3+ T cells (B), CD4+ T cells (C) and CD8+ T cells (D). Data shown as a percentage of total peripheral immune cells. (n = 3 – 4; event count range = 0 – 1748)

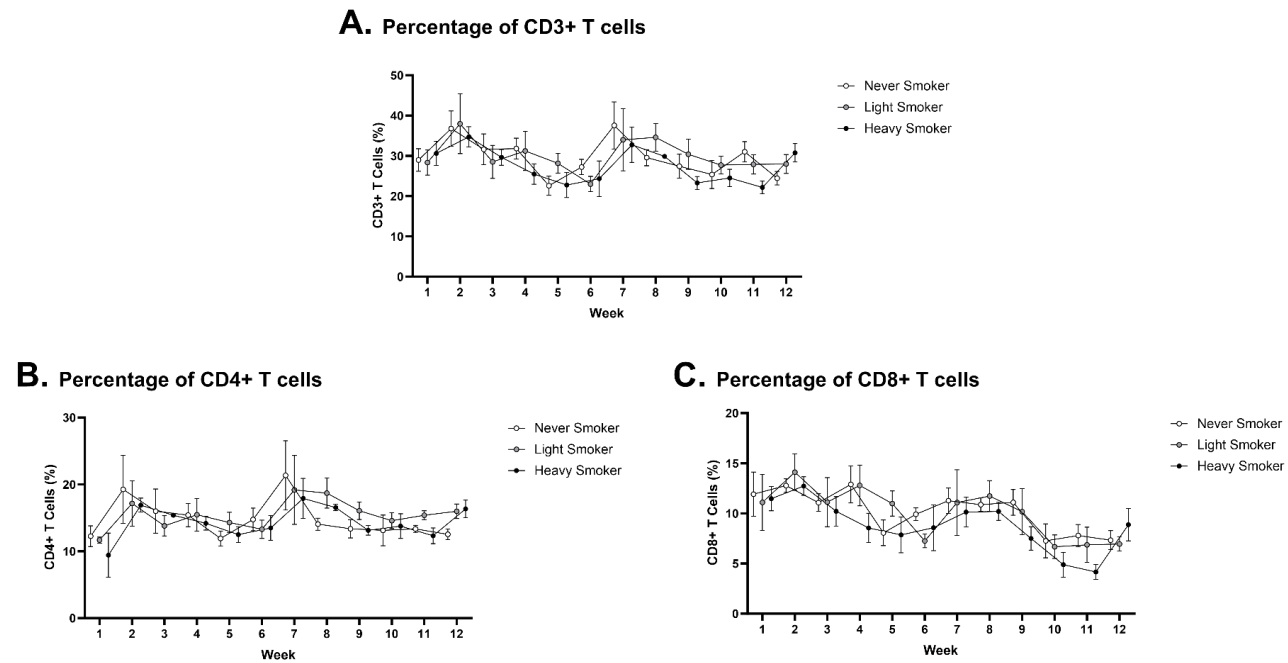


**Figure 4.3.5:- Percentage of CD3+ and proportions of CD4+ and CD8+ T cells in peripheral blood of female C57BL/6J mice during 12 weeks of CSE exposure.** Graphs show the total percentage of CD3+ T cells (A), CD4+ T cells (B) and CD8+ T cells (C). Data shown as a percentage of total peripheral immune cells. ( $n = 4$ ; event count range = 0 – 1993)

Although no differences in total T cell numbers were observed between groups, CSE exposure appeared to have an impact on the proportions of CD4<sup>+</sup> and CD8<sup>+</sup> T cells in the periphery. In male mice, exposure to 3% CSE appeared to have a negative impact on the ratio of CD4<sup>+</sup> T cells to CD8<sup>+</sup> T cells (figure 4.3.6C.i). For example, at week 9, the ratio of CD4<sup>+</sup> T cells to CD8<sup>+</sup> T cells for never-smoker and light-smoker males was approximately 1.3:1, whereas for the heavy-smoker group this ratio was approximately 2:1. The same trend was observed in female mice, with CD4<sup>+</sup> T cells found in higher abundance in comparison to CD8<sup>+</sup> T cells in the heavy-smoker groups (figure 4.3.6C.ii). At week 9, the ratio of CD4<sup>+</sup> T cells to CD8<sup>+</sup> T cells in the heavy-smoker group was 2.6:1, whereas these ratios were 1.9:1 for the never-smoker group and 2.3:1 for the light-smoker group. This may suggest that CD8<sup>+</sup> T cells are trafficking into the lungs.

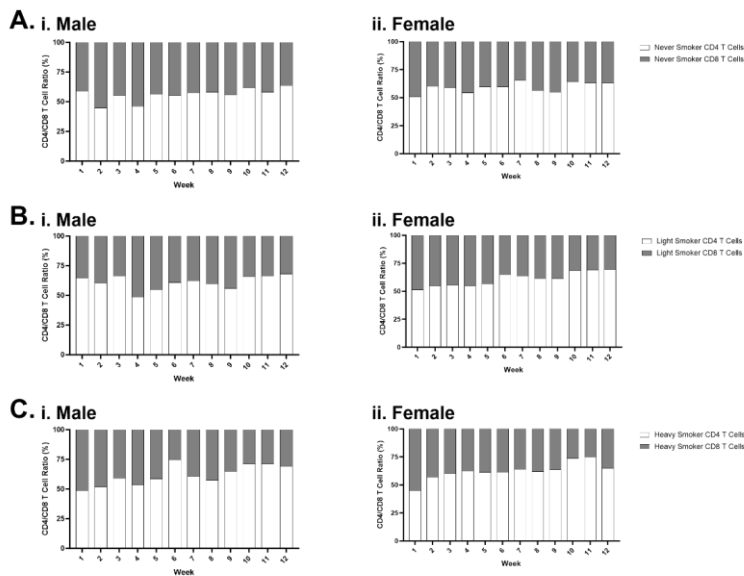


**Figure 4.3.6:- Ratios of CD4<sup>+</sup> and CD8<sup>+</sup> T cells in male and female C57BL/6J mice over a 12-week exposure period to CSE.** Graphs show distribution of CD4<sup>+</sup> and CD8<sup>+</sup> T cell populations in male (i) and female (ii) mice from never-smoker (A), light-smoker (B) and heavy-smoker (C) groups throughout the 12-week exposure period. Data shown as a percentage stacked ratio of total CD4<sup>+</sup>/CD8<sup>+</sup> T cell population as defined by CD3<sup>+</sup>CD4<sup>+</sup> and CD3<sup>+</sup>CD8<sup>+</sup> populations. (n = 3 - 4)

CD4<sup>+</sup> and CD8<sup>+</sup> T cells were then further characterised based on effector functions and cytokine production. CD4<sup>+</sup> T cells and their effector functions were gated according to the strategy defined in figure 4.3.7A and B. In both male and female mice, abundance of CCR7<sup>+</sup> CD4<sup>+</sup> T cells decreased over the course of the 12-week exposure period (figure 4.3.7C and figure 4.3.8A). This appeared to be the opposite for CD69<sup>+</sup> CD4<sup>+</sup> T cells, as CD69<sup>+</sup> populations appeared to increase over the 12-week period in both male and female mice (figure 4.3.7D and figure 4.3.8B). Higher numbers of CD69<sup>+</sup>CD25<sup>+</sup> CD4<sup>+</sup> T cells were detected in the earlier weeks of the exposure period, but beyond week 3 these numbers dropped and remained at a relatively constant level (figure 4.3.7E and figure 4.3.8C). CD4<sup>+</sup> T cells positively expressing CD25 in the absence of CD69 were defined as possible Treg subsets. Single positive CD25<sup>+</sup> CD4<sup>+</sup> T cells were found in higher abundance during the initial weeks of exposure (figure 4.3.7F and figure 4.3.8D). Beyond week 6, these numbers decreased and remained at similar levels for the remainder of the exposure period. Overall, this data suggests that over the course of model, the numbers of naïve CD4<sup>+</sup> T cells (indicated by CCR7<sup>+</sup> cells) are decreased, and early activated CD4<sup>+</sup> T cells (indicated by CD69<sup>+</sup> cells) which may contribute towards T cell differentiation are increased. No differences in these trends were observed between CSE dose groups.

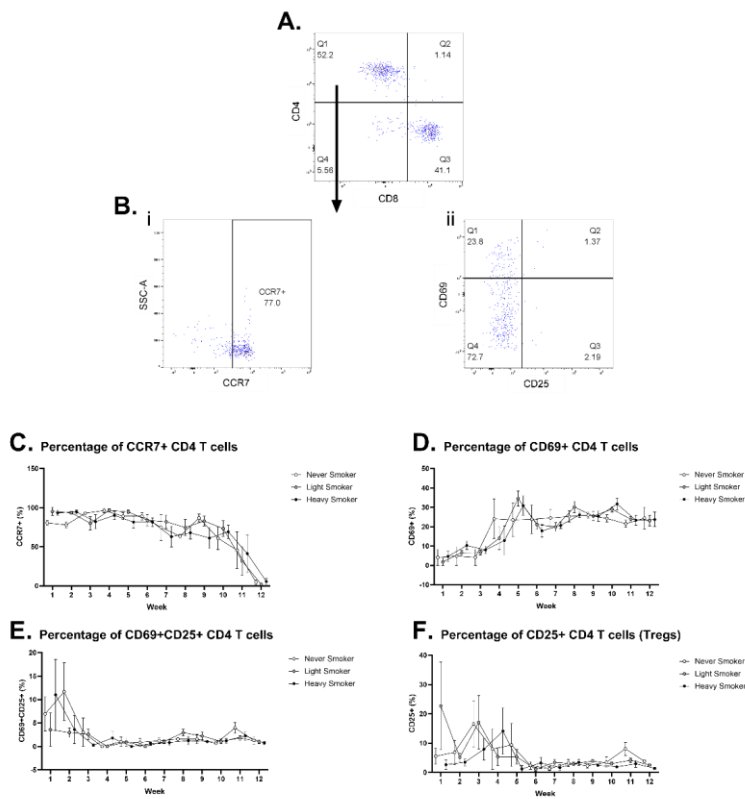


**Figure 4.3.7:- Percentage of activation marker-positive CD4+ T cells in peripheral blood of male C57BL/6J mice during 12 weeks of CSE exposure. Gating strategy is shown in A and B. Graphs show the percentage of CCR7+ (C), CD69+ (D), CD69+CD25+ (E) and CD25+ (F) expression by CD4+ T cells. Data shown as a percentage of total peripheral CD4+ T cells. (n = 3 – 4; event count range = 0 – 402)**

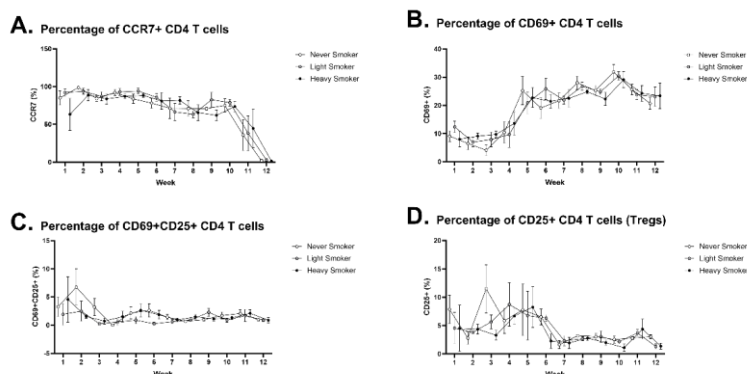


**Figure 4.3.8:- Percentage of activation marker-positive CD4<sup>+</sup> T cells in peripheral blood of female C57BL/6J mice during 12 weeks of CSE exposure.** Graphs show the percentage of CCR7<sup>+</sup> (A), CD69<sup>+</sup> (B), CD69<sup>+</sup>CD25<sup>+</sup> (C) and CD25<sup>+</sup> (D) expression by CD4<sup>+</sup> T cells. Data shown as a percentage of total peripheral CD4<sup>+</sup> T cells ( $n = 4$ ; [event count range = 0 – 568](#))

Cytokine positive CD4<sup>+</sup> T cells were defined by the gating strategy shown in figure 4.3.9A and B. In both male and female mice, IFN- $\gamma$ + CD4<sup>+</sup> T cells were increased in the early stages of the model for all groups, and minimal to no presence was detected beyond week 7 (figure 4.3.9C and figure 4.3.10A). IL-6+ CD4<sup>+</sup> T cells showed a similar trend, with increased presence between weeks 1 – 6, with a second increase at week 10, suggesting two separate increases in IL-6+ CD4<sup>+</sup> T cells (figure 4.3.9D and figure 4.3.10B). Both male and female mice demonstrated increased presence of IL-17A+ CD4<sup>+</sup> T cells in earlier stages of the model, with these numbers decreasing around week 5 and 6 before increasing again to numbers similar to those between weeks 3 – 4 (figure 4.3.9E and figure 4.3.10C). IL-17A was used as a marker for Th17 subsets of CD4<sup>+</sup> T cells, and this trend therefore suggests increased differentiation into Th17 in the periphery, though this appeared to be more prevalent in the never-smoker group and was therefore not linked to CSE exposure. TNF- $\alpha$ + CD4<sup>+</sup> T cells demonstrated a similar trend to IFN- $\gamma$  and IL-6, in that increased prevalence was detected in the earlier weeks of the model before dropping to minimal or no production beyond week 7 (figure 4.3.9F

and figure 4.3.10D). No differences in these trends were observed between CSE dose groups, therefore changes may be reflective of age-related changes in immune function. Despite this, high variation in percentages of cytokine positive CD4+ T cells was observed at week 1 in male mice in comparison to females. It is unclear why this variation was observed, and may have simply been a result of blood sampling methodology.

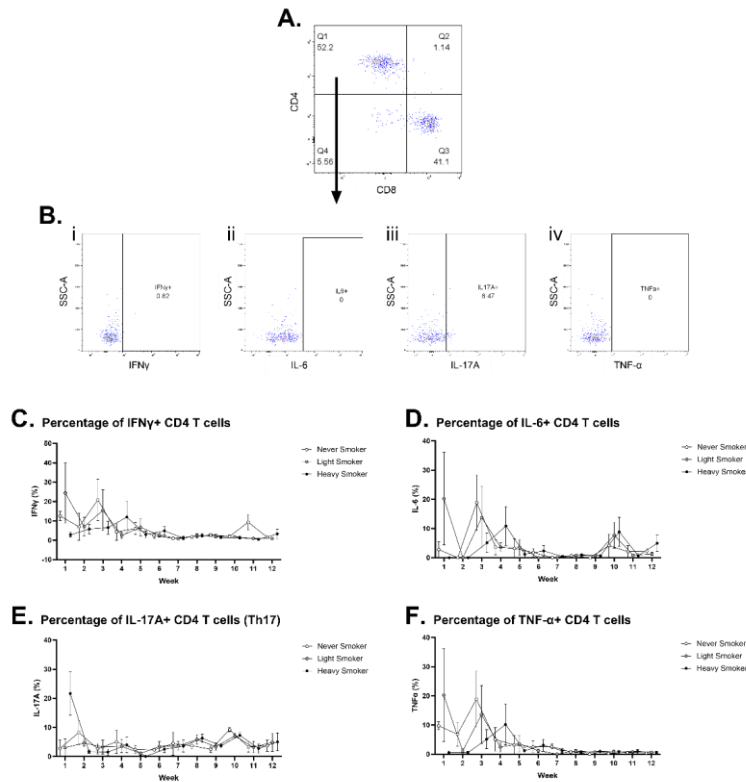


**Figure 4.3.9:- Percentages of cytokine positive CD4+ T cells in peripheral blood of male C57BL/6J mice during 12 weeks of CSE exposure.** Gating strategy is shown in A and B. Graphs show the percentage production of IFN- $\gamma$  (C), IL-6 (D), IL-17A (E) and TNF $\alpha$  (F) by CD4+ T cells. Data shown as a percentage of total peripheral CD4+ T cells. (n = 3 – 4; event count range = 0 – 34)



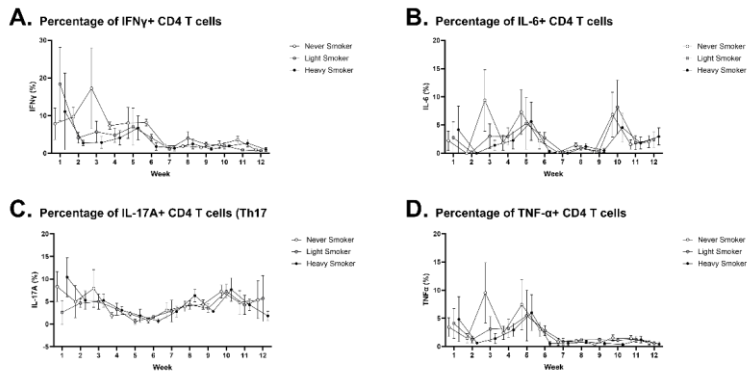


**Figure 4.3.10:- Percentages of cytokine positive CD4+ T cells in peripheral blood of female C57BL/6J mice during 12 weeks of CSE exposure.** Graphs show the percentage IFN- $\gamma$ + (A), IL-6+ (B), IL-17A+ (C) and TNF $\alpha$ + (D) CD4+ T cells. Data shown as a percentage of total peripheral CD4+ T cells. (n = 4; event count range = 0 – 59)

Imbalance of proinflammatory and anti-inflammatory immune cell types is a known contributing mechanism of COPD pathophysiology. One such imbalance that is widely reported in the literature is an imbalance of proinflammatory Th17 cells and anti-inflammatory Tregs. To determine Th17/Treg imbalance, CD4+ T cell subsets were defined as Th17 by expression of IL-17A or as Tregs by expression of CD25 in the absence of CD69. Percentage distribution of these subsets was determined proportionally according to the total numbers of Th17 and Tregs isolated per week. As shown in figure 4.3.11, Th17/Treg balance is shifted towards Treg differentiation in the first 5 weeks of exposure in all groups, however this shifts to a predominantly Th17 population from week 6 onwards. No differences in Th17/Treg ratios were observed between either sex or dose group throughout the 12-week exposure period, therefore these observed changes may be a result of ageing.

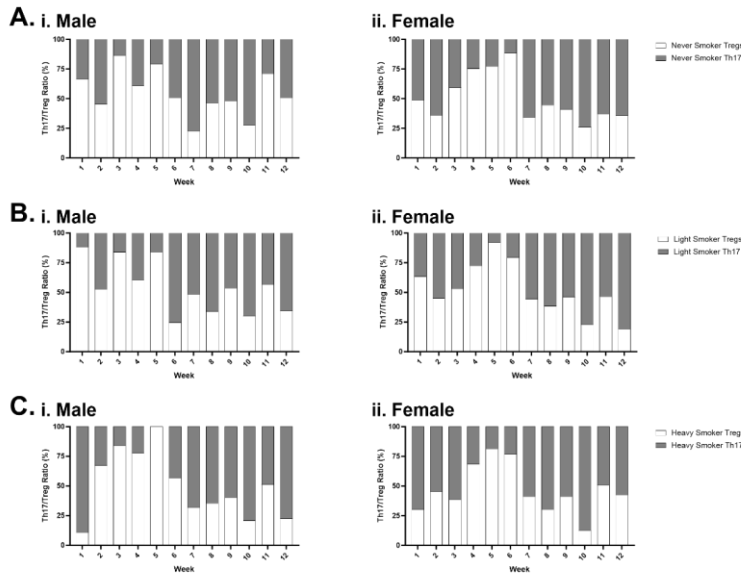


**Figure 4.3.11:- Ratios of Th17 and Tregs in male and female C57BL/6J mice over a 12-week exposure period to CSE.** Graphs show distribution of Th17 and Treg populations in male (i) and female (ii) mice from never-smoker (A), light-smoker (B) and heavy-smoker (C) groups throughout the 12-week exposure period. Data shown as a percentage stacked ratio of total Th17/Treg population as defined by CD4+IL-17A+ (Th17) and CD4+CD25+CD69- (Treg) populations. (n = 3 - 4)

CD8<sup>+</sup> T cells and activation markers were defined according to the gating strategy shown in figure 4.3.12A and B. Activation markers for CD8<sup>+</sup> T cells displayed similar trends to those observed for CD4<sup>+</sup> T cells over the 12-week exposure period. For example, abundance of CCR7<sup>+</sup> cells decreased over the 12-week period in both male and female mice (figure 4.3.12C and figure 4.3.13A). In contrast, the numbers of CD69<sup>+</sup> CD8<sup>+</sup> T cells increased, though remained at relatively constant levels beyond week 6 (figure 4.3.12D and figure 4.3.13B). Double positive CD69 and CD25 CD8<sup>+</sup> T cells were higher in abundance during the early stages of the model, though these levels dropped considerably beyond week 3 and remained at low levels for the duration of the study (figure 4.3.12E and figure 4.3.13C). CD25<sup>+</sup> CD8<sup>+</sup> T cells showed a similar trend, with higher abundance between weeks 1 – 4 and low levels for the

remainder of the model (figure 4.3.12F and 4.3.13D). Similar to the observations made for CD4<sup>+</sup> T cells, this data could possibly indicate a decrease in the numbers of naïve CD8<sup>+</sup> T cells (indicated by CCR7<sup>+</sup> cells) and an increase in early activated CD8<sup>+</sup> T cells (indicated by CD69<sup>+</sup> cells) in the periphery over the course of the model. No differences in these trends were observed between CSE dose groups and the never-smoker group.

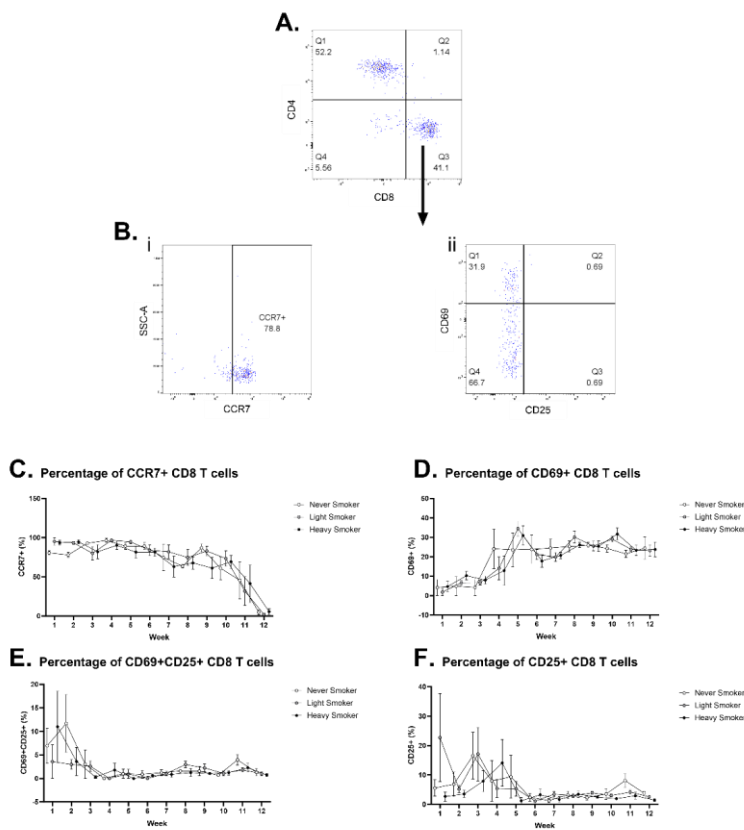


**Figure 4.3.12:- Percentage of activation marker-positive CD8<sup>+</sup> T cells in peripheral blood of male C57BL/6J mice during 12 weeks of CSE exposure.** Gating strategy is shown in A and B. Graphs show the percentage of CCR7<sup>+</sup> (C), CD69<sup>+</sup> (D), CD69<sup>+</sup>CD25<sup>+</sup> (E) and CD25<sup>+</sup> (F) CD8<sup>+</sup> T cells. Data shown as a percentage of total peripheral CD8<sup>+</sup> T cells. (n = 3 – 4; event count range = 0 – 345)

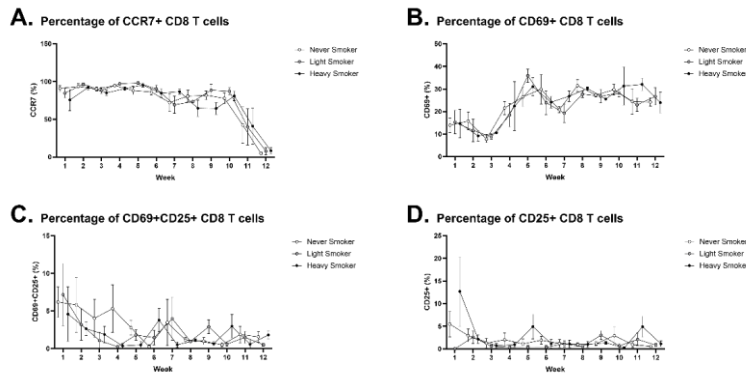


**Figure 4.3.13:- Percentage of activation marker-positive CD8+ T cells in peripheral blood of female C57BL/6J mice during 12 weeks of CSE exposure.** Graphs show the percentage of CCR7+ (A), CD69+ (B), CD69+CD25+ (C) and CD25+ (D) CD8+ T cells. Data shown as a percentage of total peripheral CD8+ T cells (n = 4; [event count range = 0 – 378](#))

Cytokines expressed by CD8<sup>+</sup> T cells were defined according to the gating strategy shown in figure 4.3.14A and B. Both male and female mice showed higher prevalence of IFN- $\gamma$ + CD8<sup>+</sup> T cells in the later stages of the model in comparison to CD4<sup>+</sup> T cells, suggesting increased activation of peripheral CD8<sup>+</sup> T cells (figure 4.3.14C and 4.3.15A). IL-6+ CD8<sup>+</sup> T cell prevalence was typically low, and did not appear to follow any trend over the 12-week exposure period, though an increase in IL-6+ CD8<sup>+</sup> T cells after week 10 was observed in both male and females (figure 4.3.14D and figure 4.3.15B). Surprisingly, presence of IL-17A+ cells was higher in CD8<sup>+</sup> T cells in comparison to CD4<sup>+</sup> T cells, particularly after week 6 (figure 4.3.14E and figure 4.3.15C). Although typically expressed by T helper subsets, particularly Th17, this data suggests that CD8<sup>+</sup> T cells may pose as a large contributing source to IL-17A levels in peripheral blood. However, this trend does not appear to be affected by proinflammatory agents such as CSE, therefore suggesting that this is a typical immune response as opposed to an immunopathogenic response. Presence of TNF- $\alpha$ + CD8<sup>+</sup> T cells was low beyond the first two weeks of exposure in both male and female mice

(figure 4.3.14F and figure 4.3.15D). No differences in these trends were observed between CSE dose groups and the never-smoker group.

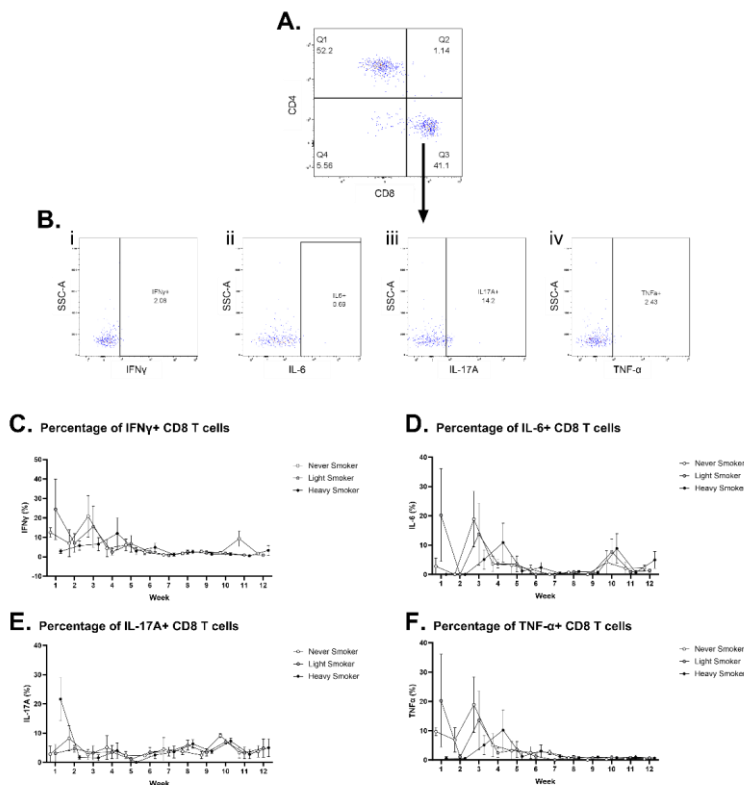


**Figure 4.3.14:- Percentage of cytokine positive CD8<sup>+</sup> T cells in peripheral blood of male C57BL/6J mice during 12 weeks of CSE exposure. Gating strategy is shown in A and B. Graphs show the percentage of IFN- $\gamma$ <sup>+</sup> (C), IL-6<sup>+</sup> (D), IL-17A<sup>+</sup> (E) and TNF $\alpha$ <sup>+</sup> (F) CD8<sup>+</sup> T cells. Data shown as a percentage of total peripheral CD8<sup>+</sup> T cells. (n = 3 - 4; event count range = 0 - 70)**

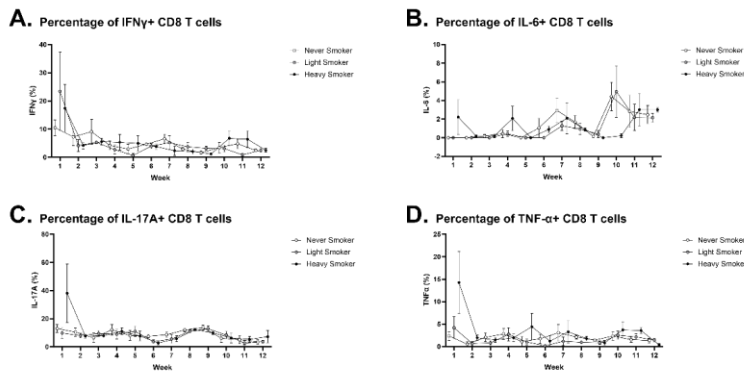


**Figure 4.3.15:- Percentage of cytokine positive CD8+ T cells in peripheral blood of female C57BL/6J mice during 12 weeks of CSE exposure.** Graphs show the percentage of IFN- $\gamma$ + (A), IL-6+ (B), IL-17A+ (C) and TNF $\alpha$ + (D) CD8+ T cells. Data shown as a percentage of total peripheral CD8+ T cells. (n = 4; event count range = 0 – 26)

#### 4.3.4. NK CELLS

NK cells are typically found in low abundance in peripheral blood, making them difficult to analyse via flow cytometry. Nonetheless, using the gating strategy shown in figure 4.3.15A and B we were able to identify NK cells from CD3 negative populations and determine cytokine positive populations. In both male and female mice, numbers of peripheral NK cells increased over the exposure period, with increases in populations being more pronounced in the heavy-smoker and light-smoker groups particularly at week 6 and again at week 10 (figure 4.3.16C and figure 4.3.17A). Due to low populations, determining trends in cytokine positive populations was challenging. This is exemplified by the fact that in both male and female mice, the percentage of IFN- $\gamma$ + NK cells appears to drastically change between highly and low between weeks 5 – 12 (figure 4.3.16D and figure 4.3.17B). A similar trend was observed for IL-6, with numbers of IL-6+ NK cells fluctuating between high and low (figure 4.3.16E), though percentage appeared to remain consistently high for heavy-smoker females between weeks 6 – 12 (figure 4.3.17C). IL-17A+ NK cell population was typically low or not expressed, though small

populations were detected in the early stages of the model (weeks 1 – 5) but this was highly variable depending on sex and dose group (figure 4.3.16F and figure 4.3.17D). TNF- $\alpha$  displayed highly variable population percentages, though in heavy-smoker males TNF- $\alpha$ + NK cell populations were relatively consistent over the 12-week period (figure 4.3.16G), though this was less consistent for the same dose group in females (figure 4.3.17E). As a result of low population numbers and highly variable data, no conclusions could be drawn as a result of the effects of CSE dose on cytokine expression by NK cells.

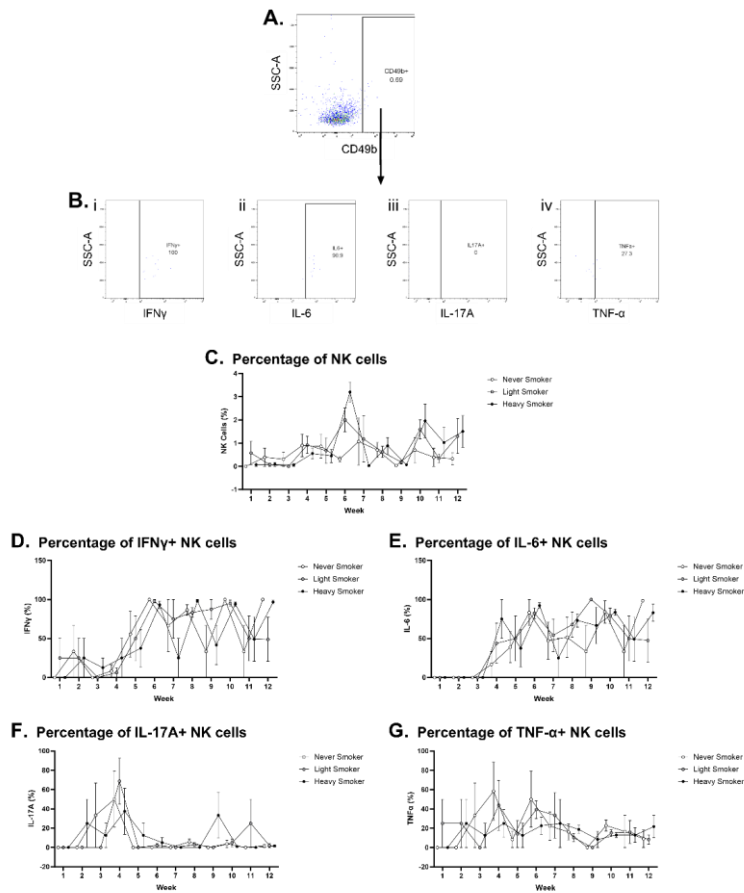


**Figure 4.3.16:- Percentage of NK cells and cytokine positive NK cells in peripheral blood of male C57BL/6J mice during 12 weeks of CSE exposure.** Gating strategy is shown in A and B. Graphs show the total percentage of CD49b<sup>+</sup> NK cells (C) and percentage of IFN- $\gamma$  (D), IL-6 (E), IL-17A (F) and TNF $\alpha$  (G) positive NK cells. Data shown as a percentage of total peripheral immune cells (C) or as a percentage of total peripheral NK cells (D - G). (n = 3 - 4; event count range = 0 - 202)



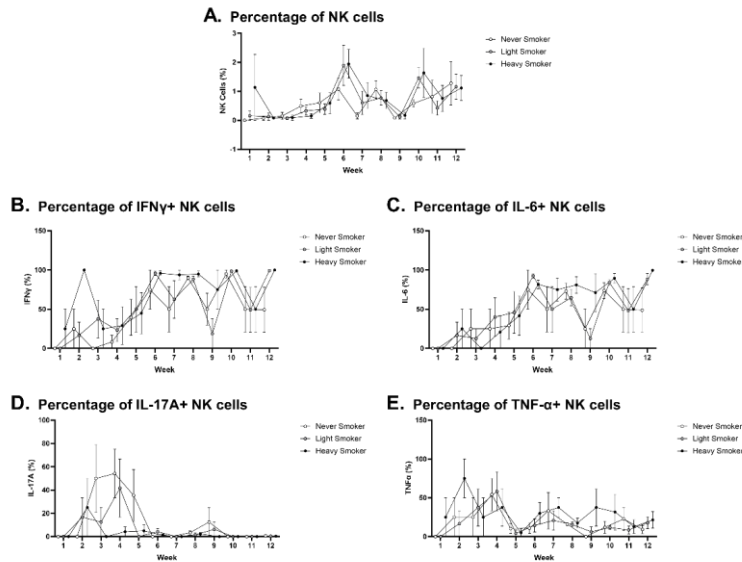


**Figure 4.3.17:- Percentage of NK cells and cytokine positive NK cells in peripheral blood of female C57BL/6J mice during 12 weeks of CSE exposure.** Graphs show the total percentage of CD49b+ NK cells (A) and percentage production of IFN- $\gamma$  (B), IL-6 (C), IL-17A (D) and TNF $\alpha$  (E) by NK cells. Data shown as a percentage of total peripheral immune cells (A) or as a percentage of total peripheral NK cells (B - E). (n = 4; event count range = 0 – 631)

#### 4.3.5. MACROPHAGES

Macrophages were defined according to the gating strategy defined in figure 4.3.18A, and cytokine positive populations were defined according to the gating strategy in figure 4.3.18B. Similar to NK cells, macrophages are found in low abundance in peripheral blood, unsurprising given that they are typically tissue-resident cells. As such, in both male and female mice low numbers of macrophages were found in peripheral blood, though detectible numbers could only be observed following week 4 of exposure in males (figure 4.3.18C) and week 3 in females (figure 4.3.19A). Interestingly, between weeks 8 – 12, macrophages were highest in the light-smoker group for males (figure 4.3.18C) and typically in the never-smoker group for females (figure 4.3.19A). This suggests that CSE exposure does not appear to impact

the percentage of macrophages found in the periphery. Cytokine profiles of macrophages from these weeks also indicate that increased numbers of macrophages are expressing proinflammatory cytokines. For example, after week 7, between 50 – 100% of macrophages from both male and female mice were shown to be positive for IFN- $\gamma$  (figure 4.3.18D and figure 4.3.19B). This trend was also observed for IL-6, with both male and female mice demonstrating increased percentage of IL-6+ macrophages in peripheral blood (figure 4.3.18E and figure 4.3.19C). For IL-17A, both male and female mice demonstrated variable percentage of IL-17A+ macrophages with no discernible trend, though a period of increased percentage between weeks 7 – 11 for males (figure 4.3.18F) and weeks 6 – 10 for heavy-smoker females (figure 4.3.19D) was observed. Similarly, percentage of TNF- $\alpha$ + macrophages was highly variable in both males and females, with numbers fluctuating between high and low between weeks 4 – 12 (figure 4.3.18G and figure 4.3.19E). Although neither sex nor CSE dose appeared to impact macrophage numbers or cytokine positive populations, a possible migration of IFN- $\gamma$  and IL-6 producing macrophages into the periphery was observed, and was thus considered a possible result of ageing.

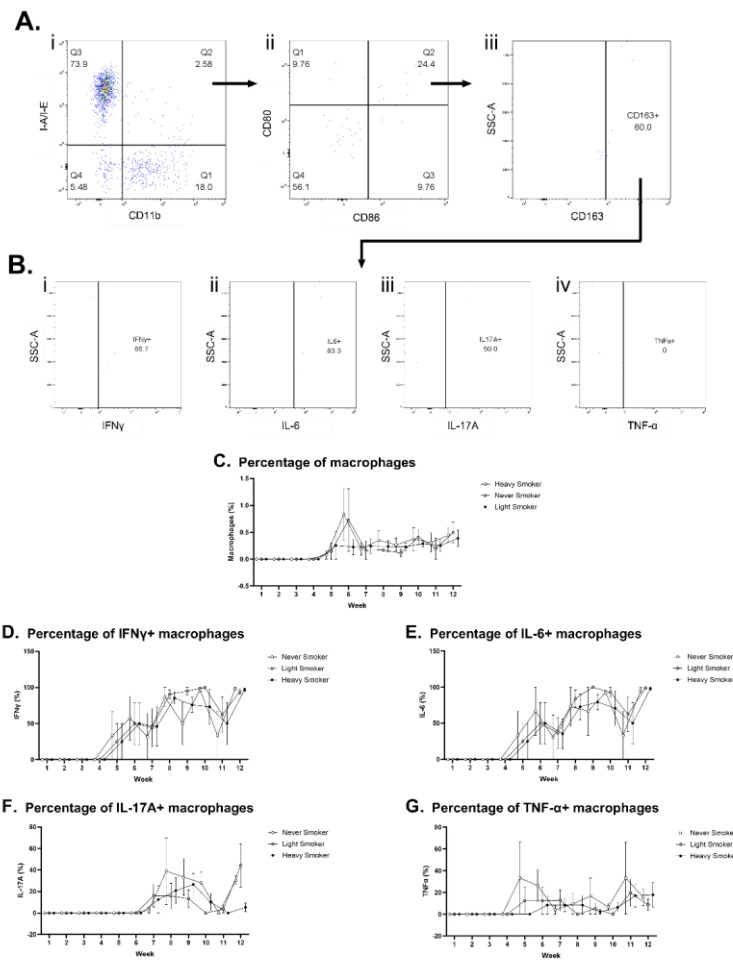


**Figure 4.3.18:- Percentage of macrophages and cytokine positive macrophages in peripheral blood of male C57BL/6J mice during 12 weeks of CSE exposure.** Gating strategy is shown in A and B. Graphs show the total percentage of CD11b+I-A/I-E+CD80+CD86+CD163+ macrophages (C) and percentage production of IFN- $\gamma$  (D), IL-6 (E), IL-17A (F) and TNF $\alpha$  (G) by macrophages. Data shown as a percentage of total peripheral immune cells (C) or as a percentage of total peripheral macrophages (D - G). (n = 3 - 4; event count range = 0 - 56)

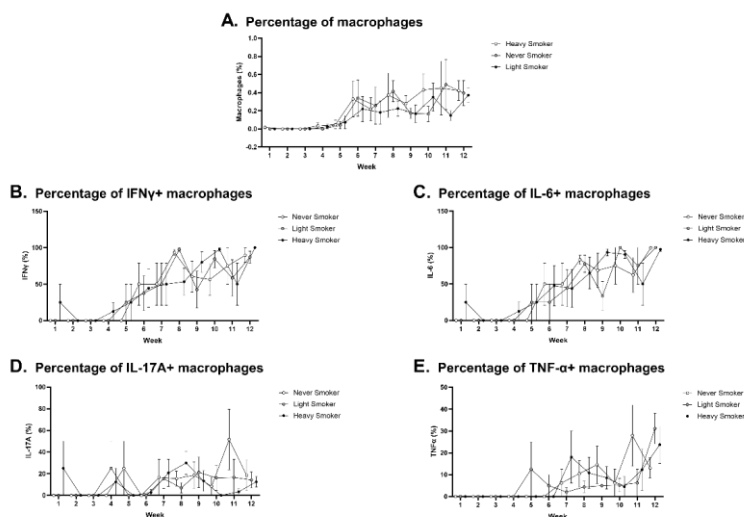


**Figure 4.3.19:- Percentage of macrophages and cytokine positive macrophages in peripheral blood of female C57BL/6J mice during 12 weeks of CSE exposure.** Graphs show the total percentage of CD11b+I-A/I-E+CD80+CD86+CD163+ macrophages (A) and percentage production of IFN- $\gamma$  (B), IL-6 (C), IL-17A (D) and TNF $\alpha$  (E) by macrophages. Data shown as a percentage of total peripheral immune cells (A) or as a percentage of total peripheral macrophages (B - E). ( $n = 4$ ; event count range = 0 – 64)

#### 4.3.6. NEUTROPHILS

Neutrophils were defined according to the gating strategy specified in figure 4.3.20A, and cytokine positive populations were defined according to the gating strategy in figure 4.3.20B. Peripheral neutrophil levels in both male and female mice demonstrated relative stability between weeks 1 – 7, though between weeks 8 – 12 percentage of peripheral neutrophils in both male and female heavy-smoker mice were shown to be slightly higher than those of never-smoker and light-smoker mice (figure 4.3.20C and figure 4.3.21A). Cytokine positive populations followed a similar trend to that observed for macrophages, with percentage of IFN- $\gamma$ + neutrophils increasing after week 4 of exposure in all groups and remaining at relatively consistent levels for the duration of

the exposure period (figure 4.3.20D and figure 4.3.21B). IL-6 followed a similar trend, with an increase in the percentage of IL-6+ cells after week 4, though this expression decreased until week 9, after which a second increase was observed (figure 4.3.20E and figure 4.3.21C). IL-17A+ neutrophils were highest in the early stages of the study irrespective of CSE dose (weeks 1 – 4) and decreased between weeks 5 – 6, after which a small increase in population was observed between weeks 7 – 9 (figure 4.3.20F and figure 4.3.21D). Similarly, TNF- $\alpha$ + neutrophils displayed no trends related to CSE dose exposure, and highest populations were observed at both the first week and between weeks 4 – 8 (figure 4.3.20G and figure 4.3.21E). It was therefore concluded that CSE did not appear to impact cytokine expression by neutrophils, though chronic exposure to 3% CSE appeared to have a small impact on overall peripheral numbers of neutrophils.

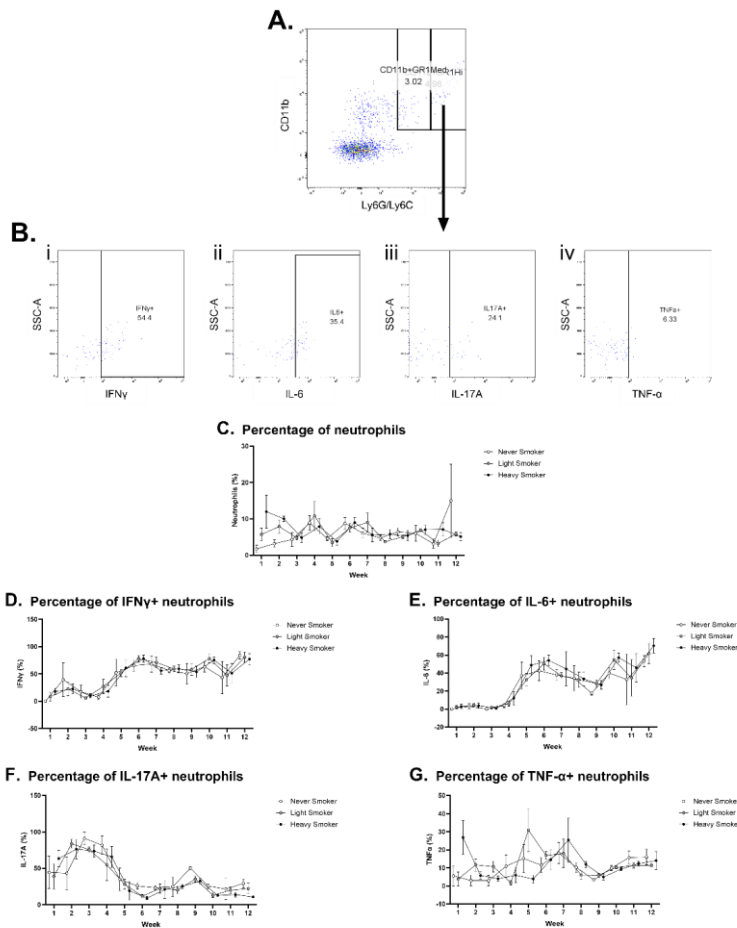


**Figure 4.3.20:- Percentage of neutrophils and cytokine positive neutrophils in peripheral blood of male C57BL/6J mice during 12 weeks of CSE exposure.** Gating strategy is shown in A and B. Graphs show the total percentage of CD11b+Gr-1hi neutrophils (C) and percentage production of IFN- $\gamma$  (D), IL-6 (E), IL-17A (F) and TNF $\alpha$  (G) by neutrophils. Data shown as a percentage of total peripheral immune cells (C) or as a percentage of total peripheral neutrophils (D - G). (n = 3 - 4; event count range = 0 - 2023)

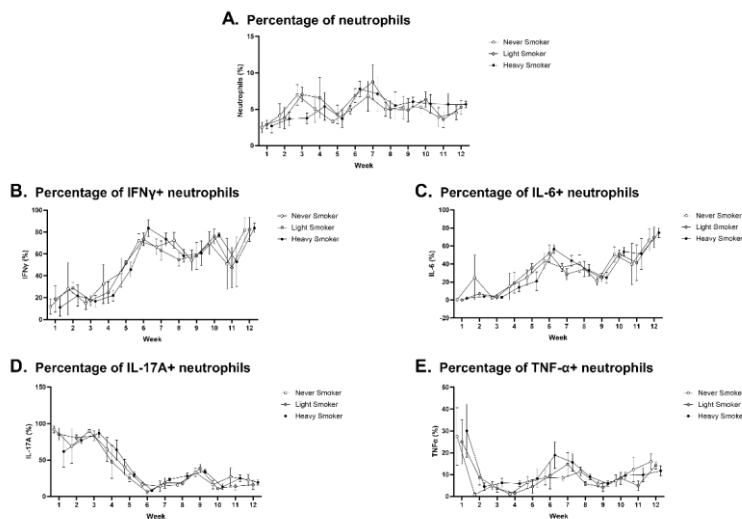


**Figure 4.3.21:- Percentage of neutrophils and cytokine positive neutrophils in peripheral blood of female C57BL/6J mice during 12 weeks of CSE exposure.** Graphs show the total percentage of CD11b+Gr-1hi neutrophils (A) and percentage production of IFN- $\gamma$  (B), IL-6 (C), IL-17A (D) and TNF $\alpha$  (E) by neutrophils. Data shown as a percentage of total peripheral immune cells (A) or as a percentage of total peripheral neutrophils (B - E). (n = 4; event count range = 0 – 2063)

#### 4.3.7. MONOCYTES

Monocytes were defined according to the gating strategy specified in figure 4.3.22A, and cytokine positive populations were further determined using the gating strategy in figure 4.3.22B. Numbers of total peripheral monocytes fluctuated in both male and female mice over the 12-week exposure period, with no distinguishable differences between CSE dose groups (figure 4.3.22C and figure 4.3.23A). Cytokine positive populations demonstrated similar trends to those observed for neutrophils, though positive populations appeared to be less stable by comparison. IFN- $\gamma$ + monocytes were shown to be somewhat increased during the acute exposure stage (weeks 1 – 4) and was then consistently substantially increased between weeks 6 – 12 (figure 4.3.22D and figure 4.3.23B) in all groups. Minimal to no IL-6+ monocytes were observed in

both male and female mice between weeks 1 – 7, which was followed by a slight increase in the numbers of monocytes expressing IL-6 between weeks 8 – 12 (figure 4.3.22E and figure 4.3.23C). IL-17A displayed highly varied expression in monocytes during the acute exposure stages, though showed a slight consistent increase in expression between weeks 6 – 12 (figure 4.3.22F and figure 4.3.23D). TNF- $\alpha$ + monocytes were shown to be consistently low across the 12-week period, with no differences observed between males and females or between dose groups (figure 4.3.22G and figure 4.3.23E). CSE dose did not appear to have any effects on cytokine expression by monocytes, nor did it impact the total percentage of peripheral monocytes.



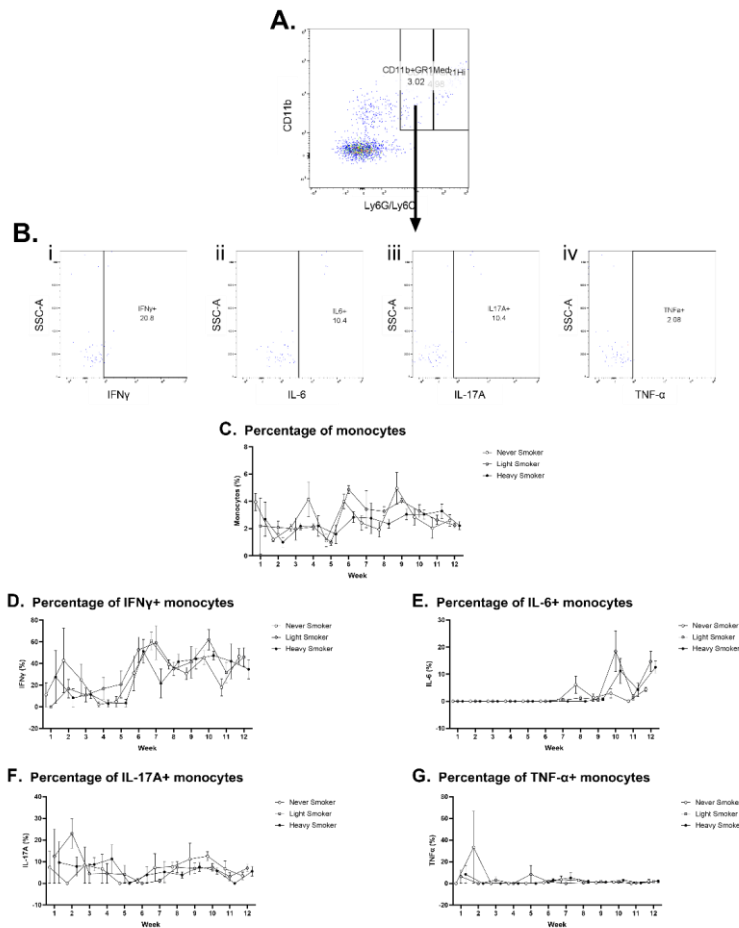


**Figure 4.3.22:- Percentage of monocytes and cytokine positive monocytes in peripheral blood of male C57BL/6J mice during 12 weeks of CSE exposure.** Gating strategy is shown in A and B. Graphs show the total percentage of CD11b+Gr-1med monocytes (C) and percentage production of IFN-γ (D), IL-6 (E), IL-17A (F) and TNFα (G) by monocytes. Data shown as a percentage of total peripheral immune cells (C) or as a percentage of total peripheral monocytes (D - G). (n = 3 – 4; event count range = 0 – 392)

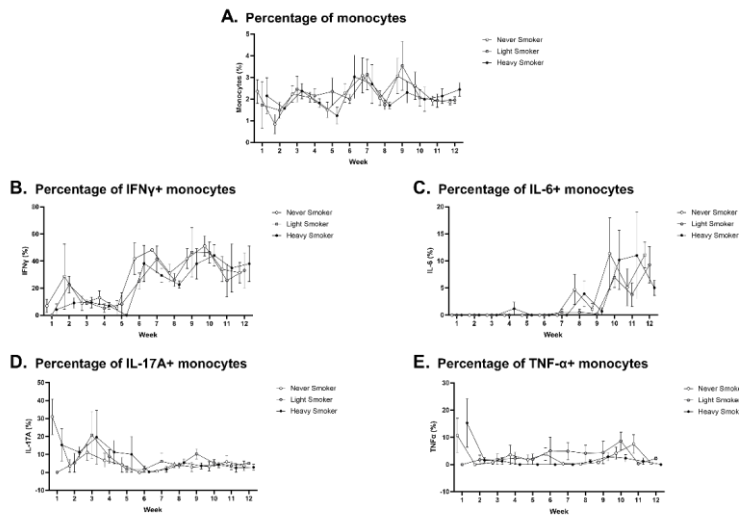


**Figure 4.3.23:- Percentage of monocytes and cytokine positive monocytes in peripheral blood of female C57BL/6J mice during 12 weeks of CSE exposure.** Graphs show the total percentage of CD11b+Gr-1med monocytes (A) and percentage production of IFN- $\gamma$  (B), IL-6 (C), IL-17A (D) and TNF $\alpha$  (E) by monocytes. Data shown as a percentage of total peripheral immune cells (A) or as a percentage of total peripheral monocytes (B - E). (n = 4; event count range = 0 – 478)

#### 4.3.8. DENDRITIC CELLS

DCs were defined according to the gating strategy specified in figure 4.3.24A, and cytokine positive populations were defined according to the gating strategy in figure 4.3.24B. In both male and female mice, numbers of circulating DCs remained at similar levels between weeks 1 – 10 before rapidly declining in abundance at weeks 11 and 12 (figure 4.3.24C and figure 4.3.25A). Low numbers of cytokine-positive DCs were observed, and most demonstrated the highest numbers during the acute exposure period. IFN- $\gamma$ + DCs were most frequent during weeks 1 – 5 in both male and female mice, with minimal populations observed for the remainder of the exposure period (figure 4.3.24D and figure 4.3.25B). IL-6+ DCs did not appear to be present, or were present at low levels between weeks 1 – 9 before a sudden increase in numbers at week 10

and again at week 12, this was more pronounced in heavy-smoker males (figure 4.3.24E) in comparison to all female dose groups (figure 4.3.25C). Expression of IL-17A by DCs appeared to gradually decrease between weeks 1 – 5, before slightly increasing over the remaining exposure period (figure 4.3.24F and figure 4.3.25D). TNF- $\alpha$ + DCs did not appear to demonstrate any particular trends between weeks 1 – 11, showing minimal to no presence across all groups, however a sharp increase in TNF- $\alpha$ + DCs was observed in never-smoker males (figure 4.3.234) and heavy-smoker females (figure 4.3.25E) at week 12. This data demonstrates that CSE exposure does not appear to have any impact on peripheral DCs, as total peripheral numbers did not appear to be impacted until weeks 11 and 12 of exposure and cytokine expression was consistently low across the 12-week exposure period.

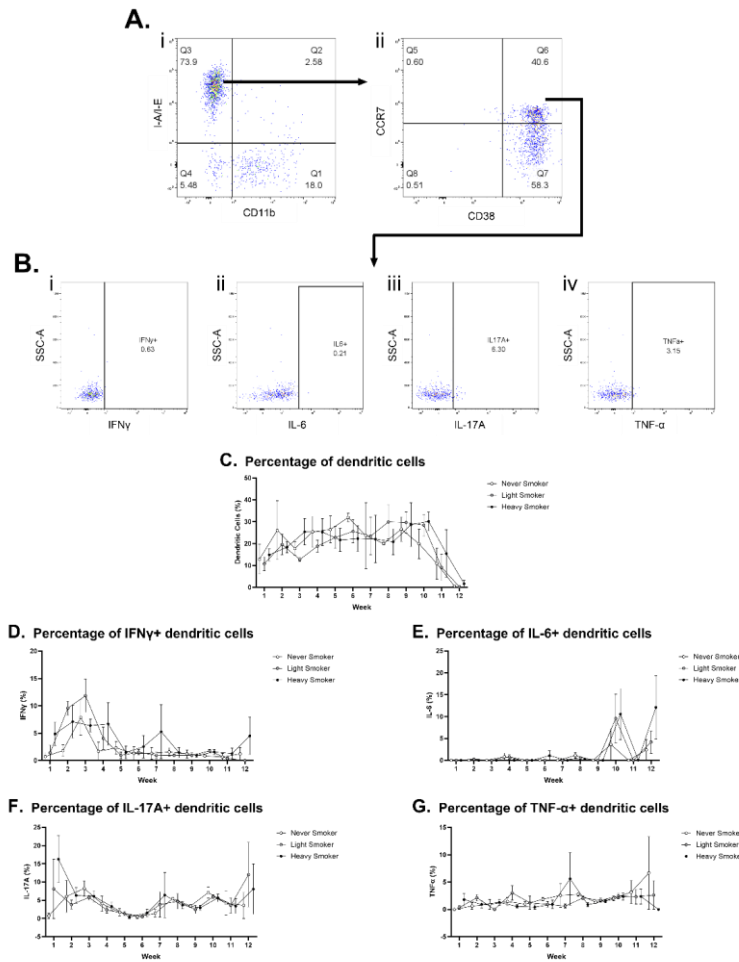


**Figure 4.3.24:- Percentage of dendritic cells and cytokine positive dendritic cells in peripheral blood of male C57BL/6J mice during 12 weeks of CSE exposure.** Gating strategy is shown in A and B. Graphs show the total percentage of CD11b-I-A/I-E+CD38+CCR7+ dendritic cells (C) and percentage production of IFN- $\gamma$  (D), IL-6 (E), IL-17A (F) and TNF $\alpha$  (G) by dendritic cells. Data shown as a percentage of total peripheral immune cells (C) or as a percentage of total peripheral dendritic cells (D - G). (n = 3 – 4; event count range = 0 – 2743)

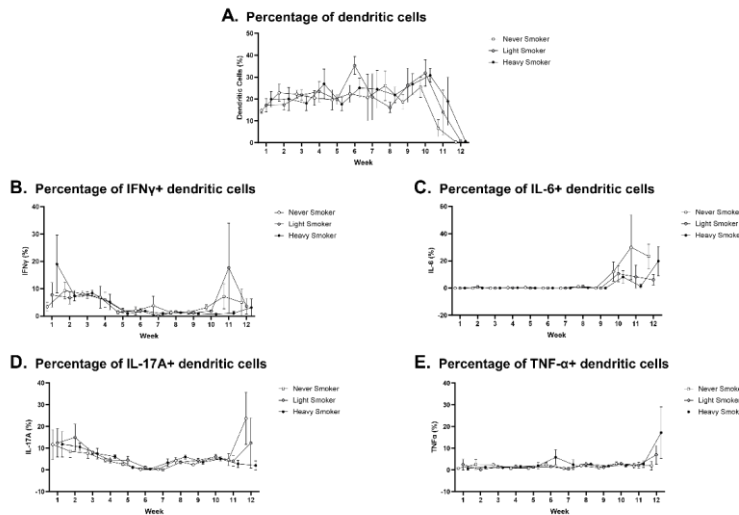


**Figure 4.3.25:- Percentage of dendritic cells and cytokine positive dendritic cells in peripheral blood of female C57BL/6J mice during 12 weeks of CSE exposure.** Graphs show the total percentage of CD11b-I-A/I-E+CD38+CCR7+ dendritic cells (A) and percentage production of IFN- $\gamma$  (B), IL-6 (C), IL-17A (D) and TNF $\alpha$  (E) by dendritic cells. Data shown as a percentage of total peripheral immune cells (A) or as a percentage of total peripheral dendritic cells (B - E). (n = 4; event count range = 0 – 1975)

#### 4.3.9. B CELLS

B cells were defined according to the gating strategy specified in figure 4.3.26A, and cytokine positive populations were further defined according to the strategy in figure 4.3.26B. In both male and female mice, B cells were consistently observed to be the most abundant cell type in the periphery, with numbers drastically increasing after week 10 (figure 4.3.26C and figure 4.3.27A). For male mice, peripheral B cells were more abundant in the heavy-smoker group in comparison to the never-smoker group across the majority of the exposure period (figure 4.3.26C), though this trend was only observed for female mice during the acute exposure period between weeks 1 – 4 (figure 4.3.27A). Similar to DCs, cytokine expression by B cells was low. IFN- $\gamma$ + B cells were highest during the acute exposure phase, with heavy-smoker male B cells expressing

higher levels of IFN- $\gamma$  compared to never-smoker males (figure 4.3.26D), though no differences between dose groups was observed for females (figure 4.3.27B). IL-6+ B cells were not observed until week 10 in both male and female mice, though the numbers of B cells expressing IL-6 was consistently low (figure 4.3.26E and figure 4.3.27C). Expression of IL-17A by B cells remained relatively consistent across the 12-week exposure period for male mice (figure 4.3.26F), though in females a potential acute increase of IL-17A+ B cells was observed between weeks 1 – 5, followed by a second increase between weeks 7 – 8 (figure 4.3.27D), but this was not dependent on CSE dose. Although expressed by a low percentage of B cells, numbers of TNF- $\alpha$ -positive B cells appeared to increase following week 6 of the exposure period, with this trend being more pronounced in heavy-smoker males in comparison to never-smoker males (figure 4.3.26G), though for females the heavy-smoker group appeared to have a lower abundance of TNF- $\alpha$ + B cells in comparison to the never-smoker group (figure 4.3.27E). This suggests that B cells may contribute towards increased TNF- $\alpha$  levels in the blood, though this may be a result of ageing as no differences were observed based on sex or CSE dose.

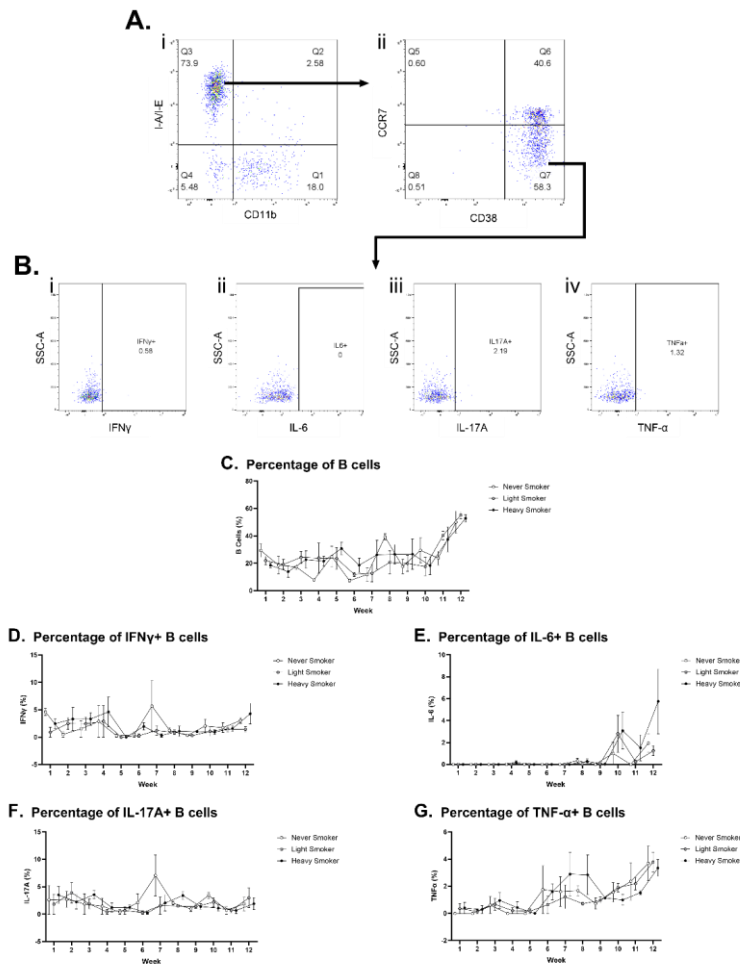


**Figure 4.3.26:- Percentage of B cells and cytokine positive B cells in peripheral blood of male C57BL/6J mice during 12 weeks of CSE exposure.** Gating strategy is shown in A and B. Graphs show the total percentage of CD11b-I-A/I-E+CD38+CCR7- B cells (C) and percentage production of IFN- $\gamma$  (D), IL-6 (E), IL-17A (F) and TNF $\alpha$  (G) by B cells. Data shown as a percentage of total peripheral immune cells (C) or as a percentage of total peripheral B cells (D - G). (n = 3 - 4; event count range = 0 - 4819)

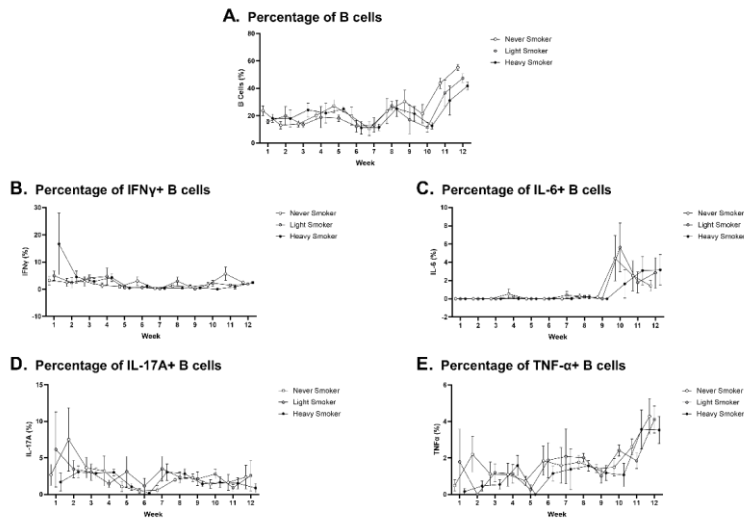


**Figure 4.3.27:- Percentage of B cells and cytokine positive B cells in peripheral blood of female C57BL/6J mice during 12 weeks of CSE exposure.** Graphs show the total percentage of CD11b-I-A/I-E+CD38+CCR7- B cells (A) and percentage production of IFN- $\gamma$  (B), IL-6 (C), IL-17A (D) and TNF $\alpha$  (E) by B cells. Data shown as a percentage of total peripheral immune cells (A) or as a percentage of total peripheral B cells (B - E). (n = 4; event count range = 0 – 5791)

#### 4.3.10. CLUSTERING ANALYSIS

Clustering analysis was performed as a means to identify immune cell populations, or “clusters”, utilising an unbiased methodology. Single viable CD45+ immune cells were first gated and data from all 12 weeks was concatenated with equal sampling measures (n = 3 with 48 events per sample). FlowSOM analysis was first performed which identified 8 unique meta-clusters which were then presented on a tSNE plot. From these clusters, the percentage distribution of each cluster between variables including sex, CSE dose, week sample was taken and disease group (e.g. never-smoker male/never-smoker female, light-smoker male/light-smoker female or heavy-smoker male/heavy-smoker female) was determined. Markers expressed by each meta-cluster were also examined to determine the possible cell type identified within each cluster. All markers (excluding CD45 and ZOMBIE-NIR) were included in





The second largest cluster, cluster 6, was shown to highly express CD4 in addition to CD3 and CCR7, thus identifying this cluster as containing CD4<sup>+</sup> T cells (figure 4.3.29).

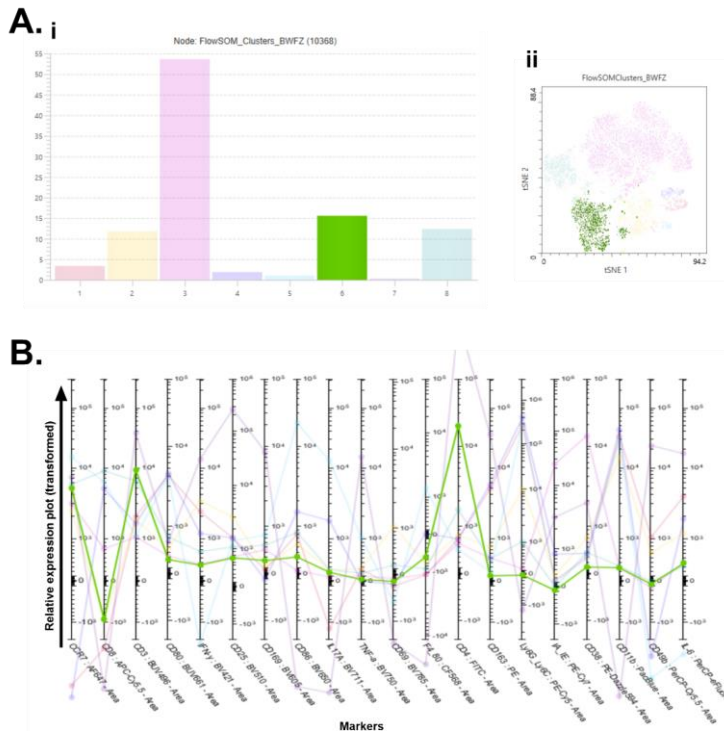


**Figure 4.3.29:- Cluster location and marker expression by Cluster 6.**

Diagrams show FlowSOM cluster by % of events (A.i) and FlowSOM cluster location (A.ii). Relative expression of markers within the cluster is shown in B. (*n* = 3; *total events analysed per sample* = 48)

Interestingly, the smallest cluster, cluster 7, expressed the highest amount of CD4 and was also shown to highly express CD3, CD25 and CCR7 (figure 4.3.30). Although it was suspected that this cluster contained Tregs, since CD69 was negatively expressed in this cluster, proinflammatory cytokines such as IFN- $\gamma$ , TNF- $\alpha$  and IL-6 were shown to be highly expressed, in addition to the NK cell marker CD49b (figure 4.3.30B). It was therefore concluded that this cluster potentially contained

a combination of activated CD4<sup>+</sup> T cells, Tregs or CD4<sup>+</sup> NKT cells, as Tregs are immunosuppressive in nature and expression of proinflammatory cytokines in this cluster was contradictory to Treg biology.

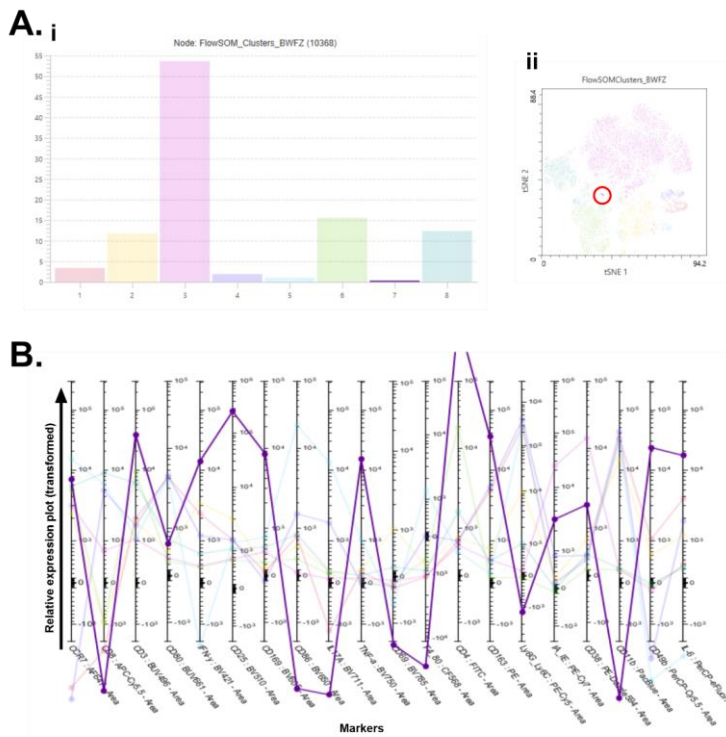


**Figure 4.3.30:- Cluster location and marker expression by Cluster 7.** Diagrams show FlowSOM cluster by % of events (A.i) and FlowSOM cluster location (A.ii, circled). Relative expression of markers within the cluster is shown in B. ( $n = 3$ ; total events analysed per sample = 48)

Cluster 8 highly expressed CD8 in addition to CD3 and CCR7, and was therefore identified as containing CD8<sup>+</sup> T cells (figure 4.3.31).

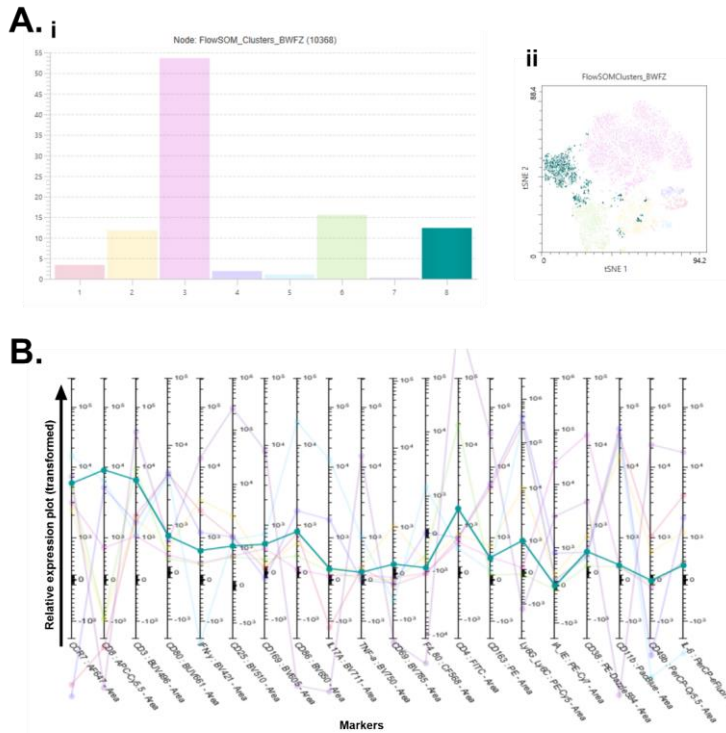


**Figure 4.3.31:- Cluster location and marker expression by Cluster 8.** Diagrams show FlowSOM cluster by % of events (A.i) and FlowSOM cluster location (A.ii). Relative expression of markers within the cluster is shown in B. (*n* = 3; *total events analysed per sample* = 48)

Cluster 4 was speculated to contain monocytes, as CD11b was highly expressed and Ly6G/Ly6C was expressed in a moderate amount compared to other clusters, which either highly expressed Ly6G/Ly6C or did not express Ly6G/Ly6C (figure 4.3.32). This cluster was also shown to moderately express CCR7 and IFN- $\gamma$ , and interestingly this cluster comprised a larger proportion of total immune cells in comparison to those observed from conventional gating strategies. Cluster 1 and cluster 4 were shown to have similar expression profiles, both highly expressing Ly6G/Ly6C and CD11b (figure 4.3.32 and figure 4.3.33). However, both clusters demonstrated different cytokine expression profiles, with cluster

1 expressing moderate amounts of IFN- $\gamma$  and IL-6, whilst cluster 4 displayed moderate expression of TNF- $\alpha$ . Interestingly, cluster 4 showed an increased expression of CD8 and a slightly increased expression of F4/80, which would indicate a potential macrophage-like cell. Both clusters expressed costimulatory markers CD80 and CD86, though levels were slightly lower in cluster 1. Based on the markers expressed by these clusters, it was concluded that cluster 1 likely contained neutrophils and cluster 4 contained a mixture of macrophages and other granulocytic cells such as eosinophils, which may also express CD11b, F4/80 and Ly6G/Ly6C.

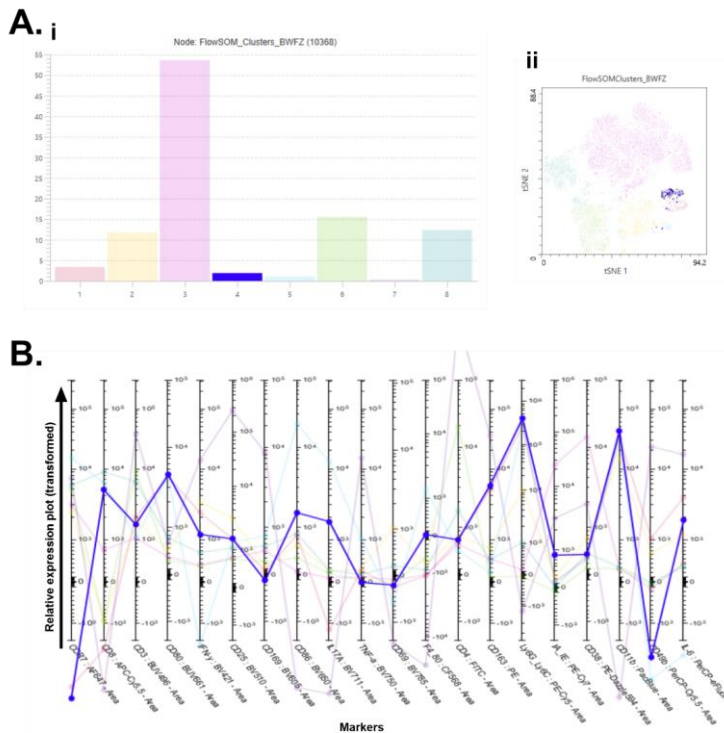


**Figure 4.3.32:- Cluster location and marker expression by Cluster 4.**

Diagrams show FlowSOM cluster by % of events (A.i) and FlowSOM cluster location (A.ii). Relative expression of markers within the cluster is shown in B. ( $n = 3$ ; total events analysed per sample = 48)

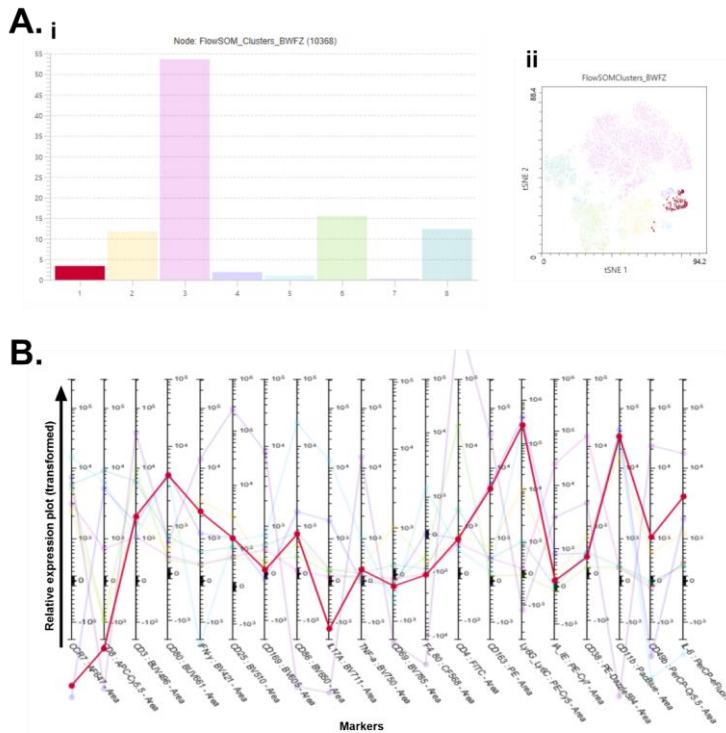


**Figure 4.3.33:- Cluster location and marker expression by Cluster 1.**

Diagrams show FlowSOM cluster by % of events (A.i) and FlowSOM cluster location (A.ii). Relative expression of markers within the cluster is shown in B. (*n* = 3; total events analysed per sample = 48)

The final cluster, cluster 5, displayed the most diverse array of markers expressed, including CCR7, CD8, CD80, CD86, IL-17A, Ly6G/Ly6C and CD11b (figure 4.3.34). This cluster expressed the highest amount of F4/80 in comparison to all other clusters, and given the wide variety and types of markers expressed it was concluded that this cluster likely contained macrophages. Therefore, based on this analysis we were able to provide evidence for the ability to differentiate multiple different cell types and populations using our flow cytometry panel in an unbiased format.

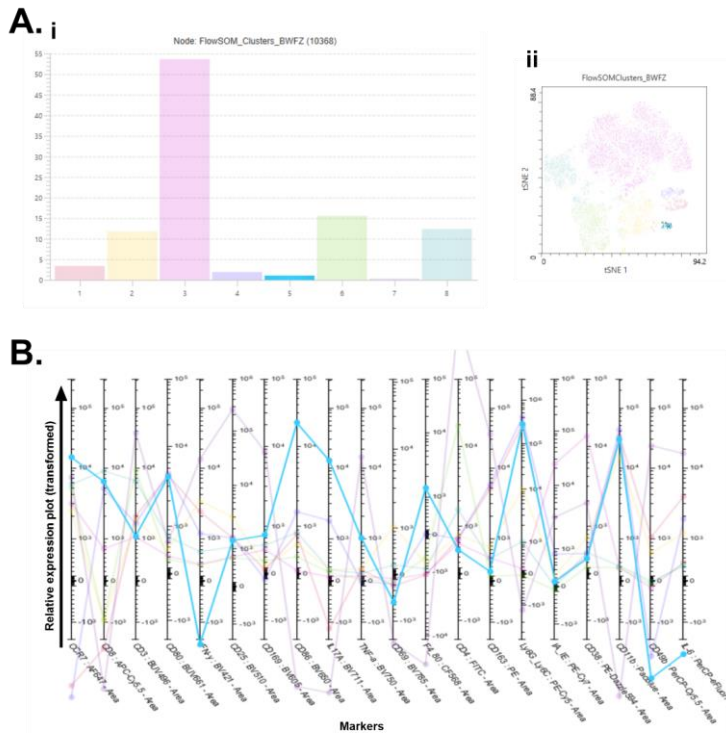


**Figure 4.3.34:- Cluster location and marker expression by Cluster 5.**

Diagrams show FlowSOM cluster by % of events (A.i) and FlowSOM cluster location (A.ii). Relative expression of markers within the cluster is shown in B. (*n* = 3; total events analysed per sample = 48)

Following the identification of possible cell types contained within each cluster, cluster distribution between study variables was examined. The impact of sex on cluster distribution was first examined, though no significant differences were identified by way of 2way ANOVA (figure 4.3.35). All clusters appeared to have equal distribution between sexes, though cluster 4 (macrophages/eosinophils/other unidentified granulocytes) appeared to slightly more prevalent in females than males and cluster 6 (CD4<sup>+</sup> T cells) were slightly more prevalent in males than females, though neither of these observations were statistically significant (figure 4.3.35E). Overall, this analysis demonstrates that sex

does not appear to impact the distribution and proportions of immune cell types in peripheral whole blood.

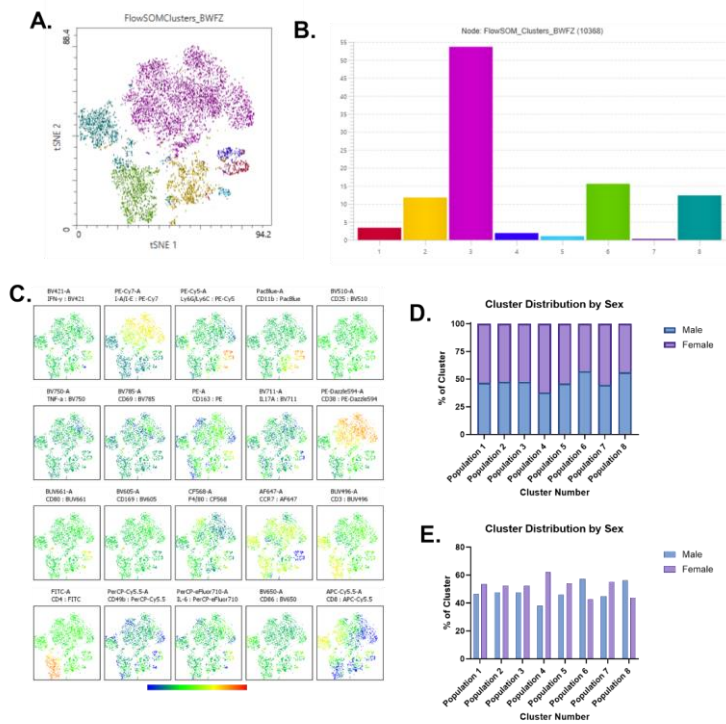


**Figure 4.3.35:- Total Immune Cell Clustering Analysis by sex.** Diagrams show FlowSOM clusters from CSE exposed mice (A) and FlowSOM clusters by % of events (B), heatmap of clusters by marker expression (C), percentage of cluster occupied by male or female mice (D) and differences between clusters of male and female mice (E). No statistical significances were detected by way of 2way ANOVA analysis with  $p < 0.05$ . ( $n = 3$ ; total events analysed per sample = 48)

Clusters were then further analysed to determine distribution by smoking status (CSE dose, e.g. 0%, 1% or 3% CSE). Similar to sex distribution, no statistical significances between cluster distribution and smoking status were detected by 2way ANOVA (figure 4.3.36). The majority of clusters appeared to be equally distributed, though cluster 5 (macrophages) was shown to be slightly increased in the light-smoker



CHAPTER 4 – SYSTEMIC EFFECTS OF CSE

groups in comparison to the never-smoker and heavy-smoker groups, and cluster 7 (activated CD4<sup>+</sup> T cells/Tregs/NKT cells) was highest in the never-smoker group (figure 4.3.36E). Although neither of these observations were statistically significant, the higher distribution of cluster 7 in the never-smoker groups suggests that this combination of cells is negatively impacted by CSE.

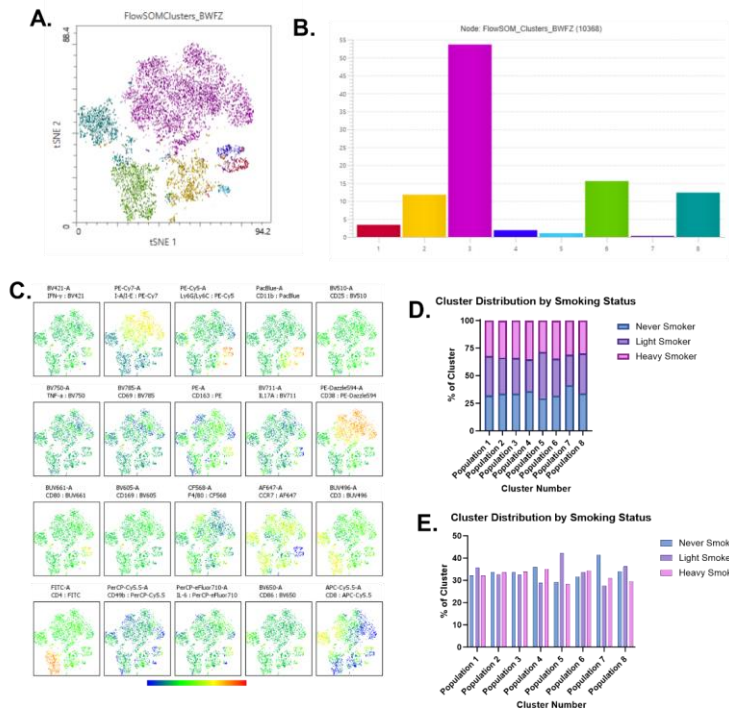


**Figure 4.3.36:- Total Immune Cell Clustering Analysis by smoking status.**

Diagrams show FlowSOM clusters from CSE exposed mice (A) and FlowSOM clusters by % of events (B), heatmap of clusters by marker expression (C), percentage of cluster occupied by never-smoker, light-smoker or heavy-smoker groups (D) and differences between clusters of never-smoker, light-smoker and heavy-smoker groups (E). No statistical significances were detected by way of 2way ANOVA analysis with  $p < 0.05$ .

( $n = 3$ ; total events analysed per sample = 48)

To determine the impact of time on cell profiles, cluster distribution was analysed by the week that each sample was taken. Since only small changes were detected on a weekly basis according to conventional gating strategies, cluster distribution was determined only for weeks 1, 4, 8 and 12. This would allow for better detection of changes between baseline (week 1), acute exposure (week 4), chronic exposure (week 8) and endpoint (week 12). As shown in figure 4.3.37D, whilst clusters 2, 3, 4 and 6 showed relatively equal distribution between the four timepoints, clusters 1, 5, 7 and 8 demonstrated skewed distribution depending on sample timepoint. Cluster 1 (neutrophils) showed the highest distribution at chronic exposure and endpoint, with no populations found at baseline and minimal at acute exposure (figure 4.3.37E). Conversely, cluster 5 (macrophages) distribution was shown to decrease over time, with the highest distribution found at acute exposure and none found at endpoint (figure 4.3.37E). This could not only suggest the possibility of macrophage migration from the periphery into inflamed sites, but also suggest a negative correlation between the cell types found in cluster 1 and cluster 5. Cluster 7 (activated CD4<sup>+</sup> T cells/Tregs/NKT cells) was found in highest abundance at baseline, with no populations found at either chronic exposure or endpoint (figure 4.3.37E). Finally, differences in cluster 8 (CD8<sup>+</sup> T cells) distribution were small, however as the timepoint increased the percentage distribution decreased, with endpoint showing the smallest distribution (figure 4.3.37E). However, as this differentiation does not account for either CSE dose or sex, it cannot be concluded that sex or CSE by itself is a contributing factor to any of these trends observed and there may be other extraneous variables that impact this data.

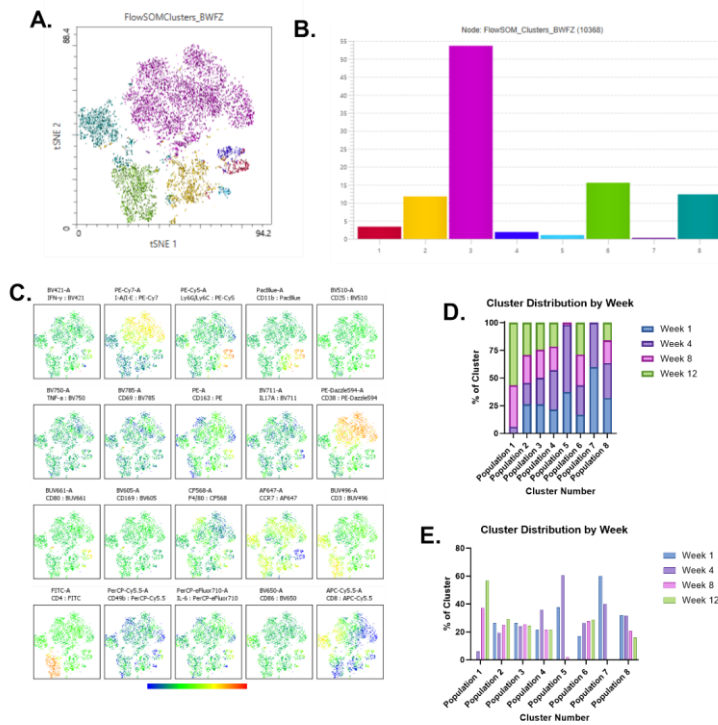


**Figure 4.3.37:- Total Immune Cell Clustering Analysis by week.** Diagrams show FlowSOM clusters from CSE exposed mice (A) and FlowSOM clusters by % of events (B), heatmap of clusters by marker expression (C), percentage of cluster occupied by data from week 1, 4, 8 or 12 (D) and differences between clusters of data from week 1, 4, 8 and 12 (E). Data in D and E is shown as a percentage of total pooled data from weeks 1, 4, 8 and 12. No statistical significances were detected by way of 2way ANOVA analysis with  $p < 0.05$ . ( $n = 3$ ; total events analysed per sample = 48)

Although no significant differences in cluster distribution was determined between either sex or smoking status, cluster distribution was further analysed by disease group. This was to determine if both sex in combination with CSE dose would alter cluster distribution. As shown in figure 4.3.38D, the majority of clusters showed equal distribution between disease groups, though small differences in distribution in cluster 4, cluster 5 and cluster 7 were observed. For example, cluster 4 (macrophages/eosinophils/unidentified granulocytes) was shown to have the highest distribution in never-smoker males (figure 4.3.38E).

Additionally, cluster 5 (macrophages) was shown to have the lowest distributions in both never-smoker males and heavy-smoker females. Finally, cluster 7 (activated CD4<sup>+</sup> T cells/Tregs/NKT cells) had the lowest distribution in light-smoker females and heavy-smoker males (figure 4.3.38E). Despite this, no significant differences were detected by 2way ANOVA, and these changes in distribution did not appear to follow any particular trend. It was therefore concluded that CSE exposure did not appear to have significant impact on immune cell profiles in peripheral blood, as all changes observed did not yield statistical significance and any changes seen were only marginal. Nonetheless, as both conventional gating and clustering analysis displayed similar population profiles and trends across CSE groups and sexes, these findings demonstrate the reliability of our flow panel to identify immune cell types and their effector functions.

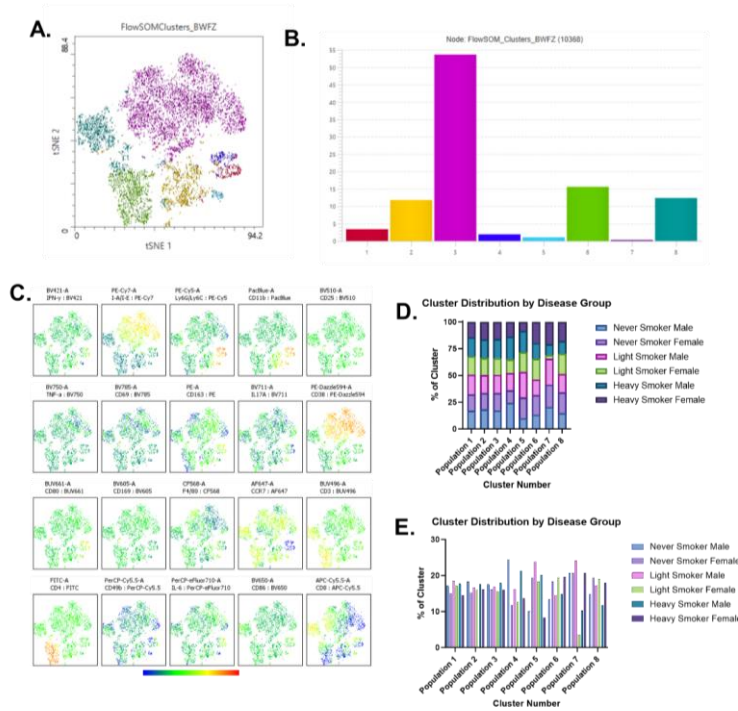


**Figure 4.3.38:- Total Immune Cell Clustering Analysis by disease group.**

Diagrams show FlowSOM clusters from CSE exposed mice (A) and FlowSOM clusters by % of events (B), heatmap of clusters by marker expression (C), percentage of cluster occupied by never-smoker male, never-smoker female, light-smoker male, light-smoker female, heavy-smoker male or heavy-smoker female mice (D) and differences between clusters of never-smoker male, never-smoker female, light-smoker male, light-smoker female, heavy-smoker male and heavy-smoker female mice (E). No statistical significances were detected by way of 2way ANOVA analysis with  $p < 0.05$ . ( $n = 3$ ; total events analysed per sample = 48)

#### 4.4. DISCUSSION

Peripheral mechanisms of COPD are critical in the understanding of immunoregulation and migration of cells into the pulmonary spaces. Immune cells are typically more abundant in specific areas within the body, such as neutrophils being typically found in circulation and macrophages typically found in tissues. Furthermore, adaptive immune cells, such as T cells and B cells mature and differentiate within the

lymphatic system, which includes the thymus, bone marrow and lymph nodes. Differentiation and maturation of adaptive immune cells is typically driven by APCs, which migrate from areas of inflammation to secondary lymphoid organs. Once T and B cells are activated and become effector cells, they leave the secondary lymphoid organs and enter the blood. Thus, activation of the immune system is highly dependent on the circulatory system, as this is often one of the swiftest ways for cells to be transported in order to carry out their effector functions. Therefore, examining alterations to immune cell profiles in the periphery can provide insight into the onset and progression of inflammatory diseases such as COPD.

Previous studies in both humans and mice have demonstrated that cytotoxic immune cells play a significant role in both COPD pathogenesis and in AECOPD. In the periphery, CD8<sup>+</sup> T cells display diminished cytotoxic function as demonstrated by decreased expression of granzyme B and perforin, and although total numbers of peripheral CD8<sup>+</sup> T cells were not different between healthy participants, smokers and COPD patients, an increased proportion of CD4<sup>+</sup> T cells to CD8<sup>+</sup> T cells in smokers and COPD patients was reported [190]. These findings are similar to those observed in our model system, as in both male and female mice the proportion of CD4<sup>+</sup> T cells to CD8<sup>+</sup> T cells increased over the exposure period, though this was observed across all dose groups and not specific to light-smoker or heavy-smoker groups (figure 4.3.6). It is hypothesised that imbalance in CD4<sup>+</sup>/CD8<sup>+</sup> T cells is a result of CD8<sup>+</sup> T cell migration into the airways and pulmonary spaces, where an increased cytotoxic function is widely reported [191, 204]. As such, investigating expression of trafficking and migration markers by cell types widely reported in the pulmonary spaces of COPD patients may provide further insight into peripheral mechanisms of COPD or effects of CSE on the peripheral immune system, and may show noticeable differences between healthy vs COPD samples.

Across all cell types, there did not appear to be any noticeable differences in cytokine expression in relation to CSE dose. Despite this,

our findings demonstrated that IL-17A<sup>+</sup> CD8<sup>+</sup> T cells were more abundant than IL-17A<sup>+</sup> CD4<sup>+</sup> T cells, implicating them as a large contributor to sources of peripheral IL-17A (figure 4.3.7 – figure 4.3.10). Although no differences between dose groups were observed for this trend, studies suggest that CD8<sup>+</sup> T cell-derived IL-17A contributes towards immune pathology in a number of inflammatory diseases, including COPD [393]. Low percentage cytokine producing B cells was also noted, though this was considered typical given that B cells are typically involved in humoral immune responses and do not typically produce cytokines to the same degree as other immune cells (figure 4.3.26 and figure 4.3.27). Nonetheless, it has been shown that cytokine production by B cells is heavily influenced by their immune microenvironment, which can drive the differentiation of B cells into subtypes which have a multitude of effects on other cells of the immune system [394]. Although we demonstrated that B cells in the periphery did not appear to express cytokines regardless of CSE dose, this may be different in the pulmonary spaces, and identifying the differences between B cell subtypes in the periphery and pulmonary spaces may provide further insight into the contributions of B cells to COPD pathophysiology.

Recent clustering analysis performed on human peripheral blood for a number of respiratory diseases has further provided insight into differences in distribution of peripheral immune cells, and identified areas for further analysis [395]. In this study, the predominant cell type found in the periphery of both COPD and AECOPD patients were neutrophils, closely followed by monocytes for COPD patients [395]. These findings do not appear to reflect the findings of our own clustering analysis, as it was suggested that B cells and DCs comprised the largest number of peripheral cells in mice (figure 4.3.28). However, it is important to note that the panel used for deep phenotyping in the aforementioned study is far more comprehensive than the one developed for our mouse model, and our data is taken over a 12-week period as opposed to a single timepoint. Additionally, while it is not specified in the study, it is likely that

a larger quantity of blood was taken from participants, thus allowing in a greater number of events to be analysed by comparison to our study. Although no statistical differences were observed between groups for all cell types and their effector functions, our data nonetheless demonstrates the ability of our flow cytometry panel to isolate and characterise a broad range of immune cell types. Clustering analysis demonstrated that markers were distinct enough to identify and isolate associated clusters with enough distinction to logically suggest the immune cell types contained within each cluster. Due to the low cell numbers and small group size, identifying trends and statistical differences over time and between groups was not possible, particularly when conventional gating strategies were used. Low cell numbers could be attributed to the limitations of blood sampling, as LASA guidelines for microsampling limit the amount of peripheral blood taken from a single animal to <10% total body volume (TBV) on a single instance in addition to <15% TBV over a 28-day period. In mice, this roughly equates to 140  $\mu$ L on a single instance, or 210  $\mu$ L over a 28-day period. As such, we were limited to taking a maximum of 20  $\mu$ L of whole blood per week, as concerns were raised regarding adverse welfare effects if higher volumes were taken particularly in the case of possible compromised respiratory function. This therefore resulted in low cell numbers available for analysis.

Given that minimal differences were observed on a weekly basis in immune cell profiles, it may therefore be more pragmatic to take peripheral blood samples on a monthly basis. This would allow for an increased volume of blood to be taken in a given sample, and therefore result in an increased number of cells available for analysis which may lead to more noticeable trends or identification of statistical differences. Nonetheless, this data demonstrates that chronic exposure to CSE does not elicit adverse welfare effects, and C57BL/6J mice show consistent tolerance to repeated CSE exposure and anaesthesia, though analysis of pulmonary effects of CSE are necessary to confirm the presence of a COPD phenotype in order to conclude that the model system mimics human disease.



## CHAPTER 5 – PULMONARY EFFECTS OF CSE EXPOSURE

### 5.1. INTRODUCTION

Alterations to the pulmonary environment are known to drive the pathogenesis and persistence of COPD and ultimately lead to significant respiratory complications, including shortness of breath, chronic cough and frequent infections. These presentations are frequently exacerbated in AECOPD and often require hospitalisation and treatment, which comprises the largest COPD-related global economic and healthcare burden [64]. As such, determining how these changes may contribute towards COPD pathology is paramount to disease understanding, allowing for the potential identification of novel targets for treatments which may reduce global burden.

Although the genetic mechanisms of COPD are poorly understood, GWAS studies have frequently identified a variety of genes in the lungs as compounding factors in COPD pathogenesis, either through changes in expression or as a result of genetic variants. A1AT deficiency is the most highly characterised genetic association of COPD and is shown to result in increased airway remodelling due to reduced inhibition of ECM-degrading proteases [135, 396]. Whilst this association is supported by a wealth of evidence, other genetic associations are speculative at best. For example, it has long been considered that the NLRP3 inflammasome contributes towards COPD pathogenesis through the production of IL-1-like cytokines, though clinical data demonstrates that indirect inhibition of the inflammasome signalling pathway has no effect on pathophysiology [397]. Conversely, other mechanisms suggest either damaging or protective roles in COPD, though strong associations have yet to be made. This is evidenced by increased expression of CRP having a greater association with mortality [398], whilst knockout of NRF2 results in increased susceptibility to COPD through dysregulation of inflammation, protease/anti-protease balance and reactive oxygen species [399]. As such, understanding genetic changes in response to

CS exposure in the lungs is critical, as many genes associated with COPD are often involved in either the onset or resolution of inflammation, particularly in regard to the recruitment of immune cells and airway remodelling.

Neutrophils are granulocytes typically found in peripheral blood, but are recruited to sites of infection or inflammation during the acute stages of the inflammatory response. Pulmonary neutrophilia is a widely reported phenotypic presentation of COPD in both humans and mice, and is known to drive the persistence of an inflammatory microenvironment within the lungs [182, 323, 400]. In particular, an increased presence of neutrophils and neutrophilic activation in the sputum and BALF of COPD patients is positively correlated to disease severity and increased risk of AECOPD [401]. Neutrophilic recruitment is driven by a number of immune mechanisms, including proinflammatory cytokines such as TNF- $\alpha$ , which are detected by neutrophils by cell surface receptors such as CXCR1 and CXCR2. Studies have shown that such receptors are often highly expressed in COPD patients, thus leading to increased migration to sites of inflammation [402]. Much like neutrophils, mast cells are granulocytes though are typically associated with allergic responses and asthma pathophysiology. Since asthma and COPD have many overlapping phenotypes and pathophysiological presentations, mast cells and their recruitment to the airways have long been speculated to have a role in COPD pathogenesis, but this research is severely limited [259, 260, 403]. Persistent recruitment of immune cells such as neutrophils into the pulmonary spaces can lead to tissue damage and airway remodelling, often demonstrated by increased presence of scar tissue and alveolar destruction [163]. These changes in lung structure, particularly to the small airways such as alveoli, are often associated with decreased lung function [152].

Following 12 weeks of CSE exposure, we dissected the lungs from each mouse in our COPD study to perform genetic and histological analysis of immune pathways and morphometry. RT-qPCR was performed on the right inferior lung lobe to assess the impact of both CSE

dose and sex on expression of genes from inflammasome signalling, TLR signalling and IL6R signalling pathways, in addition to genes encoding MMPs and other inflammatory/anti-inflammatory proteins. Toluidine blue staining was performed on fixed sections and the remaining whole lungs and trachea was used to examine mast cell infiltration and activation. H&E staining was also performed to examine evidence of pulmonary neutrophilia and airway remodelling in both large and small airways. For small airways, the degree of morphometric changes was assessed by mean linear intercept (MLI) to determine alveolar destruction. The resulting data was further interrogated through statistical analysis to identify the impact of both CSE dose and sex on outcomes.

## 5.2. METHODS

### 5.2.1. MURINE MODEL

#### 5.2.1.1. S1 cull and dissection

Full methodology for murine model work can be found in section 2.2.1. Methods – Murine COPD Model. Briefly, following 12 weeks of CSE exposure, mice were culled by IP overdose of dolethal. After loss of pedal withdrawal reflex, detectible heartbeat and permanent cessation of respiration, death was confirmed via laceration of the femoral artery (cessation of blood circulation). Following confirmation of death, the lungs and other tissues of interest were excised. The right inferior lung lobe was frozen at -80°C for RNA isolation and RT-qPCR, whilst the remainder of the lungs was fixed for histological analysis.

### 5.2.2. RT-qPCR

#### 5.2.2.1. RNA isolation and reverse transcription

Full methods for RT-qPCR can be found in section 2.2.4. Methods – RT-qPCR. In brief, RNA was extracted from the right inferior lung lobe of mice using a Qiagen RNeasy mini kit according to the manufacturer's protocol in addition to an optional on-column DNase digest step using a

Qiagen RNase-free DNase set. RNA concentrations and purity were determined using a NanoDrop spectrophotometer.

For reverse transcription, 1 µg RNA was used for optimal cDNA synthesis. A TaqMan Reverse Transcription kit was used to generate cDNA in addition to controls (no reverse transcriptase (NRT) and no template control (NTC)). Samples containing reaction mixture were placed into a thermocycler to allow reverse transcription to take place, after which resulting cDNA was diluted to 5 ng and stored at -20°C until use.

#### 5.2.2.2. Polymerase chain reaction

PCRs were performed in triplicate in 96-well PCR plates using a master mix of SYBR green reagents and FWD/REV primer mixes. Plates were sealed with an optical adhesive seal after addition of cDNA and run on an ABI Fast 7500 qPCR machine using a standard protocol for SYBR green reagents in a 10 µL volume reaction. Resulting  $\Delta\text{Ct}$  values were then exported for analysis of relative gene expression.

#### 5.2.2.3. Calculation of relative gene expression

Relative gene expression was calculated using the  $\Delta\Delta\text{Ct}$  method (see section 2.2.4.6. Methods – Calculation of relative gene expression). Calibrator wells were assigned as A12, B1 and B2, and RefFinder was used to identify the most stable housekeeping genes for normalisation. Tuba1 and SDHA were selected for normalisation factor based on RefFinder results, and relative gene expression was calculated using normalised genes and rescale means from control groups (one per sex). Data was then plotted in GraphPad Prism and analysed by 2way ANOVA.

### 5.2.3. HISTOLOGY

#### 5.2.3.1. Tissue processing and microtomy

Full methods for histology can be found in section 2.2.5. Methods – Histology. Briefly, dissected lungs were placed in 5 mL formalin overnight before being transferred to 70% EtOH. Tissues were then placed into cassettes and processed using a Leica TP1020 Tissue Processor overnight, after which tissues were embedded in paraffin wax using an embedding station. After wax blocks were solidified, 10 µm sections were cut using a microtome and three sections per slide were mounted and left to dry overnight, after which they were stored in a slide box until ready for staining.

#### 5.2.3.2. H&E staining

For H&E staining, slides were deparaffinised and rehydrated before being washed in slow running water for 2 minutes. Slides were then stained with Harris haematoxylin for 5 minutes, after which they were washed and differentiated by submerging in 1% acid alcohol and Scott's tap water. Slides were then placed into an eosin solution for 2 minutes, before being rinsed under running water and rehydrated. Slides were then mounted and left to dry overnight in preparation for imaging.

#### 5.2.3.3. Toluidine blue staining

Consecutive sections from H&E staining were used for toluidine blue staining. Slides were deparaffinised and a 1% toluidine blue solution was added to each slide and left to stain for 2 minutes. Slides were then washed three times with dH<sub>2</sub>O and dehydrated before being mounted and left to dry overnight in preparation for imaging.

#### 5.2.3.4. Picrosirius red staining

Consecutive sections from H&E and toluidine blue staining were used for picrosirius red staining. Slides were deparaffinised and

submerged in Weigert's haematoxylin for 8 minutes, before being washed and submerged in picosirius red solution for 1 hour. After staining, slides were washed twice with acidified water and dehydrated before being mounted and left to dry overnight in preparation for imaging.

#### 5.2.3.4-5.2.3.5. Image capture and analysis

Slide images were captured at 20x objective using a Zeiss AxioScan 7 Slide Scanner and 200 x 200  $\mu\text{m}$  or 500 x 500  $\mu\text{m}$  regions of interest were exported from Zeiss ZenBlue software for analysis in ImageJ. Neutrophil cell counts were performed manually from images captured from the middle region of the left lung lobe. Mean linear intercept analysis was performed using five random regions containing only alveoli from across the left lung lobe, and measurements were taken using the mean linear intercept plugin for ImageJ. Average alveolus diameter was calculated from the resulting measurements and analysed by 2way ANOVA in Prism.

### 5.3. RESULTS

#### 5.3.1. RNA PURITY FROM MURINE LUNG

RNA quality is pivotal to ensuring the generation of cDNA and therefore RT-qPCR data is valid and can be replicated. Purity of RNA is measured by the 260/280 and 260/230 values, which provide an indication of potential contamination by organic compounds, such as proteins and phenol (260/280), or inorganic compounds, such as Trizol, guanidine HCl and guanidine thiocyanate (260/230). For RNA samples, a 260/280 value of 2.0 or higher is considered "pure", whereas for 260/230 the value should ideally be between 2.0 – 2.2. Following RNA isolation from the lungs, total RNA concentration and purity of each sample was assessed by NanoDrop spectrophotometer. As shown in table 5.3.1, all samples showed 260/280 values above 2.0, indicating all samples were free of contamination with organic compounds which may inhibit or affect the reverse transcription process to generate cDNA. For

many samples however, evidence of contamination with inorganic compounds was detected, with lower 260/230 values associated with an overall lower RNA concentration (table 5.3.1). Typically, such inorganic contamination is a result of carryover of reagents from the RNA extraction process. Given the fibrous nature of lung tissues, and the fact that the weight used for some extractions exceeded the recommended 30 mg, it is possible that the columns used for RNA extraction and for DNase digest were clogged. This would have caused less efficient extraction, resulting in lower RNA yield and increased likelihood of compound carryover from extraction. Whilst many samples could be considered impure as a result of 260/230 values, typically the 260/280 value provides the greatest indication of sample purity as these compounds would more typically interfere with the reverse transcription process [404]. It was therefore concluded that these samples would be suitable for cDNA generation and RT-qPCR analysis, despite possible contamination with inorganic compounds.

**Table 5.3.1:- RNA concentrations (ng/μL), 260/280 and 260/230 values from murine lungs following 12 weeks of CSE exposure.** Abbreviations: NS – Never-smoker; LS – Light-smoker; HS – Heavy-smoker; M or F indicates sex; number indicates individual within group.

Sample ID	RNA Conc (ng/μL)	260/280	260/230
NSM1	149.8	2.10	1.91
NSM2	465.9	2.08	2.20
NSM3	171.8	2.13	1.08
NSF1	331.7	2.12	2.16
NSF2	294.0	2.11	2.15
NSF3	169.1	2.13	0.95
NSF4	205.6	2.16	1.02
LSM1	336.7	2.10	2.10
LSM2	341.9	2.17	0.71

<b>LSM3</b>	221.9	2.13	0.87
<b>LSM4</b>	324.7	2.13	2.18
<b>LSF1</b>	295.6	2.11	2.19
<b>LSF2</b>	224.3	2.08	1.75
<b>LSF3</b>	70.5	2.23	0.13
<b>LSF4</b>	194.2	2.15	0.58
<b>HSM1</b>	272.4	2.10	2.12
<b>HSM2</b>	290.8	2.09	2.15
<b>HSM3</b>	227.6	2.12	1.31
<b>HSM4</b>	245.4	2.14	1.21
<b>HSF1</b>	261.9	2.07	2.16
<b>HSF2</b>	251.4	2.07	2.00
<b>HSF3</b>	292.3	2.13	1.06
<b>HSF4</b>	98.5	2.09	0.25

### 5.3.2. RELATIVE GENE EXPRESSION

Relative gene expression was calculated by normalising genes to Tuba1 and SDHA housekeeping genes and using rescale means from control groups. To determine the impact of sex on changes in gene expression, disease groups were rescaled according to data obtained from the control group (i.e. no CSE) of the respective sex.

To assess full gene expression profiles, heatmaps were generated to visualise overall gene expression across disease groups. In male mice, it was demonstrated that the majority of these genes were upregulated, with more pronounced differences in expression between the never-smoker and light-smoker groups (figure 5.3.1A). This data possibly suggests a lower dose of CSE does not result in prominent immune dysfunction, as typically immunosuppressive genes are more highly expressed than inflammatory genes such as NLRP3, NOX2, TLR4 and IL6RA. Gene expression profiles in females displayed stark contrasts to



those observed in males, as the majority of genes analysed showed marked downregulation in the light-smoker and heavy-smoker groups in comparison to the never-smoker group (figure 5.3.2A). However, much like the trend observed in males, light-smoker females showed a more pronounced change in gene expression from never-smokers when compared to heavy-smokers. The overall profiles from heatmaps suggests that exposure to 1% CSE dampens both inflammatory and immunoregulatory gene expression, but does not have an effect on expression of PRRs and cytokine receptors such as TLR4 and IL6RA (figure 5.3.1A and 5.3.2A). In heavy-smoker mice, this profile is somewhat altered, as while most genes are downregulated, a few key inflammatory genes are highly upregulated. In particular, expression of MMP12 is increased almost 2-fold in female mice in comparison to the never-smoker group (figure 5.3.2A).

For inflammasome signalling, data from female mice could not be obtained for NLRP3 due to low signal detection. In males there was no significant changes in gene expression between disease groups (figure 5.3.1B). Additionally, no statistical differences between disease groups were detected for NOX2 for both male and female mice, although a single outlier may have skewed data for the heavy-smoker female group (figure 5.3.1C and 5.3.2B). No statistical significances as a result of sex were detected, suggesting neither CSE exposure nor sex impacts expression of genes in the inflammasome signalling pathway.

Data for TLR2 could not be obtained for both males and females due to low signal detection. No significant differences in TLR4 (figure 5.3.1D and 5.3.2C) or MyD88 (figure 5.3.1E and 5.3.2D) expression were observed between smoking groups or sexes. IL6RA expression did not show any sex or CSE-dependent differences, though it did appear that CSE differentially affected gene expression in a sex-specific manner (figure 5.3.1F and 5.3.1E). For MMP12, a significant difference between heavy-smoker males and heavy-smoker females was detected, with females showing an almost 2-fold increase in MMP12 expression (figure 5.3.1G and 5.3.1F).

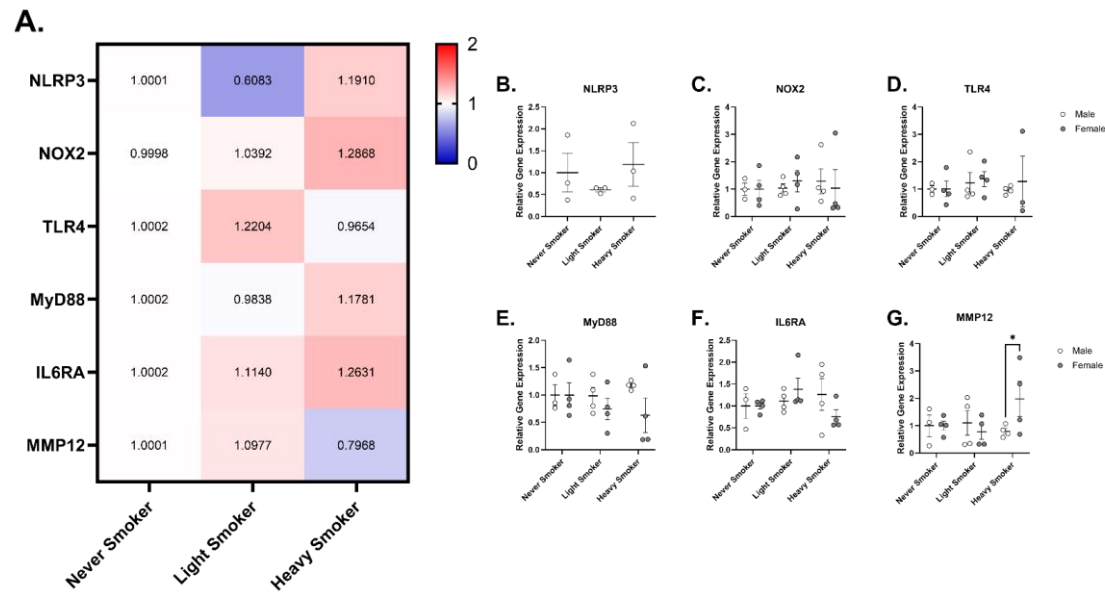


**Figure 5.3.1:- Relative gene expression and individual gene expressions in the right inferior lung lobe of male C57BL/6J mice following 12 weeks of CSE exposure.** Expression of genes between disease groups (light-smoker and heavy-smoker) were compared to a control group (never-smoker) to determine upregulation or downregulation of genes. Data plotted as a heat map (A), and individual genes expressions between male and females for NLRP3 (B), NOX2 (C), TLR4 (D), MyD88 (E), ILR6A (F) and MMP12 (G). Relative gene expression was calculated using the  $\Delta\Delta C_t$  method. Data performed in triplicate and statistics were performed using a 2way ANOVA. Data plotted as mean  $\pm$  SEM \*  $p < 0.05$ .  $n = 3 - 4$

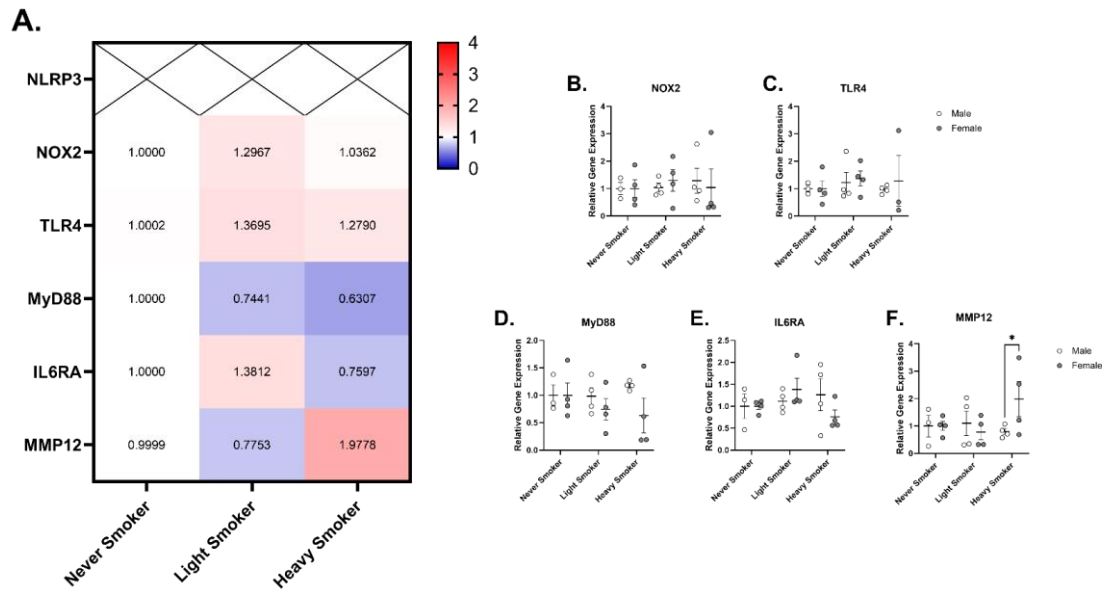


**Figure 5.3.2:- Relative gene expression and individual gene expressions in the right inferior lung lobe of female C57BL/6J mice following 12 weeks of CSE exposure.** Expression of genes between disease groups (light-smoker and heavy-smoker) were compared to a control group (never-smoker) to determine upregulation or downregulation of genes. Data plotted as a heat map (A), and individual genes expressions between male and females for NOX2 (B), TLR4 (C), MyD88 (D), IL6RA (E) and MMP12 (F). Relative gene expression was calculated using the  $\Delta\Delta C_t$  method. Data performed in triplicate and statistics were performed using a 2way ANOVA. Data plotted as mean  $\pm$  SEM \*  $p < 0.05$ .  $n = 4$

### 5.3.3. MAST CELL IDENTIFICATION

Toluidine blue staining was used to identify mast cells in lung sections, thymus and trachea. Mast cells can be easily identified through toluidine staining due to their cytoplasmic granules containing heparin, a polysaccharide which is stained violet with toluidine blue. Following image capture, mast cells were identified as dark blue/violet granular cells (figure 5.3.3, black arrowheads). Since heparin is a component of mast cell granules, toluidine blue staining can be used as an indicator of mast cell activity through the process of degranulation. As shown in figure 5.3.3 (red circle), granules secreted by mast cells retain their dark blue/violet stain and can thus be visualised outside of the mast cell cytoplasm. As mast cells only degranulate following activation in response to allergens or foreign materials, the presence and degree of degranulation in the pulmonary spaces was used as an indicator of mast cell responses to CSE exposure.

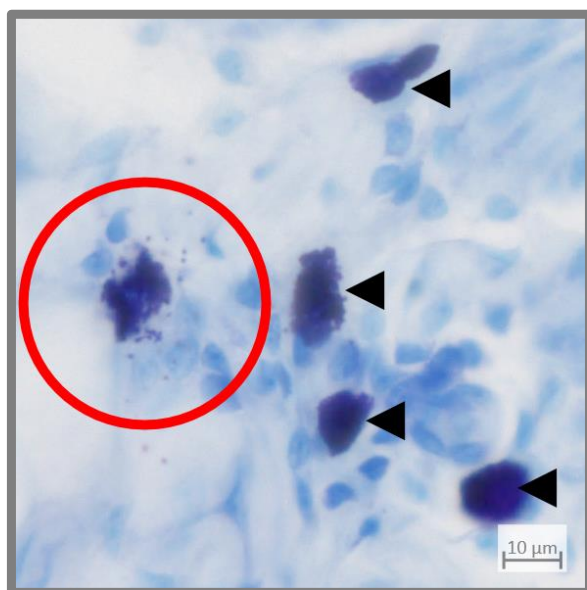


**Figure 5.3.3:- Mast cell identification using toluidine blue staining.** Mast cells were identified by dark blue staining (black arrowheads), whereas degranulating mast cells were identified as mast cells secreting small granules (red circle). Degranulating mast cells were used as an indication of activation. Scale bar = 10  $\mu$ m

#### 5.3.4. MAST CELL NUMBERS AND ACTIVITY

Infiltration and activation of mast cells was assessed by toluidine staining using images taken in the middle region of the left lung lobe, thymus and trachea of male and female mice. Due to the positioning of the thymus and trachea during embedding, sections containing these organs were not present for every individual, and therefore mast cell analysis was conducted on only one individual per group.

In male mice, mast cell infiltration was observed in the left lung and trachea across all CSE dose groups, though infiltration into the thymus was only observed in the light-smoker group (figure 5.3.4). Noticeably, mast cells in the left lung and thymus did not display signs of activation via degranulation, with the exception of the section taken from the left lung of the never-smoker male. Amongst the mast cells observed, one showed evidence of degranulation, and this was linked to the possible presence of an apoptotic body or iBALT (figure 5.3.4, red circle). While it cannot be concluded what the nature of this abnormality is without the use of immunohistochemistry, it appeared as though its presence was linked to increased presence of mast cells as few were detected outside of the captured region (data not shown). However, across all dose groups, mast cell presence in the lungs was most frequently observed in close proximity to either major airways (such as the bronchus or bronchioles) or blood vessels (figure 5.3.4). Despite this, no increased observation of mast cell degranulation was shown as a result of increased CSE dose exposure. Observations from the thymus similarly did not appear to show any differences, with mast cell presence in the light-smoker believed to simply be coincidental. The greatest difference in mast cell presence and activation were observed in the trachea. In the never-smoker, although mast cells were present these did not appear to possess any increased level of activity, however in both the light-smoker and heavy-smoker increased distribution and activation of mast cells was observed (figure 5.3.4). In particular, although the light-smoker had a greater number of overall mast cells, those found in the heavy-smoker section appeared to display a greater degree of degranulation. These

observations suggest that although CSE dose does not appear to have much of an impact on mast cell numbers and activity in the lungs or thymus, increased CSE dose may potentially elicit an allergic-type response by mast cells in the trachea. This response may be further exacerbated by higher concentrations of CSE, as demonstrated by the greater degranulation shown by male heavy-smoker mast cells in figure 5.3.4.

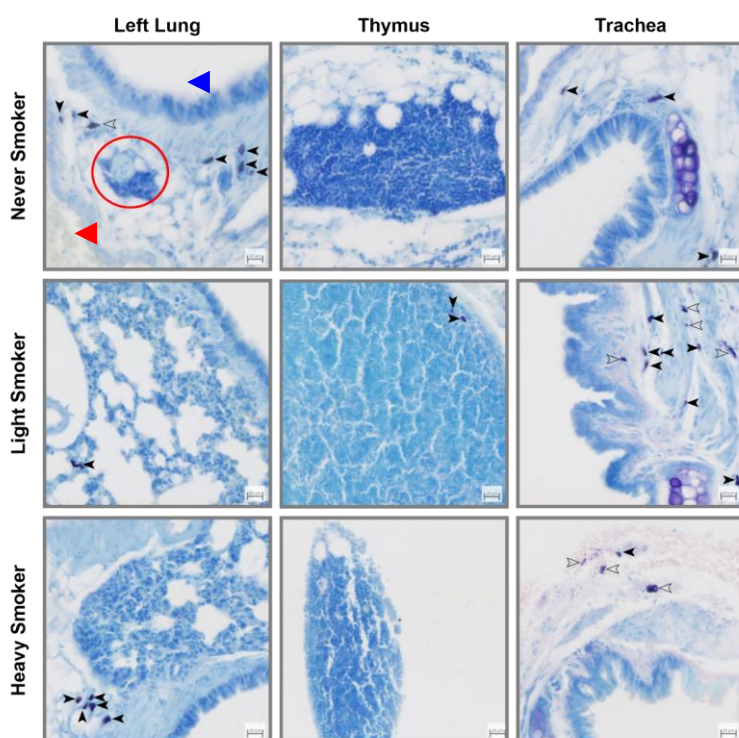


**Figure 5.3.4:- Toluidine blue staining of left middle lung, thymus and trachea of male C57BL/6J mice following 12 weeks of CSE exposure.** Mast cells are identified by black arrowheads, with mast cells displaying activation and effector functions (as demonstrated by degranulation) are identified with outlined arrowheads. Major airway identified by blue arrowhead and blood vessel identified with red arrowhead in the never-smoker lung section. A possible iBALT or apoptotic body is identified by a red circle in the never-smoker lung section. Scale bar = 50  $\mu$ m; n = 1

Similar trends to those observed in male mice were shown in female mice, although presence and activation of mast cells was considerably more prevalent in the thymus by comparison (figure 5.3.5). Mast cells were present in sections from the left lung across all dose groups, though degranulation was only observed in the heavy-smoker. Furthermore, increased infiltration was shown in the heavy-smoker, and presence of mast cells was shown to be more frequent in regions closest to major airways or blood vessels (figure 5.3.5). These observations were similar to those observed for male mice, though degranulation in the lungs was only present in the female heavy-smoker sample. Unlike male mice however, mast cell profiles in the thymus of female mice demonstrated noticeable differences. Whilst the heavy-smoker female showed no signs of mast cell infiltration or activation, a large amount of infiltration and degranulation was observed in both the never-smoker female and light-smoker female (figure 5.3.5). Lack of mast cell infiltration in the heavy-smoker thymus could be attributed to the fact that only a small region of the thymus was present in stained sections, and therefore if the whole thymus was present differences between light and heavy-smoker may have been observed. Nonetheless, these mast cells appeared to be localised to specific areas within each thymus, with those observed in the never-smoker found roughly in the cortex or medulla, whilst those in the light-smoker remained confined to the capsule. While it is unclear what the function of these mast cells and their degranulation is, it is possible that these mast cells may be involved in typical thymic and thymocyte function as their presence and activation does not appear to be dependent on CSE dose. In the trachea however, although CSE did not appear to have an effect on mast cell numbers, mast cell activity is shown to be dose dependent, with a higher CSE dose showing more pronounced degranulation in comparison to a lower CSE dose or control vehicle (figure 5.3.5). These findings are similar to those demonstrated in male mice, suggesting a possible dose-dependent activation of mast cells in the trachea. Interestingly, in both male and female mice, increased presence or degranulation of mast cells as a result of CSE exposure was shown to be typically exclusive to mucosal sites, as the

thymus did not appear to show any differences in mast cell profiles dependent on dose group (figure 5.3.4 and figure 5.3.5).

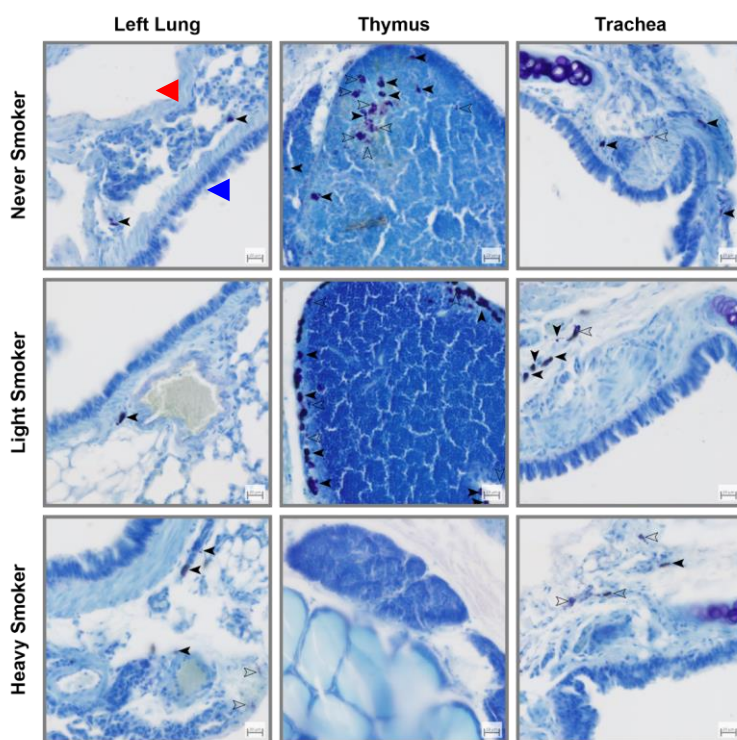


**Figure 5.3.5:- Toluidine blue staining of left middle lung, thymus and trachea of female C57BL/6J mice following 12 weeks of CSE exposure. Mast cells are identified by black arrowheads, with mast cells displaying activation and effector functions (as demonstrated by degranulation) are identified with outlined arrowheads. Major airway identified by blue arrowhead and blood vessel identified with red arrowhead in the never-smoker lung section. Scale bar = 50  $\mu$ m; n = 1**

### 5.3.5. AIRWAY STRUCTURE, COLLAGEN DEPOSITION AND NEUTROPHIL IDENTIFICATION

H&E staining was used to define and identify major and minor airway, as well as evidence of tissue injury in the form of scarring and neutrophil infiltration. Major airways, such as the bronchus and bronchioles, were defined as large airspaces surrounded by ciliated cells (figure 5.3.6, black arrowhead), which were also examined across CSE



dose groups for evidence of morphological changes or remodelling, typically in the form of loss of ciliation. Blood vessels were also identified by open spaces, typically containing red blood cells and/or enucleated cells and surrounded by a dense epithelial layer (figure 5.3.6, red arrow). Blood vessels could be further separated into major vessels (arteries and veins) and minor vessels (capillaries) based on the size of the vessel and density of epithelial lining, with arteries and veins being considerably larger and having denser epithelial linings surrounded by additional cell layers as shown in figure 5.3.6. Capillaries were observed to be much smaller by comparison, and comprised of only a single epithelial layer. Finally, alveoli were defined as small airspaces with thin epithelial walls, though the thickness of these walls would provide an indication of airway remodelling (figure 5.3.6, blue arrow).

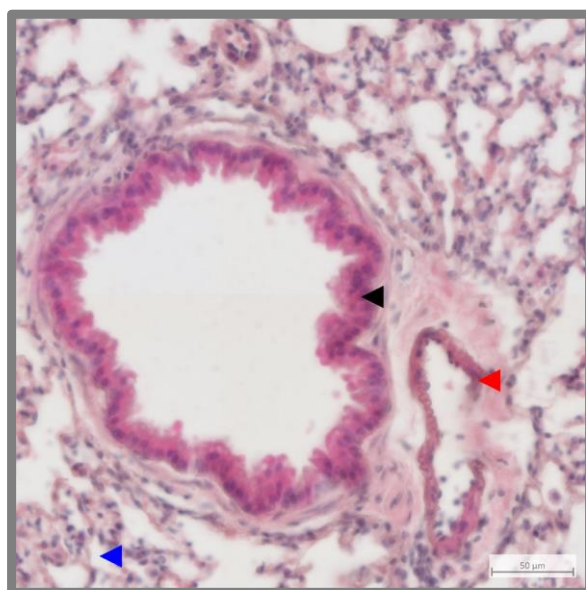


**Figure 5.3.6:- Airway structure and identification in mouse lung.** Structures were identified according to their morphology and cellular components, with major airways comprising large ciliated cell linings (black arrow), blood vessels containing red blood cells and other enucleated cells surrounded by a dense epithelial layer (red arrow), and alveoli comprising air pockets surrounded by a thin epithelial layer (blue arrow). Scale bar = 50  $\mu\text{m}$

Neutrophils were defined according to the degree of staining and the morphology of their nuclei in H&E staining. Due to the eosin counterstain, a number of cell types retain the red/pink colouration differently depending on their cellular contents. Typically, eosinophils are stained the deepest red/pink, due to containing high contents of acidophilic granules within their cytoplasm. In the case of our staining, it was found that the eosin counterstain had overstained neutrophils, to the degree that these could have easily been misidentified as eosinophils (figure 5.3.13). Neutrophils were differentiated from eosinophils by the fact that the cytoplasm did not appear to contain acidophilic granules, which would have appeared a deeper shade of red/pink, and the nucleus contained at least 3 lobes connected by isthmuses (figure 5.3.13, black arrow). As eosinophils only contain two lobes as part of their nucleus structure, this would further prevent the misidentification of cell types.

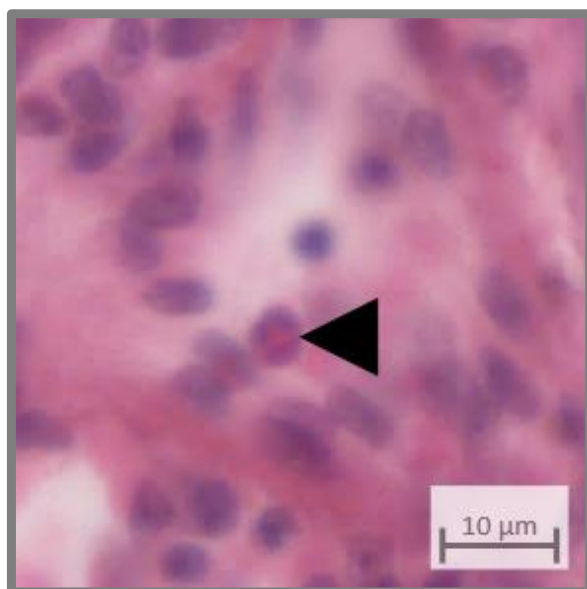


**Figure 5.3.7:- Identification of neutrophils in mouse lung.** Neutrophils were identified as bright pink cells of a similar size to other enucleated cells, but comprising of a granular appearance of the nucleus which overall gives the impression of possessing multiple nuclei (black arrow). Scale bar = 10  $\mu$ m

Collagen deposition was determined via picrosirius red staining, with collagen fibres identified by bright red staining (figure 5.3.7 black arrow). Non-collagenous fibres such as muscle, cytoplasm and red blood cells were stained yellow (figure 5.3.7 blue arrow), nuclei were stained in black (figure 5.3.7 grey arrow). Degree of collagen deposition was defined by increased presence of red collagen fibres or red staining, which is considered a hallmark characteristic of COPD pathophysiology.

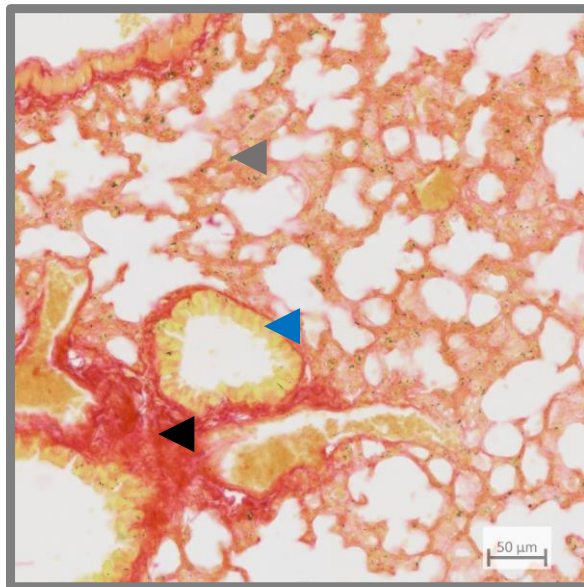


**Figure 5.3.8:- Picrosirius red staining identification of collagen deposition in the lung. Collagen fibres were identified as red stained fibres (black arrow), whilst cytoplasm, muscle fibre and red blood cells are stained in yellow (blue arrow). Nuclei may be visualised by black staining (grey arrow). Scale bar = 50  $\mu$ m**

#### 5.3.6. PULMONARY NEUTROPHILIA

Pulmonary neutrophilia was assessed in 500 x 500  $\mu$ m regions selected from the middle region of the left lung lobe. Neutrophils were counted manually to determine the degree of infiltration into the lungs. In addition, morphometric changes in airways and blood vessels were examined within each section.

In male mice, evidence of airway remodelling was observed in both the light-smoker and heavy-smoker groups, and this appeared to coincide with increased numbers of neutrophils within the airways (figure 5.3.9). In never-smoker male mice, neutrophils appeared to be typically found close to or within the epithelial lining of the airways and blood vessels. It was noted that in both light-smokers and heavy-smokers, the presence of enucleated cells surrounding both major and minor airways were drastically increased, suggesting the presence of scar tissue or tissue damage. This observation was more pronounced in heavy-smokers, and it was observed that neutrophils were frequently identified within these areas of potential scarring and damage (figure 5.3.9). Light-smokers appeared to display an intermediary phenotype between never-smokers and heavy-smokers, with neutrophils found in both epithelial linings and deeper within the lung tissue, though fewer neutrophils were observed in comparison to heavy-smokers. This therefore suggests neutrophils may drive persistent inflammation by migration and accumulation in sites of scarring and damage in response to CSE exposure in male mice.

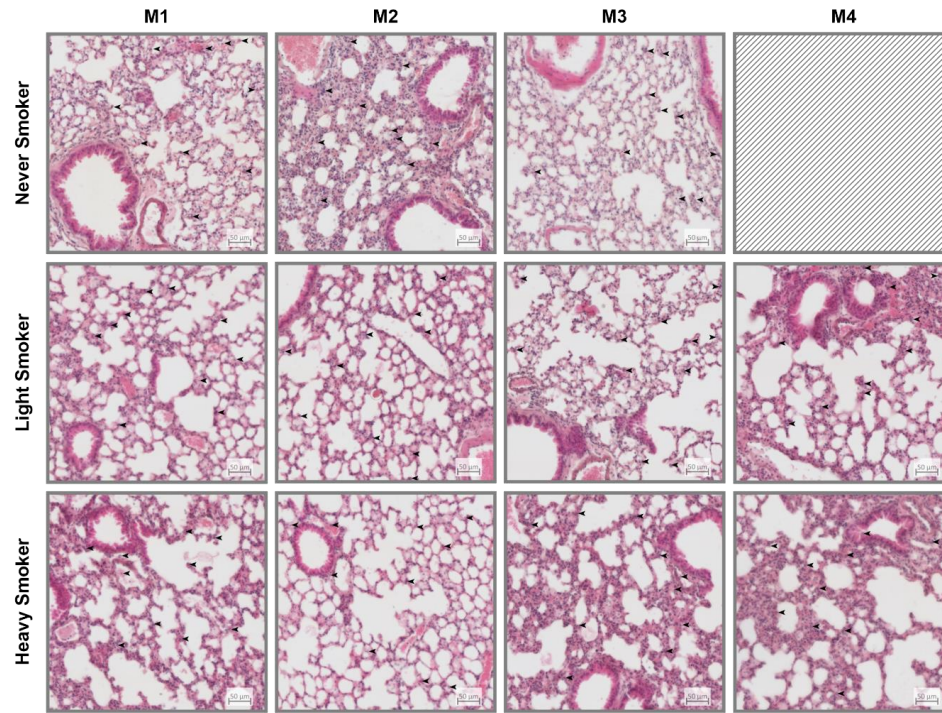
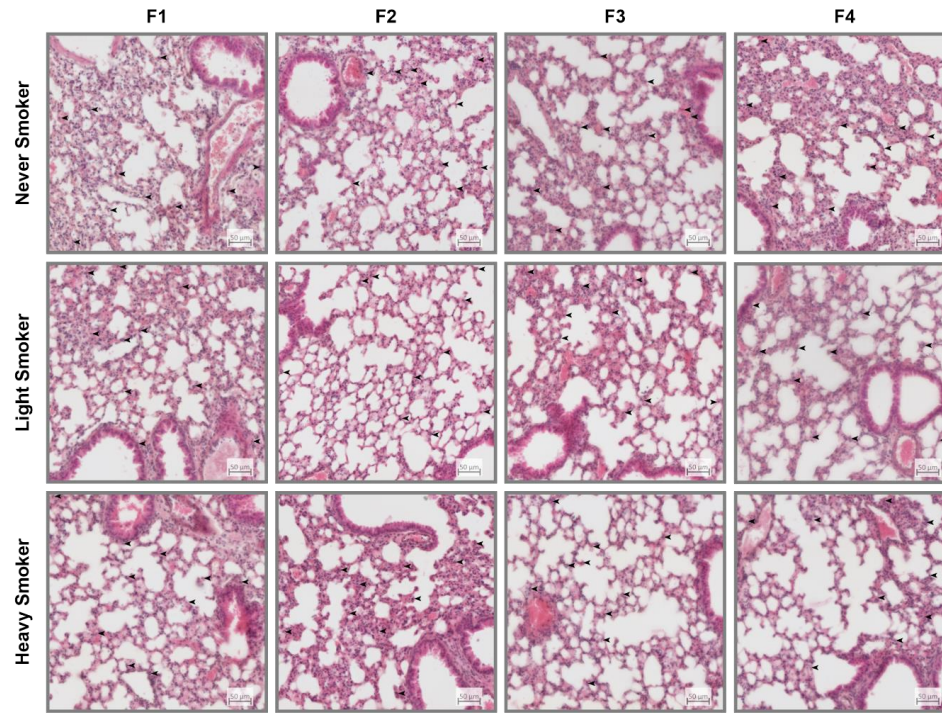


Figure 5.3.9:- H&E staining of left middle lung sections containing alveoli, major airways and major or minor blood vessels of male C57BL/6J mice following 12 weeks of CSE exposure. Neutrophils are identified by black arrowheads. Scale bar = 50  $\mu$ m; n = 3 - 4.

Female mice displayed similar phenotypes to male mice, though evidence of scarring and potential tissue damage were more pronounced in heavy-smoker females in comparison to males (figure 5.3.10). In never-smokers, neutrophils were largely localised to alveolar and bronchiole walls, or identified within and around blood vessels. This same observation was made for light-smokers, though some evidence of deeper infiltration was observed, as were increased numbers of overall neutrophils (figure 5.3.10). Much like male mice, female heavy-smokers displayed prominent evidence of airway remodelling as demonstrated by increased presence of enucleated cells surrounding airways. Additionally, these changes appeared to be more pronounced in females than males, with alveolar destruction appearing to be greater in females (figure 5.3.9 and figure 5.3.10). Additionally, neutrophils were more frequently identified within areas of possible scarring or tissue damage in comparison to never-smokers and light-smokers. These observations coincide with those shown in male mice, and further suggest increased migration of neutrophils to sites of scarring and tissue damage in response to higher doses of CSE, though this appears to be more pronounced in females.



**Figure 5.3.10:-** H&E staining of left middle lung sections containing alveoli, major airways and major or minor blood vessels of female C57BL/6J mice following 12 weeks of CSE exposure. Neutrophils are identified by black arrowheads. Scale bar = 50 μm; n = 4

Total neutrophil counts per field of view were analysed by 2way ANOVA to assess the influence of both sex and CSE dose on pulmonary neutrophilia. As shown in figure 5.3.11, in both male and female mice both 1% CSE and 3% CSE leads to a significant increase in neutrophils within the airways when compared to exposure to no CSE. In males, exposure to 1% CSE leads to almost double the number of neutrophils within the lungs, whilst the increase between 1% CSE and 3% CSE is shown to be comparably small but still significant. Female mice showed a similar increase between 1% CSE exposure and the control group, however the heavy-smoker group displayed a large significant increase in neutrophil counts between both the never-smoker and light-smoker groups (figure 5.3.11). Whilst males and females in the heavy-smoker and light-smoker groups showed comparable numbers of neutrophils, heavy-smoker females showed a significantly increased neutrophil count in comparison to heavy-smoker males (figure 5.3.11). These findings coincide with the observations made from H&E staining, where airway remodelling and presence of scar tissue or tissue damage appeared to be more pronounced in females than males. This data suggests that CSE exposure leads to an incremental increase in neutrophil infiltration into the pulmonary spaces based on dosage, and that females may be at higher risk of lung injury as a result of increased neutrophilia at high CSE doses in comparison to males.



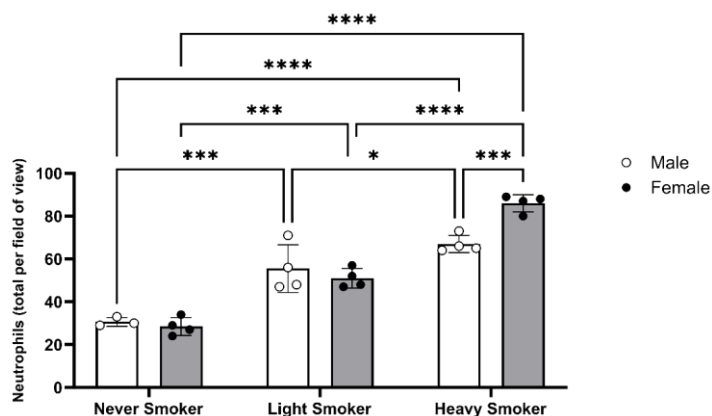


**Figure 5.3.11:- Total neutrophil counts in left middle lung sections of C57BL/6J mice following 12 weeks of CSE exposure.** Total neutrophils were counted manually across a 500 x 500  $\mu\text{m}$  section from the left middle lung lobe as an indication of pulmonary neutrophilia. Statistics were performed using a 2way ANOVA using multiple comparisons between CSE dose and sex. Data plotted as mean  $\pm$  SEM \*  $p < 0.05$ ; \*\*  $p < 0.001$ ; \*\*\*  $p < 0.0001$ ;  $n = 3 - 4$ .

### 5.3.7. COLLAGEN DEPOSITION

Following observations made during neutrophil counts, 500 x 500  $\mu\text{m}$  picosirius red stained images from the middle region of the left lung lobe were taken to determine collagen deposition as a result of CSE exposure. In male mice, increased CSE dose appeared to result in increased collagen deposition, particularly around the large airways and blood vessels (figure 5.3.12). This appeared to coincide with the appearance of small airway remodelling, suggesting a potential decrease in gas exchange efficiency as a result of increased collagen in the airways.

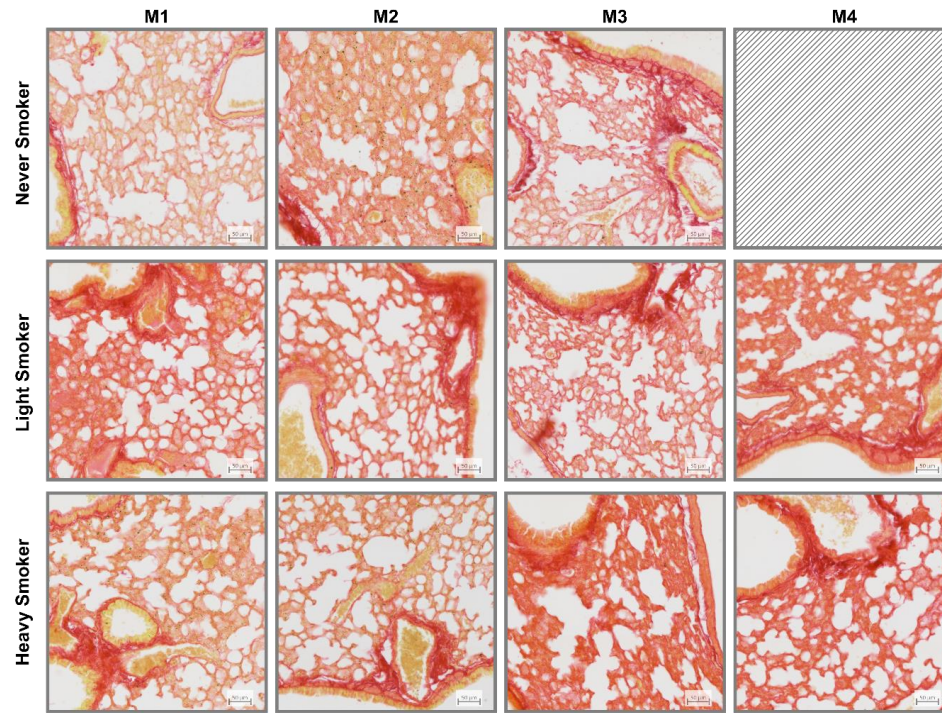


**Figure 5.3.12:-** Picosirius staining of left middle lung sections of male C57BL/6J mice following 12 weeks of CSE exposure. Scale bar = 50  $\mu\text{m}$ ;  $n = 3 - 4$ .

Female mice displayed similar degrees of collagen deposition to males, though this appeared to be more pronounced between never-smoker mice and heavy-smoker mice in comparison to male mice (figure 5.3.13). This increased collagen deposition appeared to be apparent surrounding the major airways and blood vessels, as well as within the lung parenchyma, as evidenced by increased red staining in areas where non-collagenous fibres should be abundant.

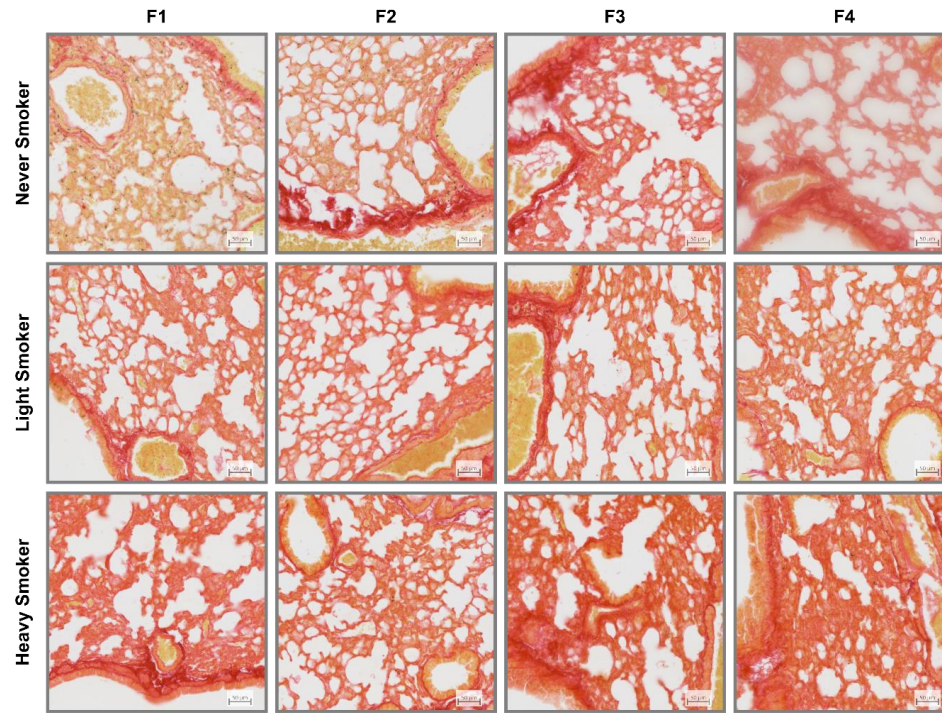


**Figure 5.3.13:-** Picrosirius red staining of left middle lung sections of female C57BL/6J mice following 12 weeks of CSE exposure. Scale bar = 50 µm; n = 4.

5.3.7.5.3.8. SMALL AIRWAY AND ALVEOLAR REMODELLING

Small airway remodelling was assessed using the mean linear intercept (MLI) method to assess free distance between alveolar airspaces as an indicator of lung injury and degree of emphysema. Five random sections from the left lung lobe containing only alveoli were selected for analysis which were used to assess chord length both horizontally and vertically using the MLI plugin for ImageJ. As demonstrated by the resulting measurements, CSE exposure resulted in an incremental increase in estimated average alveolus diameter dependent on dose concentration (figure 5.3.14). In particular, both male and female heavy-smokers showed significant evidence of airway remodelling in comparison to never-smokers as demonstrated by increased average diameter of alveoli. Whilst no differences between sexes were observed, on average females were shown to have slightly larger alveoli in comparison to males across all dose groups. It is uncertain why this was observed, however it could suggest slight sexual dimorphism in terms of lung structure, given that even in the never-smoker group females were shown to have somewhat larger alveoli (figure 5.3.14). Regardless, these findings demonstrate that chronic exposure to CSE at a high dose elicits an emphysematous phenotype in both male and female mice, as indicated by significantly increased small airway remodelling.

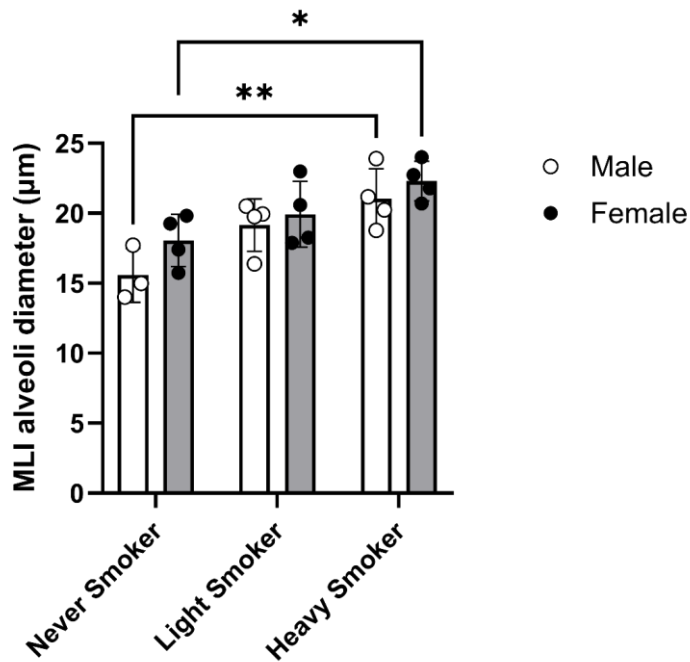


**Figure 5.3.1:- Mean linear intercept (MLI) analysis of C57BL/6J mice following 12 weeks of CSE exposure.** Five random 500 x 500 µm sections from the left lung lobe were taken and chord lengths of alveoli were measured horizontally and vertically using the MLI plugin for ImageJ. Average alveolus diameter was then calculated from the resulting data and statistics were performed using a 2way ANOVA using multiple comparisons between CSE dose and sex. Data plotted as mean ± SEM  
 \*  $p < 0.05$ ; \*\*  $p < 0.01$ ;  $n = 3 - 4$ .

#### 5.4. DISCUSSION

Chronic exposure to CS is known to cause significant inflammation and morphological changes in the lungs, and is shown to be a direct cause in the development of a number of pulmonary diseases including COPD. Here, we have demonstrated that 12 weeks of exposure to CSE leads to significant changes in the lung microenvironment, and differentially affects gene expression dependent on sex. Furthermore,

increased degranulation of mast cells in the trachea and significantly increased pulmonary neutrophilia and small airway remodelling was observed in heavy-smoker groups, with these alterations more pronounced in females than males.

Pulmonary neutrophilia is a hallmark characteristic of COPD, though given that this cell type is typically found in the circulatory system, understanding how neutrophils are trafficked and migrate into areas of inflammation is important in understanding COPD pathophysiology. Migration and trafficking of cells is typically regulated through receptor signalling pathways and production and release of cytokines and chemokines. Amongst these receptors are pattern recognition receptors (PRRs) which recognise signs of infection or tissue injury through detection of pathogen associated molecular patterns (PAMPs) or damage associated molecular patterns (DAMPs). It is widely reported that neutrophils of COPD patients express such PRRs, including TLRs, higher than individuals without COPD [180, 181, 405, 406]. This increased expression is shown to contribute towards COPD pathophysiology, as inhibition of the PRR receptor for advanced glycation end products (RAGE) in mice led to significantly reduced pulmonary neutrophilia and neutrophilic inflammation [407]. As shown in our results, increased presence of neutrophils in the airways is associated with increased CSE dose, and accumulation of neutrophils is significantly more pronounced in females than males (figure 5.3.11). Increased pulmonary neutrophilia may be related to severity of airway remodelling, as higher numbers of neutrophils in the pulmonary spaces appeared to coincide with increased airway remodelling (figure 5.3.14). Determining the impact of CS on gene expression and regulation of PRRs and their signalling pathways, particularly if a single cell type such as neutrophils are significant contributors to these changes, is thus critical in identifying mechanisms of COPD. Characterising these mechanisms and linking genetic alterations to cellular behaviours also opens avenues for future research into therapeutic targets in the treatment and management of COPD.

Whilst the role of genetics and mast cells in COPD pathophysiology is speculative at best, here we have demonstrated differences in gene profiles and mast cell activity as a result of CSE exposure. Gene regulation was shown to be subject to a degree of sexual dimorphism, with males typically showing upregulation of inflammatory genes whilst females displayed downregulation (figure 5.3.1 and figure 5.3.2). Although these differences were not statistically significant in relation to control groups, these findings highlight the importance of considering the role of sex in disease pathogenesis and pathophysiology. The role of sex as a risk factor for COPD is an ongoing debate in respiratory research, with some evidence suggesting an increased risk for women [126, 408], whilst others suggest no correlation between risk and sex [120]. Further defining these changes in gene expression and examining additional gene expressions from other pathways may provide further insight with regards to sex differences in gene expression in COPD. Understanding potential differences in pathology according to sex is important in disease treatment and management, as males and females may respond differently to the same treatment as a result of biological differences. Although no sex differences were observed in regards of mast cell accumulation or activity, it was nonetheless shown that increased CSE exposure resulted in increased presence and degranulation of mast cells in the trachea (figure 5.3.4 and figure 5.3.5). Previous studies have identified a role for mast cell tryptase in COPD pathogenesis, though these findings are from the lungs of mice as opposed to the trachea [296, 403]. Although the contents of the granules secreted by these mast cells have not been determined, this could be an area for future research in order to determine the function of these cells and their overall impact on the tracheal microenvironment. In particular, determining whether these effector functions are similar or distinct to mast cell activity reported in asthma is important in differentiating the two diseases, as they often overlap and COPD is misdiagnosed as asthma, particularly in younger individuals [19].



Despite findings suggesting airway remodelling based on MLI analysis of alveoli, it is important to note that MLI analysis should typically be conducted on inflated or insufflated lungs. Due to issues experienced during dissection, lungs from mice could not be inflated and hence the MLI analysis was conducted on collapsed alveoli. In order for MLI analysis to be considered biologically relevant, the lungs must be inflated so that the area being measured is reflective of the lung's total volume, surface area and maximal inflation [409]. Importantly, the degree of inflation has been shown to affect MLI measurements, meaning that results can vary significantly between collapsed alveoli and inflated alveoli [410]. Since this analysis was conducted on collapsed alveoli, it is likely that the true degree of remodelling as measured by free distance between alveolar walls is not being accurately estimated. In order to conclude that the findings from our MLI analysis are biologically relevant, these measurements should ideally be repeated in inflated or insufflated lungs, in order to ascertain the total average maximal volume of free air in the alveolar spaces.

Although statistical significance is reported by a number of the findings in this chapter, it is important to consider the difference between biological relevance and statistical significance, particularly within the context of human disease. A statistically significant result must be interpreted with corresponding biological processes in mind in order to determine its biological relevance or significance. If the power of the statistically significant result is too small, or does not complement or correspond to known biological processes, then the result cannot be considered biologically significant [411]. Given the small group sizes of our model, although many of our results show statistical significance, it would be unwise to fully conclude the effectiveness of this model at generating COPD in mice without further repeats to increase the power of our findings in order to conclude biological relevance and significance. Our findings are also further compounded by the fact that MLI analysis was conducted on collapsed alveoli, which would not be reflective or

biologically relevant to the state in which alveoli may be naturally observed and measured.

To summarise, here we have ~~confirmation-suggested presence~~ of an emphysematous phenotype in both male and female mice chronically exposed to CSE, and thus have ~~a-confirmed~~developed the groundwork for a novel model system of COPD. These findings open possibilities for future research in further characterising additional mechanisms of COPD, and provideing researchers in the UK with a 3Rs friendly mouse model of COPD to conduct their own research.

## CHAPTER 6 – GENERAL DISCUSSION

### 6.1. OVERVIEW

COPD is an umbrella term for persistent and progressive inflammatory respiratory conditions including emphysema and chronic bronchitis. It is highly prevalent in both high-income countries and LMICs, though the age of onset and causative factors for COPD vary depending on sociodemographic backgrounds [80]. COPD presents itself as a significant global burden on both economic and healthcare resources, as frequent exacerbations typically require hospitalisation and significant intervention and respiratory support [60, 66]. The economic burden of COPD in LMICs is particularly severe, typically attributed to a lack of healthcare resources that are otherwise available in high-income countries [65]. In high-income countries, the primary aetiological factor of COPD is cigarette smoking [97], which is known to elicit a chronic inflammatory response in the lungs and lead to airway remodelling [137]. Despite its high prevalence and global burden, the pathogenesis of COPD, particularly in the context of inflammatory mechanisms, is poorly understood, and as a result treatment and therapeutic interventions largely revolve around symptom management and management of AECOPD. Although not fully characterised, it is believed that many different immune mechanisms are involved in COPD pathogenesis, and other factors, such as genetics and sex, may increase the risk of COPD development. A1AT deficiency has been widely reported as a risk factor in COPD pathogenesis [111], and although sex differences in COPD remains a topic of much debate, many studies indicate an increased susceptibility of disease development in women compared to men [122, 126].

The immunopathogenic mechanisms of COPD consist of a number of cellular and molecular mechanisms across the innate and adaptive immune system, which contribute towards a proinflammatory environment in both the lungs and peripheral blood. Tissue-resident macrophages are well documented to contribute towards airway

remodelling in the lungs of COPD patients through the secretion of proinflammatory cytokines and production of MMPs, which cause the degradation of the ECM and lead to loss of elasticity in the pulmonary spaces [176, 177]. Similarly, neutrophils may also contribute towards airway remodelling by similar mechanisms to those of macrophages [182], though neutrophils are typically found in circulating blood as opposed to tissues. Pulmonary neutrophilia is considered a hallmark characteristic of COPD pathophysiology, and this has been linked to an overexpression of PRRs which facilitate neutrophil recruitment and activation between the peripheral blood and lungs [180]. Neutrophil recruitment into the lungs has also been shown to be driven by immature DCs [184], and these may also cause the differentiation of T cells into proinflammatory subtypes [187]. NK and NKT cells display markedly different abundance and functionality between the periphery and the lungs, where peripheral NK and NKT cells are shown to be in low abundance and exhibit blunted cytotoxic activity in COPD patients [190], whereas increased numbers are found in the pulmonary spaces and overexpress cytotoxic activity, resulting in tissue damage [191, 192]. These characteristics are also observed in CD8<sup>+</sup> T cells, with peripheral CD8<sup>+</sup> T cells showing limited cytotoxic function and pulmonary CD8<sup>+</sup> T cells overexpressing cytotoxic compounds such as perforin and granzyme B [190, 198]. CD8<sup>+</sup> T cells are also shown to be significant sources of the proinflammatory cytokine IL-17A, which is known to drive the differentiation of CD4<sup>+</sup> T cells into proinflammatory Th17 subsets [203]. An imbalance of inflammatory Th17 subsets to anti-inflammatory Treg subsets is widely reported amongst COPD patients, leading to persistent inflammatory mechanisms and reduced immune regulation mechanisms [205, 216, 217]. T cell differentiation relies on antigen presentation, which can be mediated by B cells. Although their role in COPD is unclear, studies have demonstrated that B cells in COPD patients possess autoreactive characteristics and generate antibodies which can cause lung injury and fibrosis [221, 224]. Cell migration, differentiation and effector functions are all mediated by cytokines and

chemokines, a number of which, including IL-6, IL-17A, IFN- $\gamma$  and TNF- $\alpha$  have been associated with COPD pathophysiology [228].

Due to the complex nature of COPD, animal models have been frequently used to study its pathogenesis. Whilst many different species have been used in the past, mice are the favoured species of choice due to their low cost and ease of use [292]. CS-exposure mouse models of COPD typically follow one of two designs: WB or NHO exposure. Whilst each of these models are effective in generating a COPD phenotype, there are a number of limitations in regards to both their translational ability to human disease and the welfare concerns they cause. For example, whilst WB models are effective in exposing a large number of mice to CS at once, inflammatory responses to CS were shown to be a result of ingestion of particulate matter rather than inhalation [276, 306]. In contrast, the NHO system is considered to be more clinically representative of human COPD [313], though animals are often restrained for long periods of time without free access to food and water which causes significant stress, which may in turn impact the quality of data generated [308]. As a result of the poor translational ability of the WB system and the stress concerns of the NHO system, these model designs are not permitted for use in the UK under current laws protecting animals in scientific procedures. Animal research in the UK is underpinned by the 3Rs: replacement, refinement and reduction, and the welfare of animals involved in scientific research is highly protected.

To address the lack of a murine model of COPD in the UK, we have designed a novel 3Rs friendly intranasal CSE-exposure model which reduces potential adverse welfare effects and better encapsulates the clinical presentations and exposure routes of human COPD. Using multiplexed and high-throughput analytical techniques including spectral flow cytometry and RT-qPCR, we have demonstrated that animal numbers can be reduced without impacting the quality and quantity of data generated. Furthermore, we have highlighted the necessity of including both sexes in disease research, as noticeable differences in gene expression and lung morphology were observed between male and

female mice. Although no differences in systemic immune cell profiles were detected over the 12-week exposure period, data from the pulmonary system of both male and female mice demonstrated significant evidence of alterations to gene expression, inflammation and airway remodelling. ~~We have confirmed~~Our results suggest that 12 weeks of exposure to 3% CSE elicits a moderate COPD phenotype in the lungs of male and female C57BL/6J mice, and ~~demonstrated~~ that refined dosing and sampling techniques are effective in creating a model system akin to those currently available in other countries, but is better reflective of human COPD as a whole.

## 6.2. EFFECTS OF CSE EXPOSURE ON SYSTEMIC IMMUNE CELL PROFILES

Across the 12-week exposure period, our model system did not demonstrate any differences in immune responses or cell profiles between dose groups. Nonetheless, as shown in Chapter 4, both conventional gating strategies and unbiased clustering analysis showed comparable systemic cell profiles, demonstrating the comprehensive nature of our flow cytometry panel. Furthermore, although no differences in cell profiles and effector functions were detected between control groups and disease groups, many observations made were reflective of trends typically seen in COPD patients. For example, imbalance of CD4<sup>+</sup>/CD8<sup>+</sup> T cells has been shown to be linked to COPD pathophysiology, with decreased numbers of CD8<sup>+</sup> T cells in the periphery as a result of migration into the lungs frequently observed [191, 204]. All dose groups demonstrated a shift to a majority CD4<sup>+</sup> T cell profile over the 12-week period, which although did not indicate that CSE exposure was responsible for the shift, potentially suggests that this is a natural progression of immune system changes in relation to age. It is therefore possible that whilst this shift may be observed regardless of exposure to disease-causing materials, it is exacerbated to a pathogenic extent in inflammatory diseases such as COPD, causing alterations to

cell function rather than population distribution. This could be further supported by evidence that demonstrates that cytotoxic cells such as NK, NKT and CD8<sup>+</sup> T cells show highly increased cytotoxic function in the lungs [191], but limited function in the periphery [190]. Additionally, we identified that CD8<sup>+</sup> T cells positive for IL-17A were more abundant than IL-17A<sup>+</sup> CD4<sup>+</sup> T cells, which although no differences between dose groups were observed, has been implicated in COPD pathophysiology [393]. Despite these associations however, we were not able to provide evidence of CSE having an impact on systemic immune cell profiles or mechanisms and the majority of the trends observed appeared to be more a result of ageing rather than CSE exposure. It is possible that, due to LASA guidelines for microsampling and the small blood volumes that were taken, differences in these profiles could not be determined due to low cell numbers available for analysis.

### 6.3. ALTERATIONS TO GENE EXPRESSION FOLLOWING CSE EXPOSURE

Although the majority of the genes investigated during our study showed no statistical differences between control groups and disease groups, with the exception of CRP expression in female mice, we demonstrated that gene expression is subject to a degree of sexual dimorphism. In male mice, inflammatory genes were shown to be upregulated, whilst females demonstrated downregulation of these genes. Some of these sex differences appeared to impact specific immune pathways. For example, in both the light-smoker and heavy-smoker groups, IRF3 was significantly downregulated in females when compared to males, suggesting a possible sex-specific impairment of the TRIF-dependent TLR4 signalling pathway in response to CSE. Although many genes displayed significant differences between sexes, only CRP displayed a significant difference in expression dependent on CSE dose, and this was only observed in female mice. In comparison to both female never-smoker and light-smoker mice, female heavy-smoker mice

displayed significant upregulation of CRP. In COPD, increased levels of CRP are associated with poor outcomes and can be used to predict mortality [398], and is well documented as a biomarker to predict AECOPD [412-414]. Since CRP expression did not appear to be affected by CSE dose in male mice, this suggests that CRP expression in the context of COPD is a sex-related risk factor. Differences between both male and female mice in gene expressions provide areas for future research to not only further characterise genetic associations of COPD, but also sex differences in expression within COPD.

#### 6.4. INCREASED ACTIVITY OF MAST CELLS IN THE TRACHEA

Mast cells in respiratory immunology are more typically associated with asthma and the allergic response, though due to the overlap between asthma and COPD it is theorised that mast cells may contribute in some manner to COPD pathogenesis. Nonetheless, increased numbers and activity of mast cells has been reported in the lungs and skin of smokers, suggesting a direct effect of CS on mast cell phenotypes [415]. Despite these findings however, mast cells remain a considerably overlooked cell type in COPD research, though recent research suggests that mast cells are a promising target for novel therapeutics [416]. Whilst our model did not demonstrate any distinctive changes in mast cell numbers in relation to CSE dose, increased concentrations of CSE resulted in a noticeable change in the degree of mast cell activity. This appeared to be localised within the trachea, suggesting CSE elicits an inflammatory or allergic-like response within the trachea. Furthermore, degranulation of mast cells appeared to be exacerbated in both male and female heavy-smoker mice in comparison to never-smoker and light-smoker mice. Our findings appear to coincide with those of other studies, which have demonstrated that the total numbers of mast cells in COPD patients are neither increased nor decreased compared to healthy controls, but gene expression of mast cells is shifted towards an allergic-type inflammatory response [417]. This inflammatory response has been linked to eosinophilic inflammation, and thus provides further evidence of



a role for both mast cells and eosinophils in driving an allergic-type inflammatory response in COPD, particularly in mucosal airways [258]. Although the content of secreted granules by mast cells was not analysed in this study, these findings identify a potential area for further research to determine the effector functions of mast cells following CSE exposure.

#### 6.5. DOSE-DEPENDENT INCREASE IN PULMONARY NEUTROPHILIA AND AIRWAY REMODELLING

Exposure to CSE was shown to lead to a dose-dependent increase in both pulmonary neutrophilia and airway remodelling, with some evidence of these phenotypes being exacerbated in females. Furthermore, increased presence of neutrophils was suggested to be associated with severity of airway remodelling, as higher neutrophil counts were found in groups with a greater MLI (Chapter 5). These findings appear to suggest that neutrophils may contribute towards airway remodelling, possibly as a result of the production of proinflammatory mediators which may drive recruitment of other immune cells or alterations to the ECM. This theory is supported by evidence that accumulated neutrophils in the lungs are hyperactivated, and produce large quantities of MMPs and neutrophil elastase which degrade the ECM and lead to reduced integrity and elasticity of the lungs [182, 400]. Of particular note, pulmonary neutrophilia was shown to be significantly increased in female heavy-smoker mice in comparison to all other groups, suggesting that women are possibly predisposed to accumulation of neutrophils in response to noxious particulate matter in the lungs. Further analysis of neutrophil-derived effector functions and gene expression profiles would be required to provide more evidence to support this. Given that neutrophilia, fibrosis and airway remodelling appeared to be somewhat exacerbated in female mice however, these findings highlight the importance of considering the biological impact of sex on disease pathogenesis.

## 6.6. IMPACT OF SEX ON COPD PATHOPHYSIOLOGY

Across all our findings, both subtle and significant differences were observed between sexes in response to either CSE dose or as a possible consequence of ageing. From analysis of systemic immune profiles, it appeared as though female mice often displayed changes to cell profiles approximately one week earlier than male mice. Similarly, CSE appeared to differentially affect gene expression according to sex, with male mice typically displaying upregulation of inflammatory genes as opposed to female mice, where genes were often downregulated. Importantly, however, as previously discussed, female mice showed a greater degree of pulmonary neutrophilia and slightly more pronounced fibrosis and airway remodelling in comparison to male mice. These findings highlight the importance of including both sexes in an animal model as different sexes may demonstrate different phenotypic presentations or responses to the same stimuli. This is critical for diseases where an element of sex differences or sex as a risk factor is either proven or suggested, as is the case for COPD. For complex diseases such as COPD, applying a “one size fits all” approach is not appropriate, particularly given the possible implications of increased female susceptibility. Current research into COPD using mouse models often only makes use of one sex [276, 310, 418], or fails to report the sex of animals involved at all [283, 296, 323], and very few are reported to use both sexes [419]. This issue overall reduces the integrity of reported findings from mouse models, as biological differences between males and females can be considerably dimorphic. Observed sex differences in COPD are believed to be a result of a combination of genetic, hormonal, metabolic, behavioural and environmental factors, though there is a significant lack of robust evidence to support these theories [120]. Here we have provided evidence of an increased susceptibility to immunopathogenic mechanisms that may drive COPD pathogenesis in female mice. Interestingly, our observations of earlier changes to systemic immune profiles in females in comparison to males may provide some insight to previously reported trends in COPD. It has been suggested that women

are more likely to develop COPD earlier and after having smoked for less time than men, the reasons for which are unknown and the association is speculative at best [120, 121]. If there are sex-related influences on the maturation of the immune system, then this possibly provides supporting evidence of sex as a risk factor in the development of a number of inflammatory diseases such as COPD.

### 6.7. MOUSE MODEL DESIGN

Through a 12-week exposure to CSE, we have demonstrated that our model system is effective in generating an emphysematous COPD phenotype in both male and female mice. Although concerns were raised regarding the welfare of animals during the acquisition of Home Office Licences, particularly in regards to the use of anaesthesia on mice with compromised lung function for dosing methodology, we have demonstrated that the model system has minimal to no adverse welfare effects on animals involved. This was evidenced by the fact that all animals maintained stable weight gain over the 12-week exposure period, and any adverse welfare effects that were identified were as a result of general mouse behaviour such as fighting (resulting in superficial injury) or overgrooming (resulting in lack of fur in some places or skin irritation). All instances of these welfare concerns were addressed and treated immediately, with affected animals recovering swiftly following the appropriate interventions. Importantly, all animals regardless of dose group responded well to frequent exposure to anaesthesia, and no complications as a result of anaesthesia, dosing or respiratory distress were observed. Given that the most significant evidence of COPD was observed between the never-smoker groups and the heavy-smoker groups, it can be concluded that an optimal dosing regimen of 3% CSE 3 x per week for 12 weeks is sufficient for the development of a moderate COPD phenotype. We have therefore demonstrated a robust and 3Rs friendly mouse model of COPD, that better reflects human COPD as a result of exposure methods used and can be applied in a number of research settings across the UK.

### 6.8. GENERAL LIMITATIONS

Perhaps the greatest limitation of this study is a result of the restrictions of our PPL and legislations protecting animals used in scientific procedures. Given the novel nature of our model, only small group sizes were permitted for use to ensure that no unnecessary harm or suffering occurred to animals whilst the optimal dosing regimen was determined. Ultimately, this reduces the statistical robustness of our findings, as  $n = 3 - 4$  naturally does not hold as much power as  $n = 8$ , for example. This limitation could not be avoided due to ethical and legal restrictions, nonetheless the most statistically powerful group size was used within the stipulations of our PPL and within ethical considerations in order to improve the integrity of our findings. Going forward, as the dosing regimen has been identified, further studies using this model system would have the freedom to use increased group sizes in order to improve integrity and robustness of findings. In addition to restrictions on group size, we were further limited by the volume of blood permitted to be taken each week under LASA and NC3Rs guidelines. Since we were taking samples once per week, we were only permitted to take up to 210  $\mu\text{L}$  over a 28-day period, an equivalent of just over 50  $\mu\text{L}$  per week. Due to welfare concerns and the frequency samples were taken, we opted to take 20  $\mu\text{L}$  per week to lower the risk of adverse welfare effects due to blood loss. This however resulted in low cell numbers available for analysis, and whilst some weeks over 1,000 live immune cell events were recorded from samples, at times as few as 50 events were recorded. These are staggeringly low event numbers for flow cytometry analysis, where 10,000 events is often considered the lower limit of acceptable. However, minimal differences were observed in immune cell profiles over a weekly basis, and it is therefore more appropriate to take peripheral blood samples less frequently from both a welfare and data integrity standpoint. Taking a single blood sample once per month, for example, would permit the use of LASA guidelines for blood sampling for infrequent microsampling, which would increase the blood volume limit to <10% TBV, or approximately 140  $\mu\text{L}$ . A total volume of 100  $\mu\text{L}$  whole blood

every 4 weeks would not only increase the numbers of cells available for analysis, but also allow differences in immune cell profiles to be more easily detected, and using a volume below the maximum suggested limit would minimise the risk of adverse welfare effects.

Although the analytical techniques used in this model provide a wealth of information and are considered high-throughput, specific mechanisms were not investigated in greater detail. It was anticipated that proteomic analysis would take place through the use of an RPPA panel, though as shown in Chapter 3 this previously validated panel that had been used to analyse human COPD patient samples was not cross-reactive with mouse samples despite manufacturer specifications and reports. This ultimately prevented us from performing proteomic analysis which would have provided a further additional aspect in regards to COPD pathogenesis. Furthermore, the spectral flow cytometry panel was designed to capture all major immune cell types, though due to the restrictions of both reagent availability and unmixing capabilities, this came at the cost of being able to characterise effector functions to a greater degree. Additionally, flow cytometry was not performed on lung samples, and thus critical information regarding immune cell profiles was not obtained. Acquisition of BALF had been intended for this study, though challenges in BALF retrieval were encountered and it was decided that BALF would not be collected in order to preserve tissue integrity for histological analysis. In future research, flow cytometry analysis should be performed on BALF or on immune cells isolated from the lungs through mechanical disruption in a similar manner to that used for spleens during the validation of our flow panel. Although histological analysis provided significant insight into the effects of CSE on mast cell activity, pulmonary neutrophilia and airway remodelling, further analysis using immunohistochemistry to identify presence of other immune cell types or altered functionality of structurally-related cells could have been performed. This would have allowed for the possible identification of additional immunopathogenic mechanisms. However, when it is considered that the basis of this project was to design a model system to

encapsulate human COPD in a 3Rs friendly manner, ensuring that a broad range of markers could be detected in order to demonstrate the applicability of the model itself was of greater importance. With the model system optimised and refined, these limiting factors now provide opportunities for areas of future research.

Whilst all of these limiting factors can be easily addressed in future research, a limiting factor of age of mice used for the model system is somewhat more complex. Here, 11-week-old C57BL/6J mice were used for our study, which although considered mature adults in the context of mouse biology would be age-equivalent to a human in their 20s [294]. COPD as a result of CS exposure is typically presented as a disease of old age, particularly in high-income countries, and therefore the use of animals which are not age-equivalent to those typically affected by a disease limits a study's translational ability. While COPD cannot be caused by the ageing process itself, there is evidence to suggest that natural biological processes that are altered and less efficient later in life contribute towards COPD pathogenesis [125]. Many of the hallmark characteristics of ageing and mechanisms of COPD pathogenesis overlap, as such ageing is often considered a significant risk factor in the development of COPD, especially when in combination with exposure-type risk factors such as CS or air pollutant exposure. Physiologically, the elastic recoil of the lungs declines over time, in addition to decrease in chest wall compliance which overall reduces the gaseous exchange capabilities of the lungs [420]. These characteristics can in turn lead to the development of senile emphysema, which differs from the emphysematous phenotype associated with COPD in that it displays largely homogenous airspace enlargement within the lungs by comparison [421]. The ageing process is also associated with the shortening of telomeres, repetitive sequences located on the distal ends of chromosomes involved in maintaining chromosome stability. There is evidence to suggest a role for excessive telomere shortening, particularly in inflammatory and immune cells, in COPD pathogenesis, and an association between shorter telomeres and higher risk of mortality has

been observed [422, 423]. Cellular senescence, characterised by the cessation of cell division and replication, is also known to contribute towards the ageing phenotype. Senescent cells have a distinct morphology and phenotype, which includes the production and secretion of proinflammatory cytokines to promote chronic inflammation within a given environment [424]. Increased numbers of senescent cells, particularly alveolar epithelial cells, lead to a reduction in the regenerative capabilities of the lungs and put COPD patients at increased risk of irreparable lung damage and injury [425]. From the results of our flow cytometry analysis from peripheral blood, immune cell profiles were shown to change over a 12-week period, which was attributed towards ageing of mice as opposed to CSE exposure, given that no differences between dose groups were observed. Given that COPD is often considered a disease of old age, particularly in the context of CS exposure, had we used aged mice or utilised a longer exposure period to CSE we may have seen noticeable differences in immune profiles between disease groups and control groups. The use of aged mice in COPD research has been performed before, and it was found that 52-week-old mice had increased susceptibility and accelerated development of pathophysiological characteristics of COPD in comparison to 8-week-old mice [295]. The use of aged mice would improve the biological relevance of the model system to human disease, as 8-week-old mice are considered age-equivalent to human young adults and COPD in younger individuals is typically associated more with environmental and household air pollutants [3]. Therefore, older mice, commencing a dosing period between the ages of 10 – 14 months (middle age) would be more representative of the typical patients associated with CS-induced COPD, as these would be age-equivalent to a human in their late 40s and early 50s where early onset of COPD may be observed. This does, however, lead to additional concerns with regards to the welfare of animals involved, as older mice would be at a higher risk of developing adverse welfare effects in response to CSE as a result of the biological effects of ageing. Beyond 18 – 24 months, the overall survival rate of mice begins to significantly decline as a result of biological ageing, and there is also

an increased risk of generation of misleading results due to presence of biomarkers of other age-associated diseases that may overlap with the disease of interest [294]. Furthermore, with a lower survival rate in general are potentially increased risks of poor survival following a similar CSE dosing regimen to the one used in our model system. Additionally, the use of aged mice would require the submission of an amendment to the PPL for this study, and likely require a small-scale pilot study to assess the risk of adverse welfare effects and refine the model system accordingly following the amendment's approval. Nonetheless, the use of aged mice would only further improve the biological relevance and translational ability of the model, and may assist in identifying age-related immunopathogenic mechanisms of COPD.

In all, while there are limitations to our model design, these can be easily rectified through further refinement of the model system itself and development of more comprehensive analytical panels and techniques. These limitations therefore do not significantly impact the integrity of the model design nor its potential application in future research.

### 6.9. APPLICATIONS AND FUTURE DIRECTIONS

We have now established [the framework for](#) a mouse model of COPD available for use under UK law and legislation, and are therefore able to provide researchers in the UK with an *in vivo* toolkit to further investigate COPD immunopathophysiology. In particular, the model ~~can~~ [may](#) be used for deep phenotyping to examine specific genetic, molecular or cellular mechanisms of COPD in greater detail. Based on our findings and that of previous research, this could include determining mast cell cargo in the trachea to ascertain its effect on COPD pathophysiology in the lower respiratory system, or performing single-cell RNA sequencing on neutrophils isolated from both peripheral blood and BALF to determine possible changes in PRR expression in response to CSE. Identification and further characterisation of pathogenic mechanisms could provide insight into novel targets for therapeutics, and therefore the model system



could in future be used in pre-clinical trials to assess the efficacy of novel therapeutics. In addition, the CSE used to induce COPD in mice could be modified to allow exposure to other noxious particulate matter. This includes various air pollutants and e-cigarette vape, which would allow for the examination of phenotypic differences between COPD as a result of CSE and other causative agents.

Given the small group sizes and lack of power in this study as a result, it would be imperative to increase group number sizes in future experiments in order to ensure that statistically significant results can be obtained and identified. In order to determine this, a power calculation was performed using lung neutrophil count, mean linear intercept and total peripheral immune cell count data from this study. Based on these calculations, the effect size was 5.68 for neutrophil counts, 2.35 for mean linear intercept and -0.11 for peripheral immune cell counts (table 6.9.1). Estimated required sample size per group was determined to be 1 for neutrophil counts and 5 for mean linear intercept. For total peripheral immune cell counts, estimated required sample size was determined to be 1636 per group (table 6.9.1). Given that this number is considerably high and the effect size is so small, these results should not be taken into consideration for future experiments, especially as this would contradict the 3Rs principle of reduction. Similarly, with only one animal per group it would not be possible to perform statistical analysis, as such this would not be a logical choice in future experiments. As our study makes use of 3 – 4 animals per group, and with minimal to no effect size detected for peripheral immune cell profiles, we recommended group size of between 7 – 8 or 8 – 10 animals. This would allow for the effect sizes of both lung neutrophil counts and mean linear intercept to be detected in future experiments, and account for any variability or unforeseen issues that would result in a reduction in group sizes (e.g. removal from study due or early cull as a result of welfare issues or concerns).

CHAPTER 6 – GENERAL DISCUSSION

*Table 6.9.1:- Results of power calculation to determine effect size and required sample size per group for future experiments. Calculations were performed using data for lung neutrophil count, mean linear intercept and total peripheral immune cell count*

Dataset	Effect Size	Required Sample Size Per Group
Lung Neutrophil Count	5.68	1
Mean Linear Intercept	2.35	5
Total Peripheral Immune Cells	-0.11	1636

~~Given that~~Since our model system ~~generates~~ is suggested to ~~generate~~ a moderate COPD phenotype, it can in theory be used as an infection model system, whereby mice that have developed COPD are exposed to pathogens in order to simulate AECOPD. AECOPD is a significant contributor towards the healthcare and economic burden of COPD, with frequent infections considered one of the most common causes of AECOPD [249]. Understanding how these infections take hold and how the immune system responds to infection within a COPD microenvironment can provide insight into better treatment and therapeutic strategies in AECOPD, or potentially provide insight into areas where early detection or risk of AECOPD can be assessed. A possible mechanism of COPD pathology that has yet to be widely investigated is dysbiosis or reduced diversity of the respiratory microbiome. The majority of research into host-microbiome interactions has largely focused on the role of the gut, skin and vaginal microbiota in disease pathogenesis, and it is only recently that research has begun to investigate the respiratory microbiome [426]. Unlike the gut microbiome, the lower respiratory microbiome possesses a more “fluid” dynamic to maintain low numbers of microorganisms in order to facilitate optimal gas exchange processes and maintain immune homeostasis [427-429].

- Formatted: Font: 10 pt
- Formatted: Font: 10 pt, Not Italic
- Formatted: Font: 10 pt
- Formatted Table
- Formatted: Font: 10 pt
- Formatted: Font: 10 pt
- Formatted: Font: 10 pt, Not Italic
- Formatted: Font: 10 pt
- Formatted: Font: 10 pt
- Formatted: Font: 10 pt, Not Italic
- Formatted: Font: 10 pt
- Formatted: Font: 10 pt
- Formatted: Font: 10 pt, Not Italic

Dysbiosis in COPD is often associated with colonisation of the lower respiratory microbiome with potentially pathogenic microbes (PPMs) including *Haemophilus* species, *Streptococcus pneumoniae*, *Staphylococcus aureus* and *Pseudomonas aeruginosa*, all of which are considered opportunistic pathogens that lead to the development of severe respiratory illness in individuals with compromised lung function [430]. However, the exact influence and mechanisms of lower respiratory microbiome dysbiosis on COPD pathophysiology is poorly understood, and is an area of much needed research. It is suspected that increased bacterial burden of PPMs results in immune dysregulation and exhaustion, overall leading to poor clearance of infections and promotion of a chronic inflammatory microenvironment [431, 432]. Whether or not these alterations in the lower respiratory microbiome lead directly to changes in immune and inflammatory functions or inflammation precedes dysbiosis is uncertain. However, there is enough evidence to suggest that homeostasis of the lower respiratory system is reliant on the careful balance of bacteria and microbes found within the airway and tissue-resident immune cells [433]. As such, not only could this model system be used as an infection model for common pathogens associated with COPD, but also for microbiome analysis to determine how the pulmonary microbiome is altered following CSE exposure and how this may contribute towards both COPD pathogenesis and AECOPD. This again, could lead to the identification of novel therapeutic targets for both COPD and AECOPD, or identify biomarkers for early detection or increased risk of COPD and AECOPD.

#### 6.10. CONCLUDING REMARKS

To summarise, we have developed the framework for a robust, 3Rs friendly *in vivo* system of COPD that allows-will allow for the analysis and examination of possible immunopathogenic mechanisms in disease progression and persistence. Whilst our model system did not demonstrate any systemic dose-related differences between disease and control groups, we have shown that increased concentrations of CSE

elicit increased mast cell activity, pulmonary neutrophilia and airway remodelling in the lower respiratory system of male and female C57BL/6J mice. Furthermore, RT-qPCR analysis demonstrated a possible implication of sexual dimorphism in response to CSE, with male mice shown to upregulate inflammatory genes and female mice displaying downregulation by comparison. Evidence of sexual dimorphism was present in both pulmonary neutrophilia and degree of fibrosis and airway remodelling, with heavy-smoker females showing significantly increased numbers of neutrophils within the airways in comparison to both control groups and male heavy-smoker mice, and showing evidence of slightly more pronounced fibrosis and alveolar remodelling in comparison to male mice. These findings ~~confirm~~ suggest the presence of an emphysematous COPD phenotype in mice, and thus demonstrate that with further refinement and investigation, our model ~~is~~ could be an effective system to generate a moderate COPD phenotype within the ethical and legal scope of current UK laws and guidelines for animals in scientific research. Whilst the model system has a few limitations, including group size, sample volumes taken for analysis, broad nature of the panels used for analysis and age of mice used, these can all be easily rectified and addressed in future research and model refinement. Overall, we have developed the framework for an *in vivo* system for researchers in the field of respiratory immunology to use for the analysis and characterisation of immunopathogenic mechanisms of COPD. This will hopefully lead to a better understanding of COPD pathogenesis and persistence, and aid in the identification and development of novel therapeutic targets to reduce the global burden of COPD.

## REFERENCES

1. Corlateanu A, Mendez Y, Wang Y, Garnica RdJA, Botnaru V, Sifakas N. "Chronic obstructive pulmonary disease and phenotypes: a state-of-the-art." *Pulmonology*. 2020;26(2):95-100. doi: <https://doi.org/10.1016/j.pulmoe.2019.10.006>.
2. WHO. World health statistics 2019: monitoring health for the SDGs, sustainable development goals. Geneva: World Health Organization; 2019 2019.
3. Quaderi SA, Hurst JR. The unmet global burden of COPD. *Global Health, Epidemiology and Genomics*. 2018;3. doi: 10.1017/gheg.2018.1.
4. Adelaye D, Chua S, Lee C, Basquill C, Papan A, Theodoratou E, et al. Global and regional estimates of COPD prevalence: Systematic review and meta-analysis. *J Glob Health*. 2015;5(2):020415. Epub 2016/01/13. doi: 10.7189/jogh.05.020415. PubMed PMID: 26755942; PubMed Central PMCID: PMC4693508.
5. Soriano JB, Rodríguez-Roisin R. Chronic Obstructive Pulmonary Disease Overview. *Proceedings of the American Thoracic Society*. 2011;8(4):363-7. doi: 10.1513/pats.201102-017RM. PubMed PMID: 21816993.
6. López-Campos JL, Tan W, Soriano JB. Global burden of COPD. *Respirology*. 2016;21(1):14-23. doi: 10.1111/resp.12660.
7. Mirza S, Clay RD, Koslow MA, Scanlon PD. COPD Guidelines: A Review of the 2018 GOLD Report. *Mayo Clinic Proceedings*. 2018;93(10):1488-502. doi: 10.1016/j.mayocp.2018.05.026.
8. Tilert T, Dillon C, Paulose-Ram R, Hnizdo E, Doney B. Estimating the U.S. prevalence of chronic obstructive pulmonary disease using pre- and post-bronchodilator spirometry: the National Health and Nutrition Examination Survey (NHANES) 2007–2010. *Respiratory Research*. 2013;14(1):103. doi: 10.1186/1465-9921-14-103.
9. Shirtcliffe P, Weatherall M, Marsh S, Travers J, Hansell A, McNaughton A, et al. COPD prevalence in a random population survey: a matter of definition. *European Respiratory Journal*. 2007;30(2):232-9. doi: 10.1183/09031936.00157906.
10. Buist AS, Vollmer WM, Sullivan SD, Weiss KB, Lee TA, Menezes AMB, et al. The Burden of Obstructive Lung Disease Initiative (BOLD): Rationale and Design. *COPD: Journal of Chronic Obstructive Pulmonary Disease*. 2005;2(2):277-83. doi: 10.1081/COPD-57610.
11. Vestbo J, Hurd SS, Agustí AG, Jones PW, Vogelmeier C, Anzueto A, et al. Global Strategy for the Diagnosis, Management, and Prevention of Chronic Obstructive Pulmonary Disease. *American Journal of Respiratory and Critical Care Medicine*. 2013;187(4):347-65. doi: 10.1164/rccm.201204-0596PP. PubMed PMID: 22878278.
12. Mapel DW, Dalal AA, Johnson P, Becker L, Hunter AG. A Clinical Study of COPD Severity Assessment by Primary Care Physicians and

## REFERENCES

- Their Patients Compared with Spirometry. *The American Journal of Medicine*. 2015;128(6):629-37. doi: <https://doi.org/10.1016/j.amjmed.2014.12.018>.
13. López-Campos JL, Soriano JB, Calle M. A Comprehensive, National Survey of Spirometry in Spain: Current Bottlenecks and Future Directions in Primary and Secondary Care. *Chest*. 2013;144(2):601-9. doi: <https://doi.org/10.1378/chest.12-2690>.
  14. Buist AS, McBurnie MA, Vollmer WM, Gillespie S, Burney P, Mannino DM, et al. International variation in the prevalence of COPD (The BOLD Study): a population-based prevalence study. *The Lancet*. 2007;370(9589):741-50. doi: 10.1016/S0140-6736(07)61377-4.
  15. Guindon GE, Boisclair D. Past, current and future trends in tobacco use. HNP discussion paper. 2003.
  16. Eisner MD, Anthonisen N, Coultas D, Kuenzli N, Perez-Padilla R, Postma D, et al. An Official American Thoracic Society Public Policy Statement: Novel Risk Factors and the Global Burden of Chronic Obstructive Pulmonary Disease. *American Journal of Respiratory and Critical Care Medicine*. 2010;182(5):693-718. doi: 10.1164/rccm.200811-1757ST. PubMed PMID: 20802169.
  17. Miravittles M, Soriano JB, García-Río F, Muñoz L, Duran-Tauleria E, Sanchez G, et al. Prevalence of COPD in Spain: impact of undiagnosed COPD on quality of life and daily life activities. *Thorax*. 2009;64(10):863-8. doi: 10.1136/thx.2009.115725.
  18. van Gemert F, Kirenga B, Chavannes N, Kanya M, Luzige S, Musinguzi P, et al. Prevalence of chronic obstructive pulmonary disease and associated risk factors in Uganda (FRESH AIR Uganda): a prospective cross-sectional observational study. *The Lancet Global Health*. 2015;3(1):e44-e51. doi: [https://doi.org/10.1016/S2214-109X\(14\)70337-7](https://doi.org/10.1016/S2214-109X(14)70337-7).
  19. Golpe R, Pérez de Llano L. Are the Diagnostic Criteria for Asthma-COPD Overlap Syndrome Appropriate in Biomass Smoke-Induced chronic obstructive pulmonary disease? *Arch Bronconeumol*. 2016;52(2):110. Epub 2015/03/24. doi: 10.1016/j.arbres.2014.12.016. PubMed PMID: 25799499.
  20. Postma DS, Bush A, van den Berge M. Risk factors and early origins of chronic obstructive pulmonary disease. *The Lancet*. 2015;385(9971):899-909. doi: [https://doi.org/10.1016/S0140-6736\(14\)60446-3](https://doi.org/10.1016/S0140-6736(14)60446-3).
  21. Baur X, Bakehe P, Vellguth H. Bronchial asthma and COPD due to irritants in the workplace-an evidence-based approach. *Journal of occupational medicine and toxicology*. 2012;7:1-31.
  22. Foster TS, Miller JD, Marton JP, Caloyeras JP, Russell MW, Menzin J. Assessment of the Economic Burden of COPD in the U.S.: A Review and Synthesis of the Literature. *COPD: Journal of Chronic Obstructive Pulmonary Disease*. 2006;3(4):211-8. doi: 10.1080/15412550601009396.

## REFERENCES

23. Nielsen R, Johannessen A, Benediktsdottir B, Gislason T, Buist AS, Gulsvik A, et al. Present and future costs of COPD in Iceland and Norway: results from the BOLD study. *European Respiratory Journal*. 2009;34(4):850-7. doi: 10.1183/09031936.00166108.
24. Wouters EFM. Economic analysis of the confronting COPD survey: an overview of results. *Respiratory Medicine*. 2003;97:S3-S14. doi: [https://doi.org/10.1016/S0954-6111\(03\)80020-3](https://doi.org/10.1016/S0954-6111(03)80020-3).
25. Mannino DM, Buist AS. Global burden of COPD: risk factors, prevalence, and future trends. *The Lancet*. 2007;370(9589):765-73. doi: 10.1016/s0140-6736(07)61380-4.
26. Chan-Yeung M, Ait-Khaled N, White N, Ip MS, Tan WC. The burden and impact of COPD in Asia and Africa [State of the Art]. *The International Journal of Tuberculosis and Lung Disease*. 2004;8(1):2-14.
27. Raheison C, Girodet PO. Epidemiology of COPD. *European Respiratory Review*. 2009;18(114):213-21. doi: 10.1183/09059180.00003609.
28. Blanco I, Diego I, Bueno P, Casas-Maldonado F, Miravittles M. Geographic distribution of COPD prevalence in the world displayed by Geographic Information System maps. *European Respiratory Journal*. 2019;54(1):1900610. doi: 10.1183/13993003.00610-2019.
29. Safiri S, Carson-Chahhoud K, Noori M, Nejadghaderi SA, Sullman MJM, Ahmadian Heris J, et al. Burden of chronic obstructive pulmonary disease and its attributable risk factors in 204 countries and territories, 1990-2019: results from the Global Burden of Disease Study 2019. *BMJ*. 2022:e069679. doi: 10.1136/bmj-2021-069679.
30. Gordon SB, Bruce NG, Grigg J, Hibberd PL, Kurmi OP, Lam K-bH, et al. Respiratory risks from household air pollution in low and middle income countries. *The Lancet Respiratory Medicine*. 2014;2(10):823-60. doi: 10.1016/S2213-2600(14)70168-7.
31. Britton J. Death, disease, and tobacco. *The Lancet*. 2017;389(10082):1861-2. doi: 10.1016/S0140-6736(17)30867-X.
32. Burney P, Jarvis D, Perez-Padilla R. The global burden of chronic respiratory disease in adults. *The International Journal of Tuberculosis and Lung Disease*. 2015;19(1):10-20. doi: 10.5588/ijtld.14.0446.
33. Global, regional, and national age–sex specific all-cause and cause-specific mortality for 240 causes of death, 1990–2013: a systematic analysis for the Global Burden of Disease Study 2013. *The Lancet*. 2015;385(9963):117-71. doi: [https://doi.org/10.1016/S0140-6736\(14\)61682-2](https://doi.org/10.1016/S0140-6736(14)61682-2).
34. Sin DD, Anthonisen NR, Soriano JB, Agusti AG. Mortality in COPD: role of comorbidities. *European Respiratory Journal*. 2006;28(6):1245-57. doi: 10.1183/09031936.00133805.
35. McGarvey LP, Magder S, Burkhart D, Kesten S, Liu D, Manuel RC, et al. Cause-specific mortality adjudication in the UPLIFT® COPD

## REFERENCES

- trial: Findings and recommendations. *Respiratory Medicine*. 2012;106(4):515-21. doi: <https://doi.org/10.1016/j.rmed.2011.10.009>.
36. The Effects of a Smoking Cessation Intervention on 14.5-Year Mortality. *Annals of Internal Medicine*. 2005;142(4):233-9. doi: 10.7326/0003-4819-142-4-200502150-00005 %m 15710956.
37. Berry CE, Wise RA. Mortality in COPD: Causes, Risk Factors, and Prevention. *COPD: Journal of Chronic Obstructive Pulmonary Disease*. 2010;7(5):375-82. doi: 10.3109/15412555.2010.510160.
38. Murray CJL, Vos T, Lozano R, Naghavi M, Flaxman AD, Michaud C, et al. Disability-adjusted life years (DALYs) for 291 diseases and injuries in 21 regions, 1990&#x2013;2010: a systematic analysis for the Global Burden of Disease Study 2010. *The Lancet*. 2012;380(9859):2197-223. doi: 10.1016/S0140-6736(12)61689-4.
39. Vos T, Flaxman AD, Naghavi M, Lozano R, Michaud C, Ezzati M, et al. Years lived with disability (YLDs) for 1160 sequelae of 289 diseases and injuries 1990&#x2013;2010: a systematic analysis for the Global Burden of Disease Study 2010. *The Lancet*. 2012;380(9859):2163-96. doi: 10.1016/S0140-6736(12)61729-2.
40. FUKUCHI Y, NISHIMURA M, ICHINOSE M, ADACHI M, NAGAI A, KURIYAMA T, et al. COPD in Japan: the Nippon COPD Epidemiology study. *Respirology*. 2004;9(4):458-65. doi: <https://doi.org/10.1111/j.1440-1843.2004.00637.x>.
41. Mannino DM, Doherty DE, Sonia Buist A. Global Initiative on Obstructive Lung Disease (GOLD) classification of lung disease and mortality: findings from the Atherosclerosis Risk in Communities (ARIC) study. *Respiratory Medicine*. 2006;100(1):115-22. doi: <https://doi.org/10.1016/j.rmed.2005.03.035>.
42. McGarvey LP, John M, Anderson JA, Zvarich M, Wise RA. Ascertainment of cause-specific mortality in COPD: operations of the TORCH Clinical Endpoint Committee. *Thorax*. 2007;62(5):411-5. doi: 10.1136/thx.2006.072348.
43. Mannino DM, Aguayo SM, Petty TL, Redd SC. Low Lung Function and Incident Lung Cancer in the United States: Data From the First National Health and Nutrition Examination Survey Follow-up. *Archives of Internal Medicine*. 2003;163(12):1475-80. doi: 10.1001/archinte.163.12.1475.
44. Balcells E, Antó JM, Gea J, Gómez FP, Rodríguez E, Marin A, et al. Characteristics of patients admitted for the first time for COPD exacerbation. *Respiratory Medicine*. 2009;103(9):1293-302. doi: <https://doi.org/10.1016/j.rmed.2009.04.001>.
45. Begh  B, Verduri A, Roca M, Fabbri LM. Exacerbation of respiratory symptoms in COPD patients may not be exacerbations of COPD. *European Respiratory Journal*. 2013;41(4):993-5. doi: 10.1183/09031936.00180812.



## REFERENCES

46. Fabbri LM, Beghé B, Agusti A. Cardiovascular mechanisms of death in severe COPD exacerbation: time to think and act beyond guidelines. *Thorax*. 2011;66(9):745-7. doi: 10.1136/thoraxjnl-2011-200406.
47. Vanfleteren LEGW, Spruit MA, Groenen M, Gaffron S, Empel VPMv, Bruijnzeel PLB, et al. Clusters of Comorbidities Based on Validated Objective Measurements and Systemic Inflammation in Patients with Chronic Obstructive Pulmonary Disease. *American Journal of Respiratory and Critical Care Medicine*. 2013;187(7):728-35. doi: 10.1164/rccm.201209-1665OC. PubMed PMID: 23392440.
48. Putcha N, Puhan MA, Hansel NN, Drummond MB, Boyd CM. Impact of co-morbidities on self-rated health in self-reported COPD: An analysis of NHANES 2001–2008. *COPD: Journal of Chronic Obstructive Pulmonary Disease*. 2013;10(3):324-32. doi: 10.3109/15412555.2012.744963.
49. Roberts CM, Stone RA, Lowe D, Pursey NA, Buckingham RJ. Co-morbidities and 90-day Outcomes in Hospitalized COPD Exacerbations. *COPD: Journal of Chronic Obstructive Pulmonary Disease*. 2011;8(5):354-61. doi: 10.3109/15412555.2011.600362.
50. Soler-Cataluña JJ, Martínez-García MÁ, Sánchez PR, Salcedo E, Navarro M, Ochando R. Severe acute exacerbations and mortality in patients with chronic obstructive pulmonary disease. *Thorax*. 2005;60(11):925-31. doi: 10.1136/thx.2005.040527.
51. Yohannes AM, Willgoss TG, Baldwin RC, Connolly MJ. Depression and anxiety in chronic heart failure and chronic obstructive pulmonary disease: prevalence, relevance, clinical implications and management principles. *International Journal of Geriatric Psychiatry*. 2010;25(12):1209-21. doi: <https://doi.org/10.1002/gps.2463>.
52. Schane RE, Woodruff PG, Dinno A, Covinsky KE, Walter LC. Prevalence and Risk Factors for Depressive Symptoms in Persons with Chronic Obstructive Pulmonary Disease. *Journal of General Internal Medicine*. 2008;23(11):1757-62. doi: 10.1007/s11606-008-0749-z.
53. Kühl K, Schürmann W, Rief W. Mental disorders and quality of life in COPD patients and their spouses. *International Journal of Chronic Obstructive Pulmonary Disease*. 2008;3(4):727-36. doi: 10.2147/copd.s3375.
54. Willgoss TG, Yohannes AM. Anxiety Disorders in Patients With COPD: A Systematic Review. *Respiratory Care*. 2013;58(5):858-66. doi: 10.4187/respcare.01862.
55. Ng T-P, Niti M, Tan W-C, Cao Z, Ong K-C, Eng P. Depressive Symptoms and Chronic Obstructive Pulmonary Disease: Effect on Mortality, Hospital Readmission, Symptom Burden, Functional Status, and Quality of Life. *Archives of Internal Medicine*. 2007;167(1):60-7. doi: 10.1001/archinte.167.1.60.
56. Cafarella PA, EFFING TW, USMANI Z-A, FRITH PA. Treatments for anxiety and depression in patients with chronic obstructive pulmonary

## REFERENCES

- disease: A literature review. *Respirology*. 2012;17(4):627-38. doi: <https://doi.org/10.1111/j.1440-1843.2012.02148.x>.
57. Attaway AA, Zein J, Hatipoğlu US. SARS-CoV-2 infection in the COPD population is associated with increased healthcare utilization: An analysis of Cleveland clinic's COVID-19 registry. *EClinicalMedicine*. 2020;26:100515. doi: <https://doi.org/10.1016/j.eclinm.2020.100515>.
58. Gerayeli FV, Milne S, Cheung C, Li X, Yang CWT, Tam A, et al. COPD and the risk of poor outcomes in COVID-19: A systematic review and meta-analysis. *EClinicalMedicine*. 2021;33:100789. doi: <https://doi.org/10.1016/j.eclinm.2021.100789>.
59. Puebla Neira DA, Watts A, Seashore J, Duarte A, Nishi SP, Polychronopoulou E, et al. Outcomes of Patients with COPD Hospitalized for Coronavirus Disease 2019. *Chronic Obstr Pulm Dis*. 2021;8(4):517-27. Epub 2021/10/07. doi: 10.15326/jcopdf.2021.0245. PubMed PMID: 34614553; PubMed Central PMCID: PMCPMC8686850.
60. Marron RM, Zheng M, Fernandez Romero G, Zhao H, Patel R, Leopold I, et al. Impact of Chronic Obstructive Pulmonary Disease and Emphysema on Outcomes of Hospitalized Patients with Coronavirus Disease 2019 Pneumonia. *Chronic Obstr Pulm Dis*. 2021;8(2):255-68. Epub 2021/03/30. doi: 10.15326/jcopdf.2020.0200. PubMed PMID: 33780602; PubMed Central PMCID: PMCPMC8237980.
61. Leung JM, Niiikura M, Yang CWT, Sin DD. COVID-19 and COPD. *European Respiratory Journal*. 2020;56(2):2002108. doi: 10.1183/13993003.02108-2020.
62. Halpin DMG, Criner GJ, Papi A, Singh D, Anzueto A, Martinez FJ, et al. Global Initiative for the Diagnosis, Management, and Prevention of Chronic Obstructive Lung Disease. The 2020 GOLD Science Committee Report on COVID-19 and Chronic Obstructive Pulmonary Disease. *American Journal of Respiratory and Critical Care Medicine*. 2021;203(1):24-36. doi: 10.1164/rccm.202009-3533SO. PubMed PMID: 33146552.
63. Leung JM, Yang CX, Tam A, Shaipanich T, Hackett T-L, Singhera GK, et al. ACE-2 expression in the small airway epithelia of smokers and COPD patients: implications for COVID-19. *European Respiratory Journal*. 2020;55(5):2000688. doi: 10.1183/13993003.00688-2020.
64. Viniol C, Vogelmeier CF. Exacerbations of COPD. *European Respiratory Review*. 2018;27(147):170103. doi: 10.1183/16000617.0103-2017.
65. Beran D, Zar HJ, Perrin C, Menezes AM, Burney P. Burden of asthma and chronic obstructive pulmonary disease and access to essential medicines in low-income and middle-income countries. *The Lancet Respiratory Medicine*. 2015;3(2):159-70. doi: [https://doi.org/10.1016/S2213-2600\(15\)00004-1](https://doi.org/10.1016/S2213-2600(15)00004-1).
66. Lomborg B. *Global problems, local solutions: costs and benefits*. Cambridge University Press. 2013;143:144.

---

## REFERENCES

67. Bloom DE, Cafiero E, Jané-Llopis E, Abrahams-Gessel S, Bloom LR, Fathima S, et al. The global economic burden of noncommunicable diseases. Program on the Global Demography of Aging, 2012.
68. Kim J, Rhee CK, Yoo KH, Kim YS, Lee SW, Park YB, et al. The health care burden of high grade chronic obstructive pulmonary disease in Korea: analysis of the Korean Health Insurance Review and Assessment Service data. *International Journal of Chronic Obstructive Pulmonary Disease*. 2013;8:561-8. doi: 10.2147/COPD.S48577.
69. Anzueto A, Sethi S, Martinez FJ. Exacerbations of Chronic Obstructive Pulmonary Disease. *Proceedings of the American Thoracic Society*. 2007;4(7):554-64. doi: 10.1513/pats.200701-003FM. PubMed PMID: 17878469.
70. de Queiroz MCdCAM, Moreira MAC, Jardim JR, Barbosa MA, Minamisava R, Gondim HDC, et al. Knowledge about COPD among users of primary health care services. *International Journal of Chronic Obstructive Pulmonary Disease*. 2015;10:1-6. doi: 10.2147/COPD.S71152.
71. Lou P, Zhu Y, Chen P, Zhang P, Yu J, Zhang N, et al. Vulnerability, beliefs, treatments and economic burden of chronic obstructive pulmonary disease in rural areas in China: a cross-sectional study. *BMC Public Health*. 2012;12(1):287. doi: 10.1186/1471-2458-12-287.
72. Menezes AM, Landis SH, Han MK, Muellerova H, Aisanov Z, van der Molen T, et al. Continuing to Confront COPD International Surveys: comparison of patient and physician perceptions about COPD risk and management. *International Journal of Chronic Obstructive Pulmonary Disease*. 2015;10:159-72. doi: 10.2147/COPD.S74315.
73. Mun SY, Hwang YI, Kim JH, Park S, Jang SH, Seo JY, et al. Awareness of chronic obstructive pulmonary disease in current smokers: a nationwide survey. *Korean J Intern Med*. 2015;30(2):191-7. Epub 2015/03/10. doi: 10.3904/kjim.2015.30.2.191. PubMed PMID: 25750560; PubMed Central PMCID: PMC4351325.
74. Soriano JB, Calle M, Montemayor T, Álvarez-Sala JL, Ruiz-Manzano J, Miravittles M. The General Public's Knowledge of Chronic Obstructive Pulmonary Disease and Its Determinants: Current Situation and Recent Changes. *Archivos de Bronconeumología (English Edition)*. 2012;48(9):308-15. doi: <https://doi.org/10.1016/j.arbr.2012.07.001>.
75. Bloom DE, Canning D, Fink G. Program on the global demography of aging. Harvard University Oct. 2009.
76. Lozano R, Naghavi M, Foreman K, Lim S, Shibuya K, Aboyans V, et al. Global and regional mortality from 235 causes of death for 20 age groups in 1990 and 2010: a systematic analysis for the Global Burden of Disease Study 2010. *The Lancet*. 2012;380(9859):2095-128. doi: 10.1016/S0140-6736(12)61728-0.
77. Prince MJ, Wu F, Guo Y, Gutierrez Robledo LM, O'Donnell M, Sullivan R, et al. The burden of disease in older people and implications

## REFERENCES

- for health policy and practice. *The Lancet*. 2015;385(9967):549-62. doi: 10.1016/S0140-6736(14)61347-7.
78. Rehfuess E, Organization WH. Fuel for life: household energy and health: World Health Organization; 2006.
79. Adeloje D, Agarwal D, Barnes PJ, Bonay M, Van Boven JF, Bryant J, et al. Research priorities to address the global burden of chronic obstructive pulmonary disease (COPD) in the next decade. *Journal of Global Health*. 2021;11. doi: 10.7189/jogh.11.15003.
80. Yang IA, Jenkins CR, Salvi SS. Chronic obstructive pulmonary disease in never-smokers: risk factors, pathogenesis, and implications for prevention and treatment. *The Lancet Respiratory Medicine*. 2022;10(5):497-511. doi: [https://doi.org/10.1016/S2213-2600\(21\)00506-3](https://doi.org/10.1016/S2213-2600(21)00506-3).
81. Ran P, Wang C, Yao W, Chen P, Kang J, Huang S, et al. The risk factors for chronic obstructive pulmonary disease in females in Chinese rural areas. *Zhonghua nei ke za zhi*. 2006;45(12):974-9.
82. Kulkarni N, Pierse N, Rushton L, Grigg J. Carbon in Airway Macrophages and Lung Function in Children. *New England Journal of Medicine*. 2006;355(1):21-30. doi: 10.1056/NEJMoa052972. PubMed PMID: 16822993.
83. Latzin P, Rösli M, Huss A, Kuehni CE, Frey U. Air pollution during pregnancy and lung function in newborns: a birth cohort study. *European Respiratory Journal*. 2009;33(3):594-603. doi: 10.1183/09031936.00084008.
84. Rojas-Martinez R, Perez-Padilla R, Olaiz-Fernandez G, Mendoza-Alvarado L, Moreno-Macias H, Fortoul T, et al. Lung Function Growth in Children with Long-Term Exposure to Air Pollutants in Mexico City. *American Journal of Respiratory and Critical Care Medicine*. 2007;176(4):377-84. doi: 10.1164/rccm.200510-1678OC. PubMed PMID: 17446338.
85. Thackrah CT. The effects of arts, trades, and professions: and of civic states and habits of living, on health and longevity: with suggestions for the removal of many of the agents which produce disease, and shorten and duration of life: Longman, Rees, Orme, Brown, Green, & Longman; 1832.
86. Greenhow EH. On chronic bronchitis: Lindsay and Blakiston; 1869.
87. Honeybourne D, Pickering CA. Physiological evidence that emphysema is not a feature of byssinosis. *Thorax*. 1986;41(1):6-11. doi: 10.1136/thx.41.1.6.
88. Murgia N, Gambelunghe A. Occupational COPD—The most under-recognized occupational lung disease? *Respirology*. 2022;27(6):399-410. doi: <https://doi.org/10.1111/resp.14272>.
89. Kleniewska A, Walusiak-Skorupa J, Lipińska-Ojrzanowska A, Szcześniak K, Wiszniewska M. Spirometric and hygienic criteria in

## REFERENCES

- recognition of occupational COPD in Poland—A retrospective analysis of medical records. *International journal of occupational medicine and environmental health*. 2017;31(2):139-50.
90. Coggon D, Taylor AN. Coal mining and chronic obstructive pulmonary disease: a review of the evidence. *Thorax*. 1998;53(5):398-407. doi: 10.1136/thx.53.5.398.
91. Oxman AD, Muir DCF, Shannon HS, Stock SR, Hnizdo E, Lange HJ. Occupational Dust Exposure and Chronic Obstructive Pulmonary Disease: A Systematic Overview of the Evidence. *American Review of Respiratory Disease*. 1993;148(1):38-48. doi: 10.1164/ajrccm/148.1.38. PubMed PMID: 8317812.
92. Hessel PA, Melenka LS, Michaelchuk D, Herbert FA, Cowie RL. Lung health among plumbers and pipefitters in Edmonton, Alberta. *Occupational and Environmental Medicine*. 1998;55(10):678-83. doi: 10.1136/oem.55.10.678.
93. Dumas O, Varraso R, Boggs KM, Quinot C, Zock J-P, Henneberger PK, et al. Association of Occupational Exposure to Disinfectants With Incidence of Chronic Obstructive Pulmonary Disease Among US Female Nurses. *JAMA Network Open*. 2019;2(10):e1913563-e. doi: 10.1001/jamanetworkopen.2019.13563.
94. Peacock JL, Anderson HR, Bremner SA, Marston L, Seemungal TA, Strachan DP, et al. Outdoor air pollution and respiratory health in patients with COPD. *Thorax*. 2011;66(7):591-6. doi: 10.1136/thx.2010.155358.
95. Schikowski T, Mills IC, Anderson HR, Cohen A, Hansell A, Kauffmann F, et al. Ambient air pollution: a cause of COPD? *European Respiratory Journal*. 2014;43(1):250-63.
96. Donaldson GC, Seemungal TAR, Bhowmik A, Wedzicha JA. Relationship between exacerbation frequency and lung function decline in chronic obstructive pulmonary disease. *Thorax*. 2002;57(10):847-52. doi: 10.1136/thorax.57.10.847.
97. Adeloye D, Song P, Zhu Y, Campbell H, Sheikh A, Rudan I. Global, regional, and national prevalence of, and risk factors for, chronic obstructive pulmonary disease (COPD) in 2019: a systematic review and modelling analysis. *The Lancet Respiratory Medicine*. 2022;10(5):447-58. doi: 10.1016/S2213-2600(21)00511-7.
98. Lopez AD. Global burden of disease and risk factors. 2006.
99. Mannino DM, Watt G, Hole D, Gillis C, Hart C, McConnachie A, et al. The natural history of chronic obstructive pulmonary disease. *European Respiratory Journal*. 2006;27(3):627-43. doi: 10.1183/09031936.06.00024605.
100. Rennard SI, Vestbo J. COPD: the dangerous underestimate of 15%. *The Lancet*. 2006;367(9518):1216-9.
101. Lundbäck B, Lindberg A, Lindström M, RÖNmark E, Jonsson AC, JÖNsson E, et al. Not 15 But 50% of smokers develop COPD?—Report

## REFERENCES

- from the Obstructive Lung Disease in Northern Sweden Studies. *Respiratory Medicine*. 2003;97(2):115-22. doi: <https://doi.org/10.1053/rmed.2003.1446>.
102. Gilliland FD, Li Y-F, Dubeau L, Berhane K, Avol E, McConnell R, et al. Effects of Glutathione S-Transferase M1, Maternal Smoking during Pregnancy, and Environmental Tobacco Smoke on Asthma and Wheezing in Children. *American Journal of Respiratory and Critical Care Medicine*. 2002;166(4):457-63. doi: 10.1164/rccm.2112064. PubMed PMID: 12186820.
103. Hage R, Fretz V, Schuurmans MM. Electronic cigarettes and vaping associated pulmonary illness (VAPI): A narrative review. *Pulmonology*. 2020;26(5):291-303. doi: <https://doi.org/10.1016/j.pulmoe.2020.02.009>.
104. Lee R, Vokos C, Kaur M, Austin M. E-cigarette or Vaping Use Associated Lung Injury (EVALI) - New COPD of The Young? *Pediatrics*. 2021;147(3\_MeetingAbstract):625-6. doi: 10.1542/peds.147.3MA7.625.
105. Traboulsi H, Cherian M, Abou Rjeili M, Preteroti M, Bourbeau J, Smith BM, et al. Inhalation Toxicology of Vaping Products and Implications for Pulmonary Health. *International Journal of Molecular Sciences*. 2020;21(10):3495. PubMed PMID: doi:10.3390/ijms21103495.
106. Xie Z, Ossip DJ, Rahman I, Li D. Use of Electronic Cigarettes and Self-Reported Chronic Obstructive Pulmonary Disease Diagnosis in Adults. *Nicotine & Tobacco Research*. 2019;22(7):1155-61. doi: 10.1093/ntr/ntz234.
107. Morjaria JB, Mondati E, Polosa R. E-cigarettes in patients with COPD: current perspectives. *International Journal of Chronic Obstructive Pulmonary Disease*. 2017;12(null):3203-10. doi: 10.2147/COPD.S135323.
108. Berndt A, Leme AS, Shapiro SD. Emerging genetics of COPD. *EMBO Molecular Medicine*. 2012;4(11):1144-55. doi: <https://doi.org/10.1002/emmm.201100627>.
109. Stoller JK, Aboussouan LS. A Review of  $\alpha$ 1-Antitrypsin Deficiency. *American Journal of Respiratory and Critical Care Medicine*. 2012;185(3):246-59. doi: 10.1164/rccm.201108-1428CI. PubMed PMID: 21960536.
110. Lange P, Ahmed E, Lahmar ZM, Martinez FJ, Bourdin A. Natural history and mechanisms of COPD. *Respirology*. 2021;26(4):298-321. doi: <https://doi.org/10.1111/resp.14007>.
111. Brode SK, Ling SC, Chapman KR. Alpha-1 antitrypsin deficiency: a commonly overlooked cause of lung disease. *Cmaj*. 2012;184(12):1365-71. Epub 2012/07/05. doi: 10.1503/cmaj.111749. PubMed PMID: 22761482; PubMed Central PMCID: PMC3447047.
112. Marciniuk DD, Hernandez P, Balter M, Bourbeau J, Chapman KR, Ford GT, et al. Alpha-1 Antitrypsin Deficiency Targeted Testing and Augmentation Therapy: A Canadian Thoracic Society Clinical Practice

## REFERENCES

- Guideline. *Canadian Respiratory Journal*. 2012;19:920918. doi: 10.1155/2012/920918.
113. Silverman EK. Genetics of COPD. *Annual Review of Physiology*. 2020;82(1):413-31. doi: 10.1146/annurev-physiol-021317-121224. PubMed PMID: 31730394.
114. Sakornsakolpat P, Prokopenko D, Lamontagne M, Reeve NF, Guyatt AL, Jackson VE, et al. Genetic landscape of chronic obstructive pulmonary disease identifies heterogeneous cell-type and phenotype associations. *Nature Genetics*. 2019;51(3):494-505. doi: 10.1038/s41588-018-0342-2.
115. Zhou D-C, Zhou C-F, Toloo S, Shen T, Tong S-L, Zhu Q-X. Association of a disintegrin and metalloprotease 33 (ADAM33) gene polymorphisms with the risk of COPD: an updated meta-analysis of 2,644 cases and 4,804 controls. *Molecular Biology Reports*. 2015;42(2):409-22. doi: 10.1007/s11033-014-3782-5.
116. Abd El-Zaher AH, Nagy H, Farouk G, Mohamed AS, Ghoname NF. Effect of a disintegrin and metalloprotease 33 (ADAM33) gene polymorphisms and smoking in COPD. *Egyptian Journal of Chest Diseases and Tuberculosis*. 2012;61(4):275-80. doi: <https://doi.org/10.1016/j.ejcdt.2012.08.005>.
117. Feng H-h, Mao L, Pan K, Zhang L, Rui D-s. Association between F+1 polymorphism in a disintegrin and metalloprotease 33 (ADAM33) gene and chronic obstructive pulmonary disease susceptibility: An evidence-based meta-analysis. *Gene*. 2019;719:144009. doi: <https://doi.org/10.1016/j.gene.2019.144009>.
118. Masjedy A, Salesi M, Ahmadi A, Salimian J, Azimzadeh Jamalkandi S. Association between single-nucleotide polymorphism of cytokines genes and chronic obstructive pulmonary disease: A systematic review and meta-analysis. *Cytokine*. 2023;171:156352. doi: <https://doi.org/10.1016/j.cyto.2023.156352>.
119. Korytina GF, Akhmadishina LZ, Kochetova OV, Aznabaeva YG, Izmailova SM, Zagidullin SZ, et al. Association of CRP, CD14, Pro-Inflammatory Cytokines and Their Receptors (TNFA, LTA, TNFRSF1A, TNFRSF1B, IL1B, and IL6) Genes with Chronic Obstructive Pulmonary Disease Development. *Russian Journal of Genetics*. 2020;56(8):972-81. doi: 10.1134/S1022795420080086.
120. Aryal S, Diaz-Guzman E, Mannino DM. COPD and gender differences: an update. *Translational Research*. 2013;162(4):208-18. doi: <https://doi.org/10.1016/j.trsl.2013.04.003>.
121. Gan WQ, Man SFP, Postma DS, Camp P, Sin DD. Female smokers beyond the perimenopausal period are at increased risk of chronic obstructive pulmonary disease: a systematic review and meta-analysis. *Respiratory Research*. 2006;7(1):52. doi: 10.1186/1465-9921-7-52.
122. Sørheim I-C, Johannessen A, Gulsvik A, Bakke PS, Silverman EK, DeMeo DL. Gender differences in COPD: are women more susceptible

## REFERENCES

- to smoking effects than men? *Thorax*. 2010;65(6):480-5. doi: 10.1136/thx.2009.122002.
123. Han MK, Postma D, Mannino DM, Giardino ND, Buist S, Curtis JL, et al. Gender and Chronic Obstructive Pulmonary Disease. *American Journal of Respiratory and Critical Care Medicine*. 2007;176(12):1179-84. doi: 10.1164/rccm.200704-553CC. PubMed PMID: 17673696.
124. Kanner RE, Connett JE, Altose MD, Buist AS, Lee WW, Tashkin DP, et al. Gender difference in airway hyperresponsiveness in smokers with mild COPD. The Lung Health Study. *American Journal of Respiratory and Critical Care Medicine*. 1994;150(4):956-61. doi: 10.1164/ajrccm.150.4.7921469. PubMed PMID: 7921469.
125. Brandsma C-A, Van den Berge M, Hackett T-L, Brusselle G, Timens W. Recent advances in chronic obstructive pulmonary disease pathogenesis: from disease mechanisms to precision medicine. *The Journal of Pathology*. 2020;250(5):624-35. doi: <https://doi.org/10.1002/path.5364>.
126. Foreman MG, Zhang L, Murphy J, Hansel NN, Make B, Hokanson JE, et al. Early-Onset Chronic Obstructive Pulmonary Disease Is Associated with Female Sex, Maternal Factors, and African American Race in the COPD Gene Study. *American Journal of Respiratory and Critical Care Medicine*. 2011;184(4):414-20. doi: 10.1164/rccm.201011-1928OC. PubMed PMID: 21562134.
127. Kohler M, Sandberg A, Kjellqvist S, Thomas A, Karimi R, Nyrén S, et al. Gender differences in the bronchoalveolar lavage cell proteome of patients with chronic obstructive pulmonary disease. *Journal of Allergy and Clinical Immunology*. 2013;131(3):743-51.e9. doi: <https://doi.org/10.1016/j.jaci.2012.09.024>.
128. de Torres JP, Casanova C, Pinto-Plata V, Varo N, Restituto P, Cordoba-Lanus E, et al. Gender Differences in Plasma Biomarker Levels in a Cohort of COPD Patients: A Pilot Study. *PLoS One*. 2011;6(1):e16021. doi: 10.1371/journal.pone.0016021.
129. Burgstaller G, Oehrle B, Gerckens M, White ES, Schiller HB, Eickelberg O. The instructive extracellular matrix of the lung: basic composition and alterations in chronic lung disease. *European Respiratory Journal*. 2017;50(1):1601805. doi: 10.1183/13993003.01805-2016.
130. Burgess JK, Mauad T, Tjin G, Karlsson JC, Westergren-Thorsson G. The extracellular matrix – the under-recognized element in lung disease? *The Journal of Pathology*. 2016;240(4):397-409. doi: <https://doi.org/10.1002/path.4808>.
131. Suki B, Bates JHT. Extracellular matrix mechanics in lung parenchymal diseases. *Respiratory Physiology & Neurobiology*. 2008;163(1):33-43. doi: <https://doi.org/10.1016/j.resp.2008.03.015>.
132. Faffe DS, Zin WA. Lung Parenchymal Mechanics in Health and Disease. *Physiological Reviews*. 2009;89(3):759-75. doi: 10.1152/physrev.00019.2007. PubMed PMID: 19584312.



---

## REFERENCES

133. Frantz C, Stewart KM, Weaver VM. The extracellular matrix at a glance. *Journal of Cell Science*. 2010;123(24):4195-200. doi: 10.1242/jcs.023820.
134. VLAHOVIC G, RUSSELL ML, MERCER RR, CRAPO JD. Cellular and Connective Tissue Changes in Alveolar Septal Walls in Emphysema. *American Journal of Respiratory and Critical Care Medicine*. 1999;160(6):2086-92. doi: 10.1164/ajrccm.160.6.9706031. PubMed PMID: 10588633.
135. Gooptu B, Ekeowa UI, Lomas DA. Mechanisms of emphysema in  $\alpha_1$ -antitrypsin deficiency: molecular and cellular insights. *European Respiratory Journal*. 2009;34(2):475-88. doi: 10.1183/09031936.00096508.
136. Merrilees MJ, Ching PST, Beaumont B, Hinek A, Wight TN, Black PN. Changes in elastin, elastin binding protein and versican in alveoli in chronic obstructive pulmonary disease. *Respiratory Research*. 2008;9(1):41. doi: 10.1186/1465-9921-9-41.
137. Higham A, Quinn AM, Cançado JED, Singh D. The pathology of small airways disease in COPD: historical aspects and future directions. *Respiratory Research*. 2019;20(1):49. doi: 10.1186/s12931-019-1017-y.
138. Papakonstantinou E, Karakioulakis G, Batzios S, Savic S, Roth M, Tamm M, et al. Acute exacerbations of COPD are associated with significant activation of matrix metalloproteinase 9 irrespectively of airway obstruction, emphysema and infection. *Respiratory Research*. 2015;16(1):78. doi: 10.1186/s12931-015-0240-4.
139. Papakonstantinou E, Klagas I, Roth M, Tamm M, Stolz D. Acute Exacerbations of COPD Are Associated With Increased Expression of Heparan Sulfate and Chondroitin Sulfate in BAL. *Chest*. 2016;149(3):685-95. doi: <https://doi.org/10.1378/chest.14-2868>.
140. Karakioulaki M, Papakonstantinou E, Stolz D. Extracellular matrix remodelling in COPD. *European Respiratory Review*. 2020;29(158):190124. doi: 10.1183/16000617.0124-2019.
141. Liu L, Stephens B, Bergman M, May A, Chiang T. Role of Collagen in Airway Mechanics. *Bioengineering*. 2021;8(1):13. PubMed PMID: doi:10.3390/bioengineering8010013.
142. Ito JT, Lourenço JD, Righetti RF, Tibério IFLC, Prado CM, Lopes FDTQS. Extracellular Matrix Component Remodeling in Respiratory Diseases: What Has Been Found in Clinical and Experimental Studies? *Cells*. 2019;8(4):342. PubMed PMID: doi:10.3390/cells8040342.
143. Manicone AM, Gharib SA, Gong K-Q, Eddy WE, Long ME, Frevert CW, et al. Matrix Metalloproteinase-28 Is a Key Contributor to Emphysema Pathogenesis. *The American Journal of Pathology*. 2017;187(6):1288-300. doi: <https://doi.org/10.1016/j.ajpath.2017.02.008>.
144. Suki B, Stamenović D, Hubmayr R. Lung parenchymal mechanics. *Compr Physiol*. 2011;1(3):1317-51. Epub 2011/07/01. doi:

## REFERENCES

- 10.1002/cphy.c100033. PubMed PMID: 23733644; PubMed Central PMCID: PMC3929318.
145. Weitzenblum E, Chaouat A, Kessler R. Pulmonary Hypertension in Chronic Obstructive Pulmonary Disease. *Advances in Respiratory Medicine*. 2013;81(4):390-8. PubMed PMID: doi:10.5603/ARM.34794.
146. Seimetz M, Parajuli N, Pichl A, Bednorz M, Ghofrani HA, Schermuly RT, et al. Cigarette Smoke-Induced Emphysema and Pulmonary Hypertension Can Be Prevented by Phosphodiesterase 4 and 5 Inhibition in Mice. *PLoS One*. 2015;10(6):e0129327. doi: 10.1371/journal.pone.0129327.
147. Shimoda LA, Laurie SS. Vascular remodeling in pulmonary hypertension. *Journal of Molecular Medicine*. 2013;91(3):297-309. doi: 10.1007/s00109-013-0998-0.
148. Stenmark KR, Meyrick B, Galie N, Mooi WJ, McMurtry IF. Animal models of pulmonary arterial hypertension: the hope for etiological discovery and pharmacological cure. *American Journal of Physiology-Lung Cellular and Molecular Physiology*. 2009;297(6):L1013-L32. doi: 10.1152/ajplung.00217.2009. PubMed PMID: 19748998.
149. Voelkel NF, Tuder RM. Hypoxia-induced pulmonary vascular remodeling: a model for what human disease? *The Journal of Clinical Investigation*. 2000;106(6):733-8. doi: 10.1172/JCI11144.
150. Karnati S, Seimetz M, Kleefeldt F, Sonawane A, Madhusudhan T, Bachhuka A, et al. Chronic Obstructive Pulmonary Disease and the Cardiovascular System: Vascular Repair and Regeneration as a Therapeutic Target. *Frontiers in Cardiovascular Medicine*. 2021;8. doi: 10.3389/fcvm.2021.649512.
151. Maston LD, Jones DT, Giermakowska W, Resta TC, Ramiro-Diaz J, Howard TA, et al. Interleukin-6 trans-signaling contributes to chronic hypoxia-induced pulmonary hypertension. *Pulmonary Circulation*. 2018;8(3):2045894018780734. doi: 10.1177/2045894018780734. PubMed PMID: 29767573.
152. Polosukhin VV, Gutor SS, Du R-H, Richmond BW, Massion PP, Wu P, et al. Small airway determinants of airflow limitation in chronic obstructive pulmonary disease. *Thorax*. 2021;76(11):1079-88. doi: 10.1136/thoraxjnl-2020-216037.
153. Scichilone N, La Sala A, Bellia M, Fallano K, Toghias A, Brown RH, et al. The airway response to deep inspirations decreases with COPD severity and is associated with airway distensibility assessed by computed tomography. *Journal of Applied Physiology*. 2008;105(3):832-8. doi: 10.1152/jappphysiol.01307.2007. PubMed PMID: 18617628.
154. Jones RL, Noble PB, Elliot JG, James AL. Airway remodelling in COPD: It's not asthma! *Respirology*. 2016;21(8):1347-56. doi: <https://doi.org/10.1111/resp.12841>.
155. Ito S, Ingenito EP, Brewer KK, Black LD, Parameswaran H, Lutchen KR, et al. Mechanics, nonlinearity, and failure strength of lung

## REFERENCES

- tissue in a mouse model of emphysema: possible role of collagen remodeling. *Journal of Applied Physiology*. 2005;98(2):503-11. doi: 10.1152/jappphysiol.00590.2004. PubMed PMID: 15465889.
156. Lodge KM, Vassallo A, Liu B, Long M, Tong Z, Newby PR, et al. Hypoxia Increases the Potential for Neutrophil-mediated Endothelial Damage in Chronic Obstructive Pulmonary Disease. *American Journal of Respiratory and Critical Care Medicine*. 2022;205(8):903-16. doi: 10.1164/rccm.202006-2467OC. PubMed PMID: 35044899.
157. Buchmann K. Evolution of Innate Immunity: Clues from Invertebrates via Fish to Mammals. *Frontiers in Immunology*. 2014;5. doi: 10.3389/fimmu.2014.00459.
158. Murphy K, Weaver C. *Janeway's immunobiology*: Garland science; 2016.
159. Boehm T, Swann JB. Origin and Evolution of Adaptive Immunity. *Annual Review of Animal Biosciences*. 2014;2(1):259-83. doi: 10.1146/annurev-animal-022513-114201. PubMed PMID: 25384143.
160. Kotlyarov S. Involvement of the Innate Immune System in the Pathogenesis of Chronic Obstructive Pulmonary Disease. *International Journal of Molecular Sciences*. 2022;23(2):985. PubMed PMID: doi:10.3390/ijms23020985.
161. Wittekindt OH. Tight junctions in pulmonary epithelia during lung inflammation. *Pflügers Archiv - European Journal of Physiology*. 2017;469(1):135-47. doi: 10.1007/s00424-016-1917-3.
162. Ganesan S, Comstock AT, Sajjan US. Barrier function of airway tract epithelium. *Tissue Barriers*. 2013;1(4):e24997. doi: 10.4161/tisb.24997.
163. Hadzic S, Wu C-Y, Avdeev S, Weissmann N, Schermuly RT, Kosanovic D. Lung epithelium damage in COPD – An unstoppable pathological event? *Cellular Signalling*. 2020;68:109540. doi: <https://doi.org/10.1016/j.cellsig.2020.109540>.
164. Saetta M, TURATO G, BARALDO S, ZANIN A, BRACCIONI F, MAPP CE, et al. Goblet Cell Hyperplasia and Epithelial Inflammation in Peripheral Airways of Smokers with Both Symptoms of Chronic Bronchitis and Chronic Airflow Limitation. *American Journal of Respiratory and Critical Care Medicine*. 2000;161(3):1016-21. doi: 10.1164/ajrccm.161.3.9907080. PubMed PMID: 10712357.
165. Maestrelli P, SAETTA M, MAPP CE, FABBRI LM. Remodeling in Response to Infection and Injury. *American Journal of Respiratory and Critical Care Medicine*. 2001;164(supplement\_2):S76-S80. doi: 10.1164/ajrccm.164.supplement\_2.2106067. PubMed PMID: 11734472.
166. Koo H-K, Vasilescu DM, Booth S, Hsieh A, Katsamenis OL, Fishbane N, et al. Small airways disease in mild and moderate chronic obstructive pulmonary disease: a cross-sectional study. *The Lancet Respiratory Medicine*. 2018;6(8):591-602. doi: 10.1016/S2213-2600(18)30196-6.

## REFERENCES

167. Hogg JC, Chu F, Utokaparch S, Woods R, Elliott WM, Buzatu L, et al. The Nature of Small-Airway Obstruction in Chronic Obstructive Pulmonary Disease. *New England Journal of Medicine*. 2004;350(26):2645-53. doi: 10.1056/NEJMoa032158. PubMed PMID: 15215480.
168. Faiz A, Heijink IH, Vermeulen CJ, Guryev V, van den Berge M, Nawijn MC, et al. Cigarette smoke exposure decreases CFLAR expression in the bronchial epithelium, augmenting susceptibility for lung epithelial cell death and DAMP release. *Scientific Reports*. 2018;8(1):12426. doi: 10.1038/s41598-018-30602-7.
169. Dewhurst JA, Lea S, Hardaker E, Dungwa JV, Ravi AK, Singh D. Characterisation of lung macrophage subpopulations in COPD patients and controls. *Scientific Reports*. 2017;7(1):7143. doi: 10.1038/s41598-017-07101-2.
170. Berenson CS, Kruzel RL, Eberhardt E, Sethi S. Phagocytic Dysfunction of Human Alveolar Macrophages and Severity of Chronic Obstructive Pulmonary Disease. *The Journal of Infectious Diseases*. 2013;208(12):2036-45. doi: 10.1093/infdis/jit400.
171. Liu YC, Zou XB, Chai YF, Yao YM. Macrophage polarization in inflammatory diseases. *Int J Biol Sci*. 2014;10(5):520-9. Epub 2014/06/10. doi: 10.7150/ijbs.8879. PubMed PMID: 24910531; PubMed Central PMCID: PMC4046879.
172. Wang Y, Xu J, Meng Y, Adcock IM, Yao X. Role of inflammatory cells in airway remodeling in COPD. *International Journal of Chronic Obstructive Pulmonary Disease*. 2018;13(null):3341-8. doi: 10.2147/COPD.S176122.
173. Eapen MS, Hansbro PM, McAlinden K, Kim RY, Ward C, Hackett T-L, et al. Abnormal M1/M2 macrophage phenotype profiles in the small airway wall and lumen in smokers and chronic obstructive pulmonary disease (COPD). *Scientific Reports*. 2017;7(1):13392. doi: 10.1038/s41598-017-13888-x.
174. Jundi K, Greene CM. Transcription of Interleukin-8: How Altered Regulation Can Affect Cystic Fibrosis Lung Disease. *Biomolecules*. 2015;5(3):1386-98. PubMed PMID: doi:10.3390/biom5031386.
175. Boorsma CE, Draijer C, Melgert BN. Macrophage Heterogeneity in Respiratory Diseases. *Mediators of Inflammation*. 2013;2013:769214. doi: 10.1155/2013/769214.
176. Lee J-W, Chun W, Lee HJ, Min J-H, Kim S-M, Seo J-Y, et al. The Role of Macrophages in the Development of Acute and Chronic Inflammatory Lung Diseases. *Cells*. 2021;10(4):897. PubMed PMID: doi:10.3390/cells10040897.
177. Greenlee KJ, Werb Z, Kheradmand F. Matrix Metalloproteinases in Lung: Multiple, Multifarious, and Multifaceted. *Physiological Reviews*. 2007;87(1):69-98. doi: 10.1152/physrev.00022.2006. PubMed PMID: 17237343.

## REFERENCES

178. Pelgrim CE, Wang L, Peralta Marzal LN, Korver S, van Ark I, Leusink-Muis T, et al. Increased exploration and hyperlocomotion in a cigarette smoke and LPS-induced murine model of COPD: linking pulmonary and systemic inflammation with the brain. *Am J Physiol Lung Cell Mol Physiol*. 2022;323(3):L251-L65. Epub 2022/06/15. doi: 10.1152/ajplung.00485.2021. PubMed PMID: 35699308.
179. Ellingsen J, Hedenström H, Högman M, Lisspers K, Ställberg B, Christer J, et al. The relationship between blood neutrophils, blood eosinophils and exacerbations of COPD – Results from the TIE-study. *European Respiratory Journal*. 2016;48(suppl 60):PA1013. doi: 10.1183/13993003.congress-2016.PA1013.
180. Pouwels SD, van Geffen WH, Jonker MR, Kerstjens HAM, Nawijn MC, Heijink IH. Increased neutrophil expression of pattern recognition receptors during COPD exacerbations. *Respirology*. 2017;22(2):401-4. doi: <https://doi.org/10.1111/resp.12912>.
181. Kaur M, Beardsall M, Singh D. TLR Stimulation Induces Glucocorticoid Insensitive Production Of Functional Neutrophil Chemoattractant From COPD Alveolar Macrophages. *B21 NEUTROPHIL STUDIES IN ASTHMA AND COPD2011*. p. A2560-A.
182. Sin D, Van Eeden SF. Neutrophil-mediated lung damage: a new COPD phenotype? *Respiration*. 2012;83(2):103.
183. Freeman CM, Curtis JL. Lung Dendritic Cells: Shaping Immune Responses throughout Chronic Obstructive Pulmonary Disease Progression. *American Journal of Respiratory Cell and Molecular Biology*. 2017;56(2):152-9. doi: 10.1165/rcmb.2016-0272TR. PubMed PMID: 27767327.
184. Givi ME, Folkerts G, Wagenaar GTM, Redegeld FA, Mortaz E. Cigarette smoke differentially modulates dendritic cell maturation and function in time. *Respiratory Research*. 2015;16(1):131. doi: 10.1186/s12931-015-0291-6.
185. Alkhatabi N, Todd I, Negm O, Tighe PJ, Fairclough LC. Tobacco smoke and nicotine suppress expression of activating signaling molecules in human dendritic cells. *Toxicology Letters*. 2018;299:40-6. doi: <https://doi.org/10.1016/j.toxlet.2018.09.002>.
186. Givi ME, A. Redegeld F, Folkerts G, Mortaz E. Dendritic Cells in Pathogenesis of COPD. *Current Pharmaceutical Design*. 2012;18(16):2329-35. doi: 10.2174/138161212800166068.
187. Shan M, Cheng H-F, Song L-z, Roberts L, Green L, Hacken-Bitar J, et al. Lung Myeloid Dendritic Cells Coordinately Induce T<sub>H</sub>1 and T<sub>H</sub>17 Responses in Human Emphysema. *Science Translational Medicine*. 2009;1(4):4ra10-4ra. doi: 10.1126/scitranslmed.3000154.
188. Velotti F, Barchetta I, Cimini FA, Cavallo MG. Granzyme B in Inflammatory Diseases: Apoptosis, Inflammation, Extracellular Matrix Remodeling, Epithelial-to-Mesenchymal Transition and Fibrosis. *Frontiers in Immunology*. 2020;11. doi: 10.3389/fimmu.2020.587581.

## REFERENCES

189. Fairclough L, Urbanowicz Richard A, Corne J, Lamb Jonathan R. Killer cells in chronic obstructive pulmonary disease. *Clin Sci*. 2008;114(8):533-41. doi: 10.1042/cs20070356.
190. Urbanowicz RA, Lamb JR, Todd I, Corne JM, Fairclough LC. Altered effector function of peripheral cytotoxic cells in COPD. *Respiratory Research*. 2009;10(1):53. doi: 10.1186/1465-9921-10-53.
191. Urbanowicz RA, Lamb JR, Todd I, Corne JM, Fairclough LC. Enhanced effector function of cytotoxic cells in the induced sputum of COPD patients. *Respiratory Research*. 2010;11(1):76. doi: 10.1186/1465-9921-11-76.
192. Hodge G, MUKARO V, HOLMES M, REYNOLDS PN, HODGE S. Enhanced cytotoxic function of natural killer and natural killer T-like cells associated with decreased CD94 (Kp43) in the chronic obstructive pulmonary disease airway. *Respirology*. 2013;18(2):369-76. doi: <https://doi.org/10.1111/j.1440-1843.2012.02287.x>.
193. Tsao C-C, Tsao P-N, Chen Y-G, Chuang Y-H. Repeated Activation of Lung Invariant NKT Cells Results in Chronic Obstructive Pulmonary Disease-Like Symptoms. *PLoS One*. 2016;11(1):e0147710. doi: 10.1371/journal.pone.0147710.
194. Cong J, Wei H. Natural Killer Cells in the Lungs. *Frontiers in Immunology*. 2019;10. doi: 10.3389/fimmu.2019.01416.
195. Chen C, Shen Y, Ni C-J, Zhu Y-H, Huang J-A. Imbalance of Circulating T-Lymphocyte Subpopulation in COPD and its Relationship with CAT Performance. *Journal of Clinical Laboratory Analysis*. 2012;26(2):109-14. doi: <https://doi.org/10.1002/jcla.21490>.
196. Forsslund H, Mikko M, Karimi R, Grunewald J, Wheelock ÅM, Wahlström J, et al. Distribution of T-Cell Subsets in BAL Fluid of Patients With Mild to Moderate COPD Depends on Current Smoking Status and Not Airway Obstruction. *Chest*. 2014;145(4):711-22. doi: <https://doi.org/10.1378/chest.13-0873>.
197. Siena L, Gjomarkaj M, Elliot J, Pace E, Bruno A, Baraldo S, et al. Reduced apoptosis of CD8+ T-Lymphocytes in the airways of smokers with mild/moderate COPD. *Respiratory Medicine*. 2011;105(10):1491-500. doi: <https://doi.org/10.1016/j.rmed.2011.04.014>.
198. Freeman CM, Han MK, Martinez FJ, Murray S, Liu LX, Chensue SW, et al. Cytotoxic Potential of Lung CD8+ T Cells Increases with Chronic Obstructive Pulmonary Disease Severity and with In Vitro Stimulation by IL-18 or IL-15. *The Journal of Immunology*. 2010;184(11):6504-13. doi: 10.4049/jimmunol.1000006.
199. Kim W-D, Chi H-S, Choe K-H, Oh Y-M, Lee S-D, Kim K-R, et al. A possible role for CD8+ and non-CD8+ cell granzyme B in early small airway wall remodelling in centrilobular emphysema. *Respirology*. 2013;18(4):688-96. doi: <https://doi.org/10.1111/resp.12069>.
200. Vernooy JHJ, Möller GM, Suylen RJv, Spijk MPv, Cloots RHE, Hoet PH, et al. Increased Granzyme A Expression in Type II

## REFERENCES

- Pneumocytes of Patients with Severe Chronic Obstructive Pulmonary Disease. *American Journal of Respiratory and Critical Care Medicine*. 2007;175(5):464-72. doi: 10.1164/rccm.200602-169OC. PubMed PMID: 17138956.
201. Hodge G, Nairn J, Holmes M, Reynolds PN, Hodge S. Increased intracellular T helper 1 proinflammatory cytokine production in peripheral blood, bronchoalveolar lavage and intraepithelial T cells of COPD subjects. *Clinical and Experimental Immunology*. 2007;150(1):22-9. doi: 10.1111/j.1365-2249.2007.03451.x.
202. Lethbridge MW, Kemeny DM, Ratoff JC, O'Connor BJ, Hawrylowicz CM, Corrigan CJ. A novel technique to explore the functions of bronchial mucosal T cells in chronic obstructive pulmonary disease: application to cytotoxicity and cytokine immunoreactivity. *Clinical and Experimental Immunology*. 2010;161(3):560-9. doi: 10.1111/j.1365-2249.2010.04198.x.
203. Chang Y, Nadigel J, Boulais N, Bourbeau J, Maltais F, Eidelman DH, et al. CD8 positive T cells express IL-17 in patients with chronic obstructive pulmonary disease. *Respiratory Research*. 2011;12(1):43. doi: 10.1186/1465-9921-12-43.
204. Williams M, Todd I, Fairclough LC. The role of CD8+ T lymphocytes in chronic obstructive pulmonary disease: a systematic review. *Inflammation Research*. 2021;70(1):11-8. doi: 10.1007/s00011-020-01408-z.
205. Qin K, Xu B, Pang M, Wang H, Yu B. The functions of CD4 T-helper lymphocytes in chronic obstructive pulmonary disease. *Acta Biochim Biophys Sin (Shanghai)*. 2022;54(2):173-8. Epub 2022/02/08. doi: 10.3724/abbs.2021009. PubMed PMID: 35130627; PubMed Central PMCID: PMC9827934.
206. Kheradmand F, Zhang Y, Corry DB. Contribution of adaptive immunity to human COPD and experimental models of emphysema. *Physiological Reviews*. 2023;103(2):1059-93. doi: 10.1152/physrev.00036.2021. PubMed PMID: 36201635.
207. Singh M, Lee S-H, Porter P, Xu C, Ohno A, Atmar RL, et al. Human rhinovirus proteinase 2A induces TH1 and TH2 immunity in patients with chronic obstructive pulmonary disease. *Journal of Allergy and Clinical Immunology*. 2010;125(6):1369-78.e2. doi: <https://doi.org/10.1016/j.jaci.2010.02.035>.
208. Tsoumakidou M, Tzanakis N, Chrysafakis G, Kyriakou D, Siafakas NM. Changes in sputum T-lymphocyte subpopulations at the onset of severe exacerbations of chronic obstructive pulmonary disease. *Respiratory Medicine*. 2005;99(5):572-9. doi: <https://doi.org/10.1016/j.rmed.2004.10.005>.
209. Jiang M, Liu H, Li Z, Wang J, Zhang F, Cao K, et al. ILC2s Induce Adaptive Th2-Type Immunity in Acute Exacerbation of Chronic Obstructive Pulmonary Disease. *Mediators of Inflammation*. 2019;2019:3140183. doi: 10.1155/2019/3140183.

## REFERENCES

210. Rovina N, Koutsoukou A, Koulouris NG. Inflammation and Immune Response in COPD: Where Do We Stand? Mediators of Inflammation. 2013;2013:413735. doi: 10.1155/2013/413735.
211. Huang S, He Q, Zhou L, Wei P-F. T cell responses in respiratory viral infections and chronic obstructive pulmonary disease. Chinese Medical Journal. 2021;134(13):1522-34. doi: 10.1097/CM9.0000000000001388.
212. Paats MS, Bergen IM, Hoogsteden HC, Eerden MMvd, Hendriks RW. Systemic CD4+ and CD8+ T-cell cytokine profiles correlate with GOLD stage in stable COPD. European Respiratory Journal. 2012;40(2):330-7. doi: 10.1183/09031936.00079611.
213. Vargas-Rojas MI, Ramírez-Venegas A, Limón-Camacho L, Ochoa L, Hernández-Zenteno R, Sansores RH. Increase of Th17 cells in peripheral blood of patients with chronic obstructive pulmonary disease. Respiratory Medicine. 2011;105(11):1648-54. doi: <https://doi.org/10.1016/j.rmed.2011.05.017>.
214. Korn T, Bettelli E, Oukka M, Kuchroo VK. IL-17 and Th17 Cells. Annual Review of Immunology. 2009;27(1):485-517. doi: 10.1146/annurev.immunol.021908.132710. PubMed PMID: 19132915.
215. Noack M, Miossec P. Th17 and regulatory T cell balance in autoimmune and inflammatory diseases. Autoimmunity Reviews. 2014;13(6):668-77. doi: <https://doi.org/10.1016/j.autrev.2013.12.004>.
216. Wang H, Ying H, Wang S, Gu X, Weng Y, Peng W, et al. Imbalance of peripheral blood Th17 and Treg responses in patients with chronic obstructive pulmonary disease. The Clinical Respiratory Journal. 2015;9(3):330-41. doi: <https://doi.org/10.1111/crj.12147>.
217. Zheng X, Zhang L, Chen J, Gu Y, Xu J, Ouyang Y. Dendritic cells and Th17/Treg ratio play critical roles in pathogenic process of chronic obstructive pulmonary disease. Biomedicine & Pharmacotherapy. 2018;108:1141-51. doi: <https://doi.org/10.1016/j.biopha.2018.09.113>.
218. Takemori T, Kaji T, Takahashi Y, Shimoda M, Rajewsky K. Generation of memory B cells inside and outside germinal centers. European Journal of Immunology. 2014;44(5):1258-64. doi: <https://doi.org/10.1002/eji.201343716>.
219. Polverino F, Cosio BG, Pons J, Lacho-Contreras M, Tejera P, Iglesias A, et al. B Cell-Activating Factor. An Orchestrator of Lymphoid Follicles in Severe Chronic Obstructive Pulmonary Disease. American Journal of Respiratory and Critical Care Medicine. 2015;192(6):695-705. doi: 10.1164/rccm.201501-0107OC. PubMed PMID: 26073875.
220. Agustí A, Hogg JC. Update on the Pathogenesis of Chronic Obstructive Pulmonary Disease. New England Journal of Medicine. 2019;381(13):1248-56. doi: 10.1056/NEJMra1900475. PubMed PMID: 31553836.



## REFERENCES

221. Silva-Sanchez A, Randall TD. Role of iBALT in Respiratory Immunity. In: Kabashima K, Egawa G, editors. *Inducible Lymphoid Organs*. Cham: Springer International Publishing; 2020. p. 21-43.
222. Karayama M, Inui N, Suda T, Nakamura Y, Nakamura H, Chida K. Antiendothelial Cell Antibodies in Patients With COPD. *Chest*. 2010;138(6):1303-8. doi: <https://doi.org/10.1378/chest.10-0863>.
223. Lee S-H, Goswami S, Grudo A, Song L-z, Bandi V, Goodnight-White S, et al. Antielastin autoimmunity in tobacco smoking-induced emphysema. *Nature Medicine*. 2007;13(5):567-9. doi: 10.1038/nm1583.
224. Daffa NI, Tighe PJ, Corne JM, Fairclough LC, Todd I. Natural and disease-specific autoantibodies in chronic obstructive pulmonary disease. *Clinical and Experimental Immunology*. 2015;180(1):155-63. doi: 10.1111/cei.12565.
225. Shindi R, Almehairi A, Negm OH, Kalsheker N, Gale NS, Shale DJ, et al. Autoantibodies of IgM and IgG classes show differences in recognition of multiple autoantigens in chronic obstructive pulmonary disease. *Clinical Immunology*. 2017;183:344-53. doi: <https://doi.org/10.1016/j.clim.2017.09.020>.
226. Packard TA, Li QZ, Cosgrove GP, Bowler RP, Cambier JC. COPD is associated with production of autoantibodies to a broad spectrum of self-antigens, correlative with disease phenotype. *Immunologic Research*. 2013;55(1):48-57. doi: 10.1007/s12026-012-8347-x.
227. Liang Z, Long F, Deng K, Wang F, Xiao J, Yang Y, et al. Dissociation between airway and systemic autoantibody responses in chronic obstructive pulmonary disease. *Ann Transl Med*. 2020;8(15):918. Epub 2020/09/22. doi: 10.21037/atm-20-944. PubMed PMID: 32953718; PubMed Central PMCID: PMC7475442.
228. Selvarajah S, Todd I, Tighe PJ, John M, Bolton CE, Harrison T, et al. Multiple Circulating Cytokines Are Coelevated in Chronic Obstructive Pulmonary Disease. *Mediators of Inflammation*. 2016;2016:3604842. doi: 10.1155/2016/3604842.
229. Barnes PJ. Inflammatory mechanisms in patients with chronic obstructive pulmonary disease. *Journal of Allergy and Clinical Immunology*. 2016;138(1):16-27. doi: <https://doi.org/10.1016/j.jaci.2016.05.011>.
230. Yao Y, Zhou J, Diao X, Wang S. Association between tumor necrosis factor- $\alpha$  and chronic obstructive pulmonary disease: a systematic review and meta-analysis. *Therapeutic Advances in Respiratory Disease*. 2019;13:1753466619866096. doi: 10.1177/1753466619866096. PubMed PMID: 31390957.
231. Rabolli V, Badissi AA, Devosse R, Uwambayinema F, Yakoub Y, Palmai-Pallag M, et al. The alarmin IL-1 $\alpha$  is a master cytokine in acute lung inflammation induced by silica micro- and nanoparticles. *Particle and Fibre Toxicology*. 2014;11(1):69. doi: 10.1186/s12989-014-0069-x.

## REFERENCES

232. Osei ET, Noordhoek JA, Hackett TL, Spanjer AIR, Postma DS, Timens W, et al. Interleukin-1 $\alpha$  drives the dysfunctional cross-talk of the airway epithelium and lung fibroblasts in COPD. *European Respiratory Journal*. 2016;48(2):359-69. doi: 10.1183/13993003.01911-2015.
233. Singh S, Verma SK, Kumar S, Ahmad MK, Nischal A, Singh SK, et al. Correlation of severity of chronic obstructive pulmonary disease with potential biomarkers. *Immunology Letters*. 2018;196:1-10. doi: <https://doi.org/10.1016/j.imlet.2018.01.004>.
234. Garon EB, Chih-Hsin Yang J, Dubinett SM. The Role of Interleukin 1 $\beta$  in the Pathogenesis of Lung Cancer. *JTO Clinical and Research Reports*. 2020;1(1):100001. doi: <https://doi.org/10.1016/j.jtocrr.2020.100001>.
235. Dawson RE, Jenkins BJ, Saad MI. IL-6 family cytokines in respiratory health and disease. *Cytokine*. 2021;143:155520. doi: <https://doi.org/10.1016/j.cyto.2021.155520>.
236. Wei J, Xiong X-f, Lin Y-h, Zheng B-x, Cheng D-y. Association between serum interleukin-6 concentrations and chronic obstructive pulmonary disease: a systematic review and meta-analysis. *PeerJ*. 2015;3:e1199. doi: 10.7717/peerj.1199.
237. Song W, Zhao J, Li Z. Interleukin-6 in bronchoalveolar lavage fluid from patients with COPD. *Chinese Medical Journal*. 2001;114(11):1140-2. doi: doi:10.3760/cma.j.issn.0366-6999.2001.11.109.
238. Jin Y, Wan Y, Chen G, Chen L, Zhang M-Q, Deng L, et al. Treg/IL-17 Ratio and Treg Differentiation in Patients with COPD. *PLoS One*. 2014;9(10):e111044. doi: 10.1371/journal.pone.0111044.
239. Ma R, Su H, Jiao K, Liu J. Association Between IL-17 and Chronic Obstructive Pulmonary Disease: A Systematic Review and Meta-Analysis. *International Journal of Chronic Obstructive Pulmonary Disease*. 2023;18(null):1681-90. doi: 10.2147/COPD.S412626.
240. Guo-Parke H, Linden D, Weldon S, Kidney JC, Taggart CC. Mechanisms of Virus-Induced Airway Immunity Dysfunction in the Pathogenesis of COPD Disease, Progression, and Exacerbation. *Frontiers in Immunology*. 2020;11. doi: 10.3389/fimmu.2020.01205.
241. Miller MC, Mayo KH. Chemokines from a Structural Perspective. *International Journal of Molecular Sciences*. 2017;18(10):2088. PubMed PMID: doi:10.3390/ijms18102088.
242. Hughes CE, Nibbs RJB. A guide to chemokines and their receptors. *The FEBS Journal*. 2018;285(16):2944-71. doi: <https://doi.org/10.1111/febs.14466>.
243. Henrot P, Prevel R, Berger P, Dupin I. Chemokines in COPD: From Implication to Therapeutic Use. *International Journal of Molecular Sciences*. 2019;20(11):2785. PubMed PMID: doi:10.3390/ijms20112785.
244. Barnes PJ. The Cytokine Network in Chronic Obstructive Pulmonary Disease. *American Journal of Respiratory Cell and Molecular*

## REFERENCES

- Biology. 2009;41(6):631-8. doi: 10.1165/rcmb.2009-0220TR. PubMed PMID: 19717810.
245. Mikami M, LLEWELLYN-JONES CG, BAYLEY D, HILL SL, STOCKLEY RA. The Chemotactic Activity of Sputum from Patients with Bronchiectasis. *American Journal of Respiratory and Critical Care Medicine*. 1998;157(3):723-8. doi: 10.1164/ajrccm.157.3.9606120. PubMed PMID: 9517582.
246. Zhang J, Bai C. The Significance of Serum Interleukin-8 in Acute Exacerbations of Chronic Obstructive Pulmonary Disease. *Tanaffos*. 2018;17(1):13-21. Epub 2018/08/18. PubMed PMID: 30116274; PubMed Central PMCID: PMC6087525.
247. Han MK, Quibrera PM, Carretta EE, Barr RG, Bleecker ER, Bowler RP, et al. Frequency of exacerbations in patients with chronic obstructive pulmonary disease: an analysis of the SPIROMICS cohort. *The Lancet Respiratory Medicine*. 2017;5(8):619-26. doi: 10.1016/S2213-2600(17)30207-2.
248. Donnelly LE, Barnes PJ. Chemokine receptors as therapeutic targets in chronic obstructive pulmonary disease. *Trends in Pharmacological Sciences*. 2006;27(10):546-53. doi: 10.1016/j.tips.2006.08.001.
249. Bafadhel M, McKenna S, Terry S, Mistry V, Reid C, Haldar P, et al. Acute Exacerbations of Chronic Obstructive Pulmonary Disease. *American Journal of Respiratory and Critical Care Medicine*. 2011;184(6):662-71. doi: 10.1164/rccm.201104-0597OC. PubMed PMID: 21680942.
250. Quint JK, Donaldson GC, Goldring JJP, Baghai-Ravary R, Hurst JR, Wedzicha JA. Serum IP-10 as a Biomarker of Human Rhinovirus Infection at Exacerbation of COPD. *Chest*. 2010;137(4):812-22. doi: <https://doi.org/10.1378/chest.09-1541>.
251. Kim G-D, Lim EY, Shin HS. Macrophage Polarization and Functions in Pathogenesis of Chronic Obstructive Pulmonary Disease. *International Journal of Molecular Sciences*. 2024;25(11):5631. PubMed PMID: doi:10.3390/ijms25115631.
252. Ham J, Kim J, Ko YG, Kim HY. The Dynamic Contribution of Neutrophils in the Chronic Respiratory Diseases. *Allergy Asthma Immunol Res*. 2022;14(4):361-78. Epub 2022/07/16. doi: 10.4168/aaair.2022.14.4.361. PubMed PMID: 35837821; PubMed Central PMCID: PMC9293600.
253. SAETTA M, Di STEFANO A, TURATO G, FACCHINI FM, CORBINO L, MAPP CE, et al. CD8+ T-Lymphocytes in Peripheral Airways of Smokers with Chronic Obstructive Pulmonary Disease. *American Journal of Respiratory and Critical Care Medicine*. 1998;157(3):822-6. doi: 10.1164/ajrccm.157.3.9709027. PubMed PMID: 9517597.

## REFERENCES

254. Caramori G, Casolari P, Barczyk A, Durham AL, Di Stefano A, Adcock I. COPD immunopathology. *Seminars in Immunopathology*. 2016;38(4):497-515. doi: 10.1007/s00281-016-0561-5.
255. Demedts IK, Brusselle GG, Vermaelen KY, Pauwels RA. Identification and Characterization of Human Pulmonary Dendritic Cells. *American Journal of Respiratory Cell and Molecular Biology*. 2005;32(3):177-84. doi: 10.1165/rcmb.2004-0279OC. PubMed PMID: 15576669.
256. Bu T, Wang LF, Yin YQ. How Do Innate Immune Cells Contribute to Airway Remodeling in COPD Progression? *International Journal of Chronic Obstructive Pulmonary Disease*. 2020;15(null):107-16. doi: 10.2147/COPD.S235054.
257. Zeiger RS, Tran TN, Butler RK, Schatz M, Li Q, Khattry DB, et al. Relationship of Blood Eosinophil Count to Exacerbations in Chronic Obstructive Pulmonary Disease. *The Journal of Allergy and Clinical Immunology: In Practice*. 2018;6(3):944-54.e5. doi: <https://doi.org/10.1016/j.jaip.2017.10.004>.
258. Balóira Villar A, Pallarés Sanmartín A. Chronic Obstructive Pulmonary Disease With Eosinophilia, an Emerging Phenotype? *Archivos de Bronconeumología (English Edition)*. 2016;52(4):177-8. doi: <https://doi.org/10.1016/j.arbr.2016.02.012>.
259. Mortaz E, Folkerts G, Redegeld F. Mast cells and COPD. *Pulmonary Pharmacology & Therapeutics*. 2011;24(4):367-72. doi: <https://doi.org/10.1016/j.pupt.2011.03.007>.
260. Soltani A, Ewe YP, Lim ZS, Sohal SS, Reid D, Weston S, et al. Mast cells in COPD airways: relationship to bronchodilator responsiveness and angiogenesis. *European Respiratory Journal*. 2012;39(6):1361-7. doi: 10.1183/09031936.00084411.
261. Chow L, Smith D, Chokshi K, Ezegbunam W, Charoenpong P, Foley K, et al. Animal Models of Chronic Obstructive Pulmonary. COPD: An Update in Pathogenesis and Clinical Management. 2018:1.
262. Jiang S, Mohammadtursun N, Qiu J, Li Q, Sun J, Dong J. Recent advances on animal models related to chronic obstructive pulmonary disease. *Traditional Medicine and Modern Medicine*. 2019;02(03):93-104. doi: 10.1142/s2575900019300017.
263. Laurell C-B, Eriksson S. The electrophoretic  $\alpha_1$ -globulin pattern of serum in  $\alpha_1$ -antitrypsin deficiency. *Scandinavian journal of clinical and laboratory investigation*. 1963;15(2):132-40.
264. Gross P, Pfitzer EA, Tolker E, Babyak MA, Kaschak M. Experimental emphysema: its production with papain in normal and silicotic rats. *Archives of Environmental Health: An International Journal*. 1965;11(1):50-8.
265. Busch RH, Lauhala KE, Loscutoff SM, McDonald KE. Experimental pulmonary emphysema induced in the rat by intratracheally

## REFERENCES

- administered elastase: Morphogenesis. *Environmental Research*. 1984;33(2):497-513. doi: [https://doi.org/10.1016/0013-9351\(84\)90044-6](https://doi.org/10.1016/0013-9351(84)90044-6).
266. Hayes JA, Korthy A, Snider GL. The pathology of elastase-induced panacinar emphysema in hamsters. *J Pathol*. 1975;117(1):1-14. Epub 1975/09/01. doi: 10.1002/path.1711170102. PubMed PMID: 1195057.
267. Fehrenbach H. Animal models of pulmonary emphysema: a stereologist's perspective. *European Respiratory Review*. 2006;15(101):136-47. doi: 10.1183/09059180.00010104.
268. Rydell-Törmänen K, Johnson JR. The Applicability of Mouse Models to the Study of Human Disease. In: Bertonecello I, editor. *Mouse Cell Culture: Methods and Protocols*. New York, NY: Springer New York; 2019. p. 3-22.
269. Groneberg DA, Chung KF. Models of chronic obstructive pulmonary disease. *Respiratory Research*. 2004;5(1):18. doi: 10.1186/1465-9921-5-18.
270. Irvin CG, Bates JHT. Measuring the lung function in the mouse: the challenge of size. *Respiratory Research*. 2003;4(1):1. doi: 10.1186/rr199.
271. Pan H, Deutsch GH, Wert SE, Ambalavanan N, Ansong C, Ardini-Poleske ME, et al. Comprehensive anatomic ontologies for lung development: A comparison of alveolar formation and maturation within mouse and human lung. *Journal of Biomedical Semantics*. 2019;10(1):18. doi: 10.1186/s13326-019-0209-1.
272. Janoff A, White R, Carp H, Harel S, Dearing R, Lee D. Lung injury induced by leukocytic proteases. *Am J Pathol*. 1979;97(1):111-36. Epub 1979/10/01. PubMed PMID: 495691; PubMed Central PMCID: PMC2042389.
273. Noma S, HERMAN PG, KHAN A, ROJAS KA, PIPMAN Y. Sequential Morphologic Changes of Elastase-Induced Pulmonary Emphysema in Pig Lungs: Evaluation by High-Resolution Computed Tomography. *Investigative Radiology*. 1991;26(5):446-53. PubMed PMID: 00004424-199105000-00012.
274. Scuri M, Forteza R, Lauredo I, Sabater JR, Botvinnikova Y, Allegra L, et al. Inhaled porcine pancreatic elastase causes bronchoconstriction via a bradykinin-mediated mechanism. *Journal of Applied Physiology*. 2000;89(4):1397-402. doi: 10.1152/jappl.2000.89.4.1397. PubMed PMID: 11007574.
275. Guerassimov A, Hoshino Y, Takubo Y, Turcotte A, Yamamoto M, Ghezzi H, et al. The development of emphysema in cigarette smoke-exposed mice is strain dependent. *Am J Respir Crit Care Med*. 2004;170(9):974-80. Epub 2004/07/30. doi: 10.1164/rccm.200309-1270OC. PubMed PMID: 15282203.
276. Serre J, Tanjeko AT, Mathysen C, Vanherwegen AS, Heigl T, Janssen R, et al. Enhanced lung inflammatory response in whole-body

## REFERENCES

- compared to nose-only cigarette smoke-exposed mice. *Respir Res.* 2021;22(1):86. Epub 2021/03/19. doi: 10.1186/s12931-021-01680-5. PubMed PMID: 33731130; PubMed Central PMCID: PMC7968299.
277. Williams K, Roman J. Studying human respiratory disease in animals – role of induced and naturally occurring models. *The Journal of Pathology.* 2016;238(2):220-32. doi: <https://doi.org/10.1002/path.4658>.
278. Wright JL, Churg A. Animal models of cigarette smoke-induced chronic obstructive pulmonary disease. *Expert Review of Respiratory Medicine.* 2010;4(6):723-34. doi: 10.1586/ers.10.68.
279. Shapiro SD. Transgenic and gene-targeted mice as models for chronic obstructive pulmonary disease. *European Respiratory Journal.* 2007;29(2):375-8. doi: 10.1183/09031936.00087606.
280. Tanner L, Single Andrew B. Animal Models Reflecting Chronic Obstructive Pulmonary Disease and Related Respiratory Disorders: Translating Pre-Clinical Data into Clinical Relevance. *Journal of Innate Immunity.* 2019;12(3):203-25. doi: 10.1159/000502489.
281. Hautamaki RD, Kobayashi DK, Senior RM, Shapiro SD. Requirement for Macrophage Elastase for Cigarette Smoke-Induced Emphysema in Mice. *Science.* 1997;277(5334):2002-4. doi: 10.1126/science.277.5334.2002.
282. Shan M, Yuan X, Song L-z, Roberts L, Zarinkamar N, Seryshev A, et al. Cigarette Smoke Induction of Osteopontin (SPP1) Mediates T<sub>H</sub>17 Inflammation in Human and Experimental Emphysema. *Science Translational Medicine.* 2012;4(117):117ra9-ra9. doi: 10.1126/scitranslmed.3003041.
283. Bozinovski S, Seow HJ, Chan SPJ, Anthony D, McQualter J, Hansen M, et al. Innate cellular sources of interleukin-17A regulate macrophage accumulation in cigarette-smoke-induced lung inflammation in mice. *Clin Sci.* 2015;129(9):785-96. doi: 10.1042/cs20140703. PubMed PMID: WOS:000361047600001.
284. Kearley J, Silver JS, Sanden C, Liu Z, Berlin AA, White N, et al. Cigarette smoke silences innate lymphoid cell function and facilitates an exacerbated type I interleukin-33-dependent response to infection. *Immunity.* 2015;42(3):566-79.
285. Sajjan U, Ganesan S, Comstock AT, Shim J, Wang Q, Nagarkar DR, et al. Elastase- and LPS-exposed mice display altered responses to rhinovirus infection. *American Journal of Physiology-Lung Cellular and Molecular Physiology.* 2009;297(5):L931-L44. doi: 10.1152/ajplung.00150.2009. PubMed PMID: 19748999.
286. Foronjy RF, Dabo AJ, Taggart CC, Weldon S, Geraghty P. Respiratory Syncytial Virus Infections Enhance Cigarette Smoke Induced COPD in Mice. *PLoS One.* 2014;9(2):e90567. doi: 10.1371/journal.pone.0090567.
287. Takahashi S, Ishii M, Namkoong H, Hegab AE, Asami T, Yagi K, et al. Pneumococcal Infection Aggravates Elastase-Induced Emphysema

## REFERENCES

- via Matrix Metalloproteinase 12 Overexpression. *The Journal of Infectious Diseases*. 2015;213(6):1018-30. doi: 10.1093/infdis/jiv527.
288. Hasday JD, Bascom R, Costa JJ, Fitzgerald T, Dubin W. Bacterial Endotoxin Is an Active Component of Cigarette Smoke. *Chest*. 1999;115(3):829-35. doi: <https://doi.org/10.1378/chest.115.3.829>.
289. Rylander R. Endotoxin and occupational airway disease. *Current Opinion in Allergy and Clinical Immunology*. 2006;6(1).
290. Sun L, TANG L, XU Y, WANG S, LI Y, KANG J. The effect and mechanism of action of carbocysteine on airway bacterial load in rats chronically exposed to cigarette smoke. *Respirology*. 2010;15(7):1064-71. doi: <https://doi.org/10.1111/j.1440-1843.2010.01816.x>.
291. Mizutani N, Fuchikami J-i, Takahashi M, Nabe T, Yoshino S, Kohno S. Pulmonary emphysema induced by cigarette smoke solution and lipopolysaccharide in guinea pigs. *Biological and Pharmaceutical Bulletin*. 2009;32(9):1559-64.
292. Limjunyawong N, Craig JM, Lagassé HAD, Scott AL, Mitzner W. Experimental progressive emphysema in BALB/cJ mice as a model for chronic alveolar destruction in humans. *American Journal of Physiology-Lung Cellular and Molecular Physiology*. 2015;309(7):L662-L76. doi: 10.1152/ajplung.00214.2015. PubMed PMID: 26232300.
293. Perez-Rial S, del Puerto-Nevedo L, Terron-Exposito R, Giron-Martinez A, Gonzalez-Mangado N, Peces-Barba G. Role of Recently Migrated Monocytes in Cigarette Smoke-Induced Lung Inflammation in Different Strain of Mice. *PLoS One*. 2013;8(9):9. doi: 10.1371/journal.pone.0072975. PubMed PMID: WOS:000324408400011.
294. Life span as a biomarker [cited 2023 December]. Available from: <https://www.jax.org/research-and-faculty/research-labs/the-harrison-lab/gerontology/life-span-as-a-biomarker>.
295. John-Schuster G, Gunter S, Hager K, Conlon TM, Eickelberg O, Yildirim AO. Inflammaging increases susceptibility to cigarette smoke-induced COPD. *Oncotarget*. 2016;7(21):30068-83. Epub 2015/08/19. doi: 10.18632/oncotarget.4027. PubMed PMID: 26284585; PubMed Central PMCID: PMC5058664.
296. Beckett EL, Stevens RL, Jarnicki AG, Kim RY, Hanish I, Hansbro NG, et al. A new short-term mouse model of chronic obstructive pulmonary disease identifies a role for mast cell tryptase in pathogenesis. *J Allergy Clin Immunol*. 2013;131(3):752-62. Epub 2013/02/06. doi: 10.1016/j.jaci.2012.11.053. PubMed PMID: 23380220; PubMed Central PMCID: PMC4060894.
297. Denlinger-Apte RL, Kotlyar M, Koopmeiners JS, Tidey JW, Luo X, Benowitz NL, et al. Effects of Very Low Nicotine Content Cigarettes on Smoking Behavior and Biomarkers of Exposure in Menthol and Non-menthol Smokers. *Nicotine & Tobacco Research*. 2019;21(Supplement\_1):S63-S72. doi: 10.1093/ntr/ntz160.

## REFERENCES

298. John G, Kohse K, Orasche J, Reda A, Schnelle-Kreis J, Zimmermann R, et al. The composition of cigarette smoke determines inflammatory cell recruitment to the lung in COPD mouse models. *Clin Sci*. 2014;126(3-4):207-21. doi: 10.1042/cs20130117. PubMed PMID: WOS:000330258500003.
299. Foronjy RF, Mercer BA, Maxfield MW, Powell CA, D'Armiento J, Okada Y. STRUCTURAL EMPHYSEMA DOES NOT CORRELATE WITH LUNG COMPLIANCE: LESSONS FROM THE MOUSE SMOKING MODEL. *Exp Lung Res*. 2005;31(6):547-62. doi: 10.1080/019021490951522.
300. Bracke KR, D'Hulst A I, Maes T, Moerloose KB, Demedts IK, Lebecque S, et al. Cigarette smoke-induced pulmonary inflammation and emphysema are attenuated in CCR6-deficient mice. *J Immunol*. 2006;177(7):4350-9. Epub 2006/09/20. doi: 10.4049/jimmunol.177.7.4350. PubMed PMID: 16982869.
301. Bracke KR, Verhamme FM, Seys LJ, Bantsimba-Malanda C, Cunoosamy DM, Herbst R, et al. Role of CXCL13 in cigarette smoke-induced lymphoid follicle formation and chronic obstructive pulmonary disease. *Am J Respir Crit Care Med*. 2013;188(3):343-55. Epub 2013/06/08. doi: 10.1164/rccm.201211-2055OC. PubMed PMID: 23742729.
302. Duan MC, Zhang JQ, Liang Y, Liu GN, Xiao J, Tang HJ, et al. Infiltration of IL-17-Producing T Cells and Treg Cells in a Mouse Model of Smoke-Induced Emphysema. *Inflammation*. 2016;39(4):1334-44. Epub 2016/05/07. doi: 10.1007/s10753-016-0365-8. PubMed PMID: 27150336.
303. Eppert BL, Wortham BW, Flury JL, Borchers MT. Functional characterization of T cell populations in a mouse model of chronic obstructive pulmonary disease. *J Immunol*. 2013;190(3):1331-40. Epub 2012/12/25. doi: 10.4049/jimmunol.1202442. PubMed PMID: 23264660; PubMed Central PMCID: PMC3552128.
304. Pauwels NS, Bracke KR, Maes T, Pilette C, Joos GF, Brusselle GG. The role of interleukin-6 in pulmonary and systemic manifestations in a murine model of chronic obstructive pulmonary disease. *Exp Lung Res*. 2010;36(8):469-83. doi: 10.3109/01902141003739723. PubMed PMID: WOS:000282885100004.
305. Wang H, Peng W, Weng Y, Ying H, Li H, Xia D, et al. Imbalance of Th17/Treg cells in mice with chronic cigarette smoke exposure. *Int Immunopharmacol*. 2012;14(4):504-12. Epub 2012/10/10. doi: 10.1016/j.intimp.2012.09.011. PubMed PMID: 23044435.
306. Nemmar A, Raza H, Subramaniam D, John A, Elwasila M, Ali BH, et al. Evaluation of the pulmonary effects of short-term nose-only cigarette smoke exposure in mice. *Experimental Biology and Medicine*. 2012;237(12):1449-56. doi: 10.1258/ebm.2012.012103.
307. Rinaldi M, Maes K, De Vleeschauwer S, Thomas D, Verbeken EK, Decramer M, et al. Long-term nose-only cigarette smoke exposure



## REFERENCES

- induces emphysema and mild skeletal muscle dysfunction in mice. *Disease Models & Mechanisms*. 2012;5(3):333-41. doi: 10.1242/dmm.008508.
308. Shoji H, Miyakawa T. Differential effects of stress exposure via two types of restraint apparatuses on behavior and plasma corticosterone level in inbred male BALB/cAJcl mice. *Neuropsychopharmacology Reports*. 2020;40(1):73-84. doi: <https://doi.org/10.1002/npr2.12093>.
309. Zhu Y, Klomparens EA, Guo S, Geng X. Neuroinflammation caused by mental stress: the effect of chronic restraint stress and acute repeated social defeat stress in mice. *Neurological Research*. 2019;41(8):762-9. doi: 10.1080/01616412.2019.1615670.
310. Cooper GE, Mayall J, Donovan C, Haw TJ, Budden KF, Hansbro NG, et al. Antiviral Responses of Tissue-resident CD49a1 Lung Natural Killer Cells Are Dysregulated in Chronic Obstructive Pulmonary Disease. *American Journal of Respiratory and Critical Care Medicine*. 2023;207(5):553-65. doi: 10.1164/rccm.202205-0848OC. PubMed PMID: WOS:000942062300013.
311. Gaschler GJ, Zavitz CC, Bauer CM, Skrtic M, Lindahl M, Robbins CS, et al. Cigarette smoke exposure attenuates cytokine production by mouse alveolar macrophages. *Am J Respir Cell Mol Biol*. 2008;38(2):218-26. Epub 2007/09/18. doi: 10.1165/rcmb.2007-0053OC. PubMed PMID: 17872497.
312. Wright JL, Tai H, Wang R, Wang X, Churg A. Cigarette smoke upregulates pulmonary vascular matrix metalloproteinases via TNF-alpha signaling. *Am J Physiol Lung Cell Mol Physiol*. 2007;292(1):L125-33. Epub 2006/08/15. doi: 10.1152/ajplung.00539.2005. PubMed PMID: 16905636.
313. Stevenson CS, Birrell MA. Moving towards a new generation of animal models for asthma and COPD with improved clinical relevance. *Pharmacology & Therapeutics*. 2011;130(2):93-105. doi: <https://doi.org/10.1016/j.pharmthera.2010.10.008>.
314. Kiani AK, Pheby D, Henehan G, Brown R, Sieving P, Sykora P, et al. Ethical considerations regarding animal experimentation. *J Prev Med Hyg*. 2022;63(2 Suppl 3):E255-e66. Epub 2022/12/09. doi: 10.15167/2421-4248/jpmh2022.63.2S3.2768. PubMed PMID: 36479489; PubMed Central PMCID: PMC9710398.
315. Lee HS, Park H-W. Role of mTOR in the Development of Asthma in Mice With Cigarette Smoke-Induced Cellular Senescence. *The Journals of Gerontology: Series A*. 2021;77(3):433-42. doi: 10.1093/gerona/77(3)433.
316. Lee B, Ko E, Lee J, Jo Y, Hwang H, Goh TS, et al. Soluble common gamma chain exacerbates COPD progress through the regulation of inflammatory T cell response in mice. *Int J Chron Obstruct Pulmon Dis*. 2017;12:817-27. Epub 2017/03/24. doi: 10.2147/COPD.S123405. PubMed PMID: 28331303; PubMed Central PMCID: PMC5352154.

---

## REFERENCES

317. Pelgrim CE, van Ark I, Leusink-Muis T, Brans MAD, Braber S, Garszen J, et al. Intratracheal administration of solutions in mice; development and validation of an optimized method with improved efficacy, reproducibility and accuracy. *Journal of Pharmacological and Toxicological Methods*. 2022;114:107156. doi: <https://doi.org/10.1016/j.vascn.2022.107156>.
318. Miller LM, Foster WM, Dambach DM, Doeblner D, McKinnon M, Killar L, et al. A murine model of cigarette smoke-induced pulmonary inflammation using intranasally administered smoke-conditioned medium. *Exp Lung Res*. 2002;28(6):435-55. doi: 10.1080/01902140290096728. PubMed PMID: WOS:000177493600003.
319. Xiong J, Tian J, Zhou L, Le Y, Sun Y. Interleukin-17A Deficiency Attenuated Emphysema and Bone Loss in Mice Exposed to Cigarette Smoke. *Int J Chron Obstruct Pulmon Dis*. 2020;15:301-10. Epub 2020/02/28. doi: 10.2147/COPD.S235384. PubMed PMID: 32103929; PubMed Central PMCID: PMC7020917.
320. Hubeau C, Kubera JE, Masek-Hammerman K, Williams CM. Interleukin-6 neutralization alleviates pulmonary inflammation in mice exposed to cigarette smoke and poly(I:C). *Clin Sci (Lond)*. 2013;125(10):483-93. Epub 2013/06/07. doi: 10.1042/CS20130110. PubMed PMID: 23738811.
321. Kang MJ, Homer RJ, Gallo A, Lee CG, Crothers KA, Cho SJ, et al. IL-18 is induced and IL-18 receptor alpha plays a critical role in the pathogenesis of cigarette smoke-induced pulmonary emphysema and inflammation. *J Immunol*. 2007;178(3):1948-59. Epub 2007/01/24. doi: 10.4049/jimmunol.178.3.1948. PubMed PMID: 17237446.
322. Wu M, Lai T, Jing D, Yang S, Wu Y, Li Z, et al. Epithelium-derived IL17A Promotes Cigarette Smoke-induced Inflammation and Mucus Hyperproduction. *Am J Respir Cell Mol Biol*. 2021;65(6):581-92. Epub 2021/06/30. doi: 10.1165/rcmb.2020-0424OC. PubMed PMID: 34186014.
323. Botelho FM, Bauer CM, Finch D, Nikota JK, Zavitz CC, Kelly A, et al. IL-1alpha/IL-1R1 expression in chronic obstructive pulmonary disease and mechanistic relevance to smoke-induced neutrophilia in mice. *PLoS One*. 2011;6(12):e28457. Epub 2011/12/14. doi: 10.1371/journal.pone.0028457. PubMed PMID: 22163019.
324. Li D, Wang T, Ma Q, Zhou L, Le Y, Rao Y, et al. IL-17A Promotes Epithelial ADAM9 Expression in Cigarette Smoke-Related COPD. *Int J Chron Obstruct Pulmon Dis*. 2022;17:2589-602. Epub 2022/10/22. doi: 10.2147/COPD.S375006. PubMed PMID: 36267325; PubMed Central PMCID: PMC9578481.
325. Von Staden H. Herophilus: the art of medicine in early Alexandria: edition, translation and essays: Cambridge University Press; 1989.

## REFERENCES

326. Maehle A-H. Animal experimentation from antiquity to the end of the eighteenth century: Attitudes and arguments. Vivisection in historical perspective. 1987.
327. Franco NH. Animal Experiments in Biomedical Research: A Historical Perspective. *Animals*. 2013;3(1):238-73. PubMed PMID: doi:10.3390/ani3010238.
328. Boralevi LC. Bentham and the Oppressed: Walter de Gruyter; 1984.
329. Bentham J. An introduction to the principles of morals and legislation. History of Economic Thought Books. 1781.
330. Clark JM, Clifford P, Jarrett W, Pekow C. Communicating About Animal Research with the Public. *Ilar J*. 2019;60(1):34-42. doi: 10.1093/ilar/ilz007. PubMed PMID: WOS:000514187800006.
331. Hubrecht RC, Carter E. The 3Rs and Humane Experimental Technique: Implementing Change. *Animals*. 2019;9(10):10. doi: 10.3390/ani9100754. PubMed PMID: WOS:000496757200051.
332. Hollands C. The Animals (scientific procedures) Act 1986. *Lancet*. 1986;2(8497):32-3. Epub 1986/07/05. doi: 10.1016/s0140-6736(86)92571-7. PubMed PMID: 2873327.
333. Russell WMS, Burch RL. The principles of humane experimental technique: Methuen; 1959.
334. Guidance on the operation of the Animals (Scientific Procedures) Act 1986 (ASPA): UK Home Office; [cited 2023 December]. Available from: <https://www.gov.uk/guidance/guidance-on-the-operation-of-the-animals-scientific-procedures-act-1986>.
335. ss.6 - 7 Animals (Scientific Procedures) Act 1986. Sect. s4. (1986).
336. ss.5 - 5E Animals (Scientific Procedures) Act 1986. Sect. s4. (1986).
337. s.4 Animals (Scientific Procedures) Act 1986. Sect. s4. (1986).
338. Dunn R. Brexit: A Boon or a Curse for Animals Used in Scientific Procedures? *Animals*. 2021;11(6):1547. PubMed PMID: doi:10.3390/ani11061547.
339. Unit AiSR. Identification and management of patterns of low-level concerns at licensed establishments: Home Office London, UK; 2015.
340. Percie du Sert N, Hurst V, Ahluwalia A, Alam S, Avey MT, Baker M, et al. The ARRIVE guidelines 2.0: Updated guidelines for reporting animal research\*. *Journal of Cerebral Blood Flow & Metabolism*. 2020;40(9):1769-77. doi: 10.1177/0271678x20943823. PubMed PMID: 32663096.
341. The 3Rs: National Centre for the Replacement, Refinement & Reduction of Animals in Research; [cited 2023 December]. Available from: <https://www.nc3rs.org.uk/who-we-are/3rs>.

## REFERENCES

342. Wilkinson M. The potential of organ on chip technology for replacing animal testing. *Animal Experimentation: Working Towards a Paradigm Change*: Brill; 2019. p. 639-53.
343. Herrmann K, Pistollato F, Stephens ML. Beyond the 3Rs: Expanding the Use of Human-Relevant Replacement Methods in Biomedical Research. *ALTEX-Altern Anim Exp*. 2019;36(3):343-52. doi: 10.14573/altex.1907031. PubMed PMID: WOS:000476633600002.
344. Fröhlich E. Replacement Strategies for Animal Studies in Inhalation Testing. *Sci*. 2021;3(4):45. PubMed PMID: doi:10.3390/sci3040045.
345. Cao X, Coyle JP, Xiong R, Wang Y, Heflich RH, Ren B, et al. Invited review: human air-liquid-interface organotypic airway tissue models derived from primary tracheobronchial epithelial cells—overview and perspectives. *In Vitro Cellular & Developmental Biology - Animal*. 2021;57(2):104-32. doi: 10.1007/s11626-020-00517-7.
346. Hurst JL, West RS. Taming anxiety in laboratory mice. *Nature Methods*. 2010;7(10):825-6. doi: 10.1038/nmeth.1500.
347. Ono M, Sasaki H, Nagasaki K, Torigoe D, Ichii O, Sasaki N, et al. Does the routine handling affect the phenotype of disease model mice? *Japanese Journal of Veterinary Research*. 2016;64(4):265-71.
348. Burden N, Chapman K, Sewell F, Robinson V. Pioneering Better Science through the 3Rs: An Introduction to the National Centre for the Replacement, Refinement, and Reduction of Animals in Research (NC3Rs). *Journal of the American Association for Laboratory Animal Science*. 2015;54(2):198-208.
349. Shirbache K, Nematian H, Vahdati Z, Milan N, Zanjani LO, Firouzi M, et al. *Microsurgery Achievements for Regenerative Medicine Enhancement*. 2023.
350. Movia D, Prina-Mello A. Preclinical Development of Orally Inhaled Drugs (OIDs)—Are Animal Models Predictive or Shall We Move Towards In Vitro Non-Animal Models? *Animals*. 2020;10(8):1259. PubMed PMID: doi:10.3390/ani10081259.
351. Smoking - Health Survey for England: Health and Social Care Information Centre; 2019 [cited 2024 February]. Available from: <http://healthsurvey.hscic.gov.uk/data-visualisation/data-visualisation/explore-the-trends/smoking.aspx>.
352. Part 4: Trends - Height and Weight: NHS Digital; 2024 [cited 2024 February]. Available from: <https://digital.nhs.uk/data-and-information/publications/statistical/health-survey-for-england/2021/part-4-trends>.
353. Body Weight Information for C57BL/6J (000664): The Jackson Laboratory; 2024 [cited 2024 February]. Available from: <https://www.jax.org/jax-mice-and-services/strain-data-sheet-pages/body-weight-chart-000664>.

---

## REFERENCES

354. Blood sampling: Mouse: NC3Rs; 2024 [cited 2024 January]. Available from: <https://nc3rs.org.uk/3rs-resources/blood-sampling/blood-sampling-mouse>.
355. Microsampling: NC3Rs; 2024 [cited 2024 January]. Available from: <https://nc3rs.org.uk/3rs-resources/microsampling>.
356. Gene Expression Atlas: EMBL-EBI; 2024 [cited 2024 January]. Available from: <https://www.ebi.ac.uk/gxa/home>.
357. Cell Frequencies in Common Samples: BioRad; 2024 [cited 2024 February]. Available from: <https://www.bio-rad-antibodies.com/flow-cytometry-cell-frequency.html>.
358. NovaFluor™ Antibody Conjugation Kits: Thermo Fisher; 2024 [cited 2024 January]. Available from: <https://www.thermofisher.com/order/catalog/product/K06T04L011>.
359. Lightning-Link (R) PE-Cy5.5 Antibody Labeling Kit: Novus Biologicals; 2024 [cited 2024 January]. Available from: [https://www.novusbio.com/products/lightning-link-r-pe-cy55-kit\\_761-0005](https://www.novusbio.com/products/lightning-link-r-pe-cy55-kit_761-0005).
360. Mix-n-Stain™ CF™ 568 Antibody Labeling Kit (50-100µg) | Sigma-Aldrich: Sigma-Aldrich; 2024 [cited 2024 January]. Available from: <https://www.sigmaaldrich.com/GB/en/product/sigma/mx568s100>.
361. Pierce™ BCA Protein Assay Kits: ThermoFisher Scientific; 2024 [cited 2024 January]. Available from: <https://www.thermofisher.com/order/catalog/product/23225>.
362. Livak KJ, Schmittgen TD. Analysis of Relative Gene Expression Data Using Real-Time Quantitative PCR and the 2- $\Delta\Delta$ CT Method. *Methods*. 2001;25(4):402-8. doi: <https://doi.org/10.1006/meth.2001.1262>.
363. RefFinder: LIZhen; 2024 [cited 2024 February]. Available from: <https://blogo.cn/RefFinder/?type=reference>.
364. Crowley G, Kwon S, Caraher EJ, Haider SH, Lam R, Batra P, et al. Quantitative lung morphology: semi-automated measurement of mean linear intercept. *BMC Pulmonary Medicine*. 2019;19(1):206. doi: 10.1186/s12890-019-0915-6.
365. Nolan JP, Condello D. Spectral flow cytometry. *Curr Protoc Cytom*. 2013;Chapter 1:1.27.1-1..13. Epub 2013/01/08. doi: 10.1002/0471142956.cy0127s63. PubMed PMID: 23292705; PubMed Central PMCID: PMC3556726.
366. Park LM, Lannigan J, Jaimes MC. OMIP-069: Forty-Color Full Spectrum Flow Cytometry Panel for Deep Immunophenotyping of Major Cell Subsets in Human Peripheral Blood. *Cytometry Part A*. 2020;97(10):1044-51. doi: <https://doi.org/10.1002/cyto.a.24213>.
367. Mahnke YD, Roederer M. Optimizing a multicolor immunophenotyping assay. *Clin Lab Med*. 2007;27(3):469-85, v. Epub 2007/07/31. doi: 10.1016/j.cll.2007.05.002. PubMed PMID: 17658403; PubMed Central PMCID: PMC3556726.

## REFERENCES

368. DiPiazza AT, Hill JP, Graham BS, Ruckwardt TJ. OMIP-061: 20-Color Flow Cytometry Panel for High-Dimensional Characterization of Murine Antigen-Presenting Cells. *Cytometry Part A*. 2019;95(12):1226-30. doi: <https://doi.org/10.1002/cyto.a.23880>.
369. Mincham KT, Snelgrove RJ. OMIP-086: Full spectrum flow cytometry for high-dimensional immunophenotyping of mouse innate lymphoid cells. *Cytometry Part A*. 2023;103(2):110-6. doi: <https://doi.org/10.1002/cyto.a.24702>.
370. Mincham KT, Young JD, Strickland DH. OMIP 076: High-dimensional immunophenotyping of murine T-cell, B-cell, and antibody secreting cell subsets. *Cytometry Part A*. 2021;99(9):888-92. doi: <https://doi.org/10.1002/cyto.a.24474>.
371. Unsworth A, Anderson R, Haynes N, Britt K. OMIP-032: Two multi-color immunophenotyping panels for assessing the innate and adaptive immune cells in the mouse mammary gland. *Cytometry Part A*. 2016;89(6):527-30. doi: <https://doi.org/10.1002/cyto.a.22867>.
372. Zhang X, Lan Y, Xu J, Quan F, Zhao E, Deng C, et al. CellMarker: a manually curated resource of cell markers in human and mouse. *Nucleic Acids Research*. 2018;47(D1):D721-D8. doi: 10.1093/nar/gky900.
373. Sutandy FXR, Qian J, Chen C-S, Zhu H. Overview of Protein Microarrays. *Current Protocols in Protein Science*. 2013;72(1):27.1.1-.1.16. doi: <https://doi.org/10.1002/0471140864.ps2701s72>.
374. Li S, Song G, Bai Y, Song N, Zhao J, Liu J, et al. Applications of Protein Microarrays in Biomarker Discovery for Autoimmune Diseases. *Frontiers in Immunology*. 2021;12. doi: 10.3389/fimmu.2021.645632.
375. Syu G-D, Dunn J, Zhu H. Developments and Applications of Functional Protein Microarrays \*. *Molecular & Cellular Proteomics*. 2020;19(6):916-27. doi: 10.1074/mcp.R120.001936.
376. Adams G. A beginner's guide to RT-PCR, qPCR and RT-qPCR. *The Biochemist*. 2020;42(3):48-53. doi: 10.1042/bio20200034.
377. Sadeghalvad M, Khijakadze D, Orangi M, Takei F. Flow cytometric analysis of innate lymphoid cells: challenges and solutions. *Front Immunol*. 2023;14:1198310. Epub 2023/10/09. doi: 10.3389/fimmu.2023.1198310. PubMed PMID: 37809100; PubMed Central PMCID: PMC10559883.
378. Way GW, Lu H, Wang X, Zhao D, Camarena C, Sarkar D, et al. Optimization of high throughput spectral flow cytometry for immune cell profiling in mouse liver. *Liver Research*. 2023;7(3):263-71. doi: <https://doi.org/10.1016/j.livres.2023.08.001>.
379. Juncker D, Bergeron S, Laforte V, Li H. Cross-reactivity in antibody microarrays and multiplexed sandwich assays: shedding light on the dark side of multiplexing. *Current Opinion in Chemical Biology*. 2014;18:29-37. doi: <https://doi.org/10.1016/j.cbpa.2013.11.012>.

## REFERENCES

380. Ellington AA, Kullo IJ, Bailey KR, Klee GG. Antibody-Based Protein Multiplex Platforms: Technical and Operational Challenges. *Clinical Chemistry*. 2010;56(2):186-93. doi: 10.1373/clinchem.2009.127514.
381. Bustin S, Nolan T. Talking the talk, but not walking the walk: RT-qPCR as a paradigm for the lack of reproducibility in molecular research. *European Journal of Clinical Investigation*. 2017;47(10):756-74. doi: <https://doi.org/10.1111/eci.12801>.
382. Vogels CBF, Brito AF, Wyllie AL, Fauver JR, Ott IM, Kalinich CC, et al. Analytical sensitivity and efficiency comparisons of SARS-CoV-2 RT-qPCR primer-probe sets. *Nature Microbiology*. 2020;5(10):1299-305. doi: 10.1038/s41564-020-0761-6.
383. Sule WF, Oluwayelu DO. Real-time RT-PCR for COVID-19 diagnosis: challenges and prospects. *Pan Afr Med J*. 2020;35(Suppl 2):121. Epub 2020/12/08. doi: 10.11604/pamj.suppl.2020.35.24258. PubMed PMID: 33282076; PubMed Central PMCID: PMC7687508.
384. Vandesompele J, De Preter K, Pattyn F, Poppe B, Van Roy N, De Paepe A, et al. Accurate normalization of real-time quantitative RT-PCR data by geometric averaging of multiple internal control genes. *Genome Biology*. 2002;3(7):research0034.1. doi: 10.1186/gb-2002-3-7-research0034.
385. De Spiegelaere W, Dern-Wieloch J, Weigel R, Schumacher V, Schorle H, Nettersheim D, et al. Reference Gene Validation for RT-qPCR, a Note on Different Available Software Packages. *PLoS One*. 2015;10(3):e0122515. doi: 10.1371/journal.pone.0122515.
386. Ho KH, Patrizi A. Assessment of common housekeeping genes as reference for gene expression studies using RT-qPCR in mouse choroid plexus. *Scientific Reports*. 2021;11(1):3278. doi: 10.1038/s41598-021-82800-5.
387. Elisia I, Lam V, Cho B, Hay M, Li MY, Yeung M, et al. The effect of smoking on chronic inflammation, immune function and blood cell composition. *Scientific Reports*. 2020;10(1):19480. doi: 10.1038/s41598-020-76556-7.
388. Hou J, Sun Y. Role of Regulatory T Cells in Disturbed Immune Homeostasis in Patients With Chronic Obstructive Pulmonary Disease. *Frontiers in Immunology*. 2020;11. doi: 10.3389/fimmu.2020.00723.
389. Zhu X, Gadgil AS, Givelber R, George MP, Stoner MW, Scirba FC, et al. Peripheral T Cell Functions Correlate with the Severity of Chronic Obstructive Pulmonary Disease. *The Journal of Immunology*. 2009;182(5):3270-7. doi: 10.4049/jimmunol.0802622.
390. Singh R, Belchamber KBR, Fenwick PS, Chana K, Donaldson G, Wedzicha JA, et al. Defective monocyte-derived macrophage phagocytosis is associated with exacerbation frequency in COPD. *Respiratory Research*. 2021;22(1):113. doi: 10.1186/s12931-021-01718-8.

## REFERENCES

391. Trivedi A, Bade G, Madan K, Ahmed Bhat M, Guleria R, Talwar A. Effect of Smoking and Its Cessation on the Transcript Profile of Peripheral Monocytes in COPD Patients. *International Journal of Chronic Obstructive Pulmonary Disease*. 2022;17(null):65-77. doi: 10.2147/COPD.S337635.
392. Osterburg AR, Lach L, Panos RJ, Borchers MT. Unique natural killer cell subpopulations are associated with exacerbation risk in chronic obstructive pulmonary disease. *Scientific Reports*. 2020;10(1):1238. doi: 10.1038/s41598-020-58326-7.
393. Srenathan U, Steel K, Taams LS. IL-17+ CD8+ T cells: Differentiation, phenotype and role in inflammatory disease. *Immunol Lett*. 2016;178:20-6. Epub 2016/05/14. doi: 10.1016/j.imlet.2016.05.001. PubMed PMID: 27173097; PubMed Central PMCID: PMC5046976.
394. Vazquez MI, Catalan-Dibene J, Zlotnik A. B cells responses and cytokine production are regulated by their immune microenvironment. *Cytokine*. 2015;74(2):318-26. doi: <https://doi.org/10.1016/j.cyto.2015.02.007>.
395. Song D, Yan F, Fu H, Li L, Hao J, Zhu Z, et al. A cellular census of human peripheral immune cells identifies novel cell states in lung diseases. *Clinical and Translational Medicine*. 2021;11(11):e579. doi: <https://doi.org/10.1002/ctm2.579>.
396. Veith M, Tüffers J, Peychev E, Klemmer A, Kotke V, Janciauskiene S, et al. The Distribution of Alpha-1 Antitrypsin Genotypes Between Patients with COPD/Emphysema, Asthma and Bronchiectasis. *International Journal of Chronic Obstructive Pulmonary Disease*. 2020;15(null):2827-36. doi: 10.2147/COPD.S271810.
397. Colarusso C, Terlizzi M, Molino A, Pinto A, Sorrentino R. Role of the inflammasome in chronic obstructive pulmonary disease (COPD). *Oncotarget*. 2017;8(47):81813-24. Epub 2017/11/16. doi: 10.18632/oncotarget.17850. PubMed PMID: 29137224; PubMed Central PMCID: PMC5669850.
398. Leuzzi G, Galeone C, Taverna F, Suatoni P, Morelli D, Pastorino U. C-reactive protein level predicts mortality in COPD: a systematic review and meta-analysis. *European Respiratory Review*. 2017;26(143):160070. doi: 10.1183/16000617.0070-2016.
399. Iizuka T, Ishii Y, Itoh K, Kiwamoto T, Kimura T, Matsuno Y, et al. Nrf2-deficient mice are highly susceptible to cigarette smoke-induced emphysema. *Genes to Cells*. 2005;10(12):1113-25. doi: <https://doi.org/10.1111/j.1365-2443.2005.00905.x>.
400. Arora A, Singh A. Exploring the role of neutrophils in infectious and noninfectious pulmonary disorders. *International Reviews of Immunology*. 2024;43(1):41-61. doi: 10.1080/08830185.2023.2222769.
401. Meijer M, Rijkers GT, van Overveld FJ. Neutrophils and emerging targets for treatment in chronic obstructive pulmonary disease. *Expert Review of Clinical Immunology*. 2013;9(11):1055-68. doi: 10.1586/1744666X.2013.851347.



## REFERENCES

402. Qiu Y, Zhu J, Bandi V, Atmar RL, Hattotuwa K, Guntupalli KK, et al. Biopsy Neutrophilia, Neutrophil Chemokine and Receptor Gene Expression in Severe Exacerbations of Chronic Obstructive Pulmonary Disease. *American Journal of Respiratory and Critical Care Medicine*. 2003;168(8):968-75. doi: 10.1164/rccm.200208-794OC. PubMed PMID: 12857718.
403. Mortaz E, Givi ME, Da Silva CA, Folkerts G, Redegeld FA. A relation between TGF-beta and mast cell tryptase in experimental emphysema models. *Biochim Biophys Acta*. 2012;1822(7):1154-60. Epub 2012/04/07. doi: 10.1016/j.bbadis.2012.03.006. PubMed PMID: 22481124.
404. Qiagen. What are the effects of low A260/A230 ratios in RNA preparations on downstream applications? 2024 [cited 2024 March]. Available from: <https://www.qiagen.com/us/resources/faq?id=c59936fb-4f1e-4191-9c16-ff083cb24574><=en.
405. Allam VSRR, Faiz A, Lam M, Rathnayake SNH, Ditz B, Pouwels SD, et al. RAGE and TLR4 differentially regulate airway hyperresponsiveness: Implications for COPD. *Allergy*. 2021;76(4):1123-35. doi: <https://doi.org/10.1111/all.14563>.
406. De Cunto G, Cavarra E, Bartalesi B, Lucattelli M, Lungarella G. Innate Immunity and Cell Surface Receptors in the Pathogenesis of COPD: Insights from Mouse Smoking Models. *International Journal of Chronic Obstructive Pulmonary Disease*. 2020;15(null):1143-54. doi: 10.2147/COPD.S246219.
407. Cicko S, Lucattelli M, Müller T, Lommatzsch M, De Cunto G, Cardini S, et al. Purinergic Receptor Inhibition Prevents the Development of Smoke-Induced Lung Injury and Emphysema. *The Journal of Immunology*. 2010;185(1):688-97. doi: 10.4049/jimmunol.0904042.
408. Tam A, Churg A, Wright JL, Zhou S, Kirby M, Coxson HO, et al. Sex Differences in Airway Remodeling in a Mouse Model of Chronic Obstructive Pulmonary Disease. *American Journal of Respiratory and Critical Care Medicine*. 2015;193(8):825-34. doi: 10.1164/rccm.201503-0487OC.
409. Hsia CCW, Hyde DM, Ochs M, Weibel ER. An Official Research Policy Statement of the American Thoracic Society/European Respiratory Society: Standards for Quantitative Assessment of Lung Structure. *American Journal of Respiratory and Critical Care Medicine*. 2010;181(4):394-418. doi: 10.1164/rccm.200809-1522ST. PubMed PMID: 20130146.
410. Knudsen L, Weibel ER, Gundersen HJG, Weinstein FV, Ochs M. Assessment of air space size characteristics by intercept (chord) measurement: an accurate and efficient stereological approach. *Journal of Applied Physiology*. 2010;108(2):412-21. doi: 10.1152/jappphysiol.01100.2009. PubMed PMID: 19959763.

## REFERENCES

411. Zhan X, Long Y, Zhan X, Mu Y. Consideration of Statistical vs. Biological Significances for Omics Data-Based Pathway Network Analysis. *Med One*. 2017;2(1):e170002. doi: 10.20900/mo.20170002.
412. Francis NA, Gillespie D, Wootton M, White P, Bates J, Richards J, et al. Clinical Features and C-Reactive Protein as Predictors of Bacterial Exacerbations of COPD. *International Journal of Chronic Obstructive Pulmonary Disease*. 2020;15(null):3147-58. doi: 10.2147/COPD.S265674.
413. Houlst G, Gillespie D, Wilkinson TMA, Thomas M, Francis NA. Biomarkers to guide the use of antibiotics for acute exacerbations of COPD (AECOPD): a systematic review and meta-analysis. *BMC Pulmonary Medicine*. 2022;22(1):194. doi: 10.1186/s12890-022-01958-4.
414. Phillips R, Stanton H, Singh-Mehta A, Gillespie D, Bates J, Gal M, et al. C-reactive protein-guided antibiotic prescribing for COPD exacerbations: a qualitative evaluation. *British Journal of General Practice*. 2020;70(696):e505-e13. doi: 10.3399/bjgp20X709865.
415. Wei XM, Kim HS, Kumar RK, Heywood GJ, Hunt JE, McNeil HP, et al. Effects of cigarette smoke on degranulation and NO production by mast cells and epithelial cells. *Respir Res*. 2005;6(1):108. Epub 2005/09/20. doi: 10.1186/1465-9921-6-108. PubMed PMID: 16168067; PubMed Central PMCID: PMCPMC1262779.
416. Kliment CR, Gosens R. Chymase-1: a "MAST"-er switch in COPD? *European Respiratory Journal*. 2022;60(6):2201356. doi: 10.1183/13993003.01356-2022.
417. Higham A, Dungwa J, Pham T-H, McCrae C, Singh D. Increased mast cell activation in eosinophilic chronic obstructive pulmonary disease. *Clinical & Translational Immunology*. 2022;11(9):e1417. doi: <https://doi.org/10.1002/cti2.1417>.
418. Qiu SL, Sun QX, Zhou JP, Tang HJ, Chen YQ, Chen FS, et al. IL-27 mediates anti-inflammatory effect in cigarette smoke induced emphysema by negatively regulating IFN-gamma producing cytotoxic CD8(+) T cells in mice. *Eur J Immunol*. 2022;52(2):222-36. Epub 2021/09/25. doi: 10.1002/eji.202049076. PubMed PMID: 34559883.
419. March TH, Wilder JA, Esparza DC, Cossey PY, Blair LF, Herrera LK, et al. Modulators of cigarette smoke-induced pulmonary emphysema in A/J mice. *Toxicol Sci*. 2006;92(2):545-59. Epub 2006/05/16. doi: 10.1093/toxsci/kfl016. PubMed PMID: 16699168.
420. Kukrety SP, Parekh JD, Bailey KL. Chronic obstructive pulmonary disease and the hallmarks of aging. *Lung India*. 2018;35(4):321-7. Epub 2018/07/05. doi: 10.4103/lungindia.lungindia\_266\_17. PubMed PMID: 29970772; PubMed Central PMCID: PMC6034372.
421. Janssens J, Pache J, Nicod L. Physiological changes in respiratory function associated with ageing. *European Respiratory Journal*. 1999;13(1):197-205. doi: 10.1034/j.1399-3003.1999.13a36.x.

## REFERENCES

422. Savale L, Chaouat A, Bastuji-Garin S, Marcos E, Boyer L, Maitre B, et al. Shortened Telomeres in Circulating Leukocytes of Patients with Chronic Obstructive Pulmonary Disease. *American Journal of Respiratory and Critical Care Medicine*. 2009;179(7):566-71. doi: 10.1164/rccm.200809-1398OC. PubMed PMID: 19179485.
423. Lee J, Sandford AJ, Connett JE, Yan J, Mui T, Li Y, et al. The Relationship between Telomere Length and Mortality in Chronic Obstructive Pulmonary Disease (COPD). *PLoS One*. 2012;7(4):e35567. doi: 10.1371/journal.pone.0035567.
424. Kuilman T, Michaloglou C, Mooi WJ, Peeper DS. The essence of senescence. *Genes & development*. 2010;24(22):2463-79.
425. Tsuji T, Aoshiba K, Nagai A. Alveolar Cell Senescence in Patients with Pulmonary Emphysema. *American Journal of Respiratory and Critical Care Medicine*. 2006;174(8):886-93. doi: 10.1164/rccm.200509-1374OC. PubMed PMID: 16888288.
426. Natalini JG, Singh S, Segal LN. The dynamic lung microbiome in health and disease. *Nature Reviews Microbiology*. 2023;21(4):222-35. doi: 10.1038/s41579-022-00821-x.
427. Dickson RP, Erb-Downward JR, Freeman CM, McCloskey L, Beck JM, Huffnagle GB, et al. Spatial Variation in the Healthy Human Lung Microbiome and the Adapted Island Model of Lung Biogeography. *Annals of the American Thoracic Society*. 2015;12(6):821-30. doi: 10.1513/AnnalsATS.201501-029OC. PubMed PMID: 25803243.
428. Segal LN, Clemente JC, Tsay J-CJ, Koralov SB, Keller BC, Wu BG, et al. Enrichment of the lung microbiome with oral taxa is associated with lung inflammation of a Th17 phenotype. *Nature Microbiology*. 2016;1(5):16031. doi: 10.1038/nmicrobiol.2016.31.
429. Dickson RP, Erb-Downward JR, Falkowski NR, Hunter EM, Ashley SL, Huffnagle GB. The Lung Microbiota of Healthy Mice Are Highly Variable, Cluster by Environment, and Reflect Variation in Baseline Lung Innate Immunity. *American Journal of Respiratory and Critical Care Medicine*. 2018;198(4):497-508. doi: 10.1164/rccm.201711-2180OC. PubMed PMID: 29533677.
430. Sethi S, Maloney J, Grove L, Wrona C, Berenson CS. Airway Inflammation and Bronchial Bacterial Colonization in Chronic Obstructive Pulmonary Disease. *American Journal of Respiratory and Critical Care Medicine*. 2006;173(9):991-8. doi: 10.1164/rccm.200509-1525OC. PubMed PMID: 16474030.
431. Tufvesson E, Bjermer L, Ekberg M. Patients with chronic obstructive pulmonary disease and chronically colonized with *Haemophilus influenzae* during stable disease phase have increased airway inflammation. *International Journal of Chronic Obstructive Pulmonary Disease*. 2015;10(null):881-9. doi: 10.2147/COPD.S78748.
432. Wang Z, Locantore N, Haldar K, Ramsheh MY, Beech AS, Ma W, et al. Inflammatory Endotype-associated Airway Microbiome in Chronic Obstructive Pulmonary Disease Clinical Stability and Exacerbations: A

## REFERENCES

---

Multicohort Longitudinal Analysis. *American Journal of Respiratory and Critical Care Medicine*. 2021;203(12):1488-502. doi: 10.1164/rccm.202009-3448OC. PubMed PMID: 33332995.

433. Aldonyte R, Bagdonas E, Raudoniute J, Bruzauskaite I. Novel aspects of pathogenesis and regeneration mechanisms in COPD. *International Journal of Chronic Obstructive Pulmonary Disease*. 2015:995. doi: 10.2147/copd.s82518.

## APPENDIX A: BSU STUDY PROTOCOL

**Study protocol (information required during covid-19 pandemic in red)**

For use on a study-by-study basis to supplement Section E protocols of a PPL.

- Please submit to BSU (via [bsu@nottingham.ac.uk](mailto:bsu@nottingham.ac.uk)) **before** you place your order.
- Information provided is used by BSU to facilitate collegial working, enable us to adapt to differing study requirements, and maintain high levels of animal care & welfare.
- BSU do not formally authorise Study Protocols; in other words, submitting this protocol does not remove the individual responsibility of the PIL holder to check that appropriate authorities are in place before conducting a procedure.
- Please **keep a copy of the Study Protocol in animal holding areas** together with other relevant animal records; these may be examined by the Inspector. Please remove once the study is over (initials instead of full names may be used on these versions).
- Feel free to add in additional sections according to your research group requirements.

**General study information**

Title of study	Establishing the pathophysiological impact of cigarette smoke extract in mice as a model for Chronic Obstructive Pulmonary Disease
Study reference (yours) <small>Include this on your cage card(s) AND in the 'Special Instructions box' when ordering animals on LabTracks</small>	Protocol 1: pilot study
Name of primary PILh	Adam Watkins
Names of other PILhs involved	Laura Bartlett
Grant number	RS86JF
Grant expiry date	30/09/23

**Home office licence details**

PPL holder & licence number	Adam Watkins; PP5215372
Section E protocol number(s)	1
Severity Limit	Moderate
Details of re-use/continued use:	None

**Brief aim(s) of the study**

*Note that these must coincide with the PPL objectives described in Section D of the PPL*

The aim of this study is to examine the pathophysiological development of chronic obstructive pulmonary disease (COPD) in adult male and female mice in response to a cigarette smoke extract. Currently there is a paucity of data regarding an optimal dosing regimen, both duration and concentration of extract exposure, to create a phenotype representative of COPD in humans. Furthermore, there is limited data on potential sex-specific differences in disease progression between males and females. In addition, few studies define the whole-body responses to cigarette smoke extract and the role of the peripheral immune system.

In light of the lack of detailed information from existing mouse models, this study will take the form of a pilot study to define the minimal dosing regimen (concentration and duration) to mimic phenotypic changes (lung damage, vascular smooth muscle remodelling, immune cell activation) of moderate COPD in humans.

**Animal Details**

Species/strain	Mouse; C57BL6/J	Total number	200
Sex	Males and females	Age or weight	Typically 8-week-old
Arrival date	From November 2021 onwards	Study duration	Throughout the remainder of the project

List any special requirements relating to husbandry and care

Males and females will be group housed unless welfare conditions (i.e. over grooming, fighting) require individuals to be isolated. Animals will be monitored daily for signs of ill health.

## Description of the experiment and any supporting justification

*Describe your experimental design (groups, treatments etc.) using the table below, if helpful. Please also describe your rationale for group sizes; for this you may copy relevant sections from the PPL Reduction section.*

To ensure our pilot study has the minimal impact on animal welfare, we will adopt a system in which mice (males and females) are initially exposed to the lowest concentration of extract (1%) and for the shortest duration (1 week) while under light anaesthesia. Animals will be exposed to the cigarette smoke extract three times a week via an intranasal route and will be compared against control (culture medium only) animals. Mice will be split into separate groups for blood collection, which will take place on days between dosing. We will collect a saphenous vein blood sample for the measurement of circulating inflammatory markers and immune cells, where saphenous vein sampling cannot be completed, tail vein sampling will be taken instead. Prior to commencing the pilot study, all mice will go through a 5-day conditioning regimen to acclimatise to restraint methods for blood sampling (see table 1 below). A maximal volume of typically 30  $\mu$ L will be taken weekly from each mouse to ensure adherence to NC3Rs and LASA guidelines for blood sampling. For saphenous vein bleeds, leg used to take sample will be alternated on a weekly basis to allow full recovery from the previous sampling. Full welfare checks will be performed a minimum of once to twice per week to monitor for signs of adverse health effects.

We anticipate an exposure period of approximately 12 weeks to simulate a moderate COPD phenotype, and will expose animals to either 0% (saline/culture medium vehicle alone), 1% or 3% cigarette smoke extract based upon findings from our human cell culture models and previous literature. All mice will be closely monitored throughout the duration of the study for adverse welfare effects, and the study will be ended no later than 12 weeks of exposure based on indications of COPD phenotype. Based on these parameters, we propose a maximal number of mice required under this pilot study to be 200 (100 males and 100 females).

Mice (both males and females) will be used in groups of 8 animals and compared to a control group who are exposed to the saline/culture medium vehicle alone (see table 2 below). The appropriate number of mice to be used has been determined through the use of the NC3R's online Experimental Design Assistant and existing published literature of mouse models of cigarette smoke extract. Pathophysiological data on lung morphology, circulating inflammatory markers and immune cell populations (all parameters that will be assessed under this Licence) have been taken from relevant publications (He et al, 2015, Tob Induc Dis. 13(1):6; Tabata et al. 2015. Int Immunopharmacol. 25(2):511-7; Braber et al. 2011. Am J Respir Crit Care Med. 185(8):817-24).

At specific time points, animals will be culled by overdose of anaesthetic via intraperitoneal injection for the isolation of tissues, bronchoalveolar lavage fluid and blood samples. These will be processed and analysed to determine the state of COPD disease progression. Typically, we will define tissue morphology, lung vascular smooth muscle cell remodelling, immune cell profiles and activation status and tissue gene/protein expression. If the desired COPD phenotype and no adverse welfare

effects are observed, the study will be repeated with new groups of mice using higher doses of cigarette smoke extract up to 10% over a 12-week period.

**Table 1: Schedule of conditioning regimen**

Day	Details of conditioning or reward
1	Reward placed in cages
2	Mice handled and shown restraints, allowed to freely enter restraint, reward placed in cages following handling
3	Mice handled and shown restraints, allowed to freely enter restraint, reward placed in cages following handling
4	Mice handled and placed into restraint, hind limb restrained, reward placed in cages following handling
5	Mice handled and placed into restraint, hind limb restrained, reward placed in cages following handling

**Table 2: Table of proposed experimental groups**

Experimental group ID	Extract dose	Number of mice
Never-smoker Males (NSM)	0%	4
Never-smoker Females (NSF)	0%	4
Light-smoker Males (LSM)	1%	4
Light-smoker Females (LSF)	1%	4
Heavy-smoker Males (HSM)	3%	4
Heavy-smoker Females (HSF)	3%	4

Group	Treatment	Approx n =
Adult males and females	<p>Animals will be exposed to cigarette smoke extract while under light anaesthesia. Following dosing, All animals will be allowed to recover in a warming chamber (typically for around 30 minutes) and monitored before returning to their original cages.</p> <p>The dosing regimen (both duration and concentration) may be increased incrementally dependent on results observed. We anticipate starting at a concentration of 1% for 3 weeks and then increasing incrementally by 1% and one additional week to a maximum of 10% for 12 weeks.</p>	200 (100 males and 100 females)




### Experimental procedures and sequence of events

*For example, surgical procedures, administration of compounds, behavioural tests, blood sampling. If these change during a study please amend this page and write your initials.*

*Please also highlight where records/monitoring sheets will be used (e.g. post-op monitoring sheets, weight charts). These should be kept together with the Study Protocol in the holding room.*

#### ADDITIONAL REQUIREMENTS DURING THE COVID-19 PANDEMIC

- Please provide dates and times you will need to access BSU
- Highlight times when you'll need to access holding rooms to do anything other than remove animals (e.g. health checks, weighing/monitoring, injections)
- If the protocol is approved, book theatres, procedure/behaviour rooms straight away

In light of the lack of detailed published literature on which to establish an optimal experimental set of concentration and dose parameters, we propose to conduct an initial pilot study. The aim of this pilot study will be to define the minimal dose necessary to observe pathophysiological changes in line with patients presenting with moderate COPD.

Adult (8-10 week old) male and female C57BL6/J mice will be housed in single sex groups and assigned to one of 6 study groups (Table 2). Mice will be exposed to the different cigarette smoke extract concentrations via an intranasal route while under mild anaesthesia three times per week on Mondays, Wednesdays and Fridays between 10 am – 11 am (see figure 1 below, from 05/06/23 until 11/09/23). The cigarette smoke extract will be created regularly within our research lab, batch tested and sterile filtered and brought to the BSU diluted in RPMI culture medium. Each extract will be prepared fresh on the day of dosing a maximum of 3 hours before use and will be adjusted to room temperature and neutral pH prior to administration. Animals will receive either a culture medium vehicle alone (control group) or the cigarette smoke extract at either 1% or 3% concentration based on findings from human cell culture models. Following exposure to the extract, all animals will be placed within a warming chamber and allowed to recover fully (typically for around 30 minutes). During this time animals will be continuously monitored for signs of respiratory distress.

In order to minimise workload on PIL holders, all animals will be allocated to an experimental group and dosing will begin in a staggered fashion. For this, 2 animals from each dose group (see table 2 above) will begin receiving doses of allocated cigarette smoke extract or culture medium from Monday 5<sup>th</sup> June 2023 for 12 weeks. This group will be designated Group 1 (n = 12). The remaining mice will begin the dosing period a week later on Monday 12<sup>th</sup> June 2023, and will be designated Group 2 (n = 12).

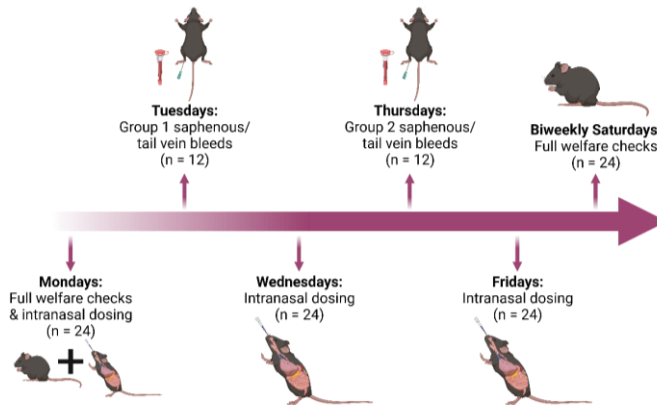
Animal health and welfare will be monitored daily for one to two weeks from the start of the experiment, with the measurement of body weight and overall appearance and demeanour checks (between 9 am – 10 am, from 05/06/23 until 16/06/23). Records of welfare checks will be taken physically and electronically through the use of score sheets and databases made available to PIL holders under the PPL. Full welfare checks will occur a minimum of once to twice per week prior to the administration of anaesthesia or blood sampling (typically Mondays and Saturdays between 9 am – 10 am, from 05/06/23 until 11/09/23). This will occur on the same day of each week and will only involve one member of our team entering the BSU to take these measurements. These activities will occur within the holding room or a designated procedure room if dosing or sampling is to take place following checks.

Once per week, blood samples will be taken from each mouse to analyse peripheral immune cells and inflammation markers. This will occur in a staggered format in a procedure room, with samples taken weekly either on Tuesdays (9 am – 10 am) or Thursdays (9 am – 10 am) (see figure 1, maximum 12 mice per group from 05/06/23 - 11/09/23). Approximately 20  $\mu$ L blood ( $\geq 10 \mu$ L and  $\leq 30 \mu$ L) will be taken typically via the saphenous vein or from the tail vein if saphenous blood sampling is not possible. For saphenous vein sampling, the back of the leg will be shaved and a local anaesthetic (e.g. EMLA cream) will be applied to the sampling area 30 minutes prior to sampling. Mice will be restrained using a 50 mL falcon tube with 1/3 of the end cut off to allow ease of breathing without anaesthesia for the duration of this procedure. All mice will be acclimatised to the necessary restraint methods through a conditioning program prior to the start of the dosing period (see table 1 above). The area for sampling will be sterilised with an antiseptic wipe and wiped clean with dry gauze, after which a 25G needle will be inserted into the saphenous vein. Blood will be collected through the use of a Gilson pipette with heparinised P-100 tips and gentle pressure will be applied to the wound after correct amount has been collected. Cessation of bleeding, and the appearance of clotting will be confirmed before the animal is removed from restraint and returned to their cage. The leg used for sampling will be alternated on a weekly basis to allow for recovery from the previous week's sampling. In the case of tail vein bleeds, mice will have a local anaesthetic (e.g. EMLA cream) applied approximately 30 minutes prior to sampling, after which they will be transferred to a warming box (37°C) for approximately 10 minutes. Once the tail vein has been dilated mice will be restrained and the same sampling procedure as described above will take place using the tail vein.

The overall exposure period is estimated to take no more than 12 weeks, though the study may be ended earlier if significant elevation of peripheral immune cell activation and inflammatory marker profiles indicative of moderate COPD phenotype are detected. Additionally, the study will be stopped at any point if investigators receive indication that continuation of the study would endanger the welfare of the animals or cause severity limit to exceed a moderate phenotype, either through welfare checks or through analysis of blood samples.

At the end of the defined duration period (maximum 12 weeks), mice will be culled by overdose of anaesthetic via intraperitoneal injection, with 2 members of our team required for rapid collections. This activity will take place in a designated procedure room. Tissues will be collected for the

analysis of established experimental endpoints typically consisting of; (i) elevated lung damage (as defined by significant increases in histological assessment of alveolar mean Linear Intercept ( $Li$ ) and Destructive Index



( $Di$ ) parameters); (ii) statistically significant remodelling and extracellular matrix deposition of the lung vasculature; (iii) decrease in blood oxygen saturation to 90%; (iv) significant infiltration of lung immune cell populations into the lung tissue and; (v) elevated peripheral immune cell activation and inflammatory mediator profiles.

**Figure 1: Weekly dosing and sampling schedule for duration of exposure period**

*Please describe what provisions are in place to complete the study should anybody be required to self-isolate:*

Our team is comprised of two members, Laura Bartlett and Dr Adam Watkins, who are both capable of continuing/completing the study should the other member be required to self-isolate.

*If more than two people from the group need to be in BSU at any one time give reasons:*

On most occasions, it will not be necessary for both members of our team to be in the BSU at any one time. However, during periods of animal dissection, both members may be required to facilitate the collection, weighting and processing of the tissues in a timely manner.

## Termination

Choose from the options below

Schedule 1 method Please specify	Overdose of anaesthetic via an intraperitoneal injection
Non-schedule 1 method Please specify	
Released from ASPA Needs NVS authorisation	
Animals to enter food chain Give withdrawal periods of any substances administered before slaughter (Sutton Bonington only)	

## Specific health & safety or animal health risks

Does your study require any of the following? (see links for further information and guidance)

### Designated containment facilities

Please detail below the requirements for any work with infectious biological agents or genetically-modified micro-organisms that may require designated containment facilities.

<http://www.nottingham.ac.uk/safety/documents/bio-gm.pdf>

Required? N

### Health & safety assessment (including COVID-19 RA)

COSHH & risk assessment forms (additional to the BSU risk assessment for Laboratory Animal Allergy) must be attached and approved by the BSU Departmental Safety Officer before the study commences if work presents a hazard to health, e.g. use of potential carcinogens. This includes pathogens/toxins, especially those listed under Schedule 5 of the Anti-terrorism, Crime and Security Act 2001, such as tetrodotoxin.

<http://www.nottingham.ac.uk/safety/policies-and-guidance/hazardous-substances/coshh/coshh.aspx>

<https://www.nottingham.ac.uk/safety/documents/bio-security-pathogens.pdf>

Required? N

### GA risk assessment

GA risk assessment forms are required for work with genetically altered (GA) animals, GA micro-organisms or where modification of genetic material will occur, e.g. using viral vectors. Copies of approved and signed off forms must be attached to this proposal and provided to the BSU Biological Safety Officer before the study commences.

<http://www.nottingham.ac.uk/safety/policies-and-guidance/bio-gm/gm.aspx>

Required? N

### Licence under the Specified Animal Pathogens Order (SAPO) regulations

If specified animal pathogens are part of the study, copies of any SAPO Licences required for working with the pathogens must be forwarded to the BSU Named Veterinary Surgeon for approval of this work before the study commences.

<http://www.hse.gov.uk/biosafety/sapo.htm>;

<http://www.hse.gov.uk/pubns/priced/hsg280.pdf>

Required? N

### Licence to work with controlled drugs

Separate licences are required for work with controlled drugs listed under schedule 1 of the Misuse of Drugs Act (e.g. cannabis, LSD). Note that the University does not hold a generic licence and a separate licence will need to be obtained by any research group that wishes to use such drugs. The relevant licence must be in place, and a copy lodged with BSU, before work commences.

Note that University research departments generally do not require a licence to possess drugs in schedules 2-5.  
<https://www.gov.uk/guidance/controlled-drugs-licences-fees-and-returns>  
Required? N

### Experimental protocol approval

I confirm, on the basis of re-examination of the appropriate project licence authority, that the purpose of the experiment is as described in **Section D** of the project licence detailed above.

The species and proposed techniques are specifically authorised in the **Section E** protocol(s) and authority is in place with respect to the personal licenses of individuals conducting the procedures.

Humane killing will be in accordance with Schedule 1 (revised 1<sup>st</sup> Jan 2013) or by methods listed in the appropriate licences and will only be conducted by competent individuals named on the University of Nottingham Schedule 1 register.

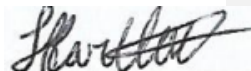
Name of PPL holder: Adam Watkins  
Date: 31/05/2023

Signature:



Name of PIL holder: Laura Bartlett  
Date: 31/05/2023

Signature:



APPENDIX B: ANIMAL WELFARE MONITORING SHEET

Mouse No.	Experiment ID	Cage No.	Sheet No.	Species/Strain	PPL holder / No.	PIL holder	Protocol No.	Model

80 % Limit	Date											
<b>Body Weight (g)</b>												
Animal presenting clinical abnormalities? (Y/N) *												
Initials												

\* If yes complete the table below. 0 = not present, 1= mild, 2= moderate and 3= severe unless specified.

<b>Normal Activity (Y/N)</b>												
<b>Body Condition Score</b> Scheduled 1 cull if score is 1												
<b>Diarrhoea (Y/N)</b> Scheduled 1 cull if Yes												
<b>Respiration Rate</b> 0-not present, 1-mild increase, 2-moderate increase, 3-breathless												
<b>Laboured breathing</b> 0 = not present, 1- intermittent, 2-persistent, 3-significant respiratory effort												
<b>Hunched (0-3)</b>												
<b>Piloerection (0-3)</b>												
<b>Dehydration (0-3)</b> 0-not present, 1-tenting + rapid return, 2-tenting + delayed return, 3-persistent tenting												
<b>Cumulative Health score</b> Sched1 if score greater than 12												

## APPENDIX C: STAIN INDEXES

For all markers selected for phenotyping, splenocytes were not subjected to activation and stained immediately following isolation or defrosting. CD45 (APC-Fire810) had the highest stain index at 1:160, but to ensure consistency across the panel a final concentration of 2 µg/mL per test (i.e. 1:100 dilution) was selected for future work (figure C.1).

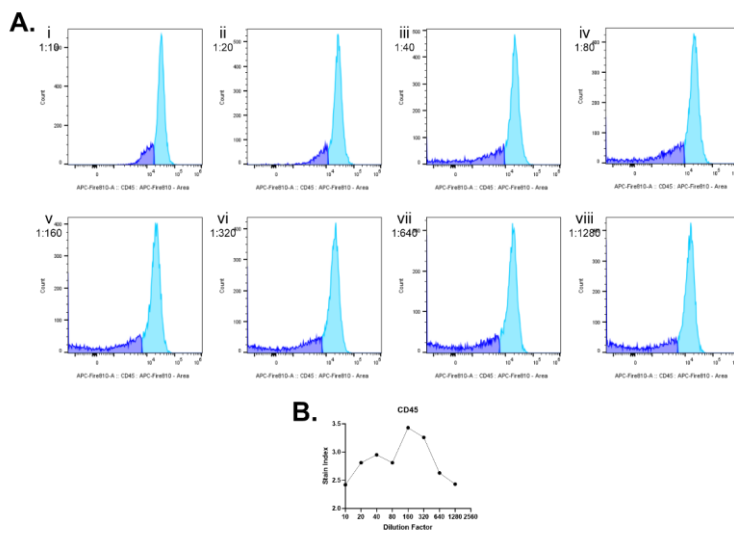


**Figure C.1:- Stain index histograms and curve for CD45 (APC Fire810).** Cells were gated according to the lymphocyte gating strategy defined in figure 3.2.1A. Histogram overlays were prepared for each dilution factor comprising of negative population (dark blue peak) and positive population (light blue peak). Dilutions were prepared in a doubling series ranging from 1:10 (A.i) to 1:1280 (A.viii). Median and standard deviation data was exported to excel and stain indexes were calculated and plotted as a standard curve in GraphPad Prism (B).

Due to difficulties presented in determining ideal concentration for CD3 (BUV496), both histograms and dot plots were created to determine location of positive and negative populations. As shown in figure C.2A, histograms appear to show nonspecific binding and lack of distinction between positive and negative populations, although the stain index curve follows a standard curve trend (figure C.2B). To confirm that gates were in the correct positions to capture positive and negative populations,

the same data was examined on SSC-A dot plots. As shown in figure C.3A, there is little distinction between the positive and negative CD3 populations, with overstaining being observed at the lowest dilutions (A.i and A.ii). However, as dilution factor increased a positively stained population could be observed (A.iv and A.v), though this distinction was lost at the highest dilution factors (A.vii and A.viii). These trends followed the same staining pattern as observed on histograms in figure C.2A, and it was therefore concluded that the stain index curves were accurate for staining efficiency (figure C.2B and C.3B). As for CD45, 2  $\mu\text{g}/\text{mL}$  per test (i.e. 1:100 dilution) was selected for CD3.

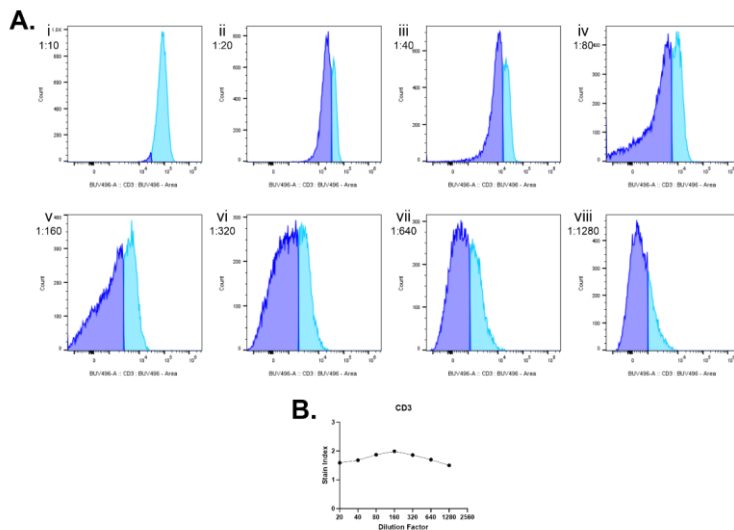


**Figure C.2:- Stain index histograms and curve for CD3 (BUV496).** Cells were gated according to the lymphocyte gating strategy defined in figure 3.2.1A. Histogram overlays were prepared for each dilution factor comprising of negative population (dark blue peak) and positive population (light blue peak). Dilutions were prepared in a doubling series ranging from 1:10 (A.i) to 1:1280 (A.viii). Median and standard deviation data was exported to excel and stain indexes were calculated and plotted as a standard curve in GraphPad Prism (B). Stain index for 1:10 dilution was excluded due to value exceeding limits of the curve.



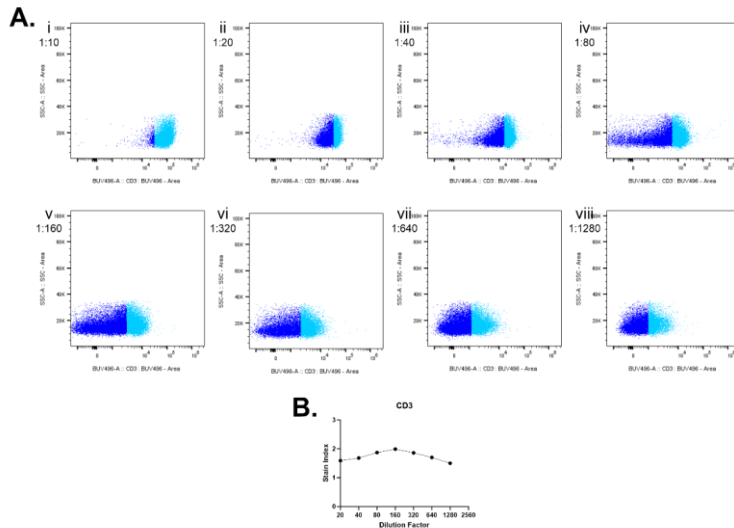


**Figure C.3:- Dot plots and stain index curve for CD3 (BUV496).** Cells were gated according to the lymphocyte gating strategy defined in figure 3.2.1A. Dot plot overlays were prepared for each dilution factor comprising of negative population (dark blue) and positive population (light blue) to ascertain population distinctions due to difficulties identifying populations via histograms. These plots confirmed the accuracy of stain index values and ensured the correct populations were gated for. Stain index for 1:10 dilution was excluded due to value exceeding limits of the curve, and dot plots confirmed overstaining.

CD4 (FITC) provides an ideal example of typical stain index profiles, where negative and positive populations can be clearly defined and separation occurs as dilution factor increases (figure C.4). Based on these results a concentration of 0.5  $\mu\text{g}/\text{mL}$  per test (i.e. 1:1000 dilution) was determined for CD4.

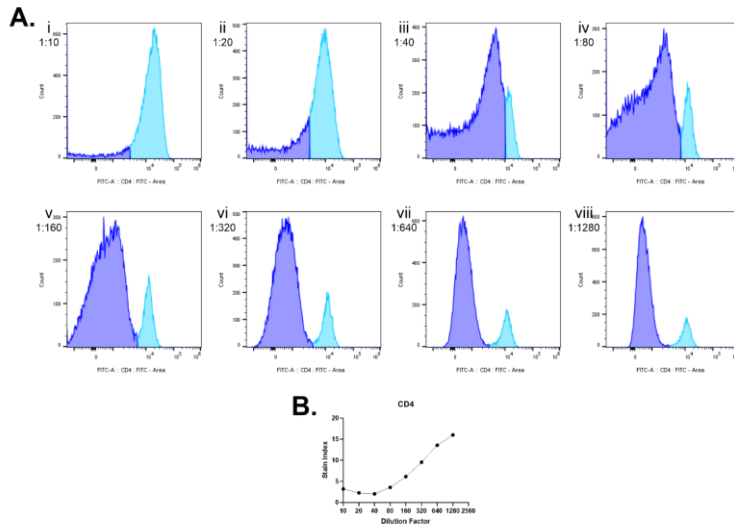


**Figure C.4:- Stain index histograms and curve for CD4 (FITC).** Cells were gated according to the lymphocyte gating strategy defined in figure 3.2.1A. Histogram overlays were prepared for each dilution factor comprising of negative population (dark blue peak) and positive population (light blue peak). Dilutions were prepared in a doubling series ranging from 1:10 (A.i) to 1:1280 (A.viii). Median and standard deviation data was exported to excel and stain indexes were calculated and plotted as a standard curve in GraphPad Prism (B).

Similar profiles were observed for CD8a (APC/Cy5.5), though as dilution factor exceeded 1:160 the separation between positive and negative peaks began to decrease (figure C.5). As a result, a concentration of 1  $\mu\text{g}/\text{mL}$  per test (i.e. 1:100 dilution) was determined.

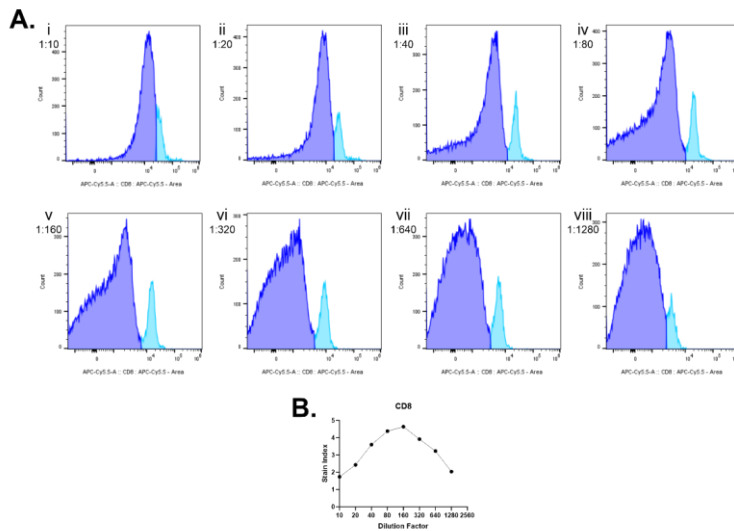


**Figure C.5:- Stain index histograms and curve for CD8 (APC-Cy5.5).** Cells were gated according to the lymphocyte gating strategy defined in figure 3.2.1A. Histogram overlays were prepared for each dilution factor comprising of negative population (dark blue peak) and positive population (light blue peak). Dilutions were prepared in a doubling series ranging from 1:10 (A.i) to 1:1280 (A.viii). Median and standard deviation data was exported to excel and stain indexes were calculated and plotted as a standard curve in GraphPad Prism (B).

Ideal concentration for ROR $\gamma$ t (PE/Cy5.5) was determined to be 5  $\mu$ g/mL per test (i.e. 1:100 dilution) (figure C.6). Stain indexes for FOXP3 were also generated (figure C.7), but it was later determined that much of the positive staining was a result of nonspecific binding. Following advice from suppliers of the conjugation kit used to generate this antibody, we were made aware that the conjugate was not suitable for intracellular staining and thus FOXP3 was dropped from the panel (figure C.7).

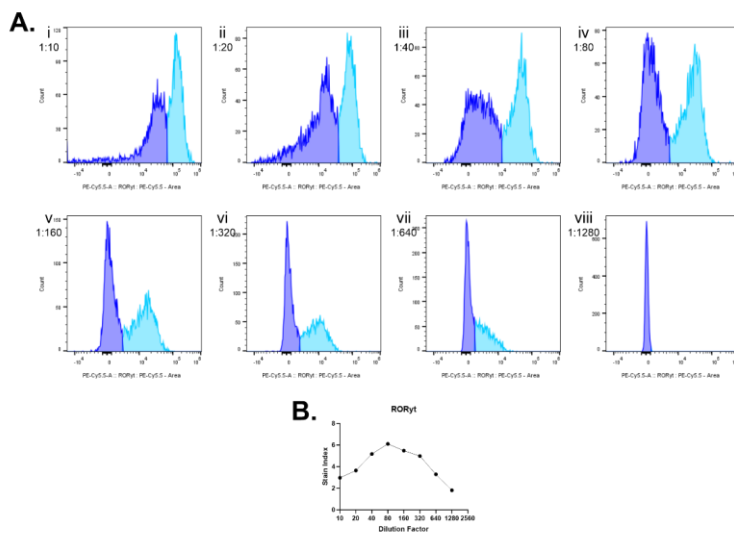


**Figure C.6:- Stain index histograms and curve for RORyt (PE-Cy5.5).** Cells were gated according to the lymphocyte gating strategy defined in figure 3.2.1A. Histogram overlays were prepared for each dilution factor comprising of negative population (dark blue peak) and positive population (light blue peak). Dilutions were prepared in a doubling series ranging from 1:10 (A.i) to 1:1280 (A.viii). Median and standard deviation data was exported to excel and stain indexes were calculated and plotted as a standard curve in GraphPad Prism (B).

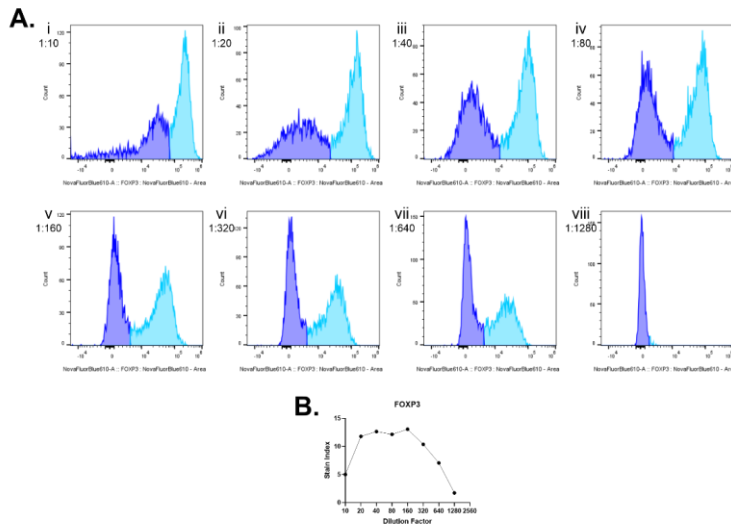


**Figure C.7:- Stain index histograms and curve for FOXP3 (NovaFluorBlue610).** Cells were gated according to the lymphocyte gating strategy defined in figure 3.2.1A. Histogram overlays were prepared for each dilution factor comprising of negative population (dark blue peak) and positive population (light blue peak). Dilutions were prepared in a doubling series ranging from 1:10 (A.i) to 1:1280 (A.viii). Median and standard deviation data was exported to excel and stain indexes were calculated and plotted as a standard curve in GraphPad Prism (B). Following conversations with fluorophore suppliers, this antibody and conjugate was dropped from the panel as it was advised that the fluorophore was not suited to intracellular staining. CD25 was added into the panel as a substitute.

In order to isolate Treg populations, CD25 (BV510) was added to the panel and validated at a concentration of 5  $\mu\text{g}/\text{mL}$  per test (i.e. 1:100 dilution) according to stain index results as higher dilutions resulted in an inability to discern negative populations from positive (figure C.8).

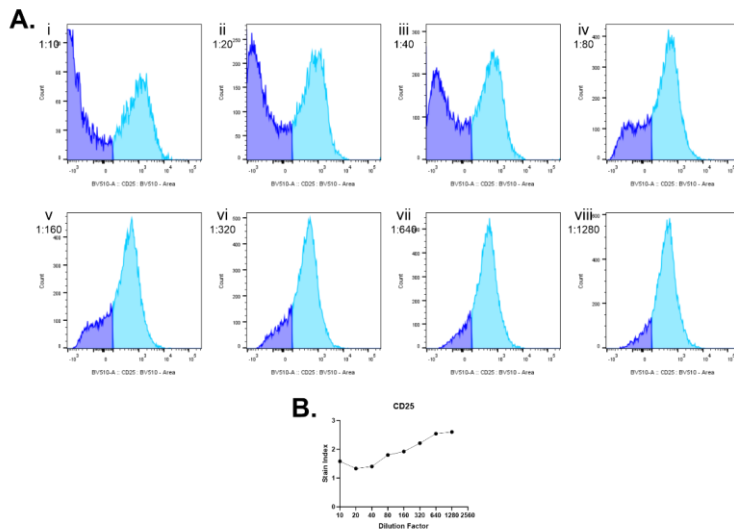


**Figure C.8:- Stain index histograms and curve for CD25 (BV510).** Cells were gated according to the lymphocyte gating strategy defined in figure 3.2.1A. Histogram overlays were prepared for each dilution factor comprising of negative population (dark blue peak) and positive population (light blue peak). Dilutions were prepared in a doubling series ranging from 1:10 (A.i) to 1:1280 (A.viii). Median and standard deviation data was exported to excel and stain indexes were calculated and plotted as a standard curve in GraphPad Prism (B).

Due to low numbers of NK cells in spleen, stain indexes could not be obtained for CD49b (PerCP/Cy5.5) using the conventional method as positive populations could not be visualised through histograms (figure C.9). As a result, populations were examined using SSC-A and the median of positive and negative populations were used to calculate the degree of separation, as defined by a greater difference between the median fluorescence intensity (MFI) of the positive and negative populations. Using this method, it was determined that 2 µg/mL per test (i.e. 1:100 dilution) concentration would be used for CD49b (figure C.10).

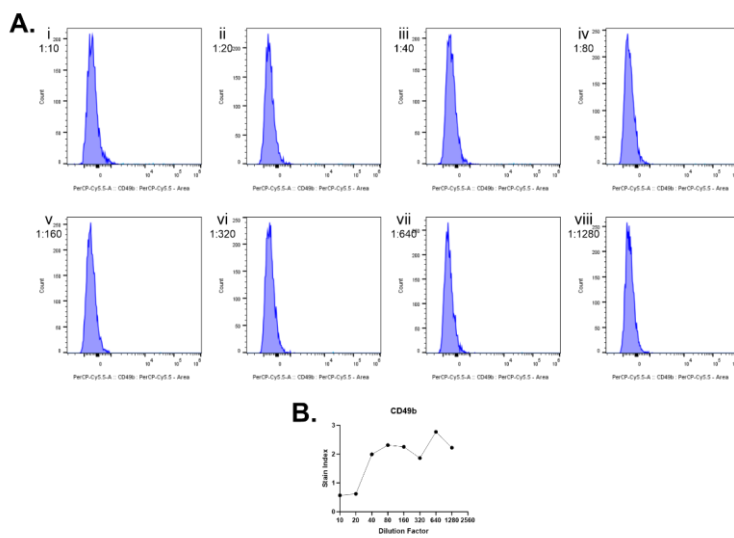


**Figure C.9:- Stain index histograms and curve for CD49b (PerCP-Cy5.5).**

Cells were gated according to the lymphocyte gating strategy defined in figure 3.2.1A. Histogram overlays were prepared for each dilution factor comprising of negative population (dark blue peak) and positive population (light blue peak). Dilutions were prepared in a doubling series ranging from 1:10 (A.i) to 1:1280 (A.viii). Due to low populations only the medians for each peak were exported and the stain index was determined by the difference between median alone, this was plotted as a standard curve in GraphPad Prism (B).

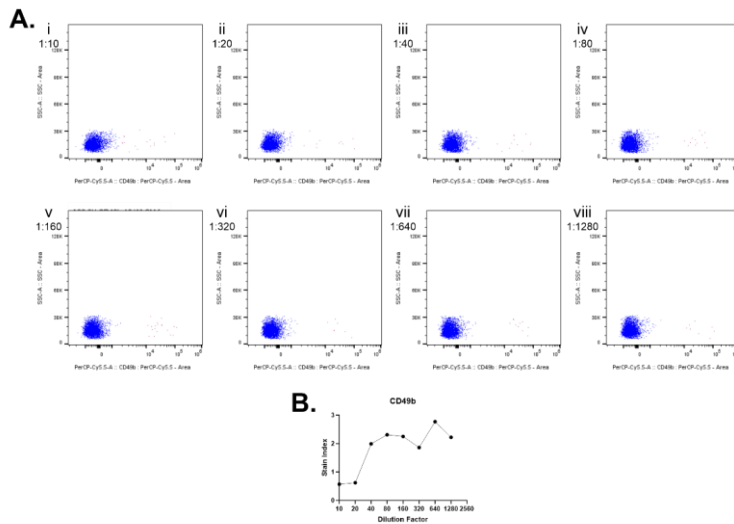


**Figure C.10:-** Dot plots and stain index curve for CD49b (PerCP-Cy5.5). Cells were gated according to the lymphocyte gating strategy defined in figure 3.2.1A. Dot plot overlays were prepared for each dilution factor comprising of negative population (dark blue) and positive population (dark pink) to ascertain population distinctions due to difficulties identifying positive peaks in histograms. This is due to low numbers of NK cells in the spleen. These plots confirmed the accuracy of stain index values and ensured the correct populations were gated for.

The ideal concentration for CD11b was determined to be between 1:640 and 1:1280, so 0.5  $\mu\text{g/mL}$  per test (i.e. 1:1000 dilution) was selected. Although signal from the positive population was low this was attributed to low frequencies of cells expressing this marker in spleen, and positive and negative populations could still be clearly defined at higher dilution factors (figure C.11).



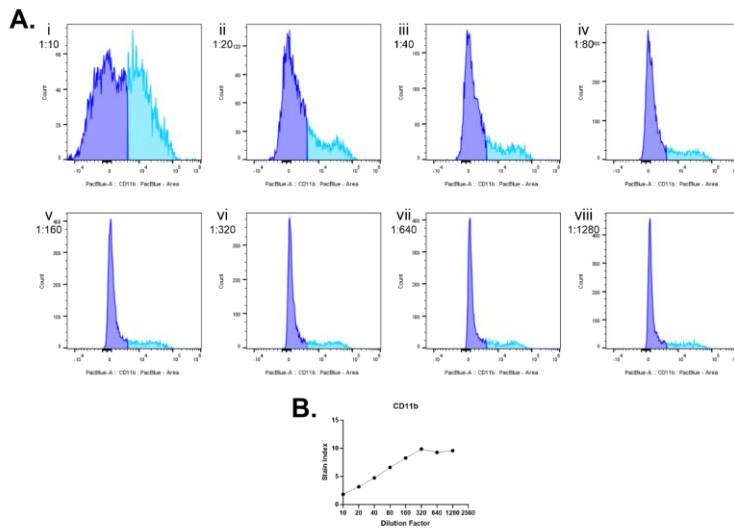


**Figure C.11:- Stain index histograms and curve for CD11b (Pacific Blue).**

Cells were gated according to the macrophage and granulocyte gating strategy defined in figure 3.2.1B. Histogram overlays were prepared for each dilution factor comprising of negative population (dark blue peak) and positive population (light blue peak). Dilutions were prepared in a doubling series ranging from 1:10 (A.i) to 1:1280 (A.viii). Median and standard deviation data was exported to excel and stain indexes were calculated and plotted as a standard curve in GraphPad Prism (B).

Due to the variable staining capacity of Ly6G/Ly6C (PE/Cy5) depending on cell and marker type, histograms for this antibody displayed two positive population peaks (figure C.12). Since the antibody binds with a higher affinity to Ly6G than Ly6C, the peak furthest to the right along the X axis was defined as the Ly6G positive population and the middle peak between this and the negative population were defined as Ly6C positive. Both positive population peaks were included in the total positive population in order to ensure that all three populations could be distinctly defined from one another. Using this strategy, ideal concentration was determined to be 2 µg/mL per test (i.e. 1:100 dilution) as higher dilutions resulted in poor separation between the negative population and the Ly6C positive population.

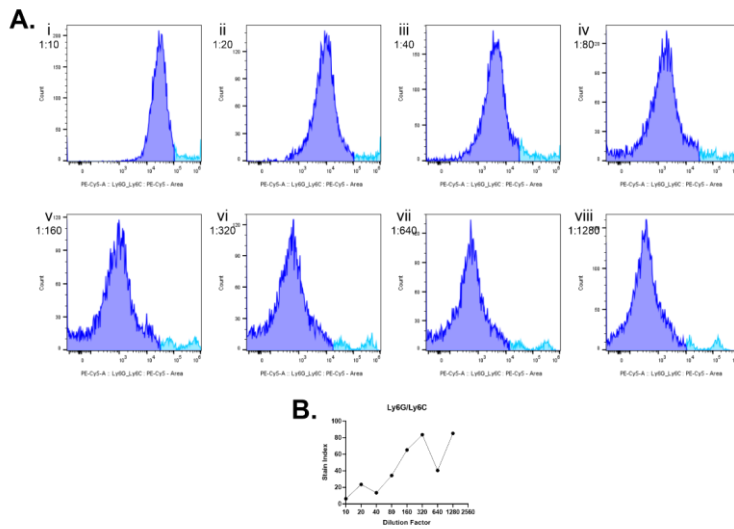


**Figure C.12:- Stain index histograms and curve for Ly6G/Ly6C (PE-Cy5).**

Cells were gated according to the macrophage and granulocyte gating strategy defined in figure 3.2.1B. Histogram overlays were prepared for each dilution factor comprising of negative population (dark blue peak) and positive population (light blue peak). The positive populations display two peaks due to staining intensity of monocytes (first light blue peaks from the left) and neutrophils (second light blue peaks from the left). Dilutions were prepared in a doubling series ranging from 1:10 (A.i) to 1:1280 (A.viii). Median and standard deviation data was exported to excel and stain indexes were calculated and plotted as a standard curve in GraphPad Prism (B).

Ideal concentration of I-A/I-E (PE/Cy7) could be easily determined as a result of clearly defined positive and negative populations, likely due to B cells being the most abundant cell type in spleen (figure C.13). Although the stain index curve peaked at a dilution of 1:40, clear separation was evident at the highest dilution factor and it was possible that lower dilutions may have resulted in nonspecific binding. Therefore, the ideal concentration of I-A/I-E was concluded to be 0.2  $\mu$ L per test (i.e. 1:1000 dilution).

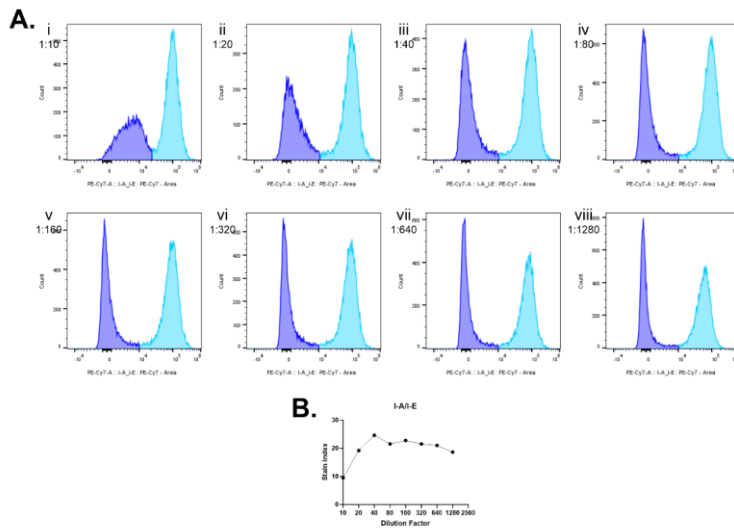


**Figure C.13:- Stain index histograms and curve for I-A/I-E (PE-Cy7).** Cells were gated according to the macrophage and granulocyte gating strategy defined in figure 3.2.1B. Histogram overlays were prepared for each dilution factor comprising of negative population (dark blue peak) and positive population (light blue peak). Dilutions were prepared in a doubling series ranging from 1:10 (A.i) to 1:1280 (A.viii). Median and standard deviation data was exported to excel and stain indexes were calculated and plotted as a standard curve in GraphPad Prism (B).

Stain index curves for macrophage markers typically did not align with the general appearance of positive and negative populations according to histograms. Despite this, ideal concentration for F4/80 (CF568) was selected at 5 µg/mL per test (i.e. 1:100 dilution) due to poor separation of populations at higher dilution factors (figure C.14).

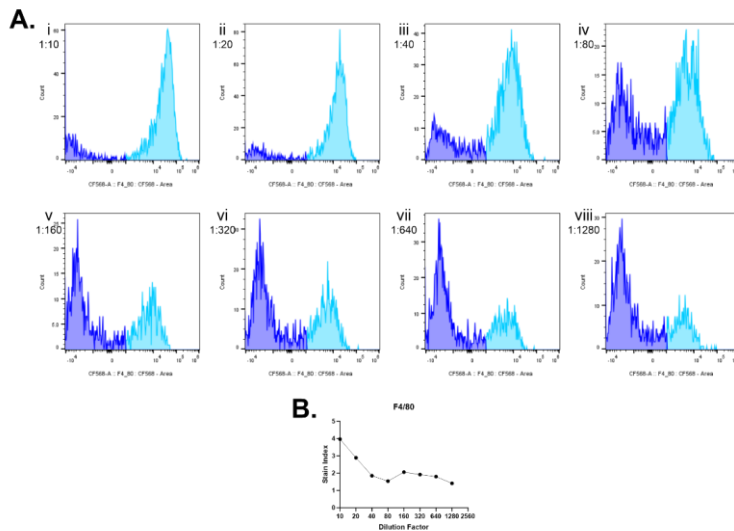


**Figure C.14:- Stain index histograms and curve for F4/80 (CF568).** Cells were gated according to the macrophage and granulocyte gating strategy defined in figure 3.2.1B. Histogram overlays were prepared for each dilution factor comprising of negative population (dark blue peak) and positive population (light blue peak). Dilutions were prepared in a doubling series ranging from 1:10 (A.i) to 1:1280 (A.viii). Median and standard deviation data was exported to excel and stain indexes were calculated and plotted as a standard curve in GraphPad Prism (B).

Although stain index curves indicated that 1:1000 were ideal dilution factors for both CD163 (PE) (figure C.15B) and CD169 (BV605) (figure C.16B), histograms suggested that ideal dilutions were in the region of 1:10 to 1:20 due to clearly defined separation of positive and negative peaks (figure C.15A and C.16A). However, examination of the same populations in dot plot format demonstrates that the majority of cells stained positive at these lower dilution factors are less granular and therefore cannot be classified as macrophages (figure C.17 and C.18). Based on these plots, macrophages can be clearly defined from the negative population at the highest dilutions and thus the stain index curve is reflective of antibody staining efficiency for the desired cell population. Based on these results, ideal concentrations for CD163 and CD169 were determined to be 0.2 µg/mL per test each (i.e. 1:1000 dilution).

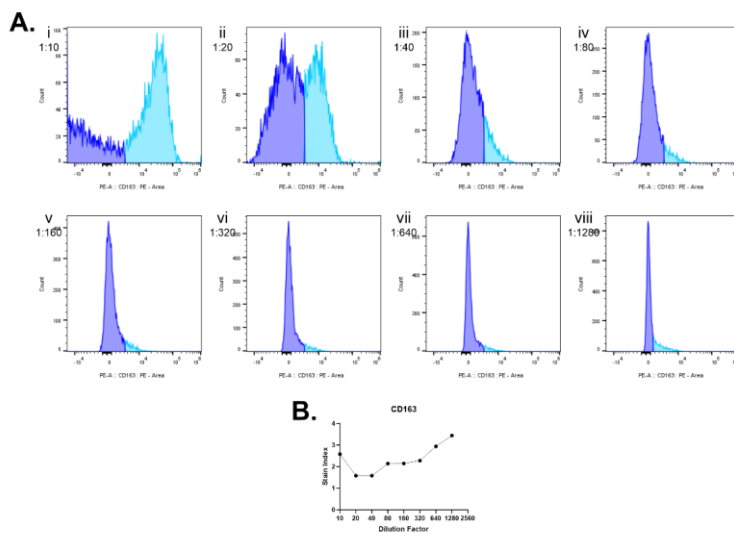


**Figure C.15:- Stain index histograms and curve for CD163 (PE).** Cells were gated according to the macrophage and granulocyte gating strategy defined in figure 3.2.1B. Histogram overlays were prepared for each dilution factor comprising of negative population (dark blue peak) and positive population (light blue peak). Dilutions were prepared in a doubling series ranging from 1:10 (A.i) to 1:1280 (A.viii). Median and standard deviation data was exported to excel and stain indexes were calculated and plotted as a standard curve in GraphPad Prism (B).

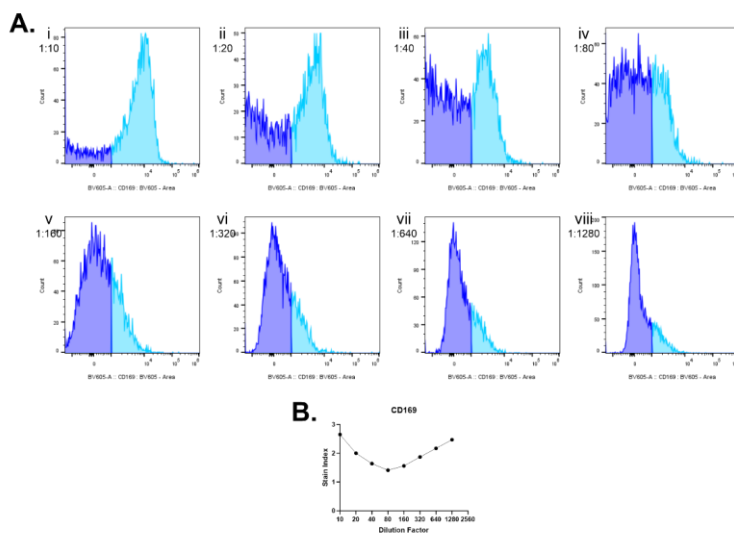


**Figure C.16:- Stain index histograms and curve for CD169 (BV605).** Cells were gated according to the macrophage and granulocyte gating strategy defined in figure 3.2.1B. Histogram overlays were prepared for each dilution factor comprising of negative population (dark blue peak) and positive population (light blue peak). Dilutions were prepared in a doubling series ranging from 1:10 (A.i) to 1:1280 (A.viii). Median and standard deviation data was exported to excel and stain indexes were calculated and plotted as a standard curve in GraphPad Prism (B).

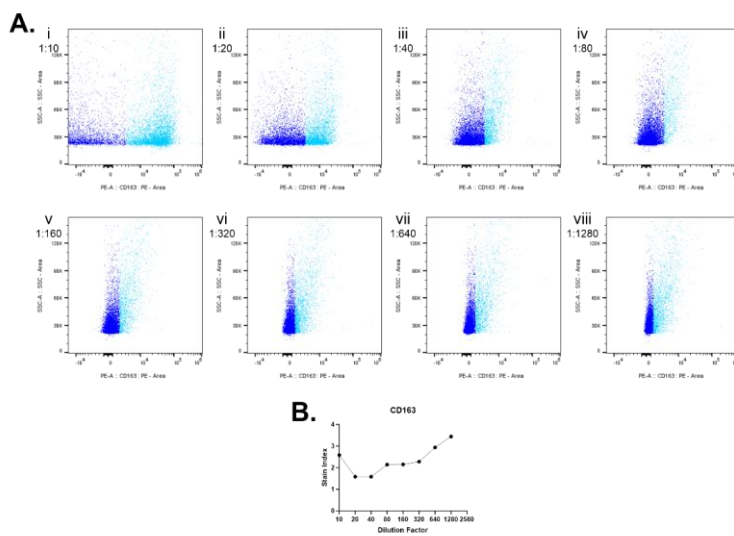


**Figure C.17:- Dot plots and stain index curve for CD163 (PE).** Cells were gated according to the macrophage and granulocyte gating strategy defined in figure 3.2.1B. Dot plot overlays were prepared for each dilution factor comprising of negative population (dark blue) and positive population (light blue) to ascertain population distinctions due to histograms appearing to misalign with stain index curves. This was found to be due to overstaining at lower dilutions, resulting in non-macrophage or granulocytic cells being positively stained for this marker. Therefore, although the histograms suggest a lower dilution factor should be used, the stain index is correct and a higher dilution factor should be used to avoid non-specific staining.

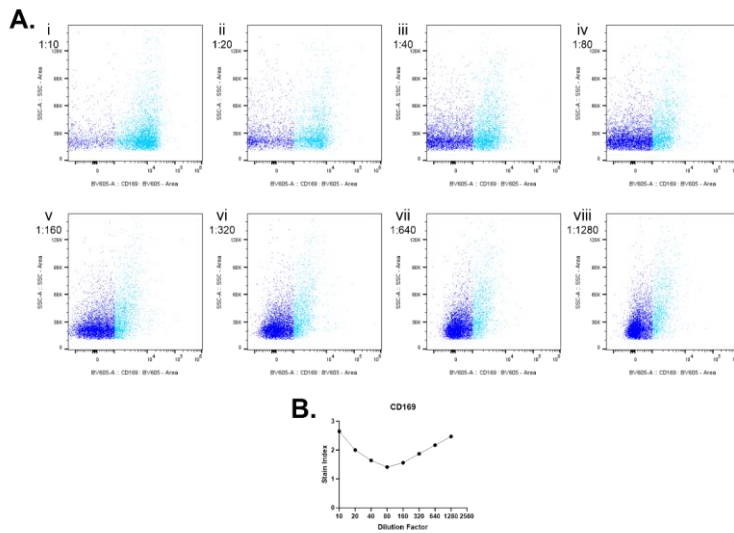


**Figure C.18:- Dot plots and stain index curve for CD169 (BV605).** Cells were gated according to the macrophage and granulocyte gating strategy defined in figure 3.2.1B. Dot plot overlays were prepared for each dilution factor comprising of negative population (dark blue) and positive population (light blue) to ascertain population distinctions due to histograms appearing to misalign with stain index curves. This was found to be due to overstaining at lower dilutions, resulting in non-macrophage or granulocytic cells being positively stained for this marker. Therefore, although the histograms suggest a lower dilution factor should be used, the stain index is correct and a higher dilution factor should be used to avoid non-specific staining.

CD80 (BUV661) and CD86 (BV650) showed similar staining patterns, with both determined to have a staining concentration of 2 µg/mL per test (i.e. 1:100 dilution) (figure C.19 and figure C.20). Clear separation of positive and negative populations for CD38 (PE/Dazzle 594) were observed at all dilutions, as such ideal antibody concentration was determined to be 0.5 µg/mL per test (i.e. 1:1000 dilution) based on stain index curve (figure C.21).



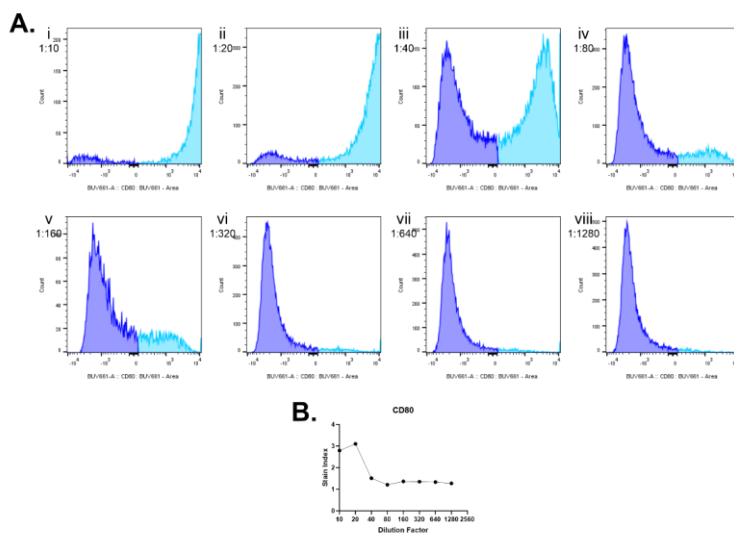


**Figure C.19:- Stain index histograms and curve for CD80 (BUV661).** Cells were gated according to the macrophage and granulocyte gating strategy defined in figure 3.2.1B. Histogram overlays were prepared for each dilution factor comprising of negative population (dark blue peak) and positive population (light blue peak). Dilutions were prepared in a doubling series ranging from 1:10 (A.i) to 1:1280 (A.viii). Median and standard deviation data was exported to excel and stain indexes were calculated and plotted as a standard curve in GraphPad Prism (B).

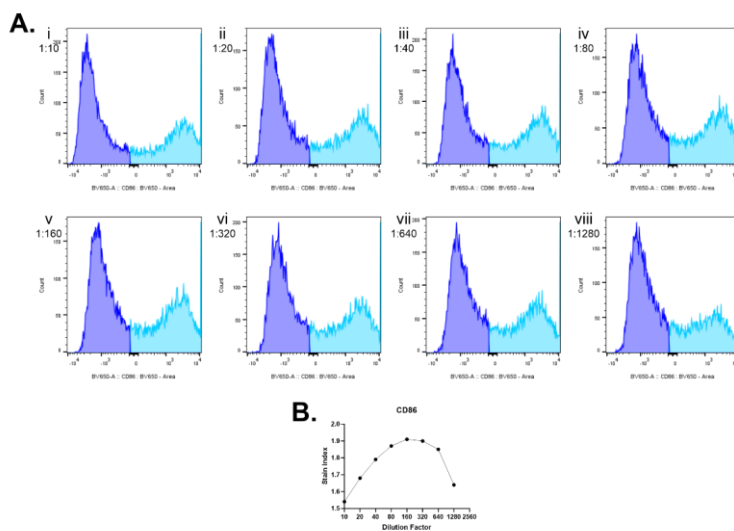


**Figure C.20:- Stain index histograms and curve for CD86 (BV650).** Cells were gated according to the macrophage and granulocyte gating strategy defined in figure 3.2.1B. Histogram overlays were prepared for each dilution factor comprising of negative population (dark blue peak) and positive population (light blue peak). Dilutions were prepared in a doubling series ranging from 1:10 (A.i) to 1:1280 (A.viii). Median and standard deviation data was exported to excel and stain indexes were calculated and plotted as a standard curve in GraphPad Prism (B).

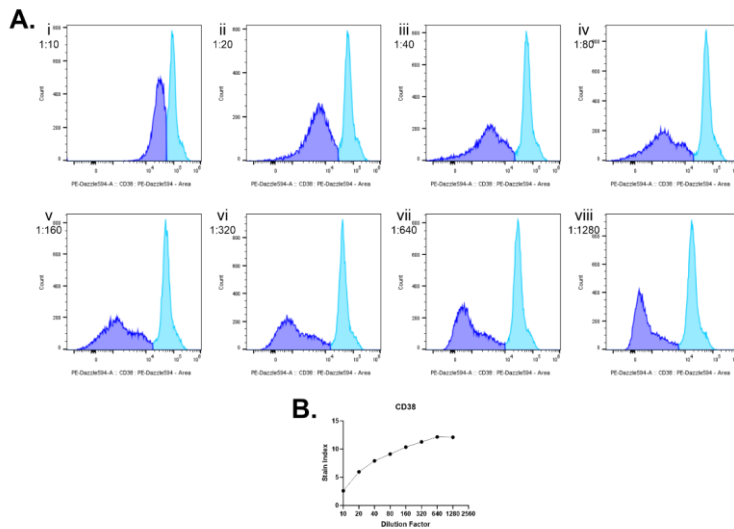


**Figure C.21:- Stain index histograms and curve for CD38 (PE-Dazzle594).**

Cells were gated according to the lymphocyte gating strategy defined in figure 3.2.1A. Histogram overlays were prepared for each dilution factor comprising of negative population (dark blue peak) and positive population (light blue peak). Dilutions were prepared in a doubling series ranging from 1:10 (A.i) to 1:1280 (A.viii). Due to low populations only the medians for each peak were exported and the stain index was determined by the difference between median alone, this was plotted as a standard curve in GraphPad Prism (B).

For T cell activation markers, splenocytes were exposed to PMA/ionomycin for 6 hours, a 0-hour control was also used to generate stain indexes for comparison. At 0 hours, CD69 (BV785) displayed minimal staining and an accurate stain index could not be obtained (figure C.22 A and B). Following activation however, staining was observed and a stain index could be obtained (figure C.22 C and D). Based on the results, a concentration of 4  $\mu\text{g}/\text{mL}$  per test (i.e. 1:50 dilution) for CD69 was determined.

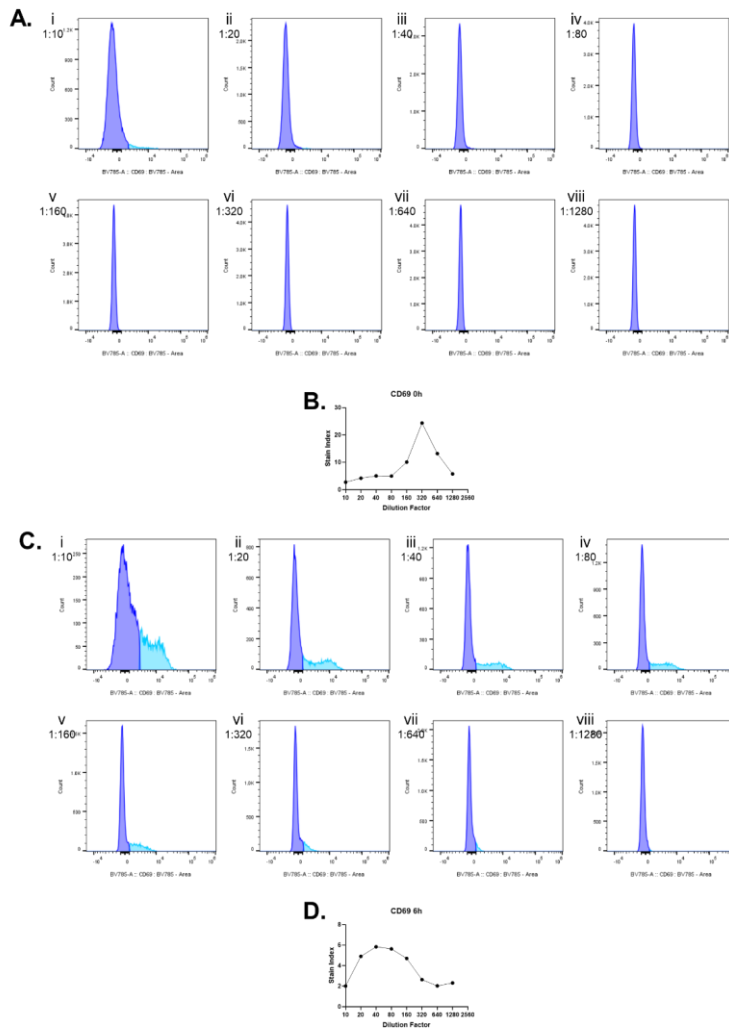


**Figure C.22:- Stain index histograms and curve for CD69 (BV785).** Cells were gated according to the lymphocyte gating strategy defined in figure 3.2.1A and stained either without activation (A and B) or after activation for 6 hours with PMA/Ionomycin (C and D). Histogram overlays were prepared for each dilution factor comprising of negative population (dark blue peak) and positive population (light blue peak). Dilutions were prepared in a doubling series ranging from 1:10 (A.i and C.i) to 1:1280 (A.viii and C.viii). Median and standard deviation data was exported to excel and stain indexes were calculated and plotted as a standard curve in GraphPad Prism (B (0h) and D (6h)).

Staining for CCR7 (AF647) was observed at both 0 hours and 6 hours and stain index curves displayed a similar trend (figure C.23). Although the curves indicated that a dilution factor around 1:1000 was ideal, histograms demonstrated that clear separation of positive and negative populations was more evident at lower dilutions. Based on these observations, CCR7 concentration was determined to be 10 µg/mL per test (i.e. 1:50 dilution).

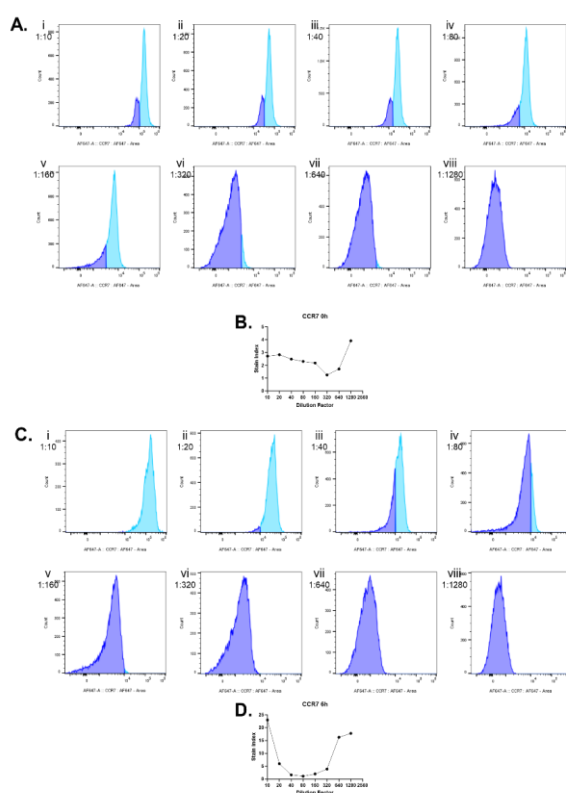


**Figure C.23:- Stain index histograms and curve for CCR7 (AF647).** Cells were gated according to the lymphocyte gating strategy defined in figure 3.2.1A and stained either without activation (A and B) or after activation for 6 hours with PMA/Ionomycin (C and D). Histogram overlays were prepared for each dilution factor comprising of negative population (dark blue peak) and positive population (light blue peak). Dilutions were prepared in a doubling series ranging from 1:10 (A.i and C.i) to 1:1280 (A.viii and C.viii). Median and standard deviation data was exported to excel and stain indexes were calculated and plotted as a standard curve in GraphPad Prism (B (0h) and D (6h)).

Stain indexes for cytokines could not be obtained for 0 hours or 6 hours due to minimal staining, therefore splenocytes were activated with LPS for 24 and 48 hours to elicit cytokine production by macrophages and granulocytes. Due to low populations of macrophages and granulocytes within the spleen, there was some difficulty in determining the ideal concentrations for each antibody. Nonetheless, similar staining patterns were observed for each marker at both 24 and 48 hours. Since stain index curves demonstrated generally atypical appearance, histograms were used to determine ideal antibody concentrations. Histograms for IFN- $\gamma$  (BV421) showed clear distinction between positive and negative populations at dilution factors between 1:10 to 1:160, but beyond this separation was not observed (figure C.24). As a result, ideal concentration was determined to be 2  $\mu\text{g}/\text{mL}$  per test (i.e. 1:100 dilution).

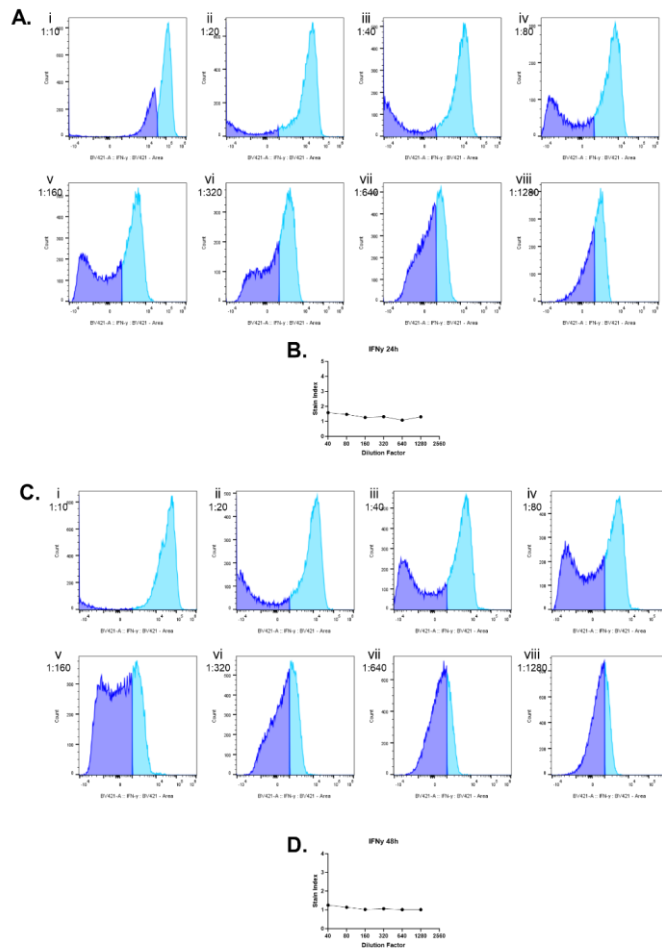


**Figure C.24:- Stain index histograms and curve for IFN- $\gamma$  (BV421).** Cells were gated according to the macrophage and granulocyte gating strategy defined in figure 3.2.1B and activated with LPS and stained at either 24 hours (A and B) or 48 hours (C and D). Histogram overlays were prepared for each dilution factor comprising of negative population (dark blue peak) and positive population (light blue peak), negative control peaks were excluded from overlays due to poor visualisation of stained populations. Dilutions were prepared in a doubling series ranging from 1:10 (A.i and C.i) to 1:1280 (A.viii and C.viii). Median and standard deviation data was exported to excel and stain indexes were calculated and plotted as a standard curve in GraphPad Prism (B (24h) and D (48h)). Stain indexes for 1:10 to 1:20 dilutions were excluded due to values exceeding limits of the curve. Data for 0h not shown due to inability to generate stain index curves as a result of low staining.

The same trend was observed for IL-6 (PerCP-eFluor 710) but only after 24 hours of activation, at 48 hours no discernible separation was observed between positive and negative populations (figure C.25). Since some degree of separation could be seen at lower antibody dilutions after 48 hours, ideal concentration for IL-6 was chosen to be 2 µg/mL per test (i.e. 1:100 dilution) as higher dilution factors at 48 hours activation resulted in no staining of IL-6.

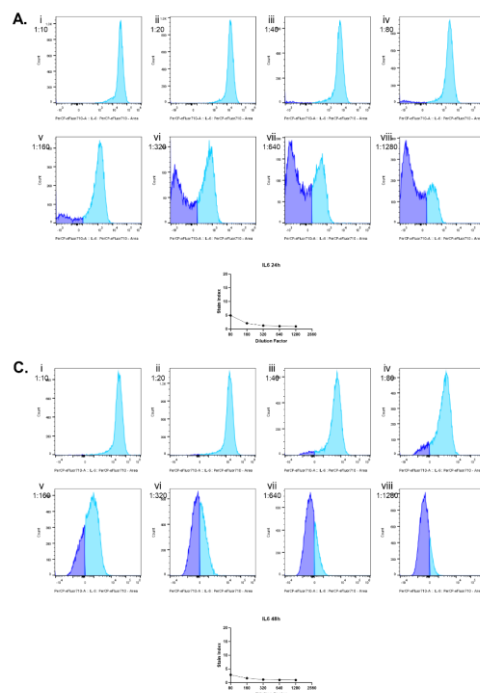


**Figure C.25:- Stain index histograms and curve for IL-6 (PerCP-eFluor710).**

Cells were gated according to the macrophage and granulocyte gating strategy defined in figure 3.2.1B and activated with LPS and stained at either 24 hours (A and B) or 48 hours (C and D). Histogram overlays were prepared for each dilution factor comprising of negative population (dark blue peak) and positive population (light blue peak), negative control peaks were excluded from overlays due to poor visualisation of stained populations. Dilutions were prepared in a doubling series ranging from 1:10 (A.i and C.i) to 1:1280 (A.viii and C.viii). Median and standard deviation data was exported to excel and stain indexes were calculated and plotted as a standard curve in GraphPad Prism (B (24h) and D (48h)). Stain indexes for 1:10 to 1:40 dilutions were excluded due to values exceeding limits of the curve. Data for 0h not shown due to inability to generate stain index curves as a result of low staining.



Clear separation between positive and negative populations were observed at both 24 and 48 hours for IL-17A (figure C.26). Above dilutions of 1:160, distinction between positive and negative populations became less clear, and therefore a concentration of 2 µg/mL per test (i.e. 1:100 dilution) was determined to be ideal.

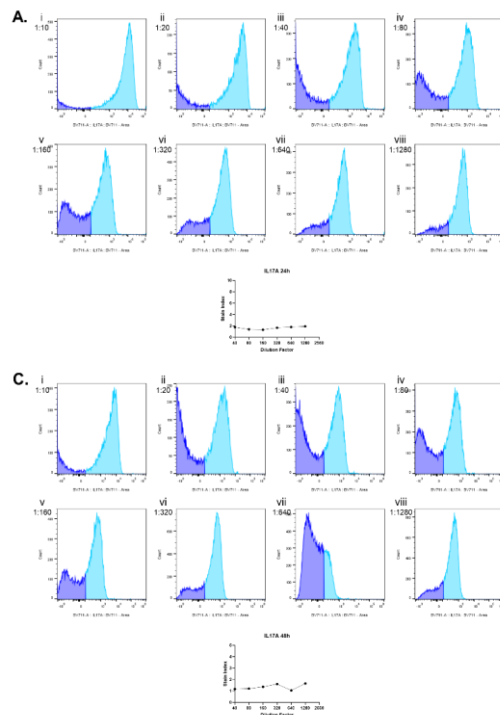


**Figure C.26:- Stain index histograms and curve for IL-17A (BV711).** Cells were gated according to the macrophage and granulocyte gating strategy defined in figure 3.2.1B and activated with LPS and stained at either 24 hours (A and B) or 48 hours (C and D). Histogram overlays were prepared for each dilution factor comprising of negative population (dark blue peak) and positive population (light blue peak), negative control peaks were excluded from overlays due to poor visualisation of stained populations. Dilutions were prepared in a doubling series ranging from 1:10 (A.i and C.i) to 1:1280 (A.viii and C.viii). Median and standard deviation data was exported to excel and stain indexes were calculated and plotted as a standard curve in GraphPad Prism (B (24h) and D (48h)). Stain indexes for 1:10 to 1:20 dilutions were excluded due to values exceeding limits of the curve. Data for 0H not shown due to inability to generate stain index curves as a result of low staining.

Staining of TNF- $\alpha$  did not produce clear separation of positive and negative peaks beyond a 1:20 dilution, and much of this positive staining was attributed to antibody saturation (figure C.27). Since populations could not be determined, a logical approach was taken based upon the results obtained from other cytokines. As all three previous cytokines were determined to have the same ideal staining concentration, it was concluded that 2  $\mu\text{g}/\text{mL}$  per test (i.e. 1:100 dilution) would likely be ideal. This would then be tested during multiplexing and adjusted accordingly if the concentration resulted in poor staining or oversaturation.

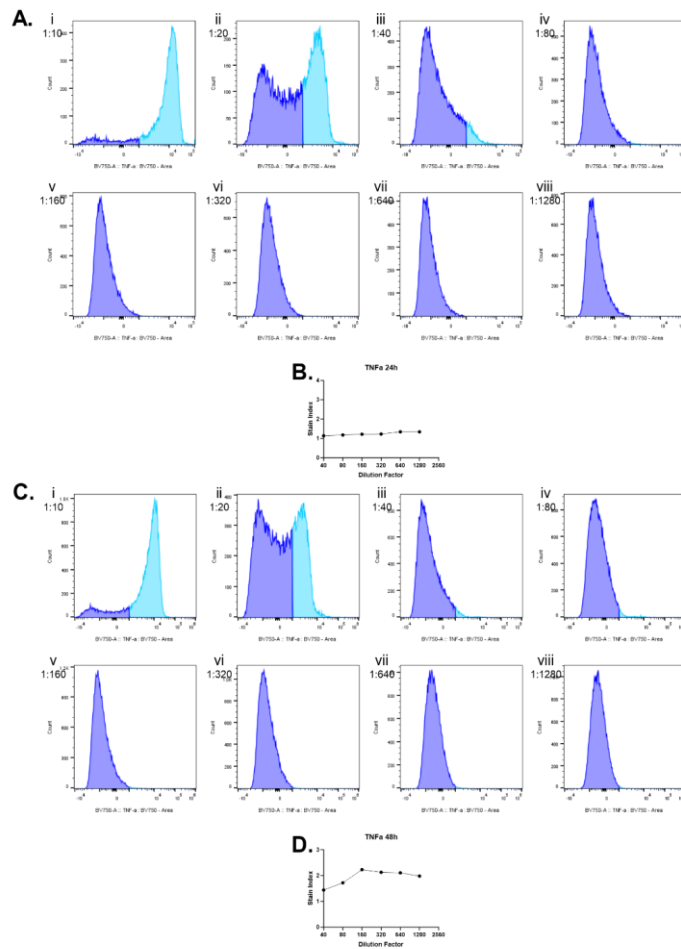


**Figure C.27:- Stain index histograms and curve for TNF- $\alpha$  (BV750).** Cells were gated according to the macrophage and granulocyte gating strategy defined in figure 3.2.1B and activated with LPS and stained at either 24 hours (A and B) or 48 hours (C and D). Histogram overlays were prepared for each dilution factor comprising of negative population (dark blue peak) and positive population (light blue peak), negative control peaks were excluded from overlays due to poor visualisation of stained populations. Dilutions were prepared in a doubling series ranging from 1:10 (A.i and C.i) to 1:1280 (A.viii and C.viii). Median and standard deviation data was exported to excel and stain indexes were calculated and plotted as a standard curve in GraphPad Prism (B (24h) and D (48h)). Stain indexes for 1:10 to 1:20 dilutions were excluded due to values exceeding limits of the curve. Data for 0h not shown due to inability to generate stain index curves as a result of low staining.

---

## APPENDIX D: PIPS REFLECTIVE STATEMENT

### NOTE TO EXAMINERS:

This statement is included as an appendix to the thesis in order that the thesis accurately captures the PhD training experienced by the candidate as a BBSRC Doctoral Training Partnership student.

The Professional Internship for PhD Students is a compulsory 3-month placement which must be undertaken by DTP students. It is usually centred on a specific project and must not be related to the PhD project. This reflective statement is designed to capture the skills development which has taken place during the student's placement and the impact on their career plans it has had.

Due to the impact of COVID-19 on the student, the PIP was shortened to 1-month as approved by the DTP team and the BBSRC.

### PLACEMENT OUTLINE

Ethical consent and approval are paramount to all scientific studies involving the use of both humans and animals to ensure that all necessary steps and precautions are taken to prevent misconduct by researchers, protect those participating in research, and maintain the integrity of science as a whole. As my PhD project has involved the use of mice as a model for COPD, I have a sound understanding of the ethical considerations within animal research, and am highly familiar with the process of the ethical review process for animal studies. However, the processes for the use of human participants, or patient data and samples, take a rather different approach in comparison to animals. In order to gain a well-rounded understanding and expertise of research ethics, I completed a placement from 1<sup>st</sup> October 2023 to 31<sup>st</sup> October 2023 with the University of Nottingham's Research Governance and Integrity Team to gain a deeper understanding of the ethical review, application and authorisation process from the human perspective. Across the month-long placement, I shadowed the Head of Research Integrity, Risk and

Compliance, and Head of Research Governance and performed tasks including reviewing previously submitted documentation for missing or incorrect information, generating example IRAS forms, attending lectures and training seminars, and at the end of the placement I gave a lecture to Master's students on the background and essentials of research ethics and integrity.

#### PLACEMENT AIMS

During the placement my aims were to:

1. Understand the processes and procedures behind Health Research Authority, NHS research and University Research Ethics approval
2. Understand the ethical considerations of designing human studies and provide solutions to areas where risk of ethical misconduct is high
3. Be able to identify mistakes or missing information in ethical application documents
4. Be able to effectively communicate and guide others through the ethics application and ethical review processes

#### PERSONAL AND PROFESSIONAL DEVELOPMENT

As part of my PIPS placement, I aimed to gain a full understanding of research governance and integrity. Due to the nature of the placement, the first items I discussed with my supervisor were the confidentiality agreements I would need to adhere by throughout and beyond the placement. As a result of this, specific details regarding patient and study information cannot be shared in this reflective report. In the beginning of my placement, my supervisor and I covered the principles of research ethics from a human perspective and we covered cases where research ethics had failed to be applied, such as the Tuskegee syphilis experiment. We further discussed scenarios where requiring ethical approval would and wouldn't be needed and discussed suggestions to researchers for

studies where the risk of ethical misconduct is high. This included studies involving vulnerable individuals, such as children, pregnant women, and those with impaired or limited mental capacity, as well as dangerous individuals such as those with criminal convictions, currently in prison, or those considered dangerous due to their political, religious or extremist associations. I believe that these discussions gave me a greater understanding of the considerations that need to be made when designing studies involving human participants, and I met my aims of understanding ethical considerations and providing solutions to scenarios where ethical misconduct is of high risk.

Having previously been involved in a study using NHS patient samples, I wanted to gain an understanding of how approval for such studies is given. I believe that I achieved this aim, as I worked with my supervisor on how to submit studies using the Integrated Research Application System (IRAS) and later reviewed an application submitted to the Research Governance and Integrity Team for mistakes or missing information. I was able to identify errors within the documentation and provide suggestions for areas where I felt the ethics of the research hadn't been considered, and thus gained confidence in my understanding of research ethics and met my first and third aims as a result. For the final part of my placement, I attended a seminar where I discussed solutions and scenarios regarding research ethics and integrity with both staff and students within the university, and gave a lecture on the same topic to Master's students. Following this lecture, I was given praise for my ability to communicate complex ethical scenarios in a clear manner, and opened up debate with the students. I therefore believe I met all aims of my placement, and as a result have gained the skills and understanding necessary to design studies involving both humans and animals of my own and consider and answer all ethical questions within said studies. This placement has given me further interest in the field of research governance and integrity, and I am seeking to further these skills through any opportunities to write grant applications, ethical approvals or patents as part of a Postdoctoral program.